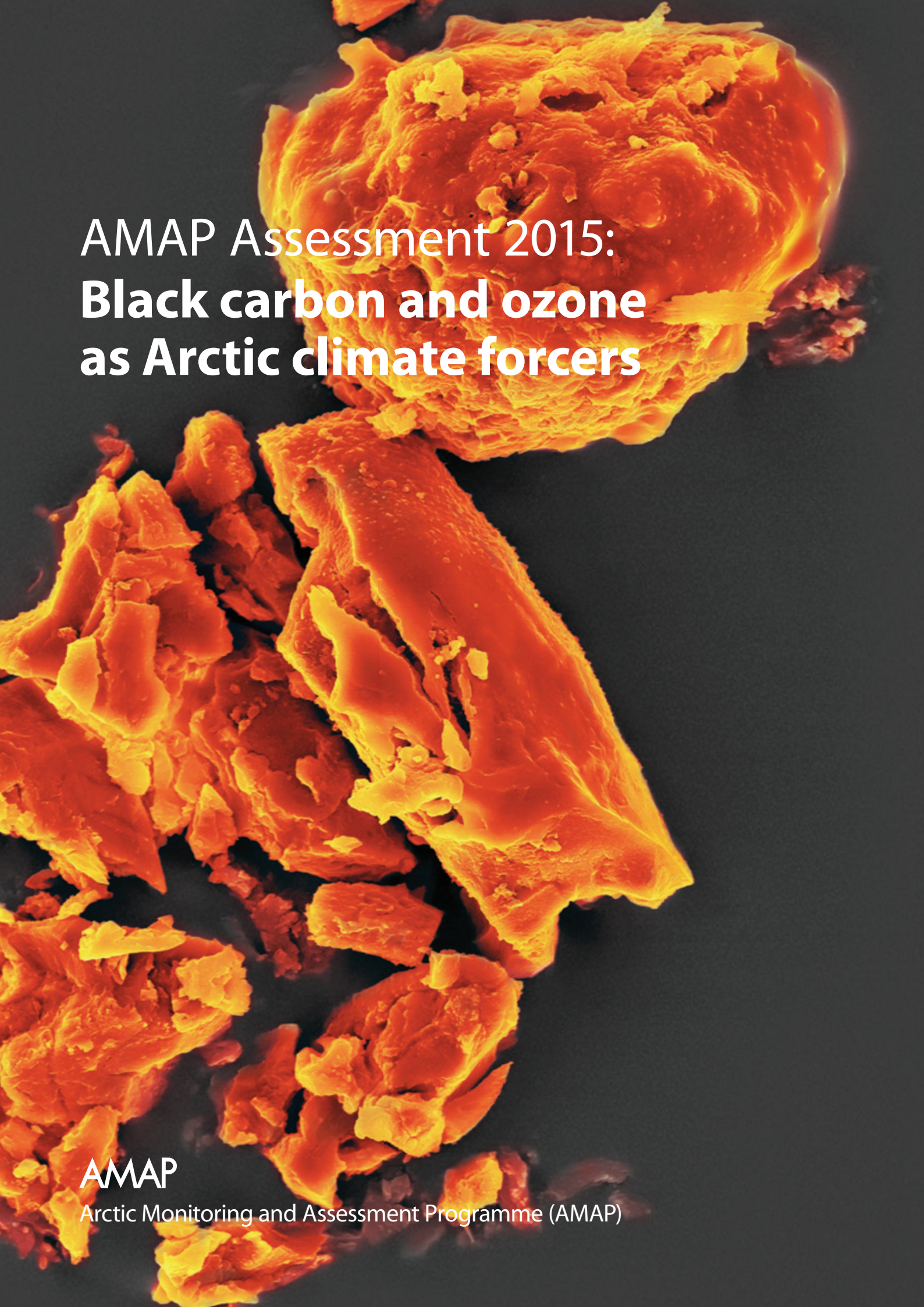

AMAP Assessment 2015:
Black carbon and ozone as Arctic climate forcers

AMAP

Arctic Monitoring and Assessment Programme (AMAP)

AMAP Assessment 2015:
Black carbon and ozone as Arctic climate forcers

AMAP

Arctic Monitoring and Assessment Programme (AMAP)
Oslo, 2015

AMAP Assessment 2015: Black carbon and ozone as Arctic climate forcers

Citation
AMAP Assessment 2015: Black carbon and ozone as Arctic climate forcers. Arctic Monitoring and Assessment Programme (AMAP), Oslo, Norway. vii + 116 pp.

ISBN – 978-82-7971-092-9

Published by
Arctic Monitoring and Assessment Programme (AMAP), Oslo, Norway (www.amap.no)

Ordering
This report can be ordered from the AMAP Secretariat, Gaustadalléen 21, N-0349 Oslo, Norway
This report is also published as electronic documents, available from the AMAP website at www.amap.no

Production

Production management
Simon Wilson (AMAP Secretariat)

Scientific, technical and linguistic editing
Carolyn Symon (carolyn.symon@btinternet.com)

Lay-out and technical production
Burnthebook, United Kingdom (www.burnthebook.co.uk)

Design and production of computer graphics
Karen Birchfield (NOAA), Derek Coffman (NOAA) and Simon Duckworth (simon@burnthebook.co.uk)

Cover photograph
Electron microscope image of soot particles
Photo: © Dennis Kunkel Microscopy, Inc.

Printing
Narayana Press, Gylling, DK-8300 Odder, Denmark (www.narayanapress.dk)

Acknowledgments

Lead Authors*

Patricia K. Quinn, Andreas Stohl, Steve Arnold, Alexander Baklanov, Terje K. Berntsen, Jesper H. Christensen, Sabine Eckhardt, Mark Flanner, Zbigniew Klimont, Ulrik Smith Korsholm, Kaarle Kupiainen, Joakim Langner, Kathy Law, Sarah Monks, Knut von Salzen, Maria Sand, Julia Schmale, Vigdis Vestreng

*See chapters for details

Bold: Assessment Leads

Contributing authors and other contributors

Markus Amann, Gerard Ancellet, Ribu Cherian, Bo Christiansen, Nikos Daskalakis, Sarah Doherty, Michael Gauss, Andreas Herber, Chris Heyes, Øivind Hodnebrog, Nis Jepsen, Chaoyi Jiao, Maria Kanakidou, Marianne Lund, Rashed Mahmood, Gunnar Myhre, Stelios Myriokefalitakis, Dirk Olivie, Ville-Veikko Paunu, Johannes Quaas, Boris Quennehen, Jean-Christophe Raut, Anke Roiger, Bjørn Samset, Hans Schlager, Michael Schulz, Sangeeta Sharma, Ragnhild Skeie, Hailong Wang, Christine Wiedinmyer

Contents

Preface

This assessment report presents the results of the 2015 AMAP Assessment of Black Carbon and Ozone as Arctic climate forcers. This assessment complements a separate 2015 AMAP assessment of methane as an Arctic climate forcer.

The Arctic Monitoring and Assessment Programme (AMAP) is a group working under the Arctic Council. The Arctic Council Ministers have requested AMAP to:

- produce integrated assessment reports on the status and trends of the conditions of the Arctic ecosystems;
- identify possible causes for the changing conditions;
- detect emerging problems, their possible causes, and the potential risk to Arctic ecosystems including indigenous peoples and other Arctic residents; and to
- recommend actions required to reduce risks to Arctic ecosystems.

This report provides the accessible scientific basis and validation for the statements and recommendations made in the *Summary for Policy-makers: Arctic Climate Issues 2015* report[i] that was delivered to Arctic Council Ministers at their meeting in Iqaluit, Canada in April 2015. It is also the basis for a related AMAP State of the Arctic Environment report *Arctic Climate Issues 2015: Overview*[ii]. It includes extensive background data and references to the scientific literature, and details the sources for figures reproduced in the overview report. Whereas the Summary for Policy-makers report contains recommendations that focus mainly on policy-relevant actions concerned with addressing short-lived climate forcers, the conclusions and recommendations presented in this report also cover issues of a more scientific nature, such as proposals for filling gaps in knowledge, and recommendations relevant to future monitoring and research work.

This assessment of black carbon and ozone as Arctic climate forcers was conducted between 2012 and 2014 by an international group of over 40 experts. Lead authors were selected based on an open nomination process coordinated by AMAP. A similar process was used to select international experts who independently reviewed this report.

Information contained in this report is fully referenced and based first and foremost on peer-reviewed and published results of research and monitoring undertaken since 2010. It also incorporates some new (unpublished) information from monitoring and research conducted according to well-established and documented national and international standards and quality assurance/quality control protocols. Care has been taken to ensure that no critical probability statements are based on non-peer-reviewed materials.

Access to reliable and up-to-date information is essential for the development of science-based decision-making regarding ongoing changes in the Arctic and their global implications. The black carbon and ozone assessment summary reports[i, ii] have therefore been developed specifically for policy-makers, summarizing the main findings of the assessment. The black carbon and ozone assessment lead authors have confirmed that both this report and its derivative products accurately and fully reflect their scientific assessment. The black carbon and ozone assessment reports are freely available from the AMAP Secretariat and on the AMAP website: www.amap.no, and their use for educational purposes is encouraged.

AMAP would like to express its appreciation to all experts who have contributed their time, efforts and data, in particular the lead authors who coordinated the production of this report. Thanks are also due to the reviewers who contributed to the black carbon and ozone assessment peer-review process and provided valuable comments that helped to ensure the quality of the report. A list of contributors is included in the acknowledgments at the start of this report and lead authors are identified at the start of each chapter. The acknowledgments list is not comprehensive. Specifically, it does not include the many national institutes, laboratories and organizations, and their staff, which have been involved in various countries in black carbon and ozone related monitoring and research. Apologies, and no lesser thanks are given to any individuals unintentionally omitted from the list.

The support from the Arctic countries and non-Arctic countries implementing research and monitoring in the Arctic is vital to the success of AMAP. The AMAP work is essentially based on ongoing activities within these countries, and the countries that provide the necessary support for most of the experts involved in the preparation of the AMAP assessments. In particular, AMAP would like to acknowledge Norway and the United States for taking the lead country role in this assessment and thank Canada, Norway and the Nordic Council of Ministers for their financial support to the black carbon and ozone assessment work. The US National Oceanic and Atmospheric Administration contribution was accomplished under NOAA PMEL contribution number 4387.

The AMAP Working Group is pleased to present its assessment to the Arctic Council and the international science community.

Andreas Stohl (Black Carbon and Ozone Assessment Co-lead, Norway)

Patricia Quinn (Black Carbon and Ozone Assessment Co-lead, USA)

Morten Olsen (AMAP Chair, April 2015)

Lars-Otto Reiersen (AMAP Executive Secretary)

Oslo, November 2015

i. AMAP, 2015. Summary for Policy-makers: Arctic Climate Issues 2015. Arctic Monitoring and Assessment Programme (AMAP), Oslo, Norway. 16 pp.

ii. AMAP, 2015. Climate Issues 2015: Overview report. Arctic Monitoring and Assessment Programme (AMAP), Oslo, Norway. 16 pp.

1. Introduction

Lead authors: Patricia Quinn, Andreas Stohl

The Arctic Monitoring and Assessment Programme (AMAP) established an Expert Group on Short-Lived Climate Forcers (SLCFs) in 2009 with the goal of reviewing the state of science surrounding short-lived climate forcers in the Arctic and recommending the science tasks that AMAP should conduct or promote in order to improve the state of knowledge and its application to policy-making. In 2011, the result of the Expert Group's work was published in *The Impact of Black Carbon on Arctic Climate* (AMAP 2011). That document focused entirely on black carbon and co-emitted particulate phase organic carbon. The current understanding of black carbon was presented including formation and properties, measurement techniques, emissions, transport pathways to the Arctic, atmosphere and snow concentrations, seasonality, and trends. In addition, two global models were used to calculate the contribution of different source regions and combustion source sectors to the atmospheric burden of black carbon in the Arctic and then to calculate the resulting radiative forcing due to each region and sector.

After publication of AMAP (2011), it was decided that the SLCFs Expert Group would continue and expand its scope to include another short-lived climate forcer, tropospheric ozone. The present report is the outcome of the extended work. In addition, a second Expert Group was formed to focus on methane.

Arctic warming is a manifestation of global warming, such that reducing global-average warming will reduce Arctic warming and slow the rate of melting of snow and ice (IPCC 2013b). Reductions in the emission of carbon dioxide are the backbone of any meaningful effort to mitigate climate forcing. But even if swift and deep reductions are made, these may not be achieved in time to delay a rapid thawing of the Arctic. Hence, the goal of constraining the length of the melt season and, in particular, delaying the onset of spring melt, may best be achieved by also targeting shorter-lived climate forcing agents; especially those that impose a surface forcing that may trigger regional-scale climate feedbacks pertaining to the melting of sea ice and snow.

Methane, ozone, and black carbon-containing aerosols are the species most commonly identified as being short-lived climate forcers. With a lifetime of about nine years (Prinn et al. 1995), methane is much shorter-lived than carbon dioxide but is still globally well-mixed. On a per molecule basis, methane is a more effective greenhouse gas than carbon dioxide, with a global warming potential a factor of 25 higher (IPCC 2013b). Radiative forcing by methane results directly from the absorption of longwave radiation and indirectly through chemical reactions that lead to the formation of other radiatively important gases (Wuebbles and Hayhoe 2002).

Tropospheric ozone, like all greenhouse gases, can affect Arctic climate by altering local radiation fluxes and modulating the transport of heat to polar regions (Shindell 2007). Ozone is not emitted directly but is formed in the atmosphere through a series of chemical reactions between precursor gases. Ozone precursors include nitrogen oxides, carbon monoxide, methane, and non-methane volatile organic compounds (Seinfeld and Pandis 2006). Reducing the atmospheric burden of tropospheric ozone to reduce warming in the Arctic requires taking into account mechanisms of ozone production that can vary depending on available precursors and their relative amounts.

Black carbon is emitted directly through incomplete combustion and remains in the atmosphere until it is removed by wet or dry deposition. Black carbon is the most efficient atmospheric particulate species at absorbing visible light (Bond et al. 2013). As a result, it exerts a warming effect that contrasts with the cooling effect of purely scattering aerosol components. Pure black carbon particles rarely occur in the atmosphere, however. Soon after emission, black carbon becomes mixed with other aerosol chemical components including sulfate and organics. Black carbon-containing aerosols can have either a warming or a cooling effect on climate depending on the albedo (i.e. reflectivity) of the underlying surface relative to the albedo of the black carbon-containing aerosol itself. The albedo of the haze depends on what other chemical species are present, their relative amounts, and whether they primarily scatter or absorb light. As a result, when determining the climate impact of black carbon and the effectiveness of a given mitigation strategy, species co-emitted with the black carbon and the altitude of the black carbon-containing aerosol must be taken into account.

Black carbon-containing aerosols in the Arctic can perturb the radiation balance in a number of ways (see Fig. 1.1). Direct aerosol forcing occurs through the absorption or scattering of solar shortwave radiation. An absorbing aerosol, such as one containing black carbon, over a highly reflective surface will result in a warming at altitudes above and within the haze layer (Shaw and Stamnes 1980). For low-altitude black carbon, the added atmospheric heating will subsequently increase the downward longwave radiation to the surface, warming the surface. Radiative forcing by black carbon can also result from aerosol-cloud interactions that affect cloud microphysical properties, albedo, extent, lifetime and longwave emissivity (Twomey 1977; Garrett et al. 2004; Garrett and Zhao 2006).

When deposited to snow and ice surfaces, black carbon can enhance the absorption of radiation, which warms the lower atmosphere and accelerates snow and ice melting (Clarke and Noone 1985). The black carbon snow/ice forcing mechanism is in addition to the stronger snow-albedo feedback process, and can trigger that process. Snow-albedo feedback occurs as snow and sea ice melt, exposing darker surfaces underneath. These darker surfaces result in enhanced absorption of radiation and surface warming. All forcing mechanisms are described in Ch. 4 in more detail.

This work builds on the results of the 2011 report by including tropospheric ozone and the particulate and non-carbon dioxide gas phase species that are co-emitted with black carbon during the combustion process. Species co-emitted with black carbon that are considered here include organic carbon, sulfur dioxide, nitrogen oxides and non-methane volatile organic carbon. Both global-scale and regional-scale chemical transport models were used to simulate transport of black carbon and co-emitted

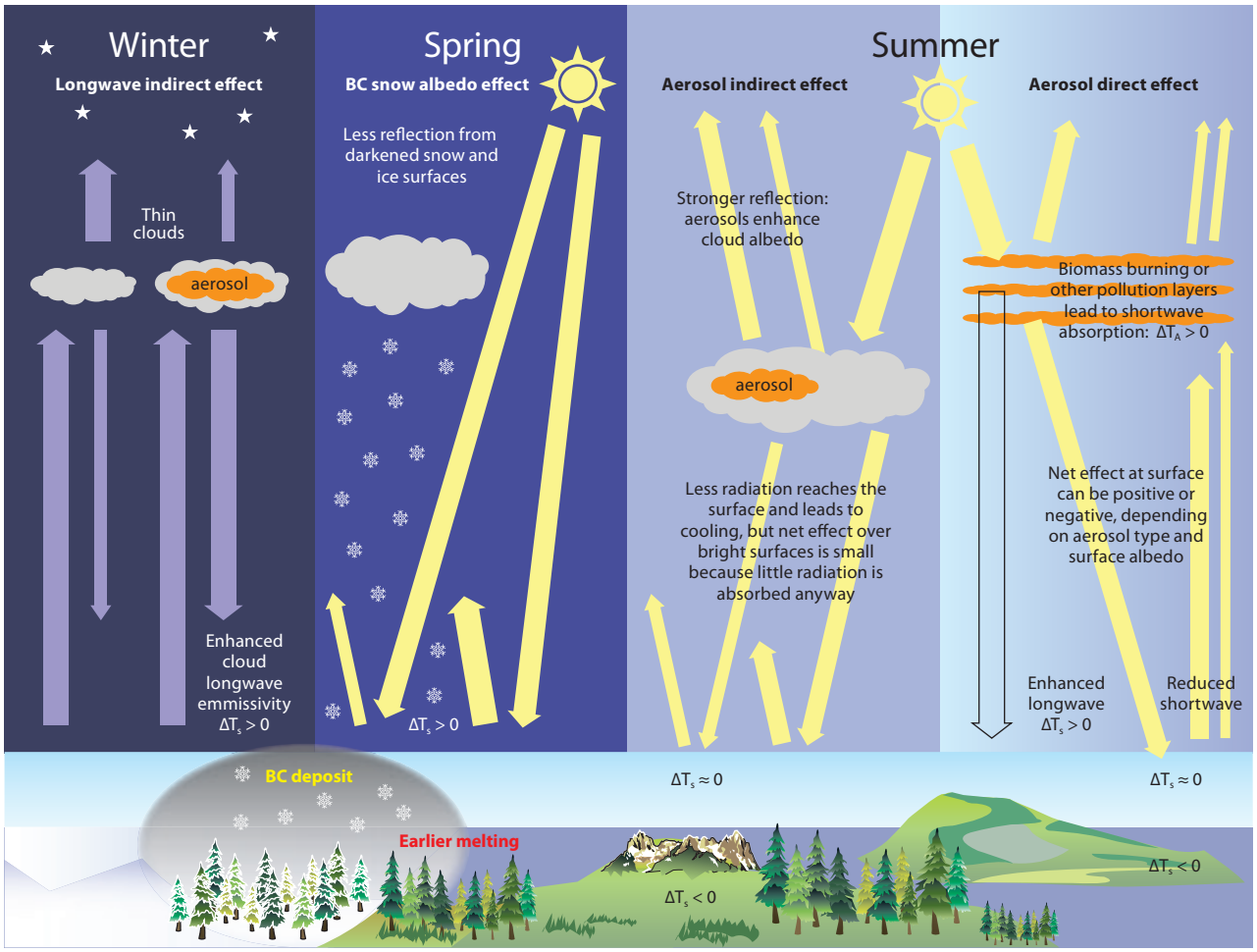

Figure 1.1 Upper panels indicate seasonal variations in forcing mechanisms in the Arctic due to black carbon. ΔT_s indicates the surface temperature response to an instantaneous forcing. Lower panel indicates seasonal climate response to the instantaneous forcing shown above. Forcing mechanisms are discussed in more detail in Ch. 4.

species to the Arctic. Additional model simulations were run for the production of tropospheric ozone, considering both remote and within-Arctic mechanisms, and transport to and within the Arctic. The contribution of specific sources (by energy sector and geographical region) to the resulting Arctic atmospheric burdens of black carbon and ozone were calculated. Similarly, radiative forcing due to specific sources was calculated for black carbon, co-emitted species, and ozone. Finally, and beyond what was done in the 2011 report, global earth system models were used to estimate the equilibrium climate response to forcing by black carbon, co-emitted species, and tropospheric ozone under different emission scenarios.

The remaining parts of this report include background information on black carbon including the properties of black carbon that make it a short-lived climate forcer, methods for measuring black carbon in the atmosphere and in snow, and a discussion of co-emitted species (Ch. 2). Chapter 3 presents background information on tropospheric ozone including the chemistry of ozone production and destruction and measurement methods. Forcing mechanisms for both black carbon and co-emitted species and tropospheric ozone are presented in Ch. 4. Emissions of black carbon and co-emitted species as well as ozone precursors as a function of energy sector and geographical region are addressed in Ch. 5. Transport of black carbon to the Arctic is reviewed in Ch. 6. Chapter 7 contains descriptions of the modeling methods used in this work. Model-measurement comparisons based on data from long-term measurement sites and recent aircraft campaigns are presented in Ch. 8. Compared species include black carbon, organic carbon, non-sea salt sulfate, ozone, carbon monoxide, nitric oxide, and peroxyacetyl nitrate. Updated trend analyses for black carbon and tropospheric ozone are presented in Ch. 9. Results of the radiative forcing and climate response model simulations are given in Ch. 10. The final two chapters of the report give the summary findings and recommendations for future research.

The report concludes with a detailed summary of the strategies used for modeling the climate response. This annex is a common contribution to the AMAP assessments on methane (AMAP 2015) and black carbon and ozone (the present report) and has been produced to facilitate an integrated understanding of the separate climate modeling exercises undertaken by the two AMAP expert groups on short-lived climate forcers (SLCFs).

2. Black carbon: Properties, measurements and co-emitted species

Lead authors: Julia Schmale, Patricia Quinn, Ulrik Smith Korsholm

2.1 Introduction

This chapter provides an overview of black carbon focusing on its properties, common measurement techniques for the atmosphere and snow, and co-emitted species. Measurements of black carbon in the atmosphere and in snow along with data from long-term monitoring programs are discussed in Ch. 8 and 9, respectively.

2.2 Properties of black carbon

Black carbon (BC) is uniquely identifiable among all particulate phase species due to its morphology, strong absorption of solar radiation, refractory nature (stability at high temperatures), and insolubility in water, alcohol and other media. BC is mainly a product of the combustion of fossil and biogenic fuels when there is insufficient oxygen to yield a complete conversion of the fuel into carbon dioxide (CO_2) and water. Through the combustion process, small graphitic particles of the order of tens of nanometers in size are formed (e.g. Slowik et al. 2004; Stier et al. 2006; Glassman and Yetter 2008). These particles change rapidly after emission as they transform into densely packed clusters (Martins et al. 1998) and serve as nuclei on which water vapor and other gas phase components can condense.

A number of different names exist in the literature for black carbon. This report uses the nomenclature suggested by Petzold et al. (2013) which is dependent on the measurement principle (see Table 2.1 for details). Briefly, BC is used as a qualitative description referring to light-absorbing carbonaceous substances in atmospheric aerosol when there is no reference to a specific measurement method. Equivalent BC (eBC) refers to the quantity derived from optical absorption methods calculated from the measured light absorption coefficient (σ_{ap}) based on an assumed mass-specific absorption cross-section (MAC). Results from methods that are specific to the carbon content of carbonaceous matter (e.g. evolved carbon or mass spectrometric methods) are reported as elemental carbon (EC). Refractory BC (rBC) is reported from incandescence methods. BC-containing particles are particles that comprise a variety of substances including a BC fraction.

Size distributions of BC-containing aerosol depend on the production mechanism of the aerosol and atmospheric processing that has occurred since emission. Freshly emitted anthropogenic BC particles are in the size range 30 nm (individual particles) to 150 nm (coagulated particles) in diameter (Petzold et al. 1999). Freshly emitted soot particles from diesel engines have a modal diameter of 60 nm (Rönkkö et al. 2006). Measured densities cover a range of 1 to 2 g/cm^3 (Ma et al. 2012 and references

Table 2.1 Measurement methods applied in the Arctic for black carbon in the atmosphere and snow.

Method	Instrument	Application	Reported value	Uncertainty / major potential artifacts	Reference
Thermal-optical	Various gasification procedures from heated filter samples in combination with transmission or reflectance measurements	Atmospheric concentration/ concentration in snow	EC	Agreement within <10% for total mass of particulate carbonaceous material/ pyrolization of non-EC carbon, different thermal sequences lead to a factor of 2 difference in mass concentration, lower size limit might be relatively high depending on filter material leading to low biases due to under-catch of particles in, for example, snow sample analysis	Forsström et al. 2013; Petzold et al. 2013 and references therein
Light absorption	Photoacoustic Spectrometer (PAS)	Atmospheric concentration	σ_{ap} or eBC	Overall uncertainty with respect to aerosol absorption is about 5%	Lack et al. 2006
Filter-based absorption photometry	Integrating Sphere/ Integrating Sandwich Spectrometer (ISSW)	Concentration in snow	eBC with MAC	Uncertainty of the derived loading is above 7% for loadings <0.2 μg/cm^2 and >6 μg/cm^2	Grenfell et al. 2011; Schwarz et al. 2012
	Particle Soot Absorption Photometer (PSAP)	Atmospheric concentration	eBC with MAC	Difference between BC mass derived from chemical and optical methods up to a factor of 7 / absorption enhancement by other components such as mineral dust, coatings etc.	Petzold et al. 2013 and references therein
	Aethalometer	Atmospheric concentration	eBC with MAC		
Laser-induced incandescence	Single Particle Soot Photometer (SP2)	Atmospheric concentration/ concentration in snow	rBC	For atmospheric measurements rBC mass concentration uncertainty is <30%, for snowmelt samples around 60%, there might be low biases in passing efficiency of particles from snow melt water into the SP2 when attached to large particles / conversion of thermal radiation into mass depends strongly on established calibration, lower size limit is around 70–80 nm	Laborde et al. 2012; Schwarz et al. 2012; Petzold et al. 2013 and refer herein

BC: black carbon, EC: elemental carbon, rBC: refractory black carbon, eBC: equivalent black carbon, MAC: mass-specific absorption cross section, σ_{ap}: light absorption coefficient.

therein). Measurements of particle size immediately after emission and their density are crucial because they are sensitive input parameters for modeling studies (Koch et al. 2009b; Ma et al. 2012). Aged plumes exhibit mass median diameters for BC cores of around 200 nm or larger with shell/core ratios of 1.3–1.6 depending on the source (Shiraiwa et al. 2008). Aged biomass burning and anthropogenic fossil fuel plumes containing BC measured in the Arctic exhibited a modal volume diameter for the whole particle of 300 nm or more (Brock et al. 2011). Particle growth occurs through coagulation and condensation of gas phase species (Fig. 2.1). As these processes occur within hours of emission, pure BC particles are rarely observed in the atmosphere, especially in remote regions like the Arctic to which BC generally has to be transported over long distances (see Sect. 2.4 and Ch. 6 on transport), although BC emission sources also exist in the Arctic (e.g. diesel engines, ships etc.). The impact of the rapid processing of BC after emission on the composition of the resulting BC-containing particles, their optical and cloud nucleating properties, and their residence time are briefly described in the rest of this section. Further details can be found in the previous AMAP technical report (AMAP 2011).

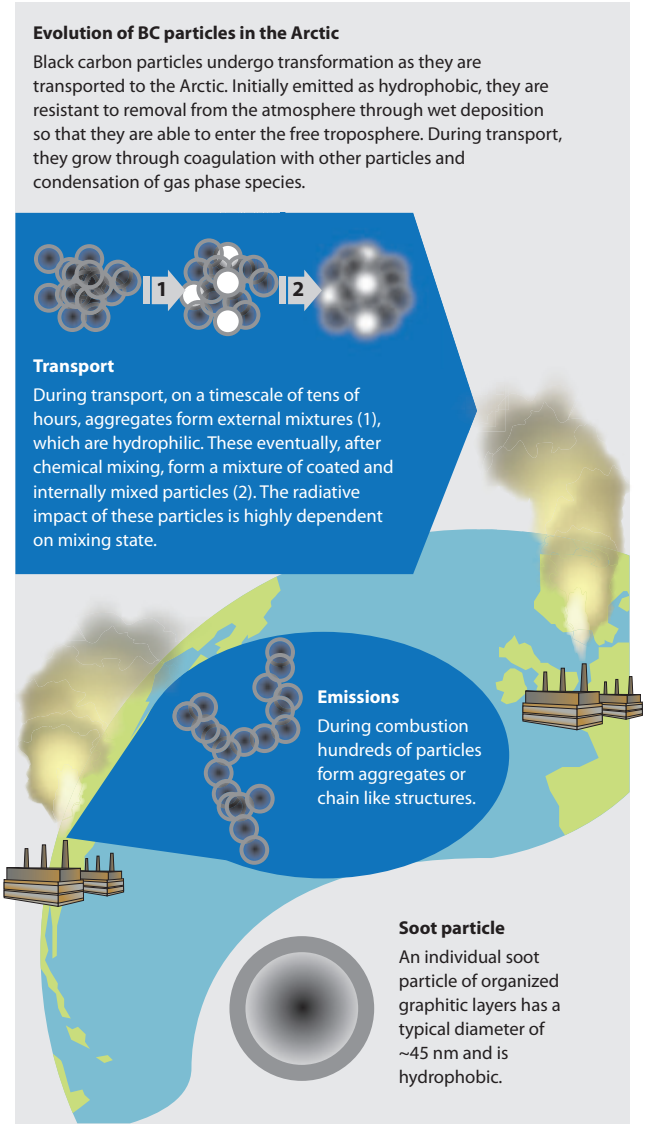

Figure 2.1 Conceptual overview of the evolution of black carbon particles during transport to the Arctic.

In addition to the aforementioned sources of BC, coal piles, such as those observed in Svalbard (Myhr 2003), may also provide a local source of BC-containing particles to the Arctic. The wind-driven production of coal dust results in considerably larger particles than combustion (Ghose and Majee 2007). Sedimentation rates increase with particle size so that particles larger than about 10 μm in diameter generally have much shorter lifetimes than submicrometer particles (i.e. hours versus days). In addition, the absorption coefficient per unit mass decreases with particle size for diameters greater than about 300 nm (Bergstrom 1973). The reason is that for small particles, light can penetrate to the center of the particle and the entire mass contributes to absorption, while in larger particles only the 'skin' can contribute (Bond and Bergstrom 2006). From a climate perspective, these large coal dust particles are expected to have only a local effect on climate through the BC-snow albedo forcing mechanism, by darkening the snow around the coal piles. Likewise other 'dark' and large particles such as debris from rock and stones can darken snow and ice surfaces. However, their short lifetime limits their impact through atmospheric forcing. The following discussion therefore focuses on fine BC particles derived from combustion.

Black carbon is hydrophobic (i.e. water-repellent) upon emission. As the particle ages, the BC-containing particle becomes increasingly hydrophilic, or hygroscopic (i.e. water-attracting), as it takes up gases, coagulates with nearby particles, and undergoes atmospheric reactions with species in the surrounding atmosphere (Abel et al. 2003). A review of observations of aerosol hygroscopicity from remote and urban regions showed that hydrophobic particles are found only near emission sources (Sweitlicki et al. 2008). These results confirm that such particles (which are indicative of BC) stay hydrophobic only on the order of hours or less in the case of biomass burning emissions (Cubison et al. 2011) before they undergo transformations in the atmosphere. As BC-containing aerosol becomes more hydrophilic, its chances of removal from the atmosphere through in-cloud scavenging and precipitation increase (Stier et al. 2006). Hence, the conversion of BC-containing particles from a hydrophobic to a more hydrophilic state changes the lifetime of BC in the atmosphere. At the same time, the BC-containing particles may alter cloud properties. The hygroscopicity of Arctic aerosol freshly emitted from biomass burning (i.e. sampled in the boundary layer near the fires) and of aged aerosol from biomass burning (i.e. long-range transported to the high Arctic) is similar owing to the rapid chemical and physical aging processes that occur immediately after emission. This leads to high mass contributions of organic carbon (OC; 93% for fresh and 78% for aged particles) with water soluble OC fractions of 0.57 and 0.80, respectively. Aged biomass burning aerosol in the Arctic is also more active as cloud condensation nuclei (CCN) than industrial pollution aerosol because the anthropogenic particles are smaller and have a lower OC content (Lathem et al. 2013). Paris et al. (2009) found the lifetime of eBC in Siberian Arctic wildfire plumes to be around five days (e-folding lifetime). This is consistent with an aged, more hygroscopic BC aerosol. Values from Arctic-focused modeling studies (Koch and Hansen 2005; Liu et al. 2005; Park et al. 2005; Wang et al. 2011) are slightly higher and variable.

The likelihood of an aerosol particle to take up water to the point that it activates and forms a cloud droplet depends on its size and composition (or hygroscopicity) and the supersaturation within the cloud. At high supersaturations, most particles will activate droplet formation regardless of size or composition. For the relatively low supersaturations of Arctic stratiform clouds, small hydrophobic particles will not form cloud droplets (Shaw 1986). Hence, freshly emitted BC particles, which are both small and hydrophobic, will make very poor nucleation sites for cloud droplets. In contrast, aged BC particles, which have grown in size and become more soluble after emission, will have an increased ability to nucleate cloud droplets (Kuwata et al. 2007; Tritscher et al. 2011). Hence, the aging of BC during transport to the Arctic is expected to affect the ability of BC-containing aerosol to form cloud droplets and influence cloud properties, and thus to affect aerosol indirect climate forcing.

The ice nucleation efficiency of BC combustion particles is currently not well understood. Some studies indicate that hydrophilic combustion particles are more efficient at nucleating ice than hydrophobic combustion particles (DeMott et al. 1999; Gorbunov et al. 2001) while other studies suggest that aging leads to reduced ice nucleation efficiency (Möhler et al. 2005; Crawford et al. 2011). However, most studies suggest that combustion particles are inefficient at nucleating ice when compared to the ability of solution droplets to form ice (Bond et al. 2013). Hence, neither aged long-range-transported combustion aerosol nor freshly emitted combustion aerosol are expected to exert large influences on the ice phase of Arctic mixed phase or cirrus clouds given the presence of non-BC ice nuclei.

The time required for transport of BC from extra-Arctic source regions to the Arctic is typically from several days to weeks (Heidam et al. 2004). This timeframe can be appreciably longer than the time required for 'aging' or conversion to a hydrophilic particle. Whether BC emitted at lower latitudes is transported to and deposited within the Arctic depends, in part, on atmospheric processing en route and whether the BC particle is removed from the atmosphere before it reaches the Arctic, as well as cloud conditions within the Arctic itself.

The transformations undergone by BC after emission also have implications for the magnitude of light absorption by the resulting internally mixed aerosol which, however, is not yet well understood. It has been shown theoretically that light absorption by an absorbing core is enhanced when the core is coated with scattering material (Fuller et al. 1999). The scattering shell serves to amplify the amount of solar radiation hitting the BC core. Calculations indicate that the core-shell configuration can enhance light absorption by particles by 50–100% (Bond et al. 2006; Shiraiwa et al. 2008). Laboratory studies indicate enhancements up to a factor of 3 (Cappa et al. 2012, and references in the supplementary material). Field measurements by Lack et al. (2012) of internally mixed BC and OC biomass burning aerosol show that absorption enhancement at a wavelength of 532 nm is on average 38%. Other observations of ambient aerosol (not significantly influenced by biomass burning) show only minimal absorption enhancements due to coating of BC cores (Cappa et al. 2012). Results from measurements made specifically in the Arctic (McNaughton et al. 2011) also show no definitive evidence for an absorption enhancement.

The preceding paragraphs show there are still significant gaps in knowledge concerning the characteristics of atmospheric BC-containing particles, their transformation in the atmosphere and transport to the Arctic. Concerning the characteristics of BC-containing particles in snow and ice, however, even less is known. For example, Schwarz et al. (2013a) found that the size of deposited and processed particles can be larger than in the atmosphere. Also, knowledge about the mobility of these particles is scarce. It has been observed that hydrophobic particles (i.e. BC and mineral dust) can accumulate in surface snow during melt events thus further decreasing the albedo while water soluble ions are flushed out (Sterle et al. 2013).

2.3 Measuring black carbon concentrations

This section provides an overview of methods used to measure BC during field campaigns. Results reported from these measurements are discussed in Ch. 8. Data from monitoring sites are presented in Ch. 9.

2.3.1 Overview of measurement methods

Measurements of BC in the Arctic and in source regions are necessary to characterize BC as it is transformed from a hydrophobic aerosol immediately after emission to an internally mixed, hydrophilic aerosol during transport. Observations of BC also provide the basis for developing, assessing, and improving emission inventories, transport models, and mitigation strategies designed to reduce the warming of the Arctic. The systematic observation of aerosols, including BC, is expanding globally through a host of national and international sampling networks. Parts of the mid-latitude source regions for the Arctic are well monitored, particularly in regions where there are public health concerns. It is anticipated that monitoring in these regions will continue to expand as mitigation policies for both air quality and climate focus on BC. In contrast, there are only a few long-term observations of BC in the Arctic. These are confined to the North American and European sectors of the Arctic and, as a result, do not give a full picture of the distribution of BC across the Arctic. There is also a significant lack of information regarding BC above the surface layer (i.e. throughout the tropospheric column) because long-term monitoring infrastructure in the Arctic is mostly limited to in-situ surface measurements with the exception of few sun-photometer and LIDAR sites. Intensive measurements do not reach high altitudes, are conducted only occasionally, and cover only a limited geographical area and time period.

The existing long-term monitoring observations, along with occasional airborne surveys and short-term intensive field campaigns, have provided information on the sources, transport, and properties of Arctic BC. An overview of monitoring efforts in the Arctic is given in Ch. 9. Intensive field campaigns that have provided snapshot, detailed pictures of the spatial distribution, properties, and transport of BC and co-emitted species to the Arctic include the AGASP (Arctic Gas and Aerosol Sampling Programs) series (e.g. Schnell

1984) which was conducted in the western Arctic in the 1980s, and the many international experiments conducted under the umbrella of POLARCAT (Polar Study using Aircraft, Remote Sensing, Surface Measurements and Models of Climate, Chemistry, Aerosols, and Transport) (Spackman et al. 2010; Law et al. 2014) during the International Polar Year (IPY) in 2008. Beginning in 2009, annual survey flights of the Polar Airborne Measurements and Arctic Regional Climate Model Simulation Project (PAMARCMiP) have been conducted to collect extensive aerosol chemical and microphysical data across the western Arctic (Herber et al. 2012). In addition, the HIAPER Pole to Pole mission (HIPPO) conducted flights in the Arctic in 2009 and 2011 (Schwarz et al. 2013b). An overview graphic for flight tracks is presented in Ch. 8. In addition to the campaigns conducted in the North American and European Arctic, since 2007 several flight campaigns have been conducted over the Russian Arctic (YAK-AEROSIB, https://yak-aerosib.lsce.ipsl.fr).

Over the same span of years (1980s to present), a few studies have been conducted on BC deposited to Arctic snow and ice. In the early 1980s, Clarke and Noone (1985) focused on BC deposited in the western Arctic. Doherty et al. (2010) reported measurements that updated and expanded the initial survey of Clarke and Noone (1985). This more recent study was conducted from 2005 to 2009 with snow collection in Alaska, Canada, Greenland, Svalbard, Norway, Russia, and the Arctic Ocean (Fig. 2.2). Additional measurements were discussed by Doherty et al. (2013). In addition, Forsström et al. (2013) measured the EC content of snow and ice in Scandinavia and the European Arctic (Fig. 2.3). However, while the spatial coverage of the data is broad, the number of samples is low. Furthermore, as the sampling is not synoptic, it is difficult to generalize findings from the campaigns in terms of BC source regions and transport and deposition mechanisms. Figures 2.2 and 2.3 provide an overview of BC and EC at snow measurement sites.

With a few exceptions, reported concentrations of BC in Arctic aerosol and snow are not based on direct measurement of BC. Methods that have been used rely on the measurement of an aerosol property from which it is assumed that BC mass can be inferred (e.g. light absorption or lack of volatility at a given temperature). BC concentrations derived from the different methods can disagree by a factor of seven or more. The different methods and their associated uncertainties are discussed in Sect. 2.3.2 and 2.3.3.

2.3.2 Measuring atmospheric black carbon

2.3.2.1 Measuring light absorption – determining equivalent black carbon

Owing to ease of remote operation, filter-based light absorption has been the most commonly used technique in the Arctic for deriving atmospheric eBC concentrations. In this method, aerosol is collected on a filter and light absorption is calculated from the change in transmission through the filter over time. Filter-based absorption instruments include the Particle Soot Absorption Photometer (PSAP) (Bond et al. 1999; Virkkula

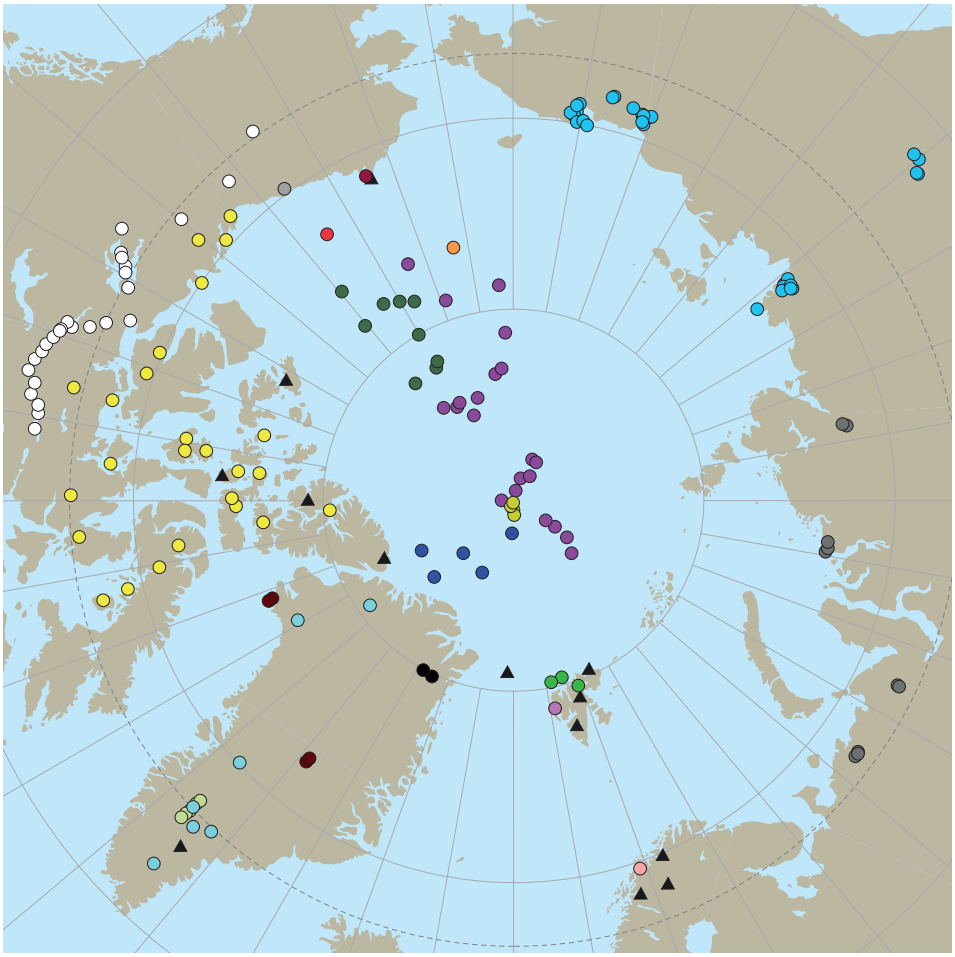

Figure 2.2 Overview of measurement sites across the Arctic for black carbon in snow (adapted from Doherty et al. 2010).

et al. 2005), currently in use at Barrow (Alaska), and the aethalometer (Hansen et al. 1992) which is currently in use at Alert (Canada) and Summit (Greenland) and has been used at Barrow (Alaska). At Zeppelin (Svalbard/Norway), both a PSAP and an aethalometer are currently in use. Filter-based methods yield an aerosol light absorption coefficient that is converted to a BC mass concentration through the use of a mass absorption cross section (MAC). The MAC for BC is defined as the amount of light absorption per unit mass of BC and has units of m^2/g. It is recommended to report the resulting BC concentration (eBC) together with the assumed MAC value as it is not based on a direct measurement of BC (Petzold et al. 2013). Typically, three different types of correction must be made: (i) a multiple scattering correction due to the scattering by filter fibers, (ii) a scattering correction due to particles embedded in the filter, and (iii) a filter-loading correction due to the reduction of the optical path when particles accumulate (Collaud Coen et al. 2010). A further caveat of filter-based methods is that they are sensitive to absorbing and non-absorbing non-BC particles.

The MAC for BC can be derived from simultaneous measurements of light absorption (such as from the PSAP or aethalometer) and EC mass concentration (from methods described in Sect. 2.3.2.2). The MAC for newly emitted BC has a fairly narrow range of 7.5 ± 1.2 m^2/g (Clarke et al. 2004; Bond and Bergstrom 2006). The MAC for aged BC is generally higher and has a much wider range of values (Quinn and Bates 2005) due to the enhancement in absorption for internally mixed aerosol and the presence of non-BC light absorbing species (e.g. OC and dust). If the measured absorption includes absorption by components other than BC (e.g. light-absorbing OC), a MAC value calculated based on assuming that all measured absorption is due to BC will be biased high. In this case, the concentration of eBC based on that MAC value will be biased low. Sharma et al. (2004, 2006) derived winter/spring and summer BC MAC values for Alert (Canada) based on three years of measurements of light absorption with an aethalometer and EC mass concentration using a thermal-optical method (see Sect. 2.3.2.1). The resulting values, 19 m^2/g for winter/spring and 29 m^2/g for summer, were used to calculate BC mass concentrations at Alert (Canada) and Barrow (Alaska). Since long-term uncertainty in the seasonally adjusted MAC values could not be assessed, it was assumed that they were valid for a trend analysis of BC concentrations that covered a span of 13 years. This assumption is not valid if aerosol sources and composition that impact light absorption changed during the 13-year period.

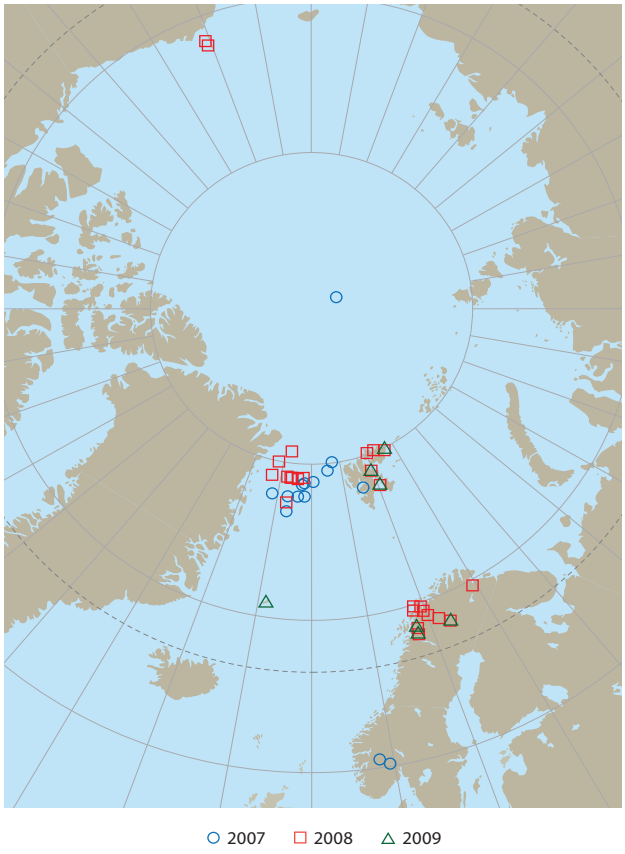

Figure 2.3 Overview of measurement sites in Scandinavia and the European Arctic for elemental carbon in snow and ice (adapted from Forsström et al. 2013).

An additional issue is that filter-based absorption methods can suffer from interferences that result in artificially high light absorption values. If the light transmission is reduced by scattering aerosol that has been collected on the filter, the absorption coefficient will be overestimated (Bond et al. 1999). The empirical schemes available to correct for the influence of scattering, yield accuracies of the PSAP of between 20% and 30% (Bond et al. 1999; Virkkula et al. 2005). However, the correction schemes are based on laboratory-generated aerosols, which may limit their application and accuracy for the measurement of atmospheric aerosols. In addition, PSAP absorption coefficients can be biased high (50–80%) when the ratio of organic aerosol to light-absorbing carbon (LAC) is high (15–20%). Lack et al. (2008) postulated that this high bias was due to the redistribution of liquid-like OC, which affected either light scattering or absorption. Other filter-based techniques, including the aethalometer, may suffer from the same bias. See Collaud Coen et al. (2010) for a detailed discussion of the five common correction algorithms for aethalometer measurements. Overall, BC mass concentrations derived from optical methods can differ by up to a factor of 7 compared to concentrations derived from chemical (thermal-optical) measurements (Petzold et al. 2013). However, in environments with limited effects from forest fires or dust particles, results from laser-induced incandescence, thermal-optical transmittance and filter-based light absorption measurements can be nearly identical (Kondo et al. 2011).

The photoacoustic spectrometer (PAS) is a non-filter based method for measuring aerosol light absorption. It was recently used in the Arctic during several intensive field campaigns associated with POLARCAT. In the PAS (Arnott et al. 1997; Lack et al. 2006), particles are drawn into a cavity and irradiated by laser light. The heat produced when the particles absorb the light is transferred to the surrounding gas creating an increase in pressure. Sensitive microphones are used to detect the standing acoustic wave that results from the pressure change. The detected signal and instrument parameters are used to calculate the absorption coefficient. The overall uncertainty of the PAS with respect to aerosol absorption has been reported at about 5% and the lower detection limit is at 0.08 Mm^{-1} (Lack et al. 2006). The uncertainty of the PAS is low, in part, because it is not subject to the sampling artifacts associated with collecting aerosol on a filter. However, the PAS is sensitive to non-BC absorbing aerosol and operates best only in dry conditions. At present the PAS is too expensive for routine deployment at multiple monitoring sites.

Briefly, in addition to in-situ measurements, absorption due to aerosol over the tropospheric column can be determined by remote sensing. A recent review focusing on the polar regions was undertaken by Tomasi et al. (2015). In the Arctic, 12 stations form part of the POLAR-AOD and AERONET programs measuring aerosol optical depth (AOD) at eight or more wavelengths roughly between 0.3 and 1.6 μm with sun photometers looking at the aerosol optical thickness throughout the atmospheric vertical column (Tomasi et al. 2007, 2015; von Hardenberg et al. 2012). Currently, absorption AOD measurements by sun photometers are the only constraint available for estimates of global radiative forcing by BC. However, in a recent closure study Koike et al. (2014) found systematic discrepancies in the BC column absorption inferred from sun photometer and Single Particle Soot Photometer (SP2) measurements. For example, the presence of mineral dust can impact results significantly.

Several other remote sensing instruments are also operated in the Arctic (e.g. Lund Myhre et al. 2007) such as Light Detection and Ranging (LIDAR) instruments that provide vertically resolved information about aerosol layers based on their backscatter signals. Further observations of AOD are made by satellite mounted instruments such as the Moderate Resolution Imaging Spectroradiometer (MODIS) or the Medium Resolution Imaging Spectometer (MERIS). However, data coverage is low compared to other regions and less accurate compared to ground-based measurements because difficulties arise from high surface albedo, high cloud cover and a large solar zenith angle causing a long path through the atmosphere (Lund Myhre et al. 2007). In addition, these remote sensing techniques are generally not BC-specific.

2.3.2.2 Measuring mass – determining elemental carbon and refractory black carbon

In many monitoring networks, BC mass concentrations are determined via thermal-optical methods by collecting aerosol on a filter and then heating the filter and measuring evolved CO_2 to discriminate between organic (volatile) and elemental (non-volatile) carbon (OC and EC). Elemental carbon is defined as the non-volatile or refractory portion of the total carbon (TC = OC + EC) measured. Frequently, the sample filter is first heated in an inert gas to volatilize OC, cooled, and then heated again with oxygen to combust the EC (Chow et al. 1993; Birch and Cary 1996). A complication is 'charring' of OC at high temperatures, which reduces its volatility and causes it to become an artifact in the EC/OC determination. Variations of this method include different temperature ramping schemes, and correcting for the charring of OC during pyrolysis by monitoring the optical reflectance (Huntzicker et al. 1982) or light transmission (Turpin et al. 1990). Comparisons between different thermal evolution protocols reveal that EC concentrations can differ by more than an order of magnitude (Schmid et al. 2001), and that much of this difference is caused by the lack of correction for charring, which leads to considerable overestimates of EC. In addition, there are significant differences in EC concentrations depending on the method used to correct for charring (Chow et al. 2004). Methods are comparable if the filter contains a shallow surface deposit of EC or if OC is uniformly distributed through the filter. If EC and OC both exist at the surface and are distributed throughout the filter, the different corrections yield different concentrations of EC. Hence, the level of agreement depends, in part, on the OC/EC ratio in the sample. As a result, the different correction schemes yield similar results for diesel exhaust, which is dominated by EC, but can differ widely for complex atmospheric mixtures that contain larger amounts of OC.

The SP2 is a newly developed instrument that is used to quantify refractory BC mass (rBC; the mass remaining after heating to ~3500 K) and optical size of individual rBC cores in a general diameter size range of 90 to 600 nm (Schwarz et al. 2006, 2008). The size range actually covered, however, depends strongly on how the instrument is operated (Laborde et al. 2012). The SP2 is currently the only instrument which can measure rBC mass more or less directly. In addition, the instrument is able to detect coatings on rBC-containing aerosol and the thickness of the coatings. The SP2 was used on several platforms involved in the recent POLARCAT and PAMARCMiP campaigns. Internal mixtures with rBC cores are identified by the laser light that is scattered as the particle is heated. Uncertainty associated with rBC mass loadings for the size range covered by the SP2 (roughly greater than 90% of the accumulation mode rBC) has been reported at 25% (Schwarz et al. 2006) and 10% during PAMARCMiP (Stone et al. 2010). Under laboratory conditions, for example in the AIDA chamber in Karlsruhe (Germany), the reproducibility of mass and size distributions of BC cores derived with the SP2 agreed within ±5% and ±10%, respectively, between different SP2s, with larger deviations in the range below 1 fg rBC (Laborde et al. 2012). However, the SP2 may provide only a poor constraint on rBC number. It is also relatively new, expensive, not suited for long-term remote operation, and a major caveat is the lower cut-off size.

2.3.3 Measuring black carbon in snow

Samples collected from the snow surface can be analyzed to characterize recent BC deposition events and from lower layers to characterize BC deposition that occurred throughout the winter and spring. Collected snow is melted and, depending on the analytical method, either analyzed directly or filtered, with the analysis performed on the BC-containing particles collected on the filter. When filtering, care must be taken not to lose BC to the walls of the filtering apparatus or through the filter (Doherty et al. 2010). Methods used for the measurement of atmospheric BC absorption and mass concentration may also be used for the quantification of snow BC.

Snowmelt that has been filtered through a quartz fiber filter can be analyzed with the thermal-optical techniques described in Sect. 2.3.2.1 for the determination of EC. However, it has been shown that a significant fraction of snowmelt EC will pass through a quartz fiber filter upon filtration (Hadley et al. 2010; Lim et al. 2014). If this method is to be used, the collection efficiency of the filters should first be tested and quantified. In addition, Forsström et al. (2013) found that the temperature protocol used by the European Supersites for Atmospheric Aerosol Research (EUSAAR2) gives, on average, EC concentrations that are double those of the National Institute for Occupational Safety and Health (NIOSH)-5040 method. Also, there are practical limitations. For example, the particle loading on the filters can be heterogeneous so that the

result of the analysis depends on the filter section chosen. In addition, large pieces of organic material such as bits of leaf or twig can interfere significantly with the thermo-optical method due to potential charring. Also, carbonates are a source of uncertainty (e.g. Ming et al. 2009) as well as pyrolized OC (Lim et al. 2014). Alternatively, an SP2 (described in Sect. 2.3.2.2) can be used to directly measure the BC mass concentration and size distribution in snowmelt (Schwarz et al. 2012, 2013a). The SP2 measurement of BC in snow has a higher uncertainty (60%) than the measurement of BC in atmospheric aerosol (10–25% for the Arctic). This is due to uncertainties related to aerosol nebulization from snow melt and the larger size of BC particles in snow than in aerosol. Careful assessment of the size dependence of the nebulization efficiency is needed as well as careful choice of the calibration material (Wendl et al. 2014). Most suitable is the jet nebulizer APEX-Q with a 75±7% efficiency (Lim et al. 2014) as nebulization is least size dependent between 10 and 1000 nm. For studies that did not take this factor into account larger uncertainties are expected (Schwarz et al. 2012). It is also possible that BC particles attached to larger particles such as mineral dust will have a lower passing efficiency or will not pass at all into the SP2. Furthermore, sample storage influences the measured concentrations. It is recommended to keep the samples frozen in polypropylene vials, to sonicate them for 25 minutes before analysis, and not to refreeze them (Wendl et al. 2014).

As with the quantification of BC in the atmosphere, the absorption due to BC in snow can be determined and converted to a mass concentration. This method was used in the pan-Arctic survey of snow eBC concentrations reported by Doherty et al. (2010). After filtering snowmelt through a Nuclepore filter, Doherty et al. (2010, 2013) used an Integrating Sphere/Integrating Sandwich Spectrometer (ISSW; Grenfell et al. 2011) to quantify light-absorbing aerosol collected on the filter (note that the collection efficiency of the filter needs to be taken into account). Spectrally resolved absorption is measured over the 300–750 or 400–750 nm wavelength range and used to discriminate between eBC and other light-absorbing species (e.g. dust and organics) for which an ångström exponent is assumed. An assumed MAC value is then used to derive an eBC mass concentration from the measured absorption (Grenfell et al. 2011).

2.4 Co-emitted species: Sources and implications for aerosol chemical composition

Shortly after emission, BC exists predominantly as internally mixed aerosol in the atmosphere. The chemical composition of this BC-containing aerosol is largely dependent on the species co-emitted during the combustion process, which, in turn, depends on the emission source. Generally, BC is emitted with other particulates such as primary organic aerosol (POA), ammonium salts and potassium, and gas phase species including sulfur dioxide (SO_2), nitrogen oxides (NO_X), carbon monoxide (CO), and a variety of volatile, gas phase organic compounds that are precursors to secondary organic aerosol. Cloud processing can also affect aerosol composition. In addition, encounters with other air masses during transport away from the source region can affect the chemical composition of the particles. The chemical composition and size of the BC-containing particles affect the way in which they age, including their degree of hygroscopicity, their ability to nucleate cloud droplets, and their absorption and scattering of solar radiation. The properties acquired during the aging process determine the atmospheric lifetime of the BC-containing aerosol.

Large dust particles are occasionally observed in biomass burning plumes (Dahlkötter et al. 2014). Globally, open burning is the most significant source of BC and can be a significant source of Arctic aerosol (Warneke et al. 2009). It has the highest POA to BC ratio – roughly 10:1 for forest, grass and woodlands (Bond et al. 2013). The SO_2:BC emission ratio for open burning is typically <1 (Bond et al. 2013). Ambient biomass burning aerosol in the Arctic is characterized by a ratio of SO_4:OC of <0.5 (Brock et al. 2011; McNaughton et al. 2011; Schmale et al. 2011). Next, in amount of total global BC emissions, is residential solid fuel burning, which is more important in the Arctic context than open burning (AMAP 2011). It has a high POA:BC ratio for biofuels and a relatively higher SO_2:BC emissions ratio – on the order of 10 for coal. Anthropogenic emissions from transport and specifically diesel engines, the third largest source of BC globally, exhibit the lowest ratio of co-emitted species to BC (Bond et al. 2013). This sector is also a significant source for the burden of BC in the Arctic (AMAP 2011). Direct measurements of BC-containing aerosol coming from anthropogenic fossil fuel burning showed an average OC:BC ratio of roughly 17 and an SO_4:BC ratio of roughly 24 during the ARCTAS campaign in 2008 (Brock et al. 2011). The OC:BC ratios in the Brock et al. (2011) measurements of ambient aerosol in the Arctic are probably much higher than those reported by Bond et al. (2013) for emissions from the same source types because of the effects of aging on the aerosols during their transport from the source to the Arctic. Emissions from oil and gas flaring that are probably particularly important for the Arctic (Stohl et al. 2013) are not well characterized.

More detailed information on emissions of BC and co-emitted species from different source regions and sectors is provided in Ch. 5. The impacts of co-emitted species on BC forcing mechanisms in both the atmosphere and snow/ice covered surfaces is given in Ch. 4. Generally, the total climate forcing of BC and co-emitted species as derived by Bond et al. (2013) is slightly negative with -0.06 W/m^2, but uncertainties are large.

2.5 Recommendations

Given the systematic biases associated with the BC measurement techniques in current use and that the measured BC concentrations can vary by up to a factor of seven depending on the approach used (Petzold et al. 2013), an Arctic in-field inter-comparison of methods is recommended. This should include as a minimum the suite of currently used BC and EC measurement methods outlined in Sect. 2.3.2 (i.e. aethalometer, PSAP, SP2 and different protocols for EC determination) and the parameters outlined in Table 2.1. As well as leading to uncertainties in ambient BC concentrations, the discrepancies can also make it difficult to use the monitoring data for identifying model biases when the spread among model results is low.

Against this background, the determination of a BC monitoring method for use in the Arctic should be a careful choice and one that considers ongoing efforts to establish harmonized BC measurements within the European Union, ongoing discussions within the International Marine Organization, and methods that are in use already for long-term Arctic datasets and worldwide datasets based on the GAW station network under the World Meteorological Organization. The reported data and metadata should follow the format shown in Table 2.1 based on Petzold et al. (2013), where the reported value (e.g. EC, eBC, rBC) and measurement method is given. The size range from which the BC was determined and deviations of the method used from other BC measurement methods should be provided if available.

3. Tropospheric ozone in the Arctic

Lead authors: Kathy Law, Steve Arnold
Authors: Joakim Langner, Ulrik Korsholm

3.1 Introduction

This chapter discusses the sources and sinks of ozone (O_3) in the Arctic troposphere, observed distributions and measurement techniques, and the origins of tropospheric O_3 in the Arctic. Information on the Arctic distributions of O_3 and its precursors from surface, ship and aircraft observations is summarized, together with information on vertical distributions from ozonesondes. Current knowledge about the key sources of Arctic O_3 at different times of the year is also discussed, based on observations and modeling studies.

Tropospheric O_3 is a secondary pollutant produced from the oxidation of carbon monoxide (CO), volatile organic compounds (VOCs) and methane (CH_4) in the presence of nitrogen oxides (NO_X) and solar radiation. At the surface, tropospheric O_3 is harmful to human health (Levy et al. 2001) and vegetation (Sitch et al. 2007), and in the mid and upper troposphere it acts as a greenhouse gas (Myhre et al. 2013b). Ozone also affects climate indirectly, as the chief precursor of the hydroxyl radical (OH), which determines the atmospheric lifetimes of potent greenhouse gases such as CH_4 (Levy 1971). In addition, increases in CH_4 emissions suppress OH, increasing CH_4 lifetime and leading to further increases in CH_4 concentration. This positive chemical feedback is estimated to increase atmospheric CH_4 concentrations by a factor of approximately 1.4 (range 1.3–1.7) for the present day (Prather et al. 2001).

Growth in anthropogenic emissions of O_3 precursors since pre-industrial times (i.e. increased emissions of CH_4, NO_X, CO and VOCs) has led to an increase in tropospheric O_3 throughout the northern hemisphere (e.g. Parrish et al. 2012b). This increase in tropospheric O_3 has contributed to the observed increase in global temperature over the past century (e.g. Stevenson et al. 2013) and is likely to have made an important contribution to the Arctic warming observed over this period (Shindell 2007; Shindell et al. 2006; see also Ch. 4).

The photochemical lifetime of O_3 in the free troposphere (weeks to months) means that O_3 can be transported between continents, including from mid-latitude source regions to the Arctic. Consequently, changes in O_3 precursor emissions from mid-latitude sources can affect the Arctic O_3 burden directly. Nevertheless, the O_3 lifetime is sufficiently short that O_3 is not well mixed in the troposphere. As a result, its impacts on air quality and climate are highly non-uniform, and dependent on interactions between chemical processing and atmospheric transport downstream of precursor emission regions. Background concentrations of surface O_3 in the northern hemisphere are in the range 35–40 ppbv, while observed surface abundances can be as low as 10 ppbv over remote tropical marine regions increasing to more than 100 ppbv downwind of large emission regions (Prather et al. 2001; Royal Society 2008). Ozone concentrations also increase with altitude due to the increasing influence of the stratosphere.

3.2 Sources and sinks

Downward transport of O_3 from the stratosphere is a substantial direct source of O_3 to the troposphere (Shapiro et al. 1987). However, O_3 is also produced photochemically from anthropogenic and natural precursor emissions. The main processes influencing Arctic tropospheric O_3 are shown schematically in Fig. 3.1.

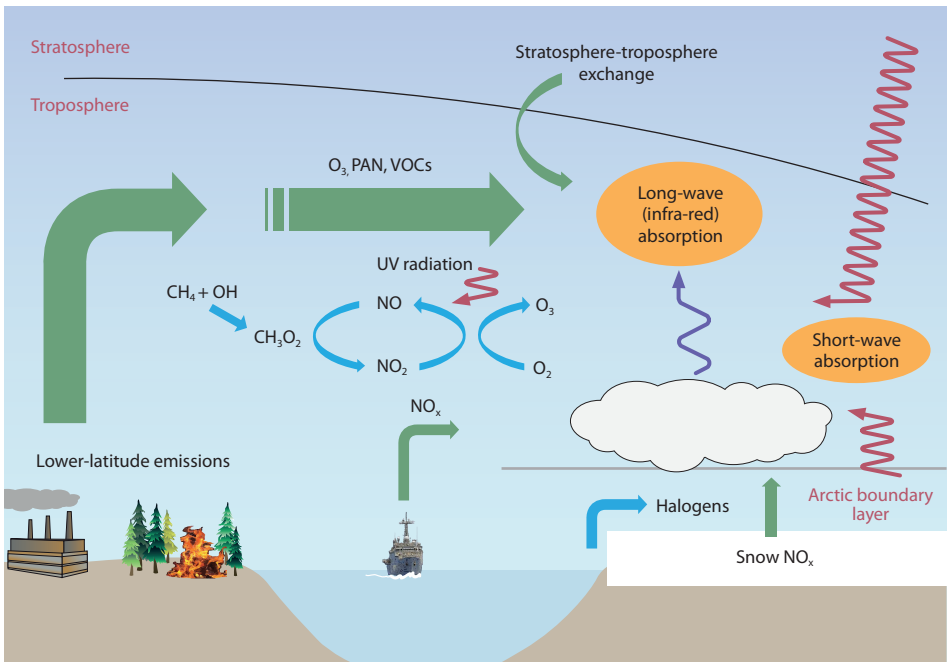

Figure 3.1 Schematic illustration of processes influencing tropospheric ozone in the Arctic, and its long- and shortwave ozone radiative impacts.

Methane oxidation leads to the production of O_3 in the presence of sufficient NO_X and it has been estimated that anthropogenic CH_4 emissions may be responsible for about half of pre-industrial to present-day O_3 radiative forcing (Stevenson et al. 2013) as well as about half of the projected future surface O_3 increases (Prather et al. 2003). CH_4 oxidation contributes to background O_3 away from emission regions, such as in the Arctic and may be responsible for a significant proportion of the positive trends in O_3 concentrations observed in the northern hemisphere over the past decades (Parrish et al. 2012b). Fiore et al. (2009) estimated that a 20% reduction in anthropogenic CH_4 emissions would lead to about a 1 ppbv decrease in tropospheric O_3, comparable to combined reductions in NO_X, CO, and VOC emissions. However, although reduced NO_X emissions lead to decreased O_3 levels, they also lead to decreased OH concentrations and therefore increased CH_4, thus offsetting the climate benefit of decreased O_3 (West et al. 2007).

Anthropogenic sources of NO_X result from high temperature combustion of fossil fuels, and include emissions from motor vehicles, power generation, and shipping. Combustion, natural gas transport and solvent use, as well as natural sources from vegetation, are sources of VOCs. Biomass burning (natural forest fires and agricultural fires) is a large global source of NO_X, CO and VOCs (Jaffe and Widger 2012). The biomass burning NO_X source is estimated at around 6 TgN/y globally (compared with ~34 Tg/y globally from anthropogenic sources) (e.g. Emmons et al. 2014). Soils and lightning are substantial natural sources of NO_X. Increased local anthropogenic emissions, such as those from shipping, may impact Arctic regional air quality and climate in the future (Granier et al. 2006; Dalsøren et al. 2013). NO_X emissions from snow may be important over snowpacks (e.g. Dibb et al. 2002).

Since O_3 and its precursors are generally less soluble than aerosols, they are not removed efficiently during frontal export from mid-latitudes to the Arctic. Consequently, transport pathways that import air masses above the Arctic dome from warmer regions such as North America and eastern Asia (described in detail in Ch. 6) have the potential to bring enhancements in O_3 and precursors to the Arctic free troposphere. In addition, peroxyacetyl nitrate (PAN), produced by the oxidation of anthropogenic and natural VOCs is stable in air masses which have been exported into the cold mid- and upper-troposphere (Singh and Hanst 1981), where it has an increased lifetime. PAN acts as a reservoir for nitrogen dioxide (NO_2), which can be re-released during PAN decomposition at higher temperatures during, for example, the Arctic summer, when it can make a significant contribution to local O_3 production (Walker et al. 2012). Other NO_X reservoirs (nitric acid, HNO_3; peroxynitric acid, HNO_4) may also contribute to Arctic O_3 production.

Ozone is destroyed by photochemistry and by dry deposition to the Earth's surface. Photochemical O_3 loss chiefly involves O_3 photolysis in the presence of water vapor or direct reaction of O_3 with hydroxy radicals (HO_2 or OH). Photochemical destruction involving the hydroperoxyl radical (HO_2) may be particularly important in the Arctic where water vapor abundances are low (Arnold et al. 2014). Dry deposition of O_3 and its precursors to ice and ocean surfaces is slower than to vegetated terrestrial surfaces at lower latitudes. The combination of suppressed dry deposition and low water vapor contribute to an enhanced tropospheric O_3 lifetime in the Arctic.

Tropospheric O_3 is also destroyed by reaction with halogens in the Arctic, since this region is a rich source of atmospheric halogen species. During Arctic spring, it is well documented that photochemical cycling of halogens in so-called 'bromine explosion' events leads to rapid depletion of surface O_3 (Barrie et al. 1988; Simpson et al. 2007). Such events are considered to be the cause of periods of near zero surface O_3 over most of the Arctic Ocean in spring (Bottenheim et al. 2009). In contrast, Thomas et al. (2012) estimated that the combined effects of snowpack NO_X and bromine destruction could lead to positive net O_3 production at Summit (Greenland) in summer. As Arctic sea ice continues to thin and decline in a warming climate, future fluxes of halogens to the Arctic boundary layer may be enhanced, with possible impacts on Arctic O_3 that are not currently well understood.

3.3 Observed distributions and measurement techniques

Observations of surface O_3 in the Arctic that can be used to analyse seasonal cycles and trends are limited to a few locations (e.g. Oltmans and Levy 1994). Concentrations are reported to the World Data Centre for Greenhouse Gases (WDCGG; http://ds.data.jma.go.jp/gmd/wdcgg) and also to the International Arctic Systems for Observing the Atmosphere (IASOA; http://www.esrl.noaa.gov/psd/iasoa/home2). The data are used to evaluate the ability of AMAP models to simulate seasonal cycles in O_3 (see Ch. 8, Fig. 8.1).

Surface O_3 is generally measured using optical methods where air samples are continuously drawn through a UV-lamp chamber. Such detectors typically measure surface O_3 in the range 0–100 ppb. Other versions of this instrument are based on the chemiluminescence of O_3 and nitrogen oxide (NO). The accuracy of the measurements varies depending on the degree of interference from other compounds such as VOCs. Williams et al. (2006) showed that interferences are small for measurements based on UV absorption even in areas with significant concentrations of potentially interfering VOCs.

Observed monthly mean O_3 concentrations vary between 10 and 50 ppbv at the surface in the Arctic with seasonal cycles exhibiting different behaviors at different locations, driven by both remote and local processes (Fig. 3.2; Hirdman et al. 2010b). Sites in proximity to the Arctic Ocean, such as Barrow (Alaska) and Alert (Canada), show evidence of halogen-influenced depletion during spring leading to very low or even near-zero O_3 concentrations close to the surface. Other sites, such as Zeppelin (Svalbard), exhibit a spring maximum. This is due to O_3 formation from precursors accumulated in Arctic Haze in the lower and middle tropopshere at this time of year (Emmons et al. 2003). Summit (Greenland) is at a higher elevation (3 km) and has a late-spring / early-summer O_3 maximum, which is likely to be due to transport of anthropogenic and boreal air masses, primarily from North America, although local snow NO_X emissions (Thomas et al. 2012) or transport from the stratosphere could also play a role (Dibb et al. 2002).

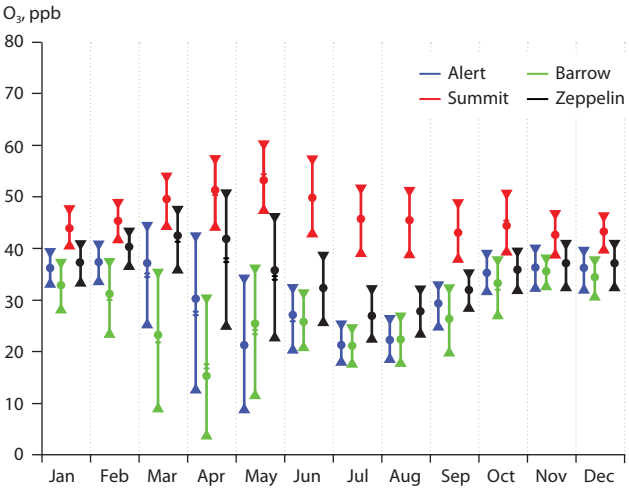

Figure 3.2 Observed seasonal cycles of ozone (O_3) at four atmospheric monitoring sites in the Arctic. Relative position of bars within month does not reflect date of sampling. Source: after Hirdman et al. (2010b).

Information on the distribution of surface O_3 over the Arctic Ocean is sparse, although there have been ship-borne field campaigns in both spring and summer (Bottenheim et al. 2009; Jacobi et al. 2010; Sommar et al. 2010). Observations from the springtime Arctic Ocean suggest surface tropospheric O_3 concentrations are often very low (<5ppbv), increasing sporadically as low pressure systems transport O_3-rich air from mid-latitudes into the Arctic basin (Jacobi et al. 2010). Mean O_3 concentrations in the summertime Arctic marine boundary layer were observed to be around 20 ppbv in July and August 2005 (Sommar et al. 2010), increasing and becoming more variable in September. Low marine springtime O_3 concentrations probably result from widespread destruction by halogens, while increased efficiency of O_3 dry deposition to the ocean surface as sea ice retreats may also contribute to low summertime concentrations.

Continuous measurements of O_3 precursors are available at a few Arctic surface sites. To date, model evaluations have largely focused on comparison with CO data (generally measured in flask samples by gas chromatography; Novelli et al. 1998). Several surface stations provide continuous CO observations (see Ch. 8, Table 8.1). Long-term records of O_3 precursors are generally not available except in northern Scandinavia, and tend not to be continuous. Weekly observations of some VOCs covering annual cycles are available at Summit (Greenland), Barrow (Alaska) and Alert (Canada) from the NOAA Global Monitoring Division/ INSTAAR network of surface sites (Helmig et al. 2009).

Ozone soundings provide a long-term record of Arctic O_3 through the depth of the troposphere. The measurements are mainly conducted using the balloon-borne Electrochemical Concentration Cell (ECC) ozonesonde, reaching an altitude of about 30 km. The overall precision of the technique is estimated at 3–5% while the accuracy is about 10% (e.g. Liu et al. 2009). An example of the vertical O_3 distribution measured over several years at Ittoqqortoormiit (Scoresbysund) in eastern Greenland is given in Fig. 3.3. Elevated concentrations in the upper troposphere show that O_3 near Ittoqqortoormiit (Scoresbysund) are regularly controlled by O_3-rich air transported downwards from the lower stratosphere. This occurs during tropopause folding events which are common in the Arctic on the flanks of low pressure systems and which result in mixing between stratospheric and tropospheric air masses (Shapiro et al. 1987). This stratospheric influence, which is stronger during spring, occasionally penetrates deeper into the troposphere and sometimes as low as 400 hPa. However, based on the analysis of aircraft data, the stratospheric influence is mainly limited to the upper troposphere and does not penetrate to lower altitudes where photochemistry is the main driver of enhanced O_3 (Emmons et al. 2003; Wespes et al. 2012).

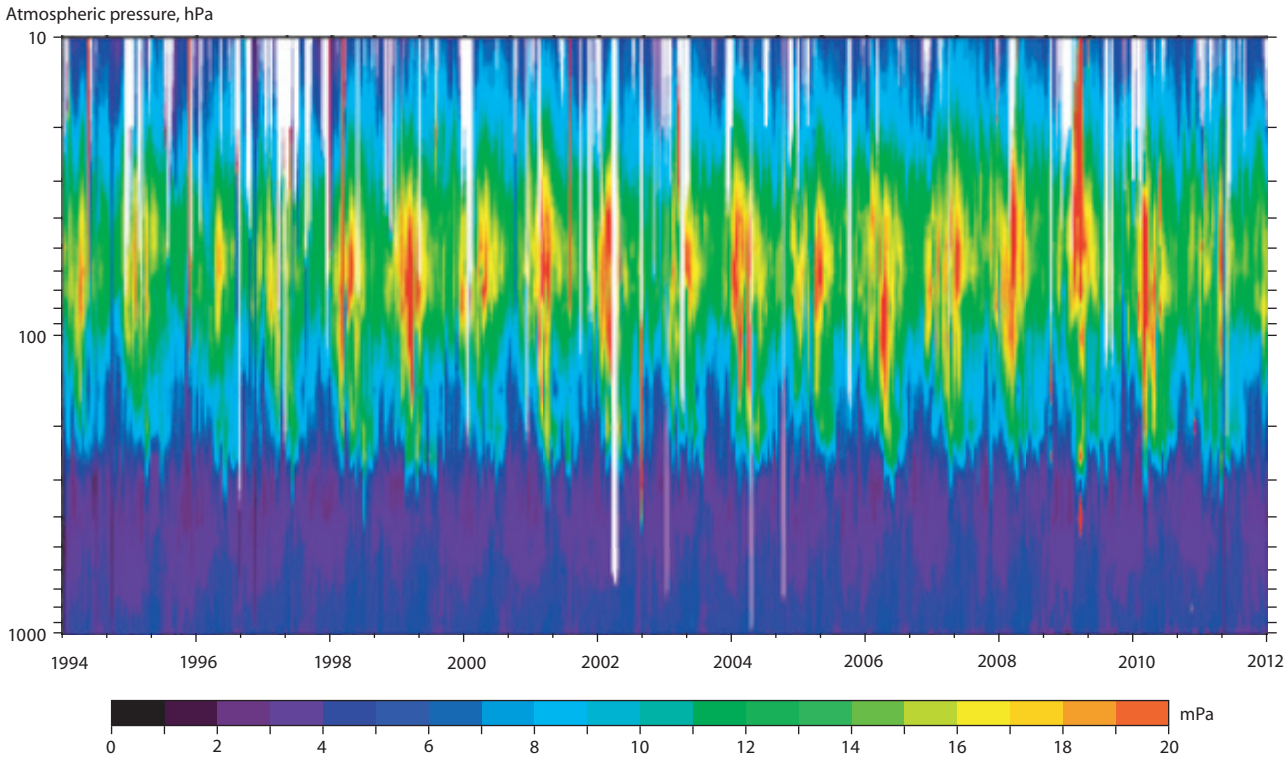

Figure 3.3 Pressure–time slice of three years of weekly ozone (O_3) partial pressure (mPa) vertical soundings at Ittoqqortoormiit (Scoresbysund) in eastern Greenland (70.48°N, 21.95°W). Source: Danish Meteorological Institute.

During spring and summer 2008, the POLARCAT (Polar Study using Aircraft, Remote Sensing, Surface Measurements and Models, of Climate, Chemistry, Aerosols, and Transport) aircraft missions provided new information on the vertical distribution of O_3 and its precursors in the Arctic free troposphere (Law et al. 2014). Observed O_3 mixing ratios showed a compact vertical distribution with higher concentrations observed during summer in the mid-upper troposphere. Concentrations ranged from <40 ppbv in the boundary layer to 60–80 ppbv between 5 and 8 km. Higher O_3 concentrations in the upper troposphere, particularly in spring, were attributable to the greater stratospheric influence at this time of year, in agreement with the ozonesonde observations discussed earlier. Aircraft observations collected during POLARCAT showed elevated PAN and CO concentrations in air masses transported from Asian and North American anthropogenic emission regions in summer 2008 (Law et al. 2014, and references therein).

3.4 Origins of Arctic tropospheric ozone

Several studies have quantified the contribution of different mid-latitude emission regions to Arctic tropospheric O_3 and its precursors. European emissions make an important contribution during winter especially in the lower troposphere (Shindell et al. 2008). However, at this time of year, strong titration (O_3 removal) due to high NO_X concentrations leads to import of air masses with lower O_3 (Hirdman et al. 2010b). Emissions from Asia and North America are important sources of Arctic O_3 in spring in the free troposphere together with stratospheric injection, although relative contributions vary between studies and years (e.g. Shindell et al. 2008; Wespes et al. 2012). The polar dome in winter (see Ch. 6) means that the influence of stratospheric air masses on O_3 and nitrogen-containing species (e.g. HNO_3) near the Arctic surface is marginal (Stohl 2006; Wespes et al. 2012).

During summer, local photochemical O_3 production from PAN exported from mid-latitude anthropogenic emission sources has been identified as an important source of Arctic tropospheric O_3 (Walker et al. 2012). Wespes et al. (2012) showed that anthropogenic contributions to Arctic tropospheric O_3 varied between ~60% and ~40% from the surface to the upper troposphere in summer, based on calculations with the MOZART-4 model. According to this study, Asian sources dominate the anthropogenic contribution to the Arctic upper troposphere, while European and North American sources dominate the lower troposphere at this time of year.

Owing to their proximity to the Arctic, boreal forest fires and agricultural fires during spring and summer are also an important source of O_3 precursors including PAN, which are transported efficiently to high latitudes (Singh et al. 2010; Brock et al. 2011). While little O_3 production appears to occur close to boreal fires (Alvarado et al. 2010; Paris et al. 2010), several recent studies have shown O_3 production downwind from boreal fires in the Arctic during summer (Parrington et al. 2012; Wespes et al. 2012; Thomas et al. 2013) when photochemistry is most active. Wespes et al. (2012) estimated that during summer 2008, the contribution to O_3 from fires varied between 5% in the upper troposphere to 22% near the surface. Arnold et al. (2014) demonstrated that a suite of global chemical transport models, run using the same specified emissions, all showed net chemical O_3 production in Arctic air dominated by fire emissions. This study also showed that Arctic O_3 production efficiency is likely to be sensitive to model organic chemistry, due to the importance of PAN as an NO_X reservoir in these air masses. Nevertheless, simulated O_3 production is generally higher in air masses influenced by anthropogenic emissions compared to those influenced by fires (Thomas et al. 2013), although relative contributions vary significantly between studies.

Source contributions to ozone radiative forcing in the Arctic are highly sensitive to the altitude at which a particular source perturbs the O_3 profile. The vertical stratification of O_3 responses to different mid-latitude emission regions implies that different sources and regions will contribute radiative impacts of differing magnitude. Radiative forcing responses to emission perturbations in different regions are dependent on both modeled source attribution (i.e. how much of a regional emission reaches the Arctic) as well as simulated photochemical O_3 production sensitivities to emissions from different regions. Forcing due to changes in Arctic surface O_3 may be most sensitive to European or local sources, whereas emissions from North American and Asian sources are more important in the mid- and upper troposphere (see Ch. 10).

3.5 Conclusions

- Long-term surface datasets are available that allow characterization of the seasonal cycles in O_3 and certain precursors, notably CO, in the European and North American Arctic.
- Springtime surface O_3 observations at sea-level coastal sites show strong influences of halogen chemistry, producing periods of very low surface O_3 abundances.
- Limited information is available on O_3 and its precursors in the free troposphere. Ozonesondes, located primarily in the western Arctic, provide an important record of regular O_3 vertical profiles in the high latitude northern hemisphere.
- New aircraft observations have recently allowed a more detailed picture of processes controlling Arctic O_3 away from the surface in the mid- and upper-troposphere, where it is more important for longwave climate forcing.
- Model studies suggest that O_3 is most sensitive to lower latitude emission sources from Asia and North America in the mid- and upper-troposphere, and to European sources in the lower troposphere.
- Observations indicate transport of polluted air from mid-latitude emission regions containing O_3 precursors, such as CO. Observations also indicate NO_X reservoir species, notably PAN, that are important for in-situ photochemical production of O_3 in the Arctic.
- Boreal fires may play a role in producing O_3 and PAN in the summertime Arctic troposphere.

4. Climate forcing mechanisms and timescales

Lead authors: Mark Flanner, Terje Berntsen

4.1 Introduction

This chapter provides a brief introduction to the mechanisms through which short-lived climate forcers (SLCFs) such as black carbon (BC) and ozone (O_3) alter the Earth's radiation budget and influence Arctic climate. It also describes the unique timescales over which SLCFs influence climate, along with metrics that can be applied to describe climate impacts on different timescales. Quantitative descriptions of radiative forcing estimates from previous literature are provided in Ch. 10, and new model results produced for this study are described in Ch. 11.

4.2 Black carbon and co-emitted species

Black carbon influences Arctic climate through several mechanisms, including direct heating of the Arctic atmosphere, darkening and increased melting of Arctic snow and sea-ice surfaces, alteration of Arctic cloud shortwave and longwave properties, and perturbation of the poleward heat flux through forcing exerted outside the Arctic. These mechanisms were described in detail by AMAP (2011). Research conducted since then has enhanced understanding of: Arctic climate impacts from BC forcing exerted outside the Arctic; the importance of the vertical distribution of Arctic atmospheric BC for its impact on local temperature change; mechanisms governing transport of BC to the Arctic and the relative importance of different sources; and the climate impacts of species co-emitted with BC.

Climate simulations by Shindell and Faluvegi (2009) showed that Arctic climate may cool in response to Arctic atmospheric BC. This counterintuitive result was due to atmospheric heating from BC being counteracted by surface dimming within the Arctic and reduced poleward heat flux into the Arctic, which in turn, is caused by a weakened latitudinal temperature gradient from BC heating of the upper troposphere. This finding motivated additional studies by Sand et al. (2013a,b) and Flanner (2013), who conducted a variety of idealized climate simulations to evaluate the robustness of this result. Sand et al. (2013a) and Flanner (2013) both found that simulated distributions of Arctic atmospheric BC, originating from all global sources and allowed to operate only within the Arctic, cool the Arctic surface (Fig. 4.1). This cooling occurs despite a positive top-of-atmosphere radiative forcing from Arctic BC. In these two studies, the concentrations of BC within the Arctic were scaled up by factors of ten and two, respectively, to achieve a substantial signal, and co-emitted species were left unchanged.

Flanner (2013) found that the surface temperature response to Arctic atmospheric BC is highly sensitive to its vertical distribution. BC above about 430 hPa cools the Arctic surface, while BC in the lower troposphere and boundary layer causes very strong surface warming (Fig. 4.2). In addition to the reasons for surface cooling mentioned above, higher-altitude BC increases cloud cover beneath the location of atmospheric heating, via the 'semi-direct' cloud effect associated with increased stability (e.g. Johnson et al. 2004; Hansen et al. 2005), helping cool the Arctic surface during summer. Low-altitude BC, on the other hand, causes very strong surface warming by depositing energy near the surface, 'burning off' low-level clouds, and decreasing atmospheric stability, all of which trigger the snow- and ice-albedo feedback that amplifies surface warming (Flanner 2013). The unusual phenomenon of surface cooling resulting from atmospheric light absorption occurs more readily in the Arctic because of the frequent occurrence of surface temperature inversions and the general persistence of stable atmospheric conditions, which serve to dynamically decouple the surface from the higher parts of the troposphere. The effect would be less pronounced in other regions where convection mixes the troposphere more thoroughly, although nuclear winter simulations have demonstrated that stratospheric soot cools the global surface (e.g. Robock et al. 2007).

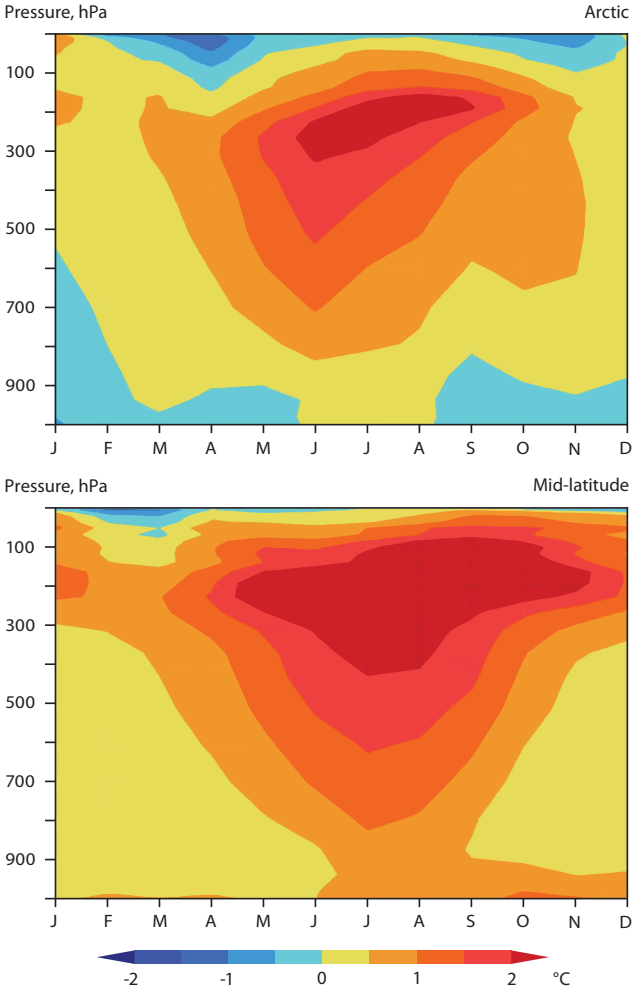

Figure 4.1 Idealized simulations by Sand et al. (2013a) showing Arctic (60° – 90°N) temperature change in response to (upper) within-Arctic atmospheric black carbon (BC) originating from all global sources and (lower) mid-latitude (28° – 60°N) atmospheric BC, also simulated with all global sources. To obtain a significant climate signal, the BC distributions were scaled up by a factor of ten in each experiment.

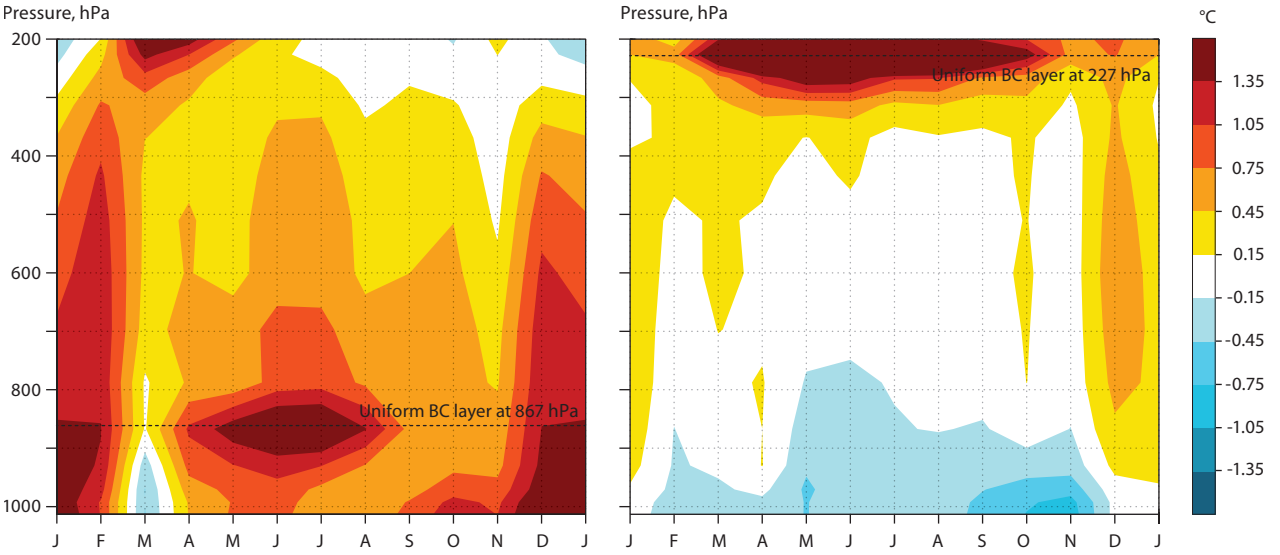

Figure 4.2 Idealized simulations by Flanner (2013) showing the Arctic equilibrium temperature response to uniform layers of black carbon (BC) in the Arctic atmosphere located at (left) 867 hPa and (right) 227 hPa. The mass of BC imposed in each experiment was identical (0.4 mg/m^2), corresponding to a uniform absorption optical depth of 0.005 in the visible spectrum.

Black carbon operating exclusively within Arctic snow and sea ice also causes strong mass-normalized warming because it directly induces albedo feedback. Flanner (2013) found that the Arctic climate sensitivity to local forcing by BC in snow and sea ice is around 1.4 °C per W/m^2, indicating that it is important to consider this contribution when quantifying climate impacts of Arctic BC. In fact, Flanner (2013) showed that the net impact of Arctic atmospheric BC plus snow- and ice-deposited BC is to warm the Arctic surface. This result was obtained through simulation of doubled global BC emissions that only interacted with radiation in the Arctic atmosphere and cryosphere. Consistent with these results, Sand et al. (2013b) found that BC emissions occurring within the Arctic induce about five-fold greater warming, normalized to the mass of emissions, than emissions from mid-latitudes. A primary reason for this is that a much higher fraction of within-Arctic emissions deposit to snow and sea ice than mid-latitude emissions. Additional references to studies describing Arctic radiative forcing and climate response from BC in snow can be found in Ch. 10.

While BC emissions within the Arctic are expected to rise with increased economic activity, these emissions currently comprise a small fraction of within-Arctic BC. Even under high-growth projections of shipping emissions, for example, ship-derived BC emissions may still contribute less than 1% of total Arctic BC deposition by 2050 (Browse et al. 2013). Consistent with this, simulations by Ménégoz et al. (2013) did not indicate a significant change in the annual duration of continental snow cover associated with high growth in Arctic shipping emissions by 2050, although impacts on sea ice were not explored in the study. Aircraft emissions from trans-Arctic flights also represent a very small source of Arctic BC, although Jacobson et al. (2012) concluded that there would be a net benefit to Arctic climate over the next several decades if flights were re-routed around the Arctic. Much of the climate benefit associated with re-routing was attributed to the fact that BC and other pollutants are removed more rapidly from the atmosphere when they are emitted at lower latitudes where precipitation is higher and atmospheric stability is lower. Readers are referred to Ch. 5 for more information on SLCF emissions within the Arctic.

Collectively, these studies highlight the point that knowledge of the mere presence of BC in the Arctic is insufficient for inferring its local climate impact, and that the vertical and seasonal distributions of BC, in particular, are critical. Moreover, different emission sources produce very different vertical distributions of Arctic BC. Figure 4.3 shows simulated vertical profiles of BC in the Arctic atmosphere caused by emissions from different latitude bands, as simulated with the CESM1 model that is described in

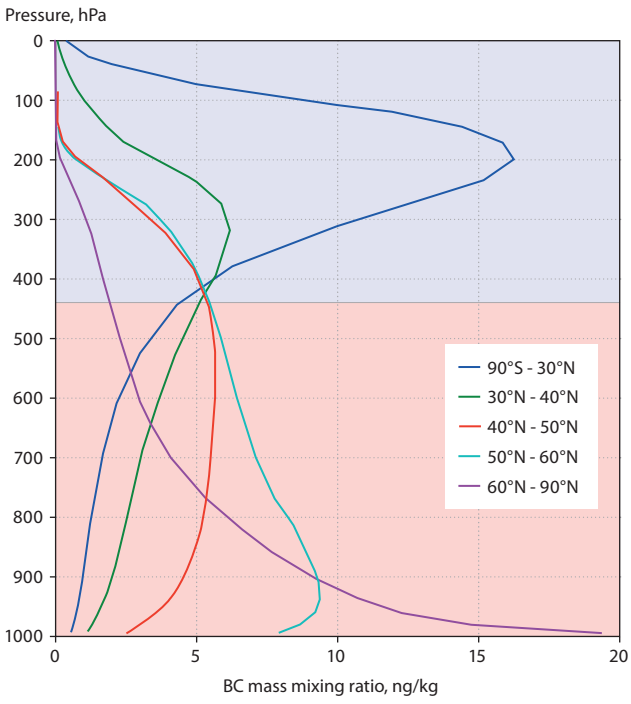

Figure 4.3 Vertical profiles of annual-mean black carbon (BC) mixing ratios in the Arctic, originating from BC emissions occurring within different latitude bands, as simulated with the CESM1 model (see Ch. 7 and 11). Blue shading indicates altitudes where BC is expected to cool the Arctic surface, on average, and red shading where BC is expected to warm the Arctic surface, on average, as determined from sensitivity studies described by Flanner (2013). The graphic illustrates how BC emissions from low latitudes that reach the Arctic are more likely to reside at high altitudes, where they exert a local cooling effect, while emissions from higher latitudes are more likely to exert forcing in the lower Arctic troposphere and deposit to cryospheric surfaces, where they can cause strong surface warming.

Ch. 7 and applied in Ch. 11. In this model, the bulk of Arctic BC originating from tropical regions and the southern hemisphere ends up at high altitudes, where it is likely to result in a cooling of the Arctic surface. The small proportion of tropical emissions (mostly from biomass burning) that reach the Arctic are able to do so because they are lofted to high altitudes, reducing their susceptibility to wet removal even after they have aged. BC emitted at higher latitudes, on the other hand, is distributed at progressively lower altitudes within the Arctic, where it is likely to exert a stronger warming influence (Fig. 4.3). High-latitude emissions are also more likely to deposit to snow and ice surfaces, further enhancing their warming effect (also see Ch. 11). The net cooling from all Arctic atmospheric BC that was found by Flanner (2013) and Sand et al. (2013a) was associated with substantial BC mass at higher altitudes. However, earlier analyses by Koch et al. (2009b) indicate that models, including the CAM4 model applied by Flanner (2013), tend to simulate excessive BC at higher altitudes in the Arctic atmosphere, while simulating too little BC at lower altitudes, suggesting a potential bias towards cooling or too little warming from Arctic atmospheric BC. A more recent analysis of BC in CMIP5 models by Allen and Landuyt (2014) shows biases in the Arctic free troposphere of different signs, depending on the observations applied. Some of the measurements showing higher BC concentrations, however, were strongly affected by biomass burning plumes that were probably not well represented in the models (also see Ch. 8). Finally, it is important to emphasize that forcing exerted outside the Arctic can strongly impact Arctic climate. Sand et al. (2013a) and Flanner (2013) both showed that forcing by BC exerted outside the Arctic warms the Arctic, and may be a stronger source of Arctic warming than within-Arctic BC in the present climate. Hence assessments of net Arctic climate impacts associated with different emissions must also consider the forcing exerted outside the Arctic. Contributions of outside-of-Arctic forcing to Arctic climate change are quantified in Ch. 11.

The seasonal cycle of BC within the Arctic is also important for radiative forcing, since insolation drops to zero during winter. Although BC within the Arctic atmosphere during winter and early spring exerts a negligible radiative forcing, particles that deposit to snow and ice surfaces can re-emerge at the surface when melt commences in the summer (e.g. Conway et al. 1996), indicating that winter transport and deposition of BC also affect Arctic climate. Moreover, although specific (mass-normalized) radiative forcing by Arctic BC peaks in the late spring and early summer, when both insolation and surface albedo are high, simulations conducted by Flanner (2013) indicate that the specific temperature response of atmospheric BC remains relatively constant throughout the late spring and summer because decreased atmospheric stability during late summer enables more effective mixing of energy between the troposphere and surface, counteracting the decrease in forcing that occurs with diminished sunlight.

Recognition of the climate importance of Arctic BC and analyses showing large biases in simulated BC distributions have motivated several recent modeling studies that explore transport of BC to the Arctic. For example, Liu et al. (2011) improved simulated Arctic BC in the GFDL AM2 model by decreasing BC aging during winter, introducing surface-dependent dry deposition velocities, and reducing wet removal efficiency of BC in ice clouds. Similarly, Browse et al. (2012) found that the transition from slow ice-cloud scavenging to more efficient warm cloud scavenging and removal with summer drizzle was critical for simulating a realistic seasonal cycle of Arctic BC in the GLOMAP model. Zhou et al. (2012) also reported strong sensitivity of Arctic BC deposition to wet removal efficiency by large-scale precipitation in the IMPACT model, but also showed that meteorological conditions from different models can strongly influence modeled long-range aerosol transport. Wang et al. (2013) showed that a package of improvements to the CAM5 model, including aerosol activation above the convective cloud base, slower BC aging into the accumulation mode, and improvements to liquid cloud removal of BC, produced more than an order-of-magnitude increase in simulated Arctic BC, improving the simulation relative to Arctic surface measurements. Jiao et al. (2014) simulated BC-in-snow concentrations using aerosol deposition fields from 25 model contributions to the AeroCom project, and evaluated these distributions against measurements from a comprehensive survey of Arctic BC in snow (Doherty et al. 2010). Although model data were poorly correlated with measurements, the multi-model mean concentrations agreed to within 25% of the observational mean, when sampled over the same grid cells, snow depths, and times as the measurements. Arctic atmospheric residence time of BC ranged from 4 to 23 days across the different models, however, indicating large differences in the treatments of aerosol removal processes in the Arctic. Moreover, Doherty et al. (2014b) recently showed that in studies such as these, where aerosol wet deposition fluxes are prescribed inconsistently with precipitation fluxes, simulated BC concentrations in the surface snow layer are biased high by factors of 1.5–2.5.

Other short-lived species that are often co-emitted with BC include particulate organic matter, sulfate precursors, nitrate precursors, O_3 precursors, and methane. These species can offset or augment the radiative forcing from BC, thus influencing the effectiveness of mitigation actions. AMAP (2011) recognized the importance of species co-emitted with BC, but focused only on BC and co-emitted organic carbon. Studies are increasingly incorporating co-emitted species into assessments of climate mitigation from short-lived forcing agents. For example, Shindell et al. (2012) explored the climate benefits associated with measures that target BC and methane emissions, but also considered the climate impacts of co-emitted or co-generated organic matter, sulfate, nitrate, and O_3. Some of the BC+methane measures explored by Shindell et al. (2012) have a strong impact on the Arctic, reducing projected warming over the next three decades by more than half. It is also worth noting, however, that some of the measures do not have much impact or actually enhance warming, and that the results are also likely to be sensitive to the model assumptions and representations of cloud indirect effects and BC albedo forcing. Bond et al. (2013) conducted a comprehensive assessment of net forcing from BC-rich sources, including co-emitted aerosol and O_3 precursors. While emissions from some sectors, like forest fires and biofuel cooking, were found to exert near climate-neutral or negative forcing, other sectors like on-road diesel cause strong emissions-normalized warming because of low emission fractions of non-BC matter. Bauer and Menon (2012), using transient simulations in a model with detailed aerosol microphysics, concluded that the regions and sectors producing the strongest net positive aerosol radiative forcing are transportation in the United States, agricultural burning and transportation in Europe, and domestic emissions in Asia.

4.3 Ozone forcing and climate response mechanism

Ozone in the troposphere causes positive radiative forcing of climate, by absorbing both longwave (LW) radiation and shortwave (SW) solar radiation. There is little spectral overlap (<5%) in the LW with other gases, as the strongest O_3 absorption band at 9.6 μm is within the so-called atmospheric window where water vapor and carbon dioxide (CO_2) only weakly absorb. Several modeling studies (e.g. Forster and Shine 1997) have shown that the LW greenhouse effect of O_3 is mainly caused by O_3 perturbations close to the tropopause. The greenhouse effect is strongest in regions where the temperature difference between the surface and the cold tropopause is large and in dry regions with little cloud cover. In the Arctic, the tropopause is generally lower and there is often a surface temperature inversion so that the temperature difference between the surface and the tropopause is relatively small. In addition, there is often extensive cloud cover, which also reduces the greenhouse effect of tropospheric O_3. Although the incoming annual mean solar radiation is lower at high latitudes, the SW absorption is only slightly reduced due to higher albedo (at the surface or above low clouds) and longer path lengths for direct solar radiation. Idealized simulations of the radiative forcing of a 10 ppb O_3 enhancement everywhere in the troposphere (Berntsen et al. 1997) showed that while the LW effect contributes about 85% of the total radiative forcing in the tropics, the contributions from LW and SW effects are about equal at high northern latitudes.

Shindell and Faluvegi (2009) estimated regional responses to regional forcings (exerted in a range of latitude bands) for several forcing agents. For O_3, the Arctic response (in terms of increase in surface air temperature) to Arctic O_3 forcing was much smaller than for equal forcings by CO_2 or scattering aerosols. This result is consistent with a larger relative contribution by SW forcing (absorption) to the total forcing in the Arctic relative to what is found globally. Hence, the climate response to the SW component of tropospheric O_3 forcing may be similar to the response to BC (Hansen et al. 1997, 2005; Shindell and Faluvegi 2009). The residence time of tropospheric O_3 is short enough to yield differences in the simulated vertical structure of Arctic O_3 perturbations, depending on the region of emissions of O_3 precursors. To date, there has not been a climate model study of the climate response to Arctic-specific O_3 perturbations at different altitudes, as was undertaken for BC by Flanner (2013). To estimate the Arctic climate response to regional emissions presented in this study (Ch. 11) regional temperature response coefficients for O_3 were applied (e.g. Shindell 2012, described in Ch. 7) and do not include the impact of differences in climate efficacy due to differences in vertical profiles of the O_3 perturbations.

4.4 Timescales

Concentrations of SLCFs such as O_3 and BC with atmospheric residence times of a month or less react rapidly to changes in emissions. The instantaneous radiative forcing per unit mass change in the atmosphere can be as high as a million times greater for BC compared to CO_2. Heat is added to the system on a short timescale through a positive radiative forcing. However, a significant fraction of the heat can reside in the system for a long time due to the inertia of the oceans. Also, mitigation policies are likely to lead to longer-term sustained reduction of emissions. The following illustrates the very different timescales in the temperature response (global mean) to emissions of BC versus CO_2. To judge if the numbers are large enough to lead to implementation of a certain strategy for reduction of BC, a policymaker needs to first define a target for the climate policy (these may be multiple, but must include a time frame for when to be achieved), then the mitigation potential and costs must be assessed. Combining this information with the emission metric numbers can then form the basis for a decision.

Commonly used metrics to describe climate impacts include radiative forcing and temperature response. Chapter 11 presents modeling assessments of radiative forcing from various short-lived forcing agents and corresponding equilibrium Arctic surface temperature responses, using techniques described in Ch. 7. While useful, neither of these metrics takes into consideration the large differences in residence time of long-lived greenhouse gases versus SLCFs including BC, which has an atmospheric residence time on the order of a week, and tropospheric O_3, which has a residence time on the order of a month.

When considering mitigation of climate change, policymakers are faced with the question of balancing the efforts to reduce long-lived greenhouse gases versus mitigation of SLCFs. A simple comparison of the radiative forcings at a certain point in time (e.g. radiative forcing at present due to concentration changes since pre-industrial times – see IPCC 2013a their fig. 5) does not accurately communicate how emissions reductions today affect future climate. Due to the large differences in atmospheric residence times and the strong thermal inertia of the climate system, total future impacts are not readily put on a common scale. To facilitate comparisons, so-called emission metrics have been developed (Shine et al. 1990; Fuglestvedt et al. 2003; Forster et al. 2007; Tol et al. 2012; Myhre et al. 2013b), the most well-known being the Global Warming Potential (GWP) which, with a 100-year time horizon, is used in the Kyoto Protocol. BC and other aerosols or precursors were not included in the Kyoto Protocol, and O_3 was only indirectly included through a modification of the GWP for methane. In all emission metrics the values are normalized to a unit mass emission of CO_2, (in kilograms) or in the case of sustained emission changes to kilograms per year.

With the use of emission metrics the net benefit associated with different policies to reduce the emissions of a suite of compounds can be readily compared without the need for simulations with complex climate models. Choosing an appropriate metric and an associated time-horizon are not pure science questions, but involve value judgments with respect to weighting of long-term and short-term impacts. In general, the metric values of SLCFs increase significantly the closer the emission reduction is to the target year, that is, the time when the temperature change target is reached. The Global Temperature change Potential (GTP) of a component *i*, is defined as the ratio of the global mean warming caused by a unit pulse emission of *i* relative to the warming caused by a similar emission of CO_2. Figure 4.4 illustrates how the GTP values of a pulse emission of components such as methane or BC with shorter residence times than CO_2 increase rapidly towards the target year. The interpretation is that the impact

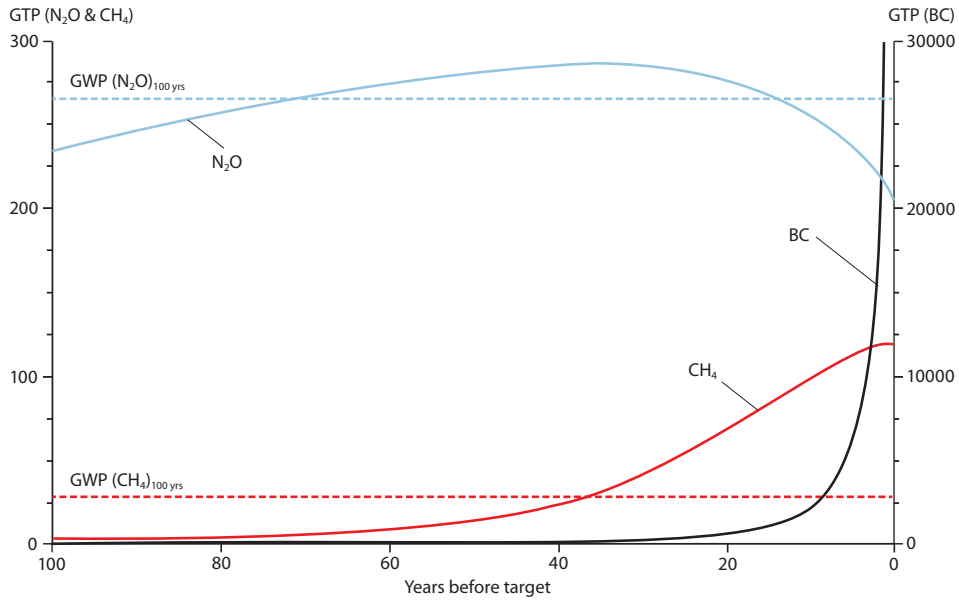

Figure 4.4 Global temperature change potential for methane (CH_4), nitrous oxide (N_2O) and black carbon (BC), shown from the time of emission to the time at which the temperature change target is reached. The (time-invariant) GWP100 is also shown for N_2O and CH_4 for comparison. Source: Myhre et al. (2013b).

of BC emissions drops off rapidly as the time between the emission reduction and the target increases, and thus the value of reducing BC emissions for a short period of time, long before the target year, is limited. However, if policymakers have defined the target not as the warming in one specific year but to slow the warming as soon as possible, then the short-term response to BC reductions would be given more weight.

Mitigation policies will, however, most likely not lead to a pulse change in emissions but to a gradual change in emissions over time. From the pulse-based model (see Fig. 4.4), metrics for different scenarios can be calculated when the future emission trajectory is known. For mitigation of SLCFs, the reductions could be expected to be phased in over a given time period (e.g. 15 years following a new technology standard), and then kept constant (as an example of one mitigation scenario). In this case there would also be emission reductions near the end of a reasonable time horizon for a climate target (e.g. two to three decades into the future). Thus the value of the emission metric will be significantly higher than in the pulse case. Figure 4.5 shows the metric values for BC for such an emissions scenario in Europe, China, and Rest of the World (ROW) for BC emissions during summer or winter as estimated by the ECLIPSE project (see Ch. 5). For this 15-year ramp-up scenario a typical GTP value of 1000 for a 50-year time horizon means that implementing an emission reduction of 1 kg/y BC for 50 years would give a similar global annual-mean temperature reduction as a corresponding emission reduction of 1000 kg/y CO_2 after 50 years. Due to the longer residence time of CO_2, the effect of continuous mitigation of CO_2 causes the radiative forcing of CO_2 to continue to decrease after the stabilization of emissions (i.e. after 15 years here). Thus the ratio of the temperature reductions by BC and CO_2 decreases over time.

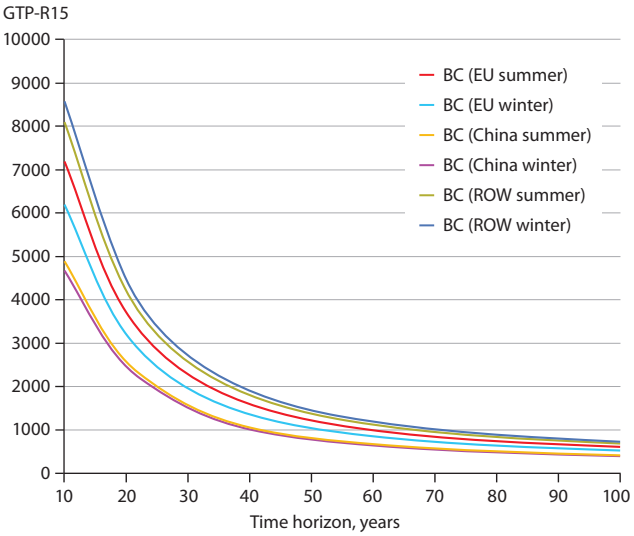

Figure 4.5 Metric values (Global temperature change potential) for a 15-year ramp up (GTP-R15) in emissions reductions of black carbon (BC) in Europe, China and the Rest of World (ROW), as estimated by the ECLIPSE Project (see Ch. 5).

4.5 Conclusions

- The Arctic surface temperature impacts from BC are sensitive to its vertical location and the season in which it is in the atmosphere or surface snow. Black carbon in the Arctic upper troposphere and stratosphere is likely to cause cooling at the surface during summer, whereas BC near the surface or within snow and ice causes strong surface warming because of its ability to trigger albedo feedback.
- Present-day global emissions of BC probably cause greater Arctic warming via radiative forcing exerted outside the Arctic than within the Arctic.
- A mass of BC emitted within the Arctic is likely to warm the Arctic several times more than the same mass of BC emitted outside the Arctic.
- Longwave heating by O_3 is less efficient in the Arctic than in other environments because the Arctic is frequently cloud covered and the temperature difference between the surface and tropopause also tends to be relatively small in the Arctic.
- Because of these features and the high surface albedo of the Arctic, shortwave and longwave radiative forcings by tropospheric O_3 in the Arctic are roughly equal, whereas longwave forcing from tropospheric O_3 is much greater than shortwave forcing in the global mean. This feature

of O_3 forcing is likely to reduce the temperature change efficacy of Arctic O_3 forcing, although more work is needed to substantiate this.

- Black carbon and O_3 have atmospheric residence times of about one week and one month, respectively; orders of magnitude less than those of long-lived greenhouse gases.
- The time response of the climate system to changes in emissions depends both on the residence time of the emitted species and on the amount of thermal inertia carried by the oceans. A much larger fraction of the total climate response to altered emissions of BC or O_3 precursors occurs within the decade following the emission change than for altered emissions of CO_2. The time horizon of societal interest therefore has a large bearing on the relative values of mitigating short-lived climate pollutants like BC and O_3 versus long-lived greenhouse gases like CO_2.

5. Emissions of short-lived climate forcers in an Arctic context

Coordinating lead author: Kaarle Kupiainen
Lead authors: Vigdis Vestreng, Jesper H. Christensen, Zbigniew Klimont
Contributing authors: Christine Wiedinmyer, Mark Flanner, Markus Amann, Patricia K. Quinn, Ville-Veikko Paunu

5.1 Introduction

This chapter addresses emissions of short-lived climate forcers (SLCFs) relevant for understanding climate impacts in the Arctic context. The discussion is largely based on the datasets used as input to models simulating the impact of SLCFs on Arctic climate (see Ch. 11) but some other anthropogenic and natural emission inventories and projections of SLCFs are also considered. National inventories and research-based inventories are included and emphasis is given to key source sectors within the Arctic. There is no unique definition of the Arctic – in this chapter the Arctic refers to the latitudinal band 60–90°N unless stated otherwise. The chapter begins by presenting the emission datasets used for modeling by the AMAP Expert Group (Sect. 5.2) and then goes on to discuss global emissions (Sect. 5.3). Comparisons with other global datasets are made in Sect. 5.4. Section 5.5 discusses emissions from Arctic nations in more detail and compares the data used in the models with those available from national submissions under the Convention on Long-range Transboundary Air Pollution (CLRTAP) and the United Nations Framework Convention on Climate Change (UNFCCC). Section 5.6 revisits the global emission datasets and examines the differences with estimates for high latitudes. Section 5.7 focuses on emissions from High Arctic sources (shipping as well as oil and gas activities) while Sect. 5.8 addresses emissions from open biomass burning. Section 5.9 outlines the uncertainties in the various emission estimates before closing with a list of key findings (Sect. 5.10).

Emission estimates are often calculated by combining information on fuel use or other activities with emission factors that define emissions per unit of activity (Granier et al. 2011). Activity data used for creating emissions inventories typically originate from international organizations and national statistics, whereas emission factors originate from published measurements or a synthesis of such measurements. The purpose of this chapter is to describe emissions that induce climatic impacts in the Arctic region as a whole. Therefore, emission sources of local relevance only are not discussed separately. This includes, for example, wind-driven coal dust particles which affect climate forcing through black carbon (BC)-snow albedo changes but which have high localized effects. In contrast, BC emissions from gas flaring emissions are discussed separately because although their impacts might be small on a global scale, they are potentially large at high latitudes. Flaring emissions might also help explain seasonal patterns of measured Arctic BC burdens and model underestimates of Arctic BC as hypothesized by Stohl et al. (2013).

5.2 Emission datasets used in AMAP modeling

This study uses the most recent emissions datasets developed within the ECLIPSE FP7 project. (Version 5 was completed in 2013–2014 and a gridded dataset is available from the project website: http://eclipse.nilu.no and will soon be available from http://eccad.sedoo.fr; see also Sect. 5.3 and 5.5.) The pollutants included in the emission datasets are black carbon (BC), organic carbon (OC) or organic matter (OM), sulfur dioxide (SO_2), methane (CH_4), carbon monoxide (CO), nitrogen oxides (NO_X), non-methane volatile organic compounds (nmVOC) and ammonia (NH_3). The discussion in this chapter focuses on emissions of BC, OC, CO, nmVOC, NO_X and SO_2. Anthropogenic CH_4 emissions are addressed by AMAP (2015). The emission data were used as input for atmospheric and climate model runs conducted for this assessment.

Anthropogenic emissions were generated using the IIASA (International Institute for Applied Systems Analysis) Greenhouse gas and Air pollutant Interactions and Synergies (GAINS) model (Amann et al. 2011). The emissions were calculated in five-year intervals, spatially distributed onto a 0.5°×0.5° latitude grid, and include monthly data for the major sectors. The GAINS model distinguishes more than 1500 emission mitigation options for each source sector allowing development of targeted technology-specific control scenarios (Amann et al. 2013). Past emissions of air pollutants and greenhouse gases were estimated for the period 1990–2010 and projections extend through 2050.

From several global scenarios developed with the GAINS model during the ECLIPSE project (Klimont et al. in prep.), two were selected for use in this assessment:

- The Current Legislation (BASELINE) scenario. This scenario includes all presently agreed legislation and adopted policies affecting air pollutant emissions; the principles and assumptions in the BASELINE scenario were described by, among others, Cofala et al. (2007).
- The SLCF mitigation scenario (MITIGATE). This scenario assumes the full implementation of a portfolio of SLCF measures by 2030 and 2050 designed to achieve large reductions in temperature response in the short term at the global scale. The principles behind the development of this scenario are the same as the reduction case reported by UNEP/WMO (2011) and Shindell et al. (2012). The measures included were selected from all existing emission control options for particulate and gaseous species in the GAINS model relying on an assessment of the potential climate impact of all measures using a climate metric (Shindell et al. 2012). The scenario eventually consists of those measures that both mitigate warming and improve air quality. However, here a GTP20 (Global Temperature Potential;

20-year horizon) metric was used for selection of measures rather than the GWP100 metric that was used by UNEP/WMO (2011) and Shindell et al. (2012). A temperature-related metric with a shorter time-span was considered more appropriate for short-lived species; however, the selection of measures is not significantly dependent on the choice between these two metrics.

Since the models used in the impact studies could not utilize the most detailed level of the GAINS model sector output, the anthropogenic emission data were aggregated into the following sectors (sector names used in figures are in brackets), feasible for the purposes of this study. The sectors are generally in line with the key sectors identified in the work of the Intergovernmental Panel on Climate Change (IPCC) and they are used in the discussion of emission data in this chapter:

- Agricultural emissions from waste burning on fields (*Agriculture – waste burning on fields*)
- Agricultural emission from animals, rice cultivation and soil (*Agriculture – Animals, rice and soil*)
- Flaring in the production of oil and gas (*Flaring in the oil and gas industry*)
- Industrial emissions from processing and combustion sources (*Industrial combustion and processing*)
- Emissions from power plants, energy conversion and extraction (*Power plants, energy conversion, extraction*)
- Emissions from residential and commercial sources, such as household heating and cooking, local heating of commercial buildings (*Residential and commercial*)
- Solvents manufacturing and use (only for nmVOCs) (*Solvent*)
- Surface transportation and inland waterways, including on-road and off-road vehicle emissions (*Surface transportation*)
- Emissions from waste treatment and disposal (*Waste*).

For atmospheric and climate model runs, the following additional emission datasets were used:

- Representative Concentration Pathway 6.0 (RCP6.0) dataset for global international shipping and air traffic. The influence of Arctic shipping was evaluated separately based on Corbett et al. (2010) and Winther et al. (2014)
- The GFED3 database for forest and grassland fires (van der Werf et al. 2010).

The data analyses and illustrations use the following regional aggregations, agreed upon by the AMAP Expert Group: Canada (CANA), United States (USAM), Nordic countries (NORD), Russia (RUSS), Non-Arctic Europe (OEUR) (other Europe, without Turkey), Asia (ASIA) that includes China, India, Japan, Singapore, South Korea (without Central Asian countries), and the Rest of the world (ROW, mostly comprising the southern hemisphere). Maps of the regions are shown in Fig. 5.1 (ROW not shown).

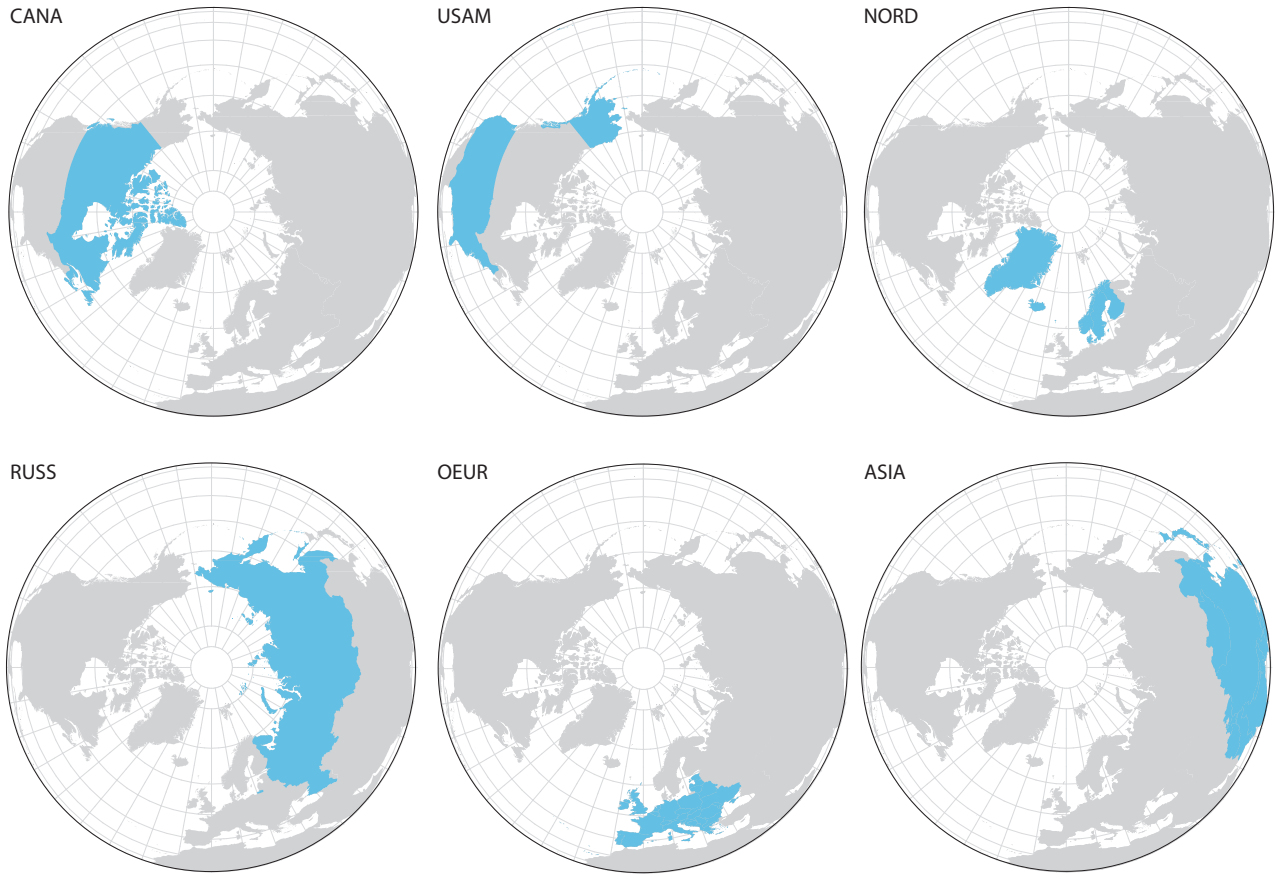

Figure 5.1 Regional definitions used for presenting the emission data and analyzing the results. From upper left to lower right: Canada (CANA), United States (USAM), Nordic countries (NORD), Russia (RUSS), Non-Arctic Europe (other Europe, without Turkey) (OEUR), Asia (without Central Asian countries) (ASIA).

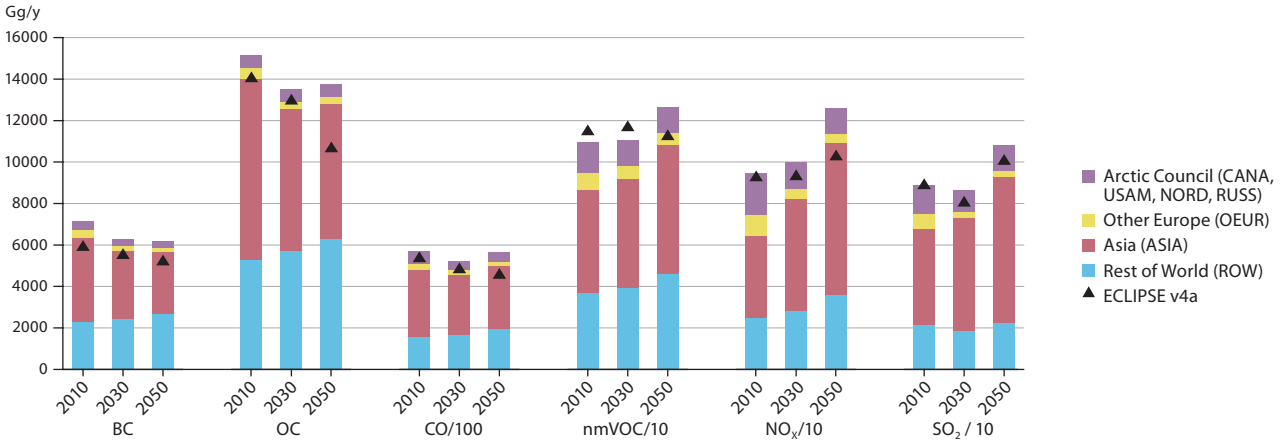

Figure 5.2 Global anthropogenic emissions of black carbon (BC), organic carbon (OC), carbon monoxide (CO), non-methane volatile organic compounds (nmVOC), nitrogen oxides (NO_X) and sulfur dioxide (SO_2) in 2010 and for the BASELINE scenario for 2030 and 2050, by region, for ECLIPSE version 5. ECLIPSE version 4a global emission values are shown as a triangle. Note that emissions for species other than BC and OC are scaled.

Owing to the timeline of the work, the atmospheric and climate model calculations used two versions of the ECLIPSE emission datasets; v4a and v5. Version 4a was used for the forcing runs, which were launched in 2013. Version 5 became available in 2014 and was the first ECLIPSE emission dataset to include the MITIGATE scenario, but it also included an update of the BASELINE scenario. The dataset was considered important for this study and was used for the transient simulation runs for climate response. Comparisons of the ECLIPSE versions 4a and 5 data sets are included in Sect. 5.3 to 5.5.

5.3 Global emissions

Figure 5.2 shows the global anthropogenic emissions of BC, OC, CO, nmVOC, NO_X and SO_2 in the BASELINE Scenario in 2010, 2030 and 2050, by region. ASIA accounts for over half of the emissions of all pollutants across all years, followed by ROW. The relative importance of emissions from the Arctic Council nations (Canada, Denmark, Finland, Iceland, Norway, Russia, Sweden, and United States) varies by pollutant and accounts for approximately 10–20% of the global totals. Emissions from Arctic nations are typically higher than for emissions from non-Arctic Europe (OEUR in Fig. 5.2). Following the BASELINE scenario, emissions in 2030 and 2050 are projected to remain relatively close to 2010 levels. For BC, OC and CO, emissions are expected to decline by 10% by 2030 and then remain relatively constant until 2050, whereas emissions of nmVOC, NO_X and SO_2 are expected to increase by 2050, mostly due to increasing trends in ASIA and ROW.

Figure 5.2 also shows ECLIPSE v4a total global emissions for comparison. The difference between the v4a and v5 datasets varies by pollutant and year. The biggest differences between v4a and v5 are for OC, CO and NO_X emissions in 2050, with v5 global emissions approximately 20% higher than v4a. BC emissions in v5 are approximately 15% higher than in v4a. For the other pollutants and years, the datasets are within 10% of each other. The primary driver behind v4a and v5 differences for 2050 is the energy use projections for the period 2035–2050. ECLIPSE v4a was developed for the period 2010–2030 and then for 2050, drawing on the International Energy Agency's (IEA) World Energy Outlook 2011 ('WEO 2011', see IEA 2011) until 2030. Long-term projections from the POLES model (developed at Joint Research Center Seville) were used for year 2050. ECLIPSE v5 was developed with the use of the Energy Technology Perspectives 2012 (IEA 2012), which extends WEO 2011 until 2050. At the global level, energy projections used in ECLIPSE v4a and v5 are both comparable to the Energy Technology Perspectives' 6°C scenario, which assumes that by 2050, energy use almost doubles compared with 2009 (IEA 2012).

Figure 5.3 shows the emission reductions in 2030 and 2050 for the MITIGATE scenario, versus the BASELINE scenario, by region, for each pollutant. A feature of the MITIGATE scenario

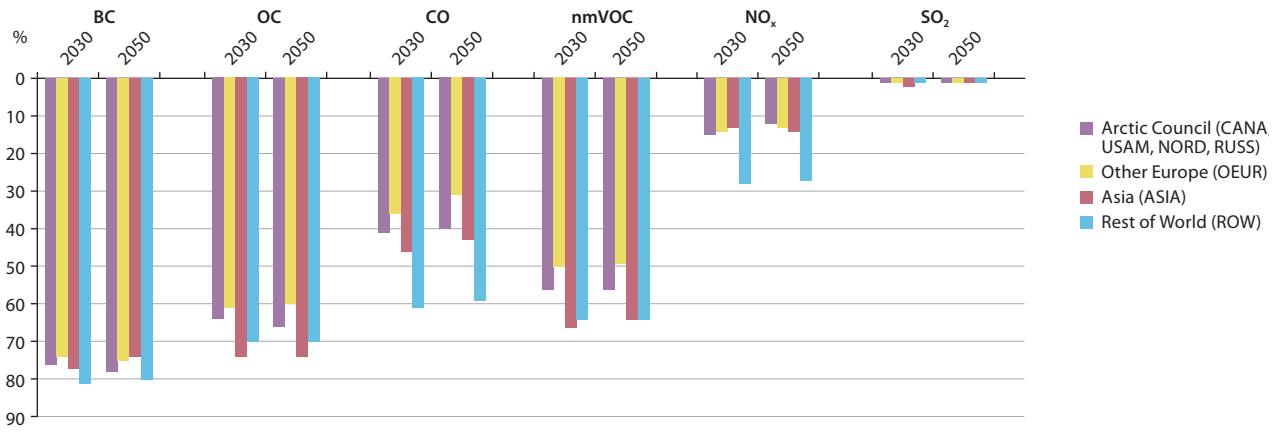

Figure 5.3 Relative emission reductions by region in the short-lived climate forcer mitigation scenario (MITIGATE) compared with the BASELINE (v5) scenario.

is that it does not prioritize mitigation of the climate-cooling SO_2 emissions, thus little SO_2 mitigation is obtained. Figure 5.3 indicates that there is significant potential for further emission reductions compared with the BASELINE scenario. This applies for all pollutants and all regions, including the Arctic Council nations. For example, reductions of BC emissions of approximately 70–80% could be achieved, but then OC would also be reduced by approximately 60–70%. CO and nmVOC reduction potentials vary between 30% and 60%. NO_X reductions are approximately 30% for ROW and around 10% for other regions. It is important to note that to achieve even part of the emission reductions that the MITIGATE scenario demonstrates, additional emission mitigation policies are required.

Figure 5.4 shows the major emission sectors in 2010. The *Surface transportation* and *Residential and commercial* sectors together account for approximately 70% of the emissions of BC and OC in the Arctic Council nations and between 80% and 90% in the other regions. In Figure 5.4, *Flaring in the oil and gas industry* is included in the *Power plants, energy conversion, extraction* sector where it accounts for 75% of the emissions. *Burning of agricultural wastes on fields* in Arctic Council nations accounts for 10% and 20% of BC and OC emissions, respectively. For the other pollutants, the importance of different sectors varies. In the case of SO_2, most of the emissions are from the *Power plants, energy conversion, extraction* sector and *Industry*. These are important sources of NO_X, in addition to *Surface transportation,* which account for 35–60% of the emissions, depending on the region.

5.4 Comparison of global anthropogenic emission datasets

Granier et al. (2011) compared publicly available global and regional emission inventories for BC, SO_2, NO_X and CO and highlighted differences between them. Emissions from anthropogenic and biomass burning sources were included in the study, and the evaluated inventories represented time periods between 1980 and 2010. Such datasets are often used by the scientific community as input for climate and regional air quality models. The comparison by Granier et al. (2011) did not include the ECLIPSE emission datasets used in this assessment, but did include an earlier dataset from the IIASA-GAINS model.

The Granier et al. (2011) evaluation showed large discrepancies between the global and regional emissions datasets. Differences between regional inventories are generally similar to or larger than the differences between global inventories. Differences between the inventories generally did not decline in the more recent years of the comparison. The evaluation did pose several challenges: the authors noted that some of the inventories are not independent of each other (Granier et al. 2011), also that the different datasets had different base years. The base year refers to the latest year when the activities are based on statistics, which can thus be considered more reliable than projections as the latter include assumptions about future development of the activities. Relevant information about underlying data and methodologies is often not available for detailed assessment of differences and uncertainties.

Figure 5.5 shows a comparison of anthropogenic emissions from different inventories for 1980 to 2000 (Granier et al. 2011). In 2000, where it is possible to compare most datasets, the difference between maximum and minimum global annual total emissions was 22% for BC, 28% for CO, 17% for NO_X and 42% for SO_2, indicating a relatively large spread in the data. For comparison, the ECLIPSE v5 global total emissions in 2010 were 7 Tg of BC, 568 Tg of CO, 95 Tg of NO_X (or 63 Tg, if expressed as NO) and 89 Tg of SO_2.

5.5 Anthropogenic emissions in the Arctic Council region

This section focuses on describing the air pollutant emissions in the Arctic Council nations. First the emissions are described by country in 2010, 2030 and 2050 based on the ECLIPSE emission data used for model simulations by the AMAP Expert Group. This is followed by a short review of national submissions of emission inventory data under CLRTAP and UNFCCC.

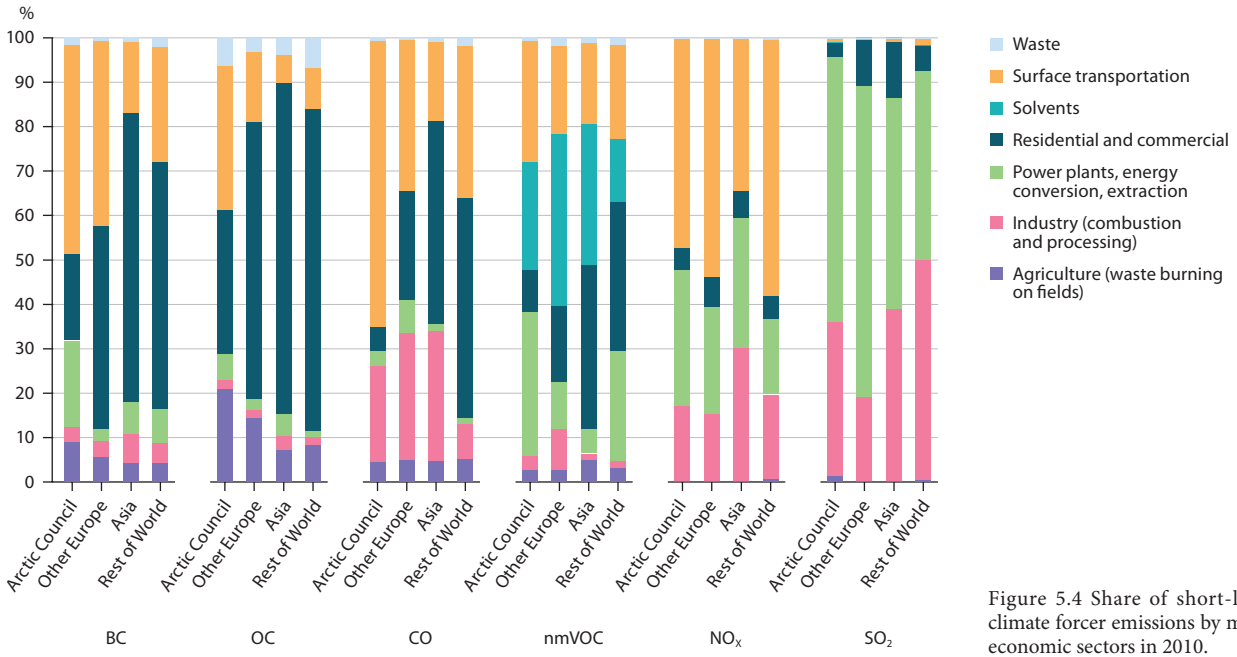

Figure 5.4 Share of short-lived climate forcer emissions by major economic sectors in 2010.

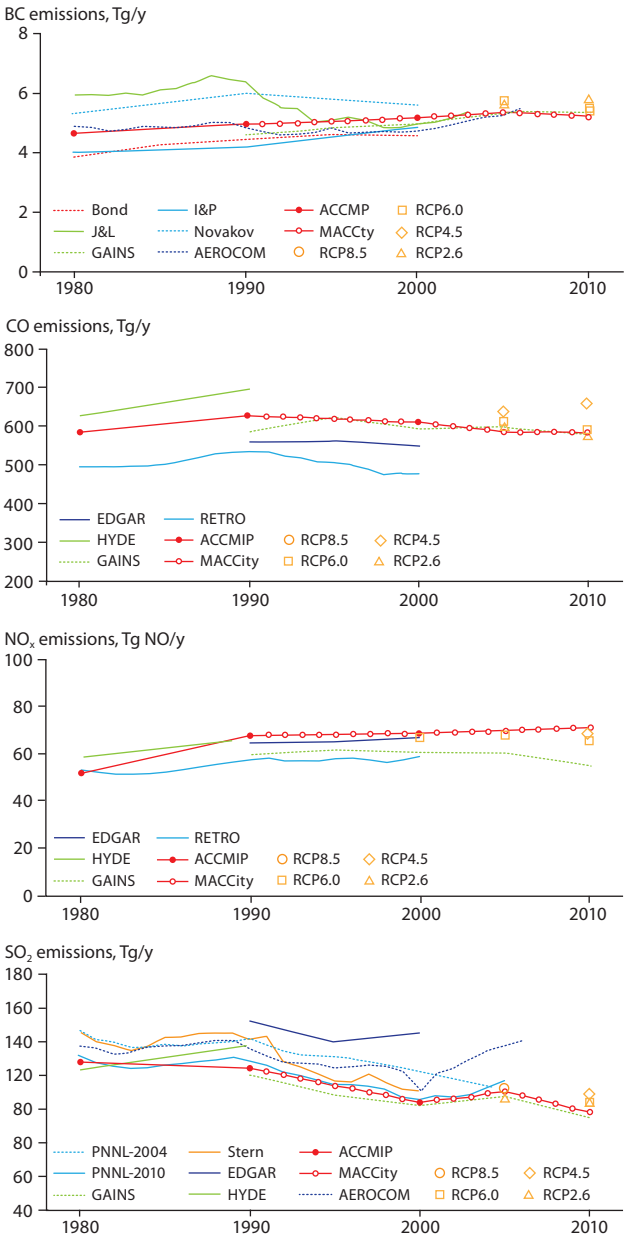

Figure 5.5 Comparison of global emissions of black carbon (BC), carbon monoxide (CO), nitrogen oxides (NO_X) and sulfur dioxide (SO_2) between 1980 and 2010 (Granier et al. 2011).

The importance of emissions from the Arctic Council region on a global scale varies by pollutant. Table 5.1 shows the percentage share of global total emissions for different pollutants as assessed by the IIASA-GAINS model in the datasets used by the AMAP Expert Group.

Figure 5.6 shows the actual (2010) and projected (2030 and 2050) emissions of BC, OC, CO, nmVOC, NO_X and SO_2 in the Arctic Council nations. Future emissions are projected for both the Current Legislation (BASELINE) and SLCF mitigation (MITIGATE) scenarios. For illustration purposes, the Nordic countries were aggregated into one region (NORD). All

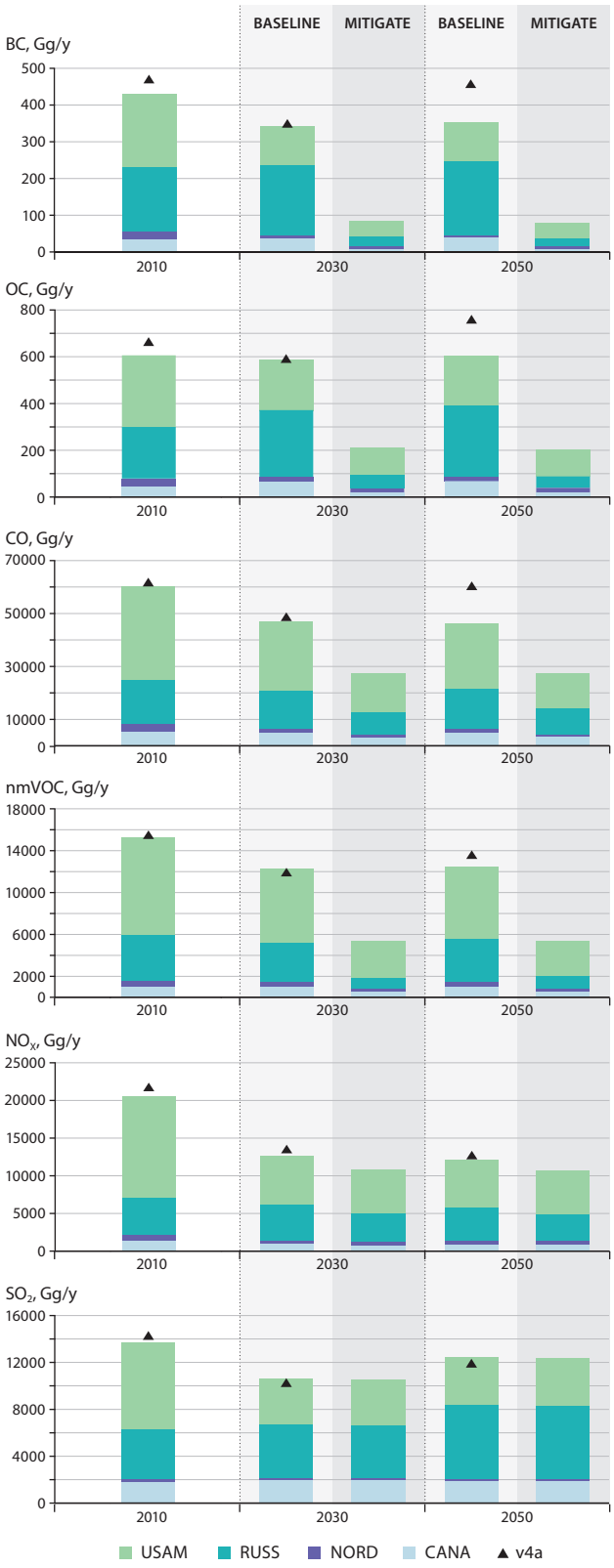

Figure 5.6 Collective emissions of selected pollutants from all Arctic Council nations in 2010, and for 2030 and 2050 under the BASELINE and MITIGATE scenarios.

Table 5.1 Percentage share of Arctic Council nations in global emissions of multiple pollutants in 2010.

Pollutant	BC	OC	OM	SO_2	CH_4	CO	NO_X	nmVOC
Arctic Council region as percentage share of global emissions	8	5	4	16	20	11	23	13

emission data were compiled from the v5 dataset, although the graphic also shows the Arctic Council nations' total emissions in the v4a dataset for comparison.

The United States (USAM) and Russia (RUSS) account for the greatest emissions shares followed by Canada (CANA) and the Nordic countries (NORD). Emissions under the BASELINE scenario (existing policies and legislation) are projected to decline between 2010 and 2030 for all pollutants other than OC, for which emissions remain at the 2010 levels. The decline is particularly apparent for USAM and NORD owing to already-stringent legislation and the impacts of recently-agreed steps to further control emissions from transport and industrial sources. In 2050, emissions projected under the BASELINE scenario are essentially similar to those in 2030.

Figure 5.7 presents a closer look at how the different economic sectors account for the changes in total emissions from the Arctic Council nations under the BASELINE scenario between 2010 and 2030. Emissions from *Surface transportation* are expected to account for large shares of the reductions in BC, OC, CO, nmVOCs and NO_X. However, in CANA and RUSS the reductions in BC and OC emissions from *Surface transportation* are offset by increased emissions especially from the *Residential and commercial* sector. SO_2 emissions are projected to decline in NORD and USAM by approximately 20% and 50%, respectively, as a result of current legislation.

The MITIGATE scenario projects significant emission reduction potential in the Arctic Council nations for BC, OC, CO and nmVOCs (Figs. 5.6 and 5.8). The reduction potential for NO_X is less and no reductions are expected for SO_2, which is a characteristic feature of the MITIGATE scenario. Most of the emission reductions will be achieved by 2030, so 2050 emissions under the MITIGATE scenario are only slightly different to the 2030 situation. The emission data for v4a and v5 are similar for the Arctic Council nations, other than for year 2050 when BC, OC and CO are lower in v5.

Figure 5.8 indicates the further emission reduction potential in 2030 by measures targeting climate effects of SLCFs under the MITIGATE scenario, versus the BASELINE scenario. BC emissions would experience the greatest relative reduction, especially in the *Residential and commercial* sector for CANA, NORD and USAM. It is notable that there is less than 15% emission reduction potential from current legislation in the *Surface transportation* sector in the Arctic Council nations, because the existing legislation already requires relatively efficient mitigation technologies of particulate matter (PM), which results in BC and OC emissions reductions. For RUSS, a big share of the

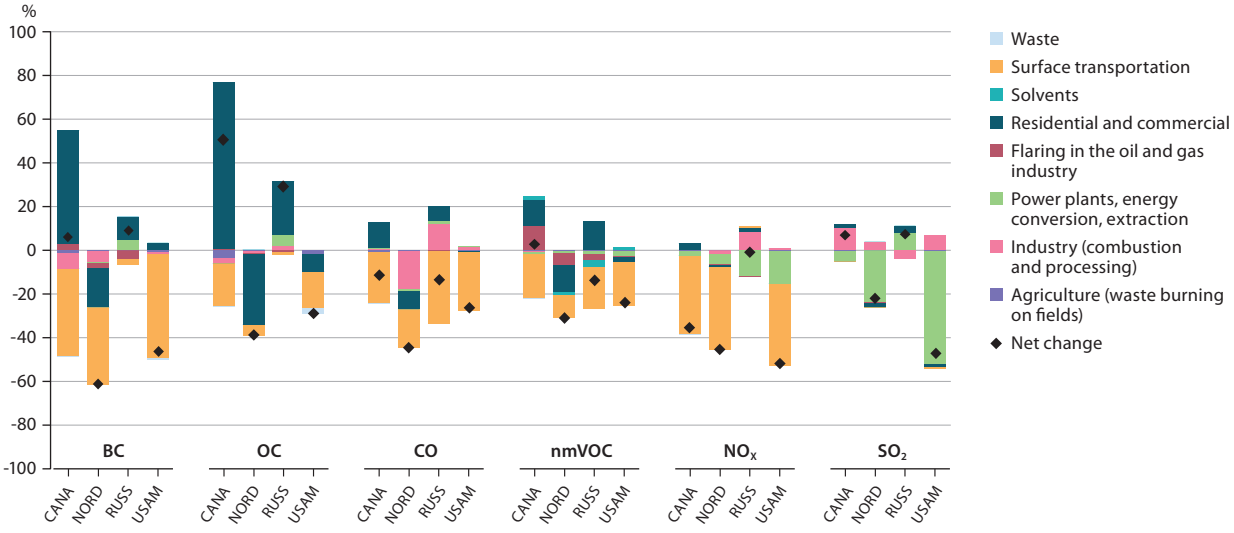

Figure 5.7 Relative change in emissions by sector and region between 2010 and 2030 under the BASELINE (existing policies and legislation) emissions scenario, for Arctic Council nations only.

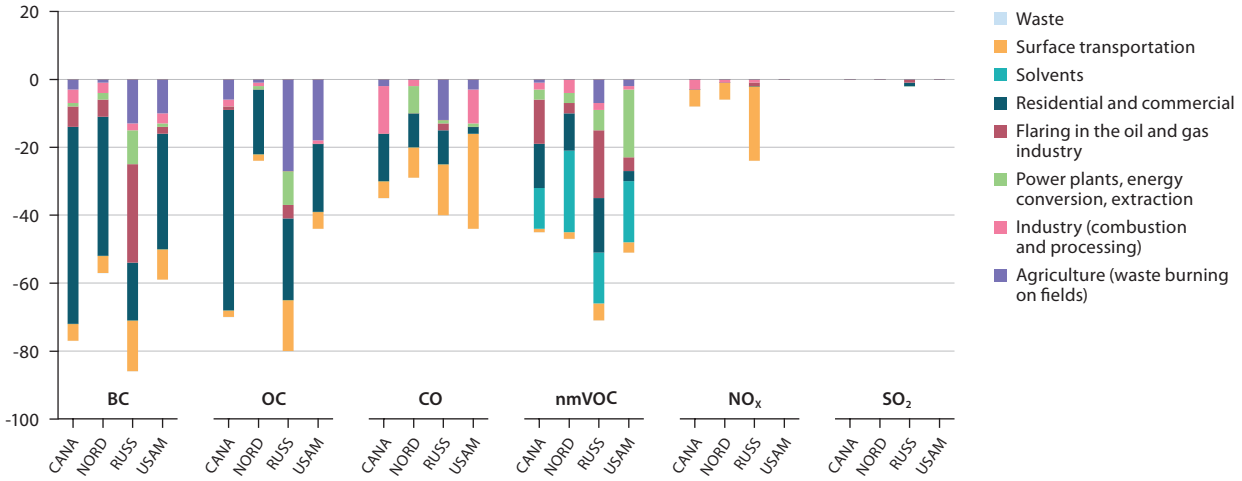

Figure 5.8 Relative difference between the change in emissions under the BASELINE scenario and the MITIGATE scenario by 2030 for the Arctic Council nations.

reduction is from measures targeting *Flaring in the oil and gas industry*. Measures addressing the *Residential and commercial*, *Surface transportation* and *Agriculture* (*waste burning on fields*) sectors are calculated to have a significant further reduction potential relative to the BASELINE scenario. The relatively large reductions in OC are due to measures targeting BC, since the two pollutants are nearly always formed and emitted from the same sources at the same time. CO is a product of incomplete combustion, similar to BC and OC, and so many of the priority sectors for further mitigation effort are the same for all the pollutants. Significant emission reductions of other SLCFs could be achieved within the *Industry* (*combustion and processing*) and *Power plants, energy conversion, extraction* sectors. In the case of nmVOC, the *Solvents* sector is a significant source of emissions, and measures exist that could further reduce SLCF emissions from this sector beyond that under the BASELINE scenario. The MITIGATE scenario does not influence emissions of SO_2 and the effect on NO_X is also minor compared to the other pollutants.

In addition to the data shown for the ECLIPSE project global datasets, Arctic Council nations also report emissions of SO_2, NO_X, CO and NH_3 under CLRTAP, while CH_4 emissions are reported under UNFCCC. Some nations also report emissions of BC and OC under CLRTAP on a voluntarily basis. Table 5.2

Table 5.2. National emissions of short-lived climate forcers in Arctic Council nations as reported under CLRTAP and UNFCCC. The sum of national emissions are calculated for Nordic countries and Arctic Council nations in respective columns where data are available. Data sources for BC and OC and other explanations listed in the table notes.

Component, Gg/y	Year	Denmark[a]	Finland[b]	Iceland	Norway[c]	Sweden[d]	Nordic countries	Canada[e]	Russian Federation[f]	USA[g]	Arctic Council nations
BC	2000	6	6	na	5	na	na	63	na	na	na
	2005	7	6	na	5	6 (5)	(24)	57	na	578	na
	2010	7	6	na	6	na	na	50	na	513	na
OC	2000	7	na	na	23	na	na	na	na	na	na
	2005	9	5	na	21	(7)	(43)	109	na	1508	na
	2010	10	6	na	22	na	na	na	na	na	na
SO_2	2000	31	79	35	27	42	214	2358	1997	14830	19613
	2005	25	69	38	24	36	192	2183	1847	13145	17559
	2010	15	67	73	19	32	207	1371	1302	7017	10103
NO_X	2000	208	201	28	204	207	848	2548	2357	21547	28148
	2005	186	169	26	199	175	755	2345	2795	18381	25031
	2010	132	167	23	180	148	650	1992	2369	13497	19158
CO	2000	490	611	21	517	815	2454	11375	10811	103844	130937
	2005	461	530	18	395	661	2065	9661	12277	73162	99229
	2010	408	485	19	336	575	1823	8712	9979	56657	78994
NH_3	2000	97	36	5	26	59	224	486	650	4453	6037
	2005	88	38	5	27	56	213	513	531	3447	4918
	2010	79	38	5	27	52	200	474	830	3742	5446
nmVOC	2000	138	166	7	381	222	914	2544	2450	15887	22709
	2005	114	136	6	219	198	674	2338	2567	14411	20663
	2010	89	116	5	142	188	540	2030	2081	13669	18860
CH_4 including LULUCF/LUCF	2000	282	260	23	241	298	1104	4549	21182	28997	56936
	2005	271	219	24	227	275	1015	4941	23027	28269	58266
	2010	268	210	25	215	242	959	4868	23893	28224	58903
CH_4 excluding LULUCF/LUCF	2000	282	258	23	241	298	1101	4477	20697	28452	55830
	2005	271	216	23	227	275	1012	4671	22560	27886	57142
	2010	268	207	24	215	242	956	4305	23385	28002	57604

na: not available; LULUCF: land use, land-use change and forestry; LUCF: land use change and forestry; WEBDAB (officially reported data under CLRTAP) http://www.ceip.at/ms/ceip_home1/ceip_home/webdab_emepdatabase/reported_emissiondata/ Note that some submissions are of different vintage, thus inconsistencies between years and countries might occur; UNFCCC emission data: http://unfccc.int/di/DetailedByParty/Event.do?event=go#

[a] BC and OC data, including Greenland and the Faroe Islands, from Winther and Nielsen (2011); [b] BC data as reported to CLRTAP and OC data from Arctic Council (2011); [c] BC and OC data from Statistics Norway (2013); [d] 2005 BC data from Kindbom and Munthe (2013), emissions in brackets from Hansson et al. (2011); [e] BC data from Environment Canada (2013), 2010 data are projected. OC data are for year 2006 and from Arctic Council (2011); [f] The WEBDAB emission data only cover the European part. [g] BC data representative for 2011 as reported to CLRTAP is posted for 2010, other BC and OC data are from US EPA (2012). The US BC and OC data include wildfire emissions of about 110 Gg BC and 672 Gg OC.

shows reported emissions for the individual Arctic countries, as well as total emissions for the Nordic countries (Denmark, Finland, Iceland, Norway and Sweden) and the Arctic Council nations calculated from the country-specific data. Some national BC and OC data published elsewhere by individual countries were also included in the table and referenced in the table notes.

The coverage of reported national data from Arctic nations on SLCFs other than BC and OC is complete. In recent years many Arctic Council nations have increased efforts to estimate and publish BC and OC data, and more inventories are now being updated and developed. This is partly due to the focus on inventory development under the Task Force on SLCF (Arctic Council 2011). Projects that target individual sources have also been launched within the Arctic Council, for example the ACAP project on emissions from domestic wood burning (ACAP 2014). Such projects, together with the development of Guidelines for reporting of BC and OC emissions under CLRTAP, are likely to result in more comparable BC and OC inventories across countries in the near future.

According to the national submissions, there was a downward trend in most SLCFs between 2000 and 2010 for the Arctic Council nations collectively, but CH_4 emissions increased between 2000 and 2010 (Table 5.2). Relative emission reductions of nmVOC and NH_3 were considerably lower than for SO_2, NO_X and CO.

A comparison between emissions reported by the Arctic Council nations under CLRTAP and UNFCCC, and those from the ECLIPSE v5 inventory is shown in Table 5.3. For BC and OC, the national emissions are higher for all regions. Some of the differences could be linked to the emission sources covered. For example, for USAM the national emissions include wildfire emissions and prescribed burning of forests not included in ECLIPSE. After subtracting the wildfire emissions, the national reported BC emissions for USAM are twice as high as those in the ECLIPSE dataset, while the OC data are almost three times higher. After subtracting BC emissions from prescribed burning of forests the USAM national emission inventory is 1.5 times higher than the ECLIPSE emissions. A detailed sectoral split was not available for all countries so similar comparison was not possible. All countries emphasize that their BC and OC data are preliminary and that the inventories must be viewed as a work in progress.

For the other emission components, the comparability and completeness of the national submissions should be much better. However, emissions can be either higher or lower than the ECLIPSE data, depending on the pollutant and country. For Russia, the ECLIPSE emissions are higher than the national estimates for all components except NH_3. The ratio between national emissions and ECLIPSE data varies between 0.66 and 2.07 for other regions and pollutants. A detailed explanation for the differences is beyond the scope of this study, but should be one of the aims for further work.

5.6 Comparison of northern hemispheric anthropogenic emission datasets

To assess emissions that are expected to have a more direct impact on the Arctic, a comparison of available SLCF emission inventories for areas in the latitude bands 40–90°N, 60–90°N and

Table 5.3 Comparison of nationally reported emissions (different years, see table notes for Table 5.2 for further details) and the ECLIPSE v5 emission data used for AMAP modeling in 2010. Unit: Gg/y.

Region	National	ECLIPSE v5	National/ ECLIPSE v5
BC			
CANA	50	34	1.45
NORD	24	22	1.11
RUSS	na	174	na
USAM	405	200	2.03
OC			
CANA	109	43	2.52
NORD	43	37	1.17
RUSS	na	220	na
USAM	836	305	2.74
SO_2			
CANA	1371	1889	0.73
NORD	207	163	1.27
RUSS	1302	4231	0.31
USAM	7017	7389	0.95
NO_X			
CANA	1992	1521	1.31
NORD	650	608	1.07
RUSS	2369	4941	0.48
USAM	13497	13396	1.01
CO			
CANA	8712	5377	1.62
NORD	1823	2744	0.66
RUSS	9979	16707	0.60
USAM	56657	35370	1.60
NH_3			
CANA	474	636	0.74
NORD	200	167	1.20
RUSS	830	750	1.11
USAM	3742	3736	1.00
nmVOC			
CANA	2030	982	2.07
NORD	540	581	0.93
RUSS	2081	4344	0.48
USAM	13669	9259	1.48
CH_4 excluding LULUCF/LUCF			
CANA	4305	4195	1.03
NORD	956	1013	0.94
RUSS	23385	34234	0.68
USAM	28002	31795	0.88

CANA: Canada; NORD: Nordic countries; RUSS: Russia; USAM: United States.

Table 5.4. Description of global emission datasets.

Dataset[a]	Pollutants	Home institute	Documentation
ACCMIP	BC, OC, SO_2, NO_X, CO, NH_3, CH_4, nmVOC	Atmospheric Chemistry & Climate Model Intercomparison Project (www.igacproject.org/ACCMIP)	Lamarque et al. 2010
GAINS (v4a, v5) (unep)	BC, OC, SO_2, NO_X, CO, NH_3, CH_4, nmVOC	International Institute for Applied Systems Analysis (gains.iiasa.ac.at)	http://eclipse.nilu.no; UNEP/WMO 2011; Shindell et al. 2012; Klimont et al. in prep.
Junker and Liousse	BC, OC	Laboratoire d'Aérologie, Université Paul Sabatier, Toulouse, France	Junker and Liousse 2008
PEGASOS	BC, OC, SO_2, NO_X, CO, NH_3, CH_4, nmVOC	Netherlands Environmental Impact Assessment Agency & International Institute for Applied Systems Analysis	Janssens-Maenhout et al. 2011
RCP3D	BC, OC, SO_2, NO_X, CO, NH_3, CH_4, nmVOC	Netherlands Environmental Impact Assessment Agency	van Vuuren et al. 2007
RCP4.5	BC, OC, SO_2, NO_X, CO, NH_3, CH_4, nmVOC	Pacific Northwest National Laboratory, Joint Global Change Research Institute	Smith and Wigley 2006; Clarke et al. 2007; Wise et al. 2009
RCP6.0	BC, OC, SO_2, NO_X, CO, NH_3, CH_4, nmVOC	National Institute for Environmental Studies, Japan	Fujino et al. 2006; Hijioka et al. 2008
RCP8.5	BC, OC, SO_2, NO_X, CO, NH_3, CH_4, nmVOC	International Institute for Applied Systems Analysis	Riahi et al. 2007
Edgar v4.2	BC, OC, SO_2, NO_X, CO, NH_3, CH_4, nmVOC	Joint Research Center (http://edgar.jrc.ec.europa.eu/)	EC-JRC/PBL. EDGAR version 4.2. http://edgar.jrc.ec.europa.eu/, 2011
RETRO	CO, NO_X	REanalysis of the TROpospheric chemical composition over the past 40 years (http://retro.enes.org/index.shtml)	Schultz et al. 2008
SPEW	BC, OC	Department of Civil & Environmental Engineering, University of Illinois at Urbana-Champaign (www.hiwater.org/)	Bond et al. 2007

[a]Information on RCPs available from: http://tntcat.iiasa.ac.at:8787/RcpDb/dsd?Action=htmlpage&page=about

Table 5.5 Ratios between maximum and minimum emissions from the global emission inventories listed in Table 5.4, for several northern hemisphere latitude bands. Green (values <1.3), yellow (values 1.3–1.7), red (>1.7).

		Global	40–90°N	60–90°N	70–90°N
BC	2000	1.30	1.15	1.53	3.01
	2005	1.08	1.17	3.91	4.49
	2010	1.20	1.40	3.09	3.52
OC	2000	2.43	1.94	2.09	1.97
	2005	1.09	1.61	1.93	4.83
	2010	1.21	1.61	2.32	5.67
SO_2	2000	1.20	1.09	2.39	1.51
	2005	1.13	1.13	1.23	1.25
	2010	1.22	1.32	1.58	2.82
NO_X	2000	1.28	1.26	3.51	7.19
	2005	1.12	1.14	1.42	2.37
	2010	1.17	1.23	1.46	2.46
CO	2000	1.60	1.70	2.91	13.31
	2005	1.19	1.32	1.25	1.55
	2010	1.38	1.48	2.30	10.47

70–90°N was conducted. This analysis used spatially-distributed global emission datasets downloaded from the ECCAD-GEIA website (http://eccad.sedoo.fr), described in Table 5.4.

Emissions of SLCFs for the years 2000, 2005 and 2010 were summed within three latitude bands (40–90°N, 60–90°N and 70–90°N) to examine the share of high latitude emissions to global totals as well as differences in the emissions in the vicinity of, versus within, the Arctic. This showed that, in general, emissions north of 40°N were about 20% of the global totals for BC, OC, CO and CH_4, and about 30% for SO_2, NO_X and NH_3. Emissions north of 60°N comprised about 0.5–1.5% of the global totals for all pollutants, and north of 70°N less than 0.1%.

The different emission inventories (see Table 5.4) were compared using the method described by Granier et al. (2011). The resulting ratios between the inventories with the highest and lowest emissions are shown in Table 5.5, with the magnitude of

the differences highlighted using color. Although the emission inventories included in the analysis are not exactly the same as those used by Granier et al. (2011), the ratios obtained in the present study for global 2000 and 2005 BC, SO_2, NO_X and CO are similar.

The ratio between the maximum and minimum emissions from different inventories generally increases with latitude. North of 40°N the ratio varied somewhat but was always below 2. However, for emissions north of 60°N and 70°N, the ratios were significantly higher, ranging from about 2 to over 10. The differences are probably due to different methodologies used to spatially distribute the emission data. They are also likely to reflect differences in total emissions arising from how some data about high latitude regions or sources such as flaring in oil and gas exploration and shipping are addressed (e.g. Stohl et al. 2013). At high latitudes the total emissions are lower and variability in emission estimates for regionally important source sectors translates into higher relative uncertainties than for the global perspective. The variability in emission estimates reflects uncertainties in key parameters, activities and emission factors, and further work is needed to improve their accuracy. More attention is also needed on identifying the location of high latitude sources and on improving the accuracy of the spatial distribution of emissions in the vicinity of and within the Arctic. Emission location is especially important when estimating the impacts of SLCFs, which are relatively quickly removed from the atmosphere and thus have higher concentrations close to their sources.

5.7 High-Arctic emission sources

This section focuses on two emission source sectors: Arctic shipping and flaring in the Arctic oil and gas industries (e.g. Corbett et al. 2010; Peters et al. 2011; Stohl et al. 2013; Winther et al. 2014). Characteristic for both sources are that the emissions occur at high latitudes and that activities in the Arctic associated with these sources may increase significantly in the future.

5.7.1 Arctic shipping

Both the thickness and extent of multi-year sea ice as well as the minimum extent of the sea-ice cover in the Arctic have declined over the past few decades (ACIA 2005; Arctic Council 2009; AMAP 2012; IPCC 2013b), and this decline is expected to continue as the Arctic continues to warm (IPCC 2013b). This is expected to result in the opening up of new shipping routes, such as the Northwest and Northeast Passages as well as polar routes across the North Pole between Europe/North America and Asia (Fig. 5.9), which are likely to decrease the travel distances between these regions by 25–50%. Corbett et al. (2010) estimated that in 2050, between 1.8% (Business as Usual scenario) and 5% (High Growth scenario) of the global ship traffic could shift to these new shipping routes.

Several Arctic shipping emission inventories exist. Corbett et al. (2010), referred to as 'C2010' in further discussion, published an Arctic shipping inventory for the year 2004 that includes BC and OC emissions from transit (international shipping) and fishing vessels based on shipping activity reported by Arctic Council

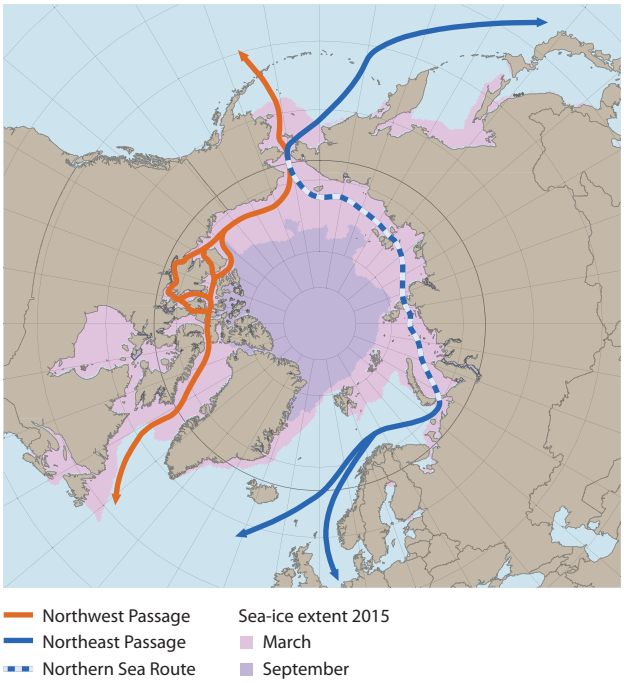

Figure 5.9 Arctic shipping routes and maximum and minimum sea-ice extent in 2015.

nations (Arctic Council 2009), and the most recent estimates of emission factors. Peters et al. (2011), referred to as 'P2011' in further discussion, estimated emissions from transpolar (transit) and in-Arctic petroleum extraction related shipping activities for the year 2004. Winther et al. (2014), referred to as 'W2014' in further discussion, published an emission inventory for the year 2012 drawing on satellite AIS (Automatic Information System) data for 13 different ship types with distinct ship activity, ship engine power functions, and emission factors. All discussion of shipping emissions in the Arctic in this chapter is based on these three emission inventories.

Direct comparisons of the estimates are not necessarily meaningful since there are important differences in the approaches used. Most notable are differences in shipping activity estimates, including which vessel types have been included and what area is considered Arctic. For example, P2011 did not include passenger ships or fishing vessels whereas C2010 and W2014 did. In addition, although the areas used by C2010 and P2011 are relatively similar, C2010 followed the definition of the Arctic region given by the Arctic Council Arctic Marine Shipping Assessment (Arctic Council 2009), while P2011 followed that of AMAP (e.g. AMAP 2011). In contrast, W2014 defined the area north of 58.95°N as Arctic. The W2014 Arctic region includes shipping activities in the Baltic Sea (e.g. Gulf of Finland and Gulf of Bothnia), not covered by the other two inventories, but excludes some areas in the North Atlantic and south of the Bering Strait which are covered by the other two inventories. All three inventories seem to have used relatively similar emission factors, except for SO_2, for which emissions are lower in W2014, reflecting the change in fuel sulfur content between 2004 (C2010, P2011) and 2012 (W2014).

Despite the differences in the approaches across these emission inventories, the orders of magnitude in Fig. 5.10 indicate that SO_2 and NO_X emissions from current Arctic shipping activities are approximately a third of those from other anthropogenic

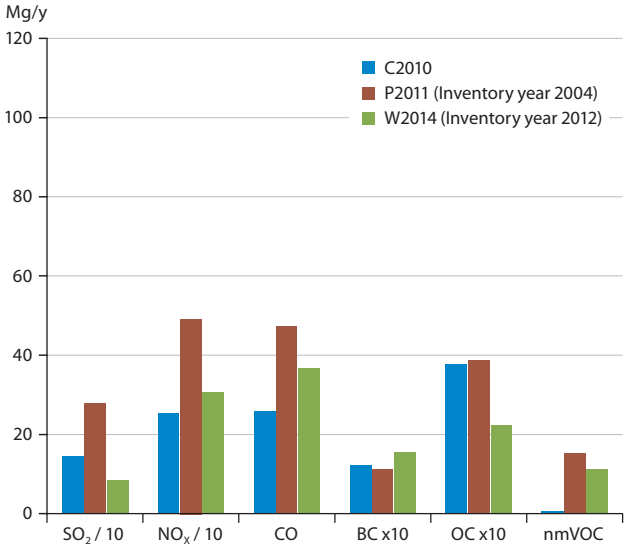

Figure 5.10 Comparison of Arctic shipping emission estimates for year 2004 or 2012 according to the emission inventories C2010 (Corbett et al. 2010), P2011 (Peters et al. 2011), and W2014 (Winther et al. 2014).

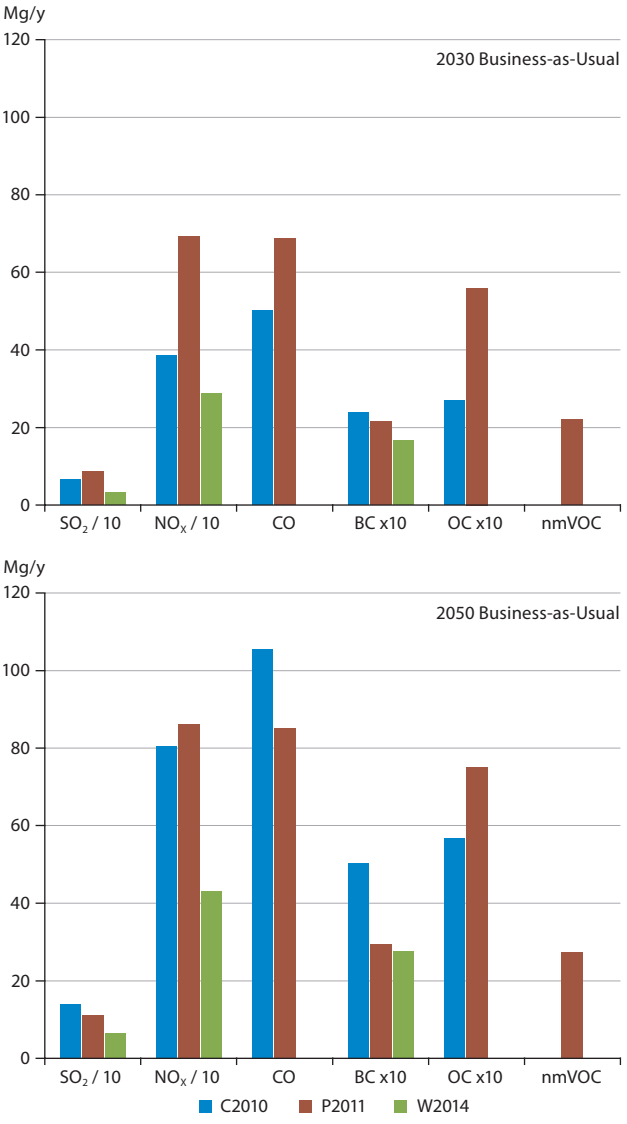

Figure 5.11 Projected change in Arctic shipping emissions for year 2030 (upper) and 2050 (lower) under a Business-as-Usual scenario for the emission inventories C2010 (Corbett et al. 2010), P2011 (Peters et al. 2011), and W2014 (Winther et al. 2014). Emissions include diversion/transit and exclude fishing vessels. P2011 excludes passenger ships.

emissions north of 60°N, and BC and OC shipping emissions are less than 5–10% (e.g. AMAP 2011 and discussion in Sect. 5.6).

The three emission inventories also projected emissions for 2030 and 2050. W2014 used the same scenarios of different ship type activities as C2010, while P2011 used several different models of future sea-ice conditions and cost benefit analyses to assess future shipping activity levels in the Arctic. All three included emission projections for the new shipping routes between Europe and Asia. W2014 also took account of expectations about future changes in energy efficiency changes in ships.

In the Business-as-Usual scenario, emissions are estimated to roughly double by 2030 relative to the base year (see Figs. 5.10 and 5.11). Most of the increase in shipping activity and emissions is due to the shift in global traffic away from the traditional routes into Arctic waters. In addition, traffic along routes within the Arctic area is expected to increase (Corbett et al. 2010; Peters et al. 2011; Winther et al. 2014). By 2050 in the Business-as- Usual scenario, C2010 projects a further doubling of emissions compared with 2030, while P2011 projects an approximate 1.3-fold increase (Fig. 5.11). W2014 projects emissions increases that fall between the two.

C2010 and W2014 also gave projections for a High-Growth scenario, which set an upper bound to the Arctic shipping emission estimates. In the High-Growth scenario the emissions could increase considerably and reached about the 2050 Business-as-Usual emission levels (Fig. 5.11) by 2030. Between 2030 and 2050 the emissions increased about four-fold (Fig. 5.12). The reason for the relatively high emission levels in the High-Growth scenario is mostly the increased shipping activity in the Arctic waters along the new shipping routes between Europe/North America and Asia, which would bring global shipping to Arctic waters. The emission levels in 2050 in the High-Growth scenario comprise a major share of the anthropogenic emissions north of 60°N.

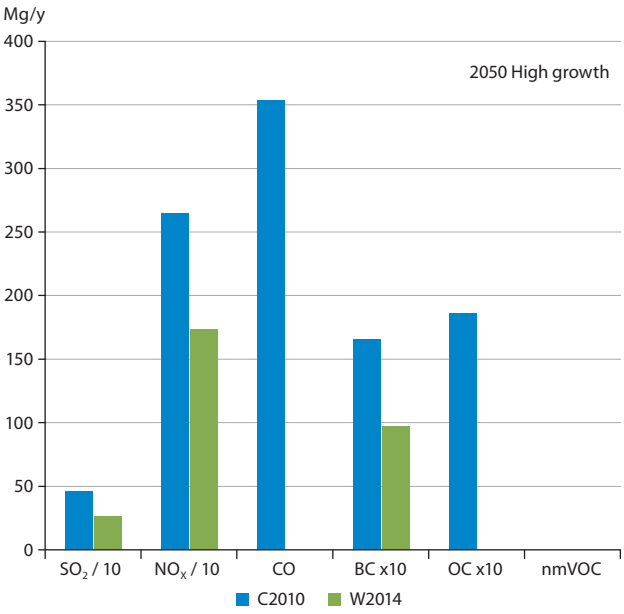

Figure 5.12 Arctic shipping emissions projected for year 2050 in the High-Growth scenario for C2010 (Corbett et al. 2010) and W2014 (Winther et al. 2014). Emissions include diversion/transit and exclude fishing vessels.

Det Norske Veritas (DNV) has also developed an inventory for 2012 shipping emissions, which is spatially distributed based on AIS data (Table 5.6) (DNV 2013). The emissions are calculated for the Arctic area as defined in the IMO Polar Code guidelines (IMO 2010) and shown in Fig. 5.13. The calculations highlight the sensitivity of the emission estimates to the definition of 'the Arctic'. The W2014 inventory is a factor of 29, 19 and 57 higher than the DNV inventory for BC, NO_X and SO_2, respectively and the difference appears to be related to the area defined as the Arctic.

Defining the Arctic as all the area north of 60°N makes a big difference in the amount of ship activity compared to the IMO Polar Code Guideline definition used in the DNV (2013) study. Total sailed distance inside the Arctic as defined in the IMO Polar Code Guideline is only 10–15% of the traffic amount north of 60°N. The ice-free areas around Iceland and north/west of Norway, not included in the IMO Polar Code guideline and the DNV study, constitute a major proportion of the ship traffic north of 60°N.

Table 5.6 Shipping emissions for 2012 according to the definition of the Arctic as defined by the IMO Polar Code guidelines. These emissions are about 3% higher than reported by DNV (2013) because they have not been corrected for the Russian nuclear fleet and icebreakers.

Compound	2012 emissions, tonnes
BC	54
OC	180
NO_X	16,440
SO_2	1550
PM	826
CO_2	957,100
CO	2230

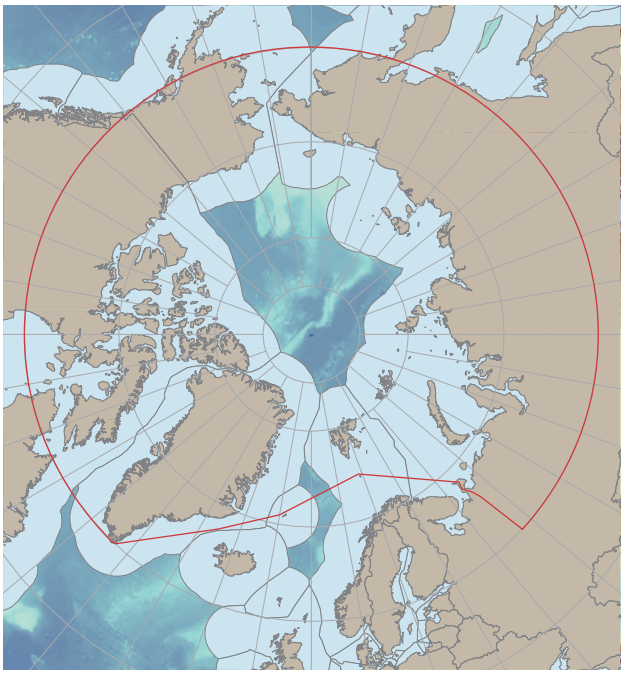

Figure 5.13 Arctic area as defined by the International Maritime Organization (IMO 2010) and Det Norske Veritas (DNV 2013).

5.7.2 Oil and gas activities in the Arctic

The first commercial oil and gas activities in the Arctic began in the 1920s and 1930s (AMAP 2007). Between the 1950s and early 1990 production increased rapidly (Peters et al. 2011), but the collapse of the former Soviet Union led to an 80% decline by the mid-1990s. Current oil and gas production is again close to its peak levels (Peters et al. 2011). More than 5% of the world's oil reserves, over 20% of the world's gas reserves, and a quarter of the undiscovered reservoirs occur in the Arctic, especially in Arctic Russia, so an increase in oil and gas activities in the Arctic area is possible (AMAP 2007). This poses a risk of increased emissions to the air.

Peters et al. (2011) estimated emissions of multiple pollutants from oil and gas extraction operations in the Arctic. However, their work did not identify specific emission factors for flaring, resulting in high uncertainty in areas with a high degree of flaring (Peters et al. 2011). Figure 5.14 shows oil and gas production in 2004, 2030 and 2050 in the Arctic in the reference scenario of Peters et al. (2011). This scenario assumes a future oil price of USD80 per barrel of oil equivalent, which would lead to a slight decline in total production until 2030 but an increase to 2004 levels by 2050. Figure 5.14 also shows the corresponding emissions for a range of air pollutants, assuming constant emission factors and assuming no advanced emission control technologies applied in the future. Emissions of CO and NO_X increase, whereas emissions for the other pollutants follow the trend in production. According to Peters et al. (2011) there is a relatively high potential for emission reductions: as much as 60–90% depending on the pollutant by 2050, assuming the adoption of advanced control technologies across the Arctic region.

In the oil and gas industry's offshore and onshore sites, production installations, and refineries, the excess gaseous and liquid hydrocarbons associated with production are either released directly to the atmosphere via venting or flaring, or are recovered and used. Ideally, both venting and flaring

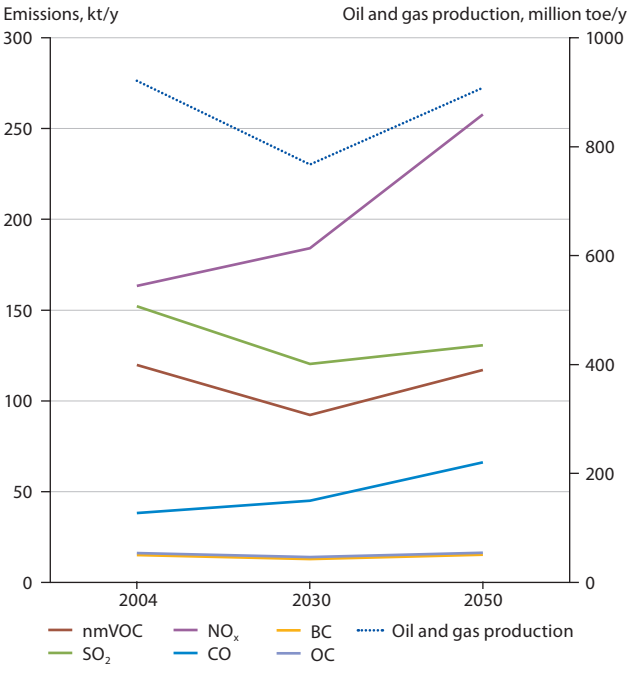

Figure 5.14 Projected oil and gas production in the Arctic region and associated emissions of selected air pollutants (Peters et al. 2011).

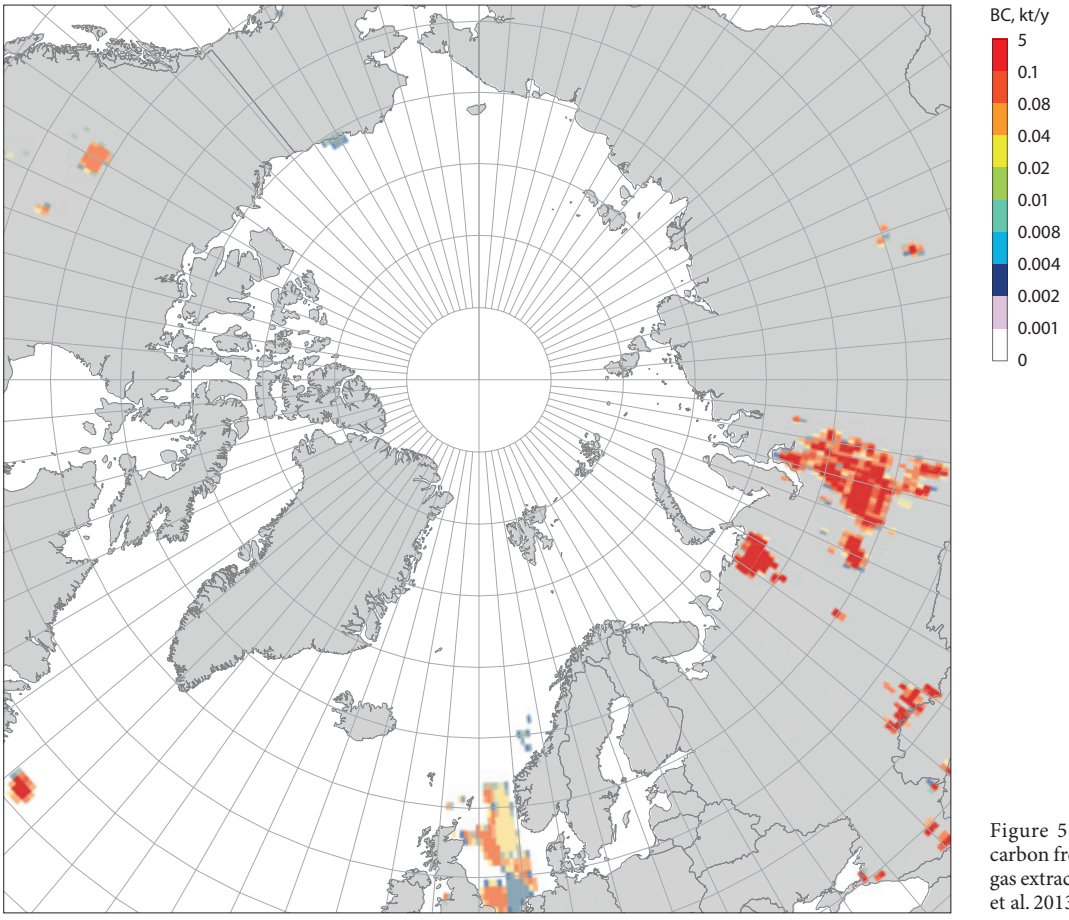

Figure 5.15 Emissions of black carbon from flaring during oil and gas extraction activities (after Stohl et al. 2013).

should be eliminated in favor of recovery and utilization, but in Arctic conditions this can be challenging. Venting emissions are flammable and a major source of CH_4, so flaring is often the preferred alternative for safety and climate impact considerations, that is, carbon dioxide has a lower global warming potential than CH_4 (which is a major component of vented gas). However, flaring may be a significant source of black carbon in the Arctic (Stohl et al. 2013).

AMAP (2011) discussed flaring as an emissions source that could affect the Arctic due to the high latitude location of some of the exploration areas. The report presented a first estimate of emissions in the Arctic nations based on a calculation using the IIASA-GAINS model (Arctic Council 2011; AMAP 2011). However, the AMAP assessment was limited because the spatial distribution of the Arctic flaring activities at the time was highly uncertain. Also, Peters et al. (2011) noted that emission factors in areas with a high degree of flaring were more uncertain. Since then, better spatial proxies have been developed using, for example, satellite images and this seems to have resulted in improved consistency between measurements and modeling data (Stohl et al. 2013). The updated results are included in the present study and discussed in the Arctic Council context in Sect. 5.5.

Stohl et al. (2013) found that BC emissions from flaring estimated with the GAINS model accounted for a relatively large fraction of the overall Arctic BC emissions in 2010: 33% north of 60°N and 66% north of 66°N. The emissions were concentrated in the large oil and gas extraction areas of northwestern Russia (Fig. 5.15). For comparison, the contributions to the global total and to emissions north of 40°N were much less at 3% and 6%, respectively. The total amount of BC from flaring was estimated at 52,000 tonnes north of 60°N and 26,000 tonnes north of 66°N (Stohl et al. 2013), which indicates, despite the different definitions of the Arctic area, higher emissions from flaring than estimated by Peters et al. (2011) for all oil and gas activities. The analysis by Stohl et al. (2013) showed that including flaring emissions in high northerly latitudes with daily varying emissions from residential combustion resulted in a better match between modeled and observed concentrations of BC in the Arctic. However, as Stohl et al. (2013) pointed out, there are still significant uncertainties in quantifying BC emissions from flaring.

Carbon Limits addressed associated petroleum gas flaring in Russia, Kazakhstan, Turkmenistan and Azerbaijan (Carbon Limits 2013). Flared volumes were estimated to be at least double the volumes in the national statistics. In the case of Russia, which is the largest producer of associated petroleum gas, the satellite data indicate approximately 38 billion cubic meters flared in 2010 (http://ngdc.noaa.gov/eog/interest/gas_flares.html) while the national statistics report around 17 billion cubic meters. The study suggests three contributory causes for the discrepancies: uncertainties from the satellite estimates, difference of scope between the satellite and the national estimates, and uncertainties in national statistics due to the lack of gas flaring measurements.

In addition to uncertainty in flared volumes from many countries there is a lack of reliable emission factors, particularly for BC. It is unclear whether petroleum-producing countries other than Norway have attempted to estimate BC emissions from flaring. In Norway, flaring is only permitted for security

reasons, and the flared volumes and the composition of the gas are relatively well known. The BC emission factor was taken from the literature (McEwen and Johnson 2012). It is acknowledged that this factor is not representative of the flaring conditions in Norway, but such that better emission factors were not available (Carbon Limits 2013).

5.8 Open biomass burning

AMAP addressed open biomass burning in the Arctic context (AMAP 2011, and references therein) and noted some key characteristics: (i) fire regimes of open biomass burning are under notable human influence (e.g. human ignition as well as extinction and prevention, changes in forestry practices); (ii) fire regimes are also under strong direct climate influence, for instance in the remote parts of boreal forests, or when specific weather patterns lead to uncontrollable burning; (iii) climate change and atmospheric CO_2 concentration will affect future fire regimes (including intensity, severity, location and seasonality); (iv) fire activities from forest and grassland fires are concentrated spatially and seasonally, which reflects (especially in the case of fires from managed grassland) anthropogenic burn practices, as well as the co-occurrence of dry litter and ignition sources; (v) in the boreal zones north of 60°N, fires occur most often between March and October; (vi) significant interannual variations in the occurrence and scale of boreal wildfires have been identified for many geographic regions in response to climatic and weather variation; and (vii) direct policy measures to reduce open biomass burning can only be of limited influence, by targeting, for instance, the time of burning.

Whether ignited by anthropogenic or natural (e.g. lightning) causes, open biomass burning in ecosystems surrounding and within the Arctic is a substantial contributor of air pollutant emissions. Not only are emissions from fires within the Arctic important, but the Arctic atmosphere can be impacted by fires far from the region. Wildfires can effectively inject emissions higher up into the atmosphere than other ground-based emission sources. Depending on the scale of the fire, fire plumes may penetrate the top of the boundary layer and so pollute the upper troposphere and even the stratosphere, where residence times are much longer and the pollutants can be transported greater distances (AMAP 2011).

Emissions from open burning are dependent on the location and size of the burn, the type of vegetation burned, and the amount of pollutant emitted per mass of fuel burned. Fire emission inventories are often derived using a bottom-up approach, such as combining satellite remote sensing information with a biogeochemical model (AMAP 2011). Fire location, timing and burned area can be derived from remote sensing products and combined with information on vegetation type and cover and a biogeochemical model of vegetation productivity to estimate the amount of plant material available for combustion. Plant or vegetation-specific emission factors are used to estimate the amount of pollutant emitted per mass of fuel burned. The spatial and temporal resolution of inventories depends on the resolution of the underlying remote sensing products. Despite the advances in remote sensing products used to develop fire emission inventories, the emission estimates remain highly uncertain. Sources of uncertainties in these emission inventories include the underestimation of area burnt, an over- or underestimation of combusted biomass, and use of emission factors that do not distinguish plant or fire types correctly.

Table 5.7 shows global emission estimates of biomass burning in 2005 by GFAS (Kaiser et al. 2012), GFED2 (van der Werf et al. 2006), GFED3 (van der Werf et al. 2010), GICC (Mieville et al. 2010), MACCity (e.g. van der Werf et al. 2006; Lamarque et al. 2010) and FINN (Wiedinmyer et al. 2011). Biomass burning emissions account, on average, for approximately 50% of BC, 150% of OC, 3% of SO_2, 16% of NO_X, 70% of CO, 21% of NH_3, and 7% of CH_4 emissions from anthropogenic sources shown in Fig. 5.2. The variability between the maximum and minimum emission estimates for global biomass burning is 1.4–2.3 times depending on the pollutant.

Table 5.8 shows the emissions from biomass burning north of 60°N in 2005 extracted from the same inventories as for Table 5.7. There is considerably more variability between the emission estimates north of 60°N with ratios of 4–7.5 between the maximum and minimum estimate. The emissions north of 60°N account for about 1–11% of the global total emissions from biomass burning (Table 5.9) depending on the pollutant and the inventory.

5.9 Uncertainties in emissions estimates

Most of the emission estimates presented in this chapter rely on methodologies in which the emissions are calculated by combining information on fuel use or other activities with emission factors that define emissions per unit of activity. Activity data used for creating emissions inventories typically originate from international organizations and national statistics, and emission factors originate from published measurements or a synthesis of such measurements. The emission estimates are limited by the availability and completeness of data, both for activities as well as emission factors (Amann et al. 2013; Bond et al. 2013).

Global emissions of NO_X and SO_2 are considered to be relatively well understood, with uncertainties within 10–40% (Amann et al. 2013). For BC, OC, CO and nmVOC the uncertainties are more significant (Amann et al. 2013). For example, Bond et al. (2013, 2004) estimated that the uncertainty in global anthropogenic BC emissions is about a factor of two. The factors contributing to the BC emission uncertainty are discussed by Bond et al. (2013).

In spatially and temporally distributed emission inventories, uncertainty is also introduced via the inaccuracies in the proxy data used to distribute the emissions by location and time, as discussed in previous sections of this chapter. For regional emission estimates the uncertainties can be higher or lower than for global emission estimates depending on, for example, data availability and data quality. Section 5.6 noted higher relative differences between emissions estimates for high latitudes compared to global estimates and concluded this to be an outcome of inaccuracies in the spatial representation of emissions, as well as generally lower total emissions combined with a high variability in emission estimates for regionally important source sectors. In general it is important to study and acknowledge the uncertainties as well as to continuously and systematically work towards narrowing these uncertainties in order to generate more robust emission estimates in the future.

Table 5.7 Emission estimates for global emissions from biomass burning in 2005 (Tg/y), plus the ratio of maximum to minimum estimate for each pollutant.

	GFAS	GFED2	GFED3	GICC	MACCity	FINN	Ratio of maximum to minimum estimate
BC	2.0	2.8	2.2	3.9	2.6	2.3	1.76
OC	18	22	18	31	22	23	1.67
SO_2	2.3	na	2.4	3.0	3.6	2.5	1.50
NO_X	10	12	10	13	11	13	1.33
CO	358	415	357	504	504	375	1.41
NH_3	na	na	na	6.9	10	4.5	2.31
CH_4	20	21	19	26	25	18	1.42

Table 5.8 Emission estimates for biomass burning north of 60°N in 2005 (Tg/y), plus the ratio of maximum to minimum estimate for each pollutant.

	GFAS	GFED2	GFED3	GICC	MACCity	FINN	Ratio of maximum to minimum estimate
BC	0.08	0.05	0.09	0.22	0.03	0.03	7.48
OC	1.4	0.5	1.4	2.2	0.6	0.55	3.99
SO_2	0.15	na	0.16	0.35	0.22	0.06	5.77
NO_X	0.5	0.3	0.5	1.1	0.2	0.28	5.37
CO	19	8	17	38	38	7	5.44
NH_3	na	na	na	0.5	0.9	0.14	6.17
CH_4	1.1	0.3	0.7	1.7	1.0	0.3	5.51

Table 5.9 Percentage share of biomass burning emissions north of 60°N from global total emissions in 2005.

	GFAS	GFED2	GFED3	GICC	MACCity	FINN
BC	4	2	4	6	1	1
OC	8	2	8	7	3	2
SO_2	7	na	6	11	6	2
NO_X	5	2	5	8	2	2
CO	5	2	5	8	8	2
NH_3	na	na	na	7	8	3
CH_4	6	2	4	6	4	2

5.10 Key findings

- The contribution of anthropogenic emissions in the ECLIPSE inventory from Arctic Council nations to global totals is about 10% for BC and ranges from 5% for OC to 23% for NO_X. All other co-emitted aerosol and ozone precursors fall within this range.
- Sulfur emission reductions implemented to improve air quality are enhancing climate warming. A mitigation strategy which also reduces SLCF components (especially CH_4 and BC) could help offset this warming, especially in the Arctic.
- A mitigation case study indicates there is considerable potential for reducing global and Arctic Council SLCF emissions beyond the current emission legislation. Provided that the full reduction potential of all available reduction measures could be mobilized, a focused SLCF policy would result in further BC emission reductions of up to 70–80% by 2030 in all world regions, including the Arctic region. Significant reductions in ozone precursors would also occur. The measures included in the SLCF-focused emission reduction policy do not affect SO_2 emissions, but OC reductions would be significant, up to 60–70%. The greatest reductions could be achieved by mobilizing reduction measures in the residential and commercial sector, flaring in the oil and gas industries, transport and agricultural waste burning.
- Flaring emissions of SLCFs are potentially very large in and near the Arctic, but uncertainties for this source are high, as neither flaring volumes nor emission factors are well known. One previous study and this assessment suggest a large impact of flaring emissions on Arctic BC.
- On average, biomass burning emissions account globally for approximately 50% of BC, 150% of OC, 3% of SO_2, 16% of NO_X, 70% of CO, 21% of NH_3, and 7% of CH_4 emissions from anthropogenic sources. Emissions north of 60°N account

for about 1–11% of the global total emissions from biomass burning, depending on the pollutant and the inventory.

- There are significant uncertainties in emission estimates of key short-lived species, especially black carbon. A comparison of global emission datasets indicated high relative differences between the estimates in high latitudes which is an outcome of inaccuracies in the spatial representation of emissions, as well as high variability in emission estimates of individual source sectors, important for the region.

6. Atmospheric transport of short-lived climate forcers to and within the Arctic

Lead author: Andreas Stohl
Authors: Maria Sand, Steve Arnold, Alexander Baklanov, Knut von Salzen

6.1 Introduction

As the emissions of short-lived climate forcers (SLCFs) within the Arctic (north of 67°N) are currently small compared to other world regions (see Ch. 5), the Arctic SLCF budget is mainly a balance between atmospheric import of SLCFs from source regions outside the Arctic, transformation and removal within the Arctic, and export of remaining SLCFs to mid-latitudes. The purpose of this chapter is to describe the relevant transport and removal processes. As transport of black carbon (BC) was covered extensively by AMAP (2011), its description here has been shortened but new results added, especially with respect to SLCFs other than BC. Removal processes are also covered in greater detail here than in the previous AMAP report (AMAP 2011).

6.2 Conceptual overview of transport processes

Surfaces of constant potential temperature form shells over the Arctic, with minimum values in the Arctic boundary layer, thus building the so-called polar dome (Fig. 6.1) (Klonecki et al. 2003; Stohl 2006). Strong inversions lead to extremely high static stability of the air mass inside the dome, with associated low turbulence intensities (Strunin et al. 1997; Zilitinkevich and Baklanov 2002; Zilitinkevich et al. 2002). This limits the vertical exchange between the boundary layer and the free troposphere and leads to slow dry deposition of pollutants to the ground. While the inversions are often surface-based in winter, a cloud-topped shallow boundary layer forms in summer, where turbulence can be generated due to radiative cloud-top cooling and interaction with gravity waves. Dry deposition, especially over open leads in the sea ice, reduces BC concentrations near the ground and produces a positive vertical gradient of BC (Spackman et al. 2010). In fact, aircraft and helicopter measurements during POLARCAT (Polar Study using Aircraft, Remote Sensing, Surface Measurements and Models of Climate, Chemistry, Aerosols and Transport; Law et al. 2014) and ASCOS (Arctic Summer Cloud Ocean Study; Tjernström et al. 2014) have shown that strong pollution layers resulting from long-range transport were present in the High Arctic in spring and summer 2008 only above the sea-ice inversion layer and did not reach the (sea-ice) surface (Brock et al. 2011; Kupiszewski et al. 2013). The stable stratification also prevents constituents emitted locally from reaching the free troposphere. This often means that for the aerosol population near the surface, local sources are more important than long-range transport (Kupiszewski et al. 2013). Such sources include bubble bursting in open leads, emission of dimethyl sulfide (DMS) from phytoplankton in the marginal ice zone (DMS oxidation products can condense onto existing aerosols) or the release of accumulation-mode particles from evaporating cloud droplets. As a result, measurement data collected at Arctic surface stations or by ships is not necessarily representative for the Arctic troposphere as a whole (see Ch. 8 for more details).

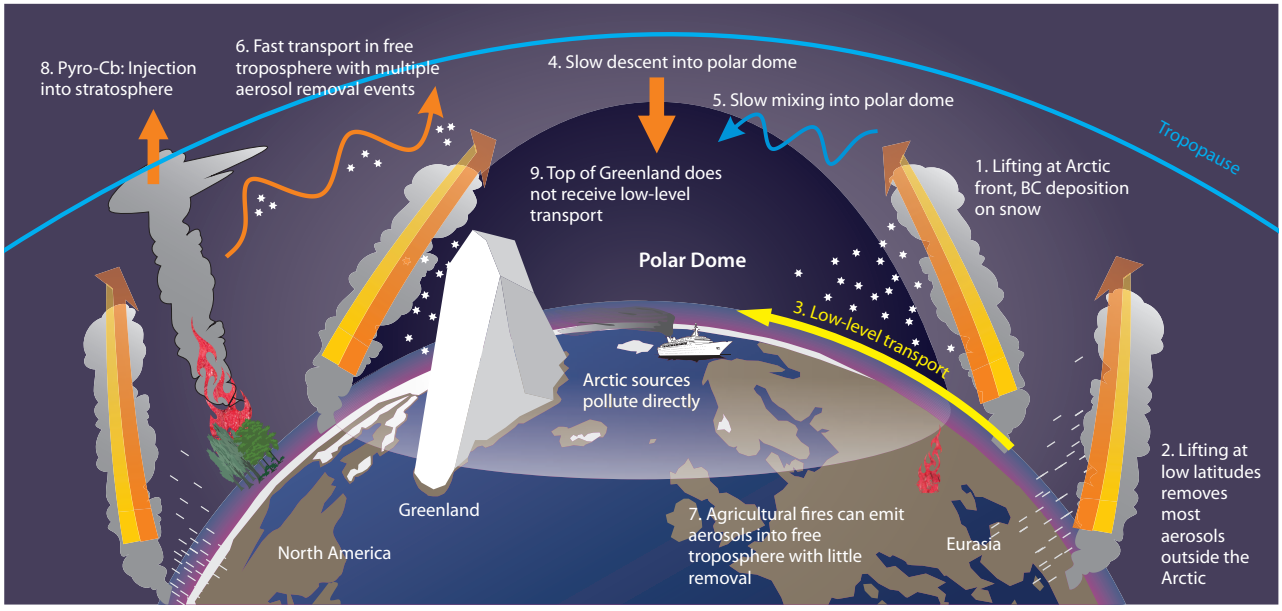

Figure 6.1 Schematic illustration of processes relevant for transport of trace pollutants into the Arctic based on the study by Stohl (2006), from AMAP (2011). In reality, the polar dome is asymmetric and its extent is temporally highly variable. In addition, its southernmost extent is greatest over Eurasia. The placement of the polar dome is more typical of the winter/spring situation, whereas in summer the dome is much smaller. Also note that the dome is not homogeneous but is itself highly stratified with strong vertical gradients.

The Arctic lower troposphere is also isolated towards lower latitudes, by a transport barrier called the 'Arctic front' (Barrie 1986), which shifts seasonally as shown in Fig. 6.2. For polluted air to reach the lower troposphere in the Arctic on time scales shorter than a few weeks, the pollution source regions must be sufficiently cold and thus located north of the Arctic front. This situation only occurs in winter and early spring over northern Eurasia where the Arctic front can be located as far south as 40°N in January (Barrie 1986; see also Fig. 6.2). Strong diabatic cooling of the air at the snow-covered surfaces not only helps to establish the polar dome itself but also allows polluted air containing aerosols and ozone (O_3) precursors from northern Eurasia to cross the entire Arctic at low altitudes on time scales of 10 to 15 days (Stohl 2006; pathway 3 in Fig. 6.1).

Pollution emitted into the relatively warm air masses south of the Arctic front can reach the Arctic only by (approximately) following sloping surfaces of constant potential temperature (isentropic surfaces) upwards into the Arctic middle or upper troposphere, that is, pathways 1 and 2 in Fig. 6.1 (Carlson 1981; Heintzenberg 1982; Iversen 1984; Barrie 1986). The lifting is typically associated with cloud formation and precipitation by which soluble pollutants and aerosols can be scavenged from the atmosphere. This is almost the only pathway by which emissions from the densely populated areas of eastern North America and southeastern Asia can reach the Arctic (Stohl 2006). Most wet deposition, however, occurs along the North Atlantic or North Pacific storm tracks (at the so-called polar front, not to be confused with the Arctic front) south of the Arctic (pathway 2). Lifting at the Arctic front where aerosol is more likely to be deposited over snow and ice surfaces (pathway 1), occurs only if the source regions are further north (Europe, eastern Asia). Indeed, BC mass concentrations in snow samples taken in different parts of Arctic Eurasia are on average a factor of three to four higher than concentrations in snow in Arctic Canada (Doherty et al. 2010).

Figure 6.2 The mean position of the Arctic air mass in winter (January) and summer (July) according to Li et al. (1993), superimposed on the frequency of major poleward transport routes (Iversen 1996).

Air can also penetrate the polar dome by slow descent from above (pathway 4) and by incorporation of extra-Arctic air via mixing into the polar dome (pathway 5). Both pathways require radiative cooling, which is a slow process (about 1 K/d). Descent from the upper troposphere to the surface typically takes several weeks. Air participating in this descent involves a mixture of background air that has been cleaned during (often several cycles of) uplift (pathway 6), stratospheric air, as well as agricultural (pathway 7) and wildfire plumes (pathway 8) from various mid-latitude source regions (Warneke et al. 2009, 2010; Brock et al. 2011). The biomass burning plumes are often injected to higher altitudes directly above the source and are thus often not subject to equally efficient deposition processes. The probability of stratospheric air (and thus O_3) reaching the Arctic surface within 10 days varies between only about 0.1% and 1%, with highest values in winter and spring (Stohl 2006), but it reaches the mid-troposphere more quickly.

Biomass burning plumes from fires outside the Arctic follow transport pathways to the Arctic that depend on the injection height of the plume. Fire-driven convection can inject aerosols and O_3 precursors directly into the free troposphere (pathway 7) and even the stratosphere (pathway 8), thus reducing the efficiency of dry and wet deposition. This results in distinct aerosol layers in the high-latitude free troposphere, which subsequently can be incorporated into the polar dome via pathways 4 and 5. In fact, strong pollution layers consisting of a mix of anthropogenic and biomass burning pollution have been found in the Arctic upper troposphere and lower stratosphere (Roiger et al. 2011), with O_3 probably originating both from the stratosphere and photochemical O_3 production. Warm conveyor belts associated with mid-latitude cyclones (Eckhardt et al. 2004) are mainly responsible for the upward lifting into the high-latitude upper troposphere (Harrigan et al. 2011; Sodemann et al. 2011).

Owing to these different transport pathways, the pollutant source regions for Arctic receptor locations near the surface differ from those in the middle or upper troposphere (Hirdman et al. 2010b). Figure 6.3 shows the footprint emission sensitivity for four Arctic monitoring stations for transport times of up to 20 days. The station Summit on Greenland (3216 m above sea level) is much less sensitive to surface emissions (excluding local emissions from the snow pack or camp pollution) in the Arctic than the other stations but is more sensitive to emissions at low latitudes. This is due to the high altitude of the Greenland Ice Sheet, which is located far above the lower shells of the polar dome (pathway 9). BC or other pollutant records obtained from high-altitude Greenland ice cores (McConnell et al. 2007) may therefore not be representative for lower altitudes.

Radiative forcing is determined not only by surface air concentrations of SLCFs but also by their concentrations higher in the troposphere and – in the case of BC – by concentrations in the snow. Therefore, attribution of radiative forcing must consider all the various transport pathways, not only those relevant for

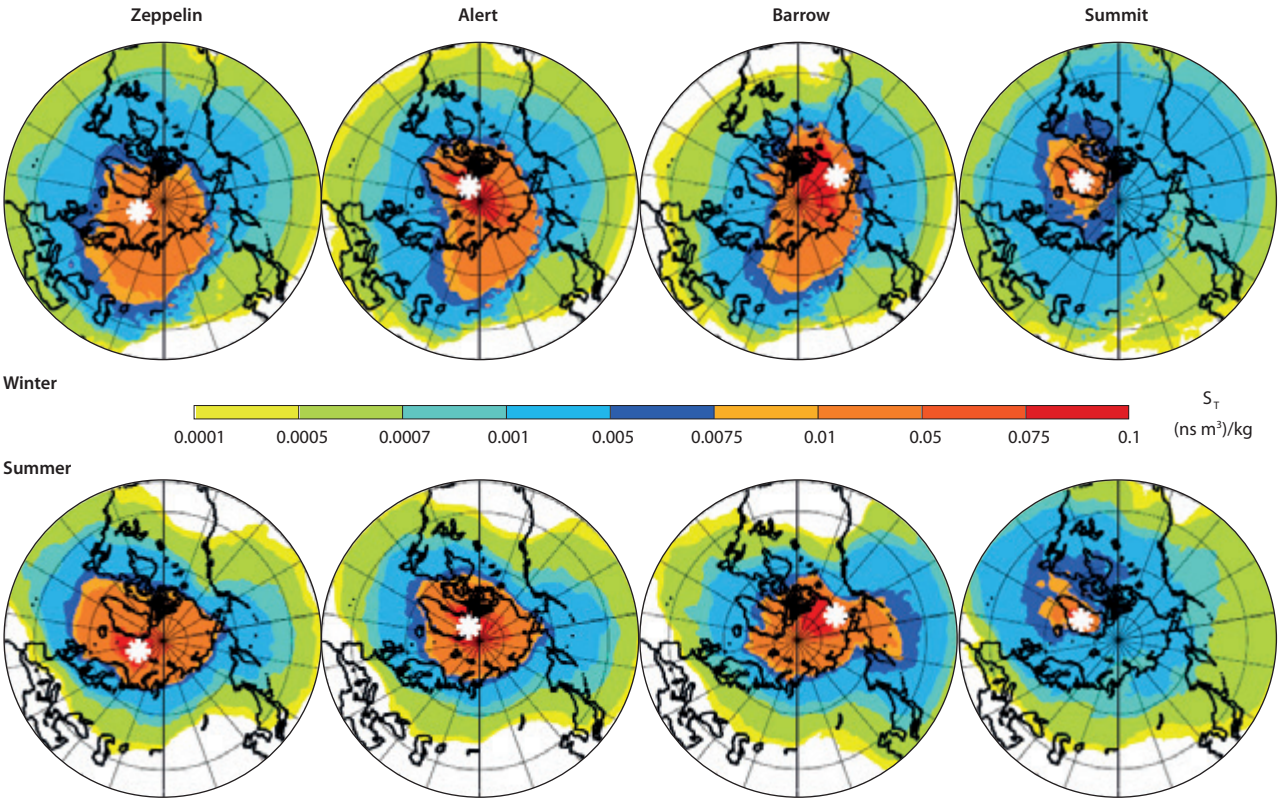

Figure 6.3 Transport climatologies of emission sensitivities for winter (upper row) and summer (lower row) for four Arctic monitoring stations for the years 2000–2007. Station locations are marked by a white asterisk. Source: Hirdman et al. (2010b).

BC or other aerosols measured near the surface and which have been the focus of most past work (e.g. Sharma et al. 2006; Eleftheriadis et al. 2009; Hirdman et al. 2010b). Since O_3 and its precursors are not efficiently wet scavenged, Arctic tropospheric O_3 can show strong sensitivities to lower latitude sources in the upper troposphere (e.g. lightning, aircraft emissions), in addition to higher latitude Eurasian sources in the lower troposphere (Wespes et al. 2012). In addition, it is important to note that BC deposited to Arctic snow (Doherty et al. 2010) can originate from dry deposition (Spackman et al. 2010) as well as wet scavenging from higher altitudes. The sources of BC in Arctic snow will therefore be a mixture of the sources contributing to near-surface air and sources contributing to altitudes at and below cloud level.

The transport pathways also vary seasonally. In winter, the Arctic front is located much further south than in summer (Barrie 1986; Heidam et al. 2004; see Fig. 6.2), especially over Eurasia. This allows emissions from high-latitude Eurasia to enter the Arctic (here loosely defined as the area north of 67°N) via the low-level transport route, pathway 3. In summer, the Arctic front approximately follows the northern coastline of Eurasia (Fig. 6.2), which eliminates this pathway. This is clearly visible in seasonal maps of nighttime aerosol extinction derived from space-borne lidar measurements for different height layers (Di Pierro et al. 2013, their fig. 10). The northward retreat of the Arctic front is one of the reasons why aerosol concentrations in the Arctic are much lower in summer than winter (Stohl 2006). However, increased efficiency of wet scavenging in summer is also important for driving the seasonal cycle of aerosols (Garrett et al. 2010). Since O_3 is produced photochemically in the troposphere, sensitivity of Arctic O_3 to different source regions depends on seasonal changes in both the transport pathways and in the balance between production and loss processes (Hirdman et al. 2010b) (see discussion in Section 6.4).

Transport pathways to the Arctic vary considerably on interannual time scales. The North Atlantic Oscillation (NAO), a redistribution of atmospheric mass between the Arctic and the subtropical Atlantic (Hurrell 1995) and a prominent pattern of atmospheric variability in the northern hemisphere, is particularly important in this respect. For instance, during the positive phase of the NAO, transport from all three northern hemisphere continents (Europe, North America and Asia in order of the magnitude of the NAO transport variability signal) into the Arctic is enhanced (Duncan and Bey 2004; Eckhardt et al. 2004). The efficiency of transport from the mid-latitudes into the Arctic influences the interannual variability of Arctic BC mass concentrations (e.g. Gong et al. 2010; Hirdman et al. 2010a), but the trends in transport are not strong enough to drive the overall decadal BC and sulfate trends in the Arctic (Hirdman et al. 2010b). These concentration trends must therefore be mainly due to emission changes (Hirdman et al. 2010b).

The idealized concept outlined above can be perturbed. For instance, in the summer of 2012 the unusual passage of a cyclone deep into the Arctic caused destabilization of sea ice (Zhang et al. 2013) and probably also brought lower-latitude air into the Arctic and led to large-scale stirring of air within the Arctic. While the summer 2012 cyclone was an extreme event, cyclones are quite common in the Arctic in winter.

While transport of pollution into the Arctic has been high on the research agenda, outflow of Arctic air into the mid-latitudes can also be of interest. For instance, during a ship cruise Gilman et al. (2010) observed air over the sub-polar North Atlantic Ocean that was depleted in O_3 as a result of Arctic tropospheric O_3 depletion and Heintzenberg et al. (2003) observed Arctic Haze over Central Europe.

6.3 Seasonality and removal mechanisms

Near the surface, the concentrations of most SLCFs (aerosols but also many gas-phase species like carbon monoxide, CO) peak during the Arctic Haze season in winter and early spring and are lowest in summer (see Ch. 8). The build-up of Arctic Haze is generally attributed to the inefficiency of removal processes during winter (Shaw 1995). This includes lower oxidation rates due to lower hydroxyl (OH) radical concentrations in dark winter periods leading to accumulation of, for example, volatile organic compounds (VOCs or CO) in the Arctic during winter and early spring. Based on the analysis of observation data, Garrett et al. (2010, 2011) argued that aerosol seasonality in the Arctic is controlled by seasonal differences in wet scavenging. In particular, warm rain and drizzle production at temperatures above freezing in summer seems to be associated with efficient scavenging of aerosols (Garrett et al. 2010). The wet scavenging efficiently removes accumulation-mode aerosol, thus also shaping the aerosol number size distribution (Tunved et al. 2013). However, it is also important to notice that the slow transport in summer leads to longer exposure of aerosols to precipitation before they reach the Arctic than in winter (Stohl 2006). This would lead to lower Arctic aerosol concentrations even if the scavenging efficiency itself was constant. Tropospheric O_3, driven by photochemistry and transport, is not subject to wet removal processes and thus its seasonal cycle does not follow this pattern (see Ch. 3). On the other hand, many nitrogen oxide (NO_X) or oxidant reservoir species, important for O_3 photochemistry, are subject to wet (and dry) removal (e.g. nitric acid, formaldehyde).

Quantification of the overall strength of pollutant removal and the relative contributions by different processes ultimately requires model simulations. However, models have long struggled to reproduce the seasonal cycle of aerosols in the Arctic and have generally strongly underestimated the peak aerosol concentrations during the Arctic Haze season (Shindell et al. 2008; Koch et al. 2009b; AMAP 2011). While problems remain, there has been a lot of progress and current models capture aerosol seasonality much better than the previous generations (e.g. Liu et al. 2011; Browse et al. 2012; Sharma et al. 2013; Breider et al. 2014). The models used in this assessment are evaluated in Ch. 8.

Recent studies have shown that the simulated aerosol seasonality is strongly dependent on how aerosol removal processes are represented in a model. For instance, Vignati et al. (2010) found that changes in a model's aerosol scheme (i.e. treatment of microphysical properties, size distribution and atmospheric removal of BC) alone can change simulated concentrations by more than an order of magnitude in remote regions such as the Arctic. Implementing a realistic aerosol microphysical scheme in another model increased the simulated Arctic BC mass concentrations near the surface in winter, which is in better agreement with the observations – however, at the same time it exacerbated model overestimates at higher altitudes (Lund and Berntsen 2012).

Liu et al. (2011) found that calculated Arctic BC mass concentrations were very sensitive to parameterizations of BC aging (conversion from hydrophobic to hydrophilic properties) and wet scavenging. Figure 6.4 shows a comparison of measured and simulated surface BC mass concentrations for three Arctic stations using the Liu et al. (2011) original model version and the version with improved BC aging and deposition parameterizations. Winter concentrations of BC in the Arctic simulated with the improved model are increased by a factor of 100 throughout the tropospheric column and the seasonality in concentrations is more in line with observations. Huang et al. (2010a) also found that enhanced below-cloud scavenging led to much improved simulations of the BC seasonal cycle.

Another model study attributed the seasonal decrease of aerosol concentrations from winter to summer in the Arctic to the different efficiency of scavenging by different types of clouds. There is a transition from ice-phase cloud scavenging in winter to more efficient warm cloud scavenging in summer, and there is also the appearance of warm drizzling cloud in the late spring and summer boundary layer (Browse et al. 2012). Including

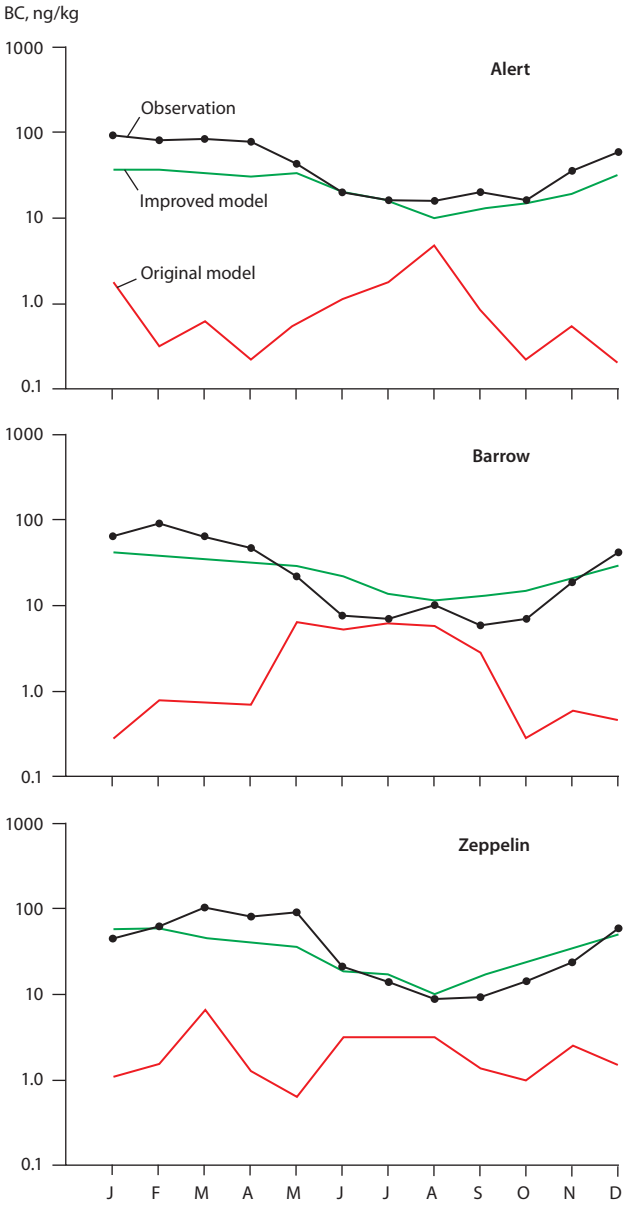

Figure 6.4 Monthly averaged concentrations of measured equivalent BC and simulated (red line represents results from original AM3 model and green line improved AM3 model) BC at the surface at Alert (Canada), Barrow (Alaska) and Zeppelin (Ny-Ålesund, Svalbard). Measurements were made between 2000 and 2007. The simulations use observed sea ice and sea-surface temperature from 1996 to 2000. Source: Liu et al. (2011).

these processes in a model clearly improved model performance both in terms of absolute concentrations as well as seasonality for BC and sulfate (Fig. 6.5). This also seems to be in agreement with the observation-based findings that scavenging efficiencies increase in summer both for light-scattering as well as for light-absorbing aerosols (Garrett et al. 2010, 2011). Another modeling problem may be excessive convective transport and underestimation of the associated wet scavenging in convective clouds, which can lead to model overestimates of BC in the upper troposphere and lower stratosphere (Allen and Landuyt 2014; Wang et al. 2014a).

The relative importance of dry versus wet deposition is also still not well understood. While Bourgeois and Bey (2011) estimated global and Arctic annual BC loss by dry deposition at only 2% of the total loss, other studies find much higher fractions. For instance, Sharma et al. (2013) found that dry deposition contributes between about 10% (in summer) and some 70% (in winter) to total BC deposition in the Arctic. Huang et al. (2010a) found that the seasonal cycle of Arctic BC mass concentrations is controlled by below-cloud scavenging which accounts for 48% of all BC removal in the Arctic, but that both in-cloud scavenging (27%) and dry deposition (25%) were also important.

Similarly, models generally underestimate Arctic CO concentrations in winter and spring at the surface (Shindell et al. 2008). Recently, Monks et al. (2015) showed that this low CO bias persists through the depth of the Arctic troposphere based on comparisons with aircraft and satellite observations. This study demonstrated that inter-model differences in Arctic CO burdens were likely to be explained more by model differences in CO oxidation by OH than differences in transport from mid-latitudes. However, the universal underestimate of CO by models is more likely to be due to emission errors or transport errors common across all models. Mao et al. (2013) suggested that heterogeneous loss of the hydroperoxyl (HO_2) radical onto aerosol particles can increase CO at high latitudes (through resultant OH decreases) to be more consistent with observed concentrations; however it is not yet clear if this process is fully consistent with observations of O_3.

6.4 Source regions and source types

Determining the source regions and/or source types of Arctic SLCFs is challenging. Five types of approach have generally been used: detailed case studies; statistical analysis of measurement data; statistical analysis of trajectories, often in conjunction with measurement data; inverse modeling and solving the adjoint problem for source term determination; and explicit calculation of SLCF source contributions with global chemistry transport models. For secondary pollutants, such as tropospheric O_3, there are additional challenges in understanding not only the sources of precursors and their transport, but also non-linear photochemical processes during transport to the Arctic or within the Arctic troposphere.

Case studies using a combination of aerosol and trace gas measurements as well as model information often allow reliable identification of the cause of observed enhancements. For instance, Stohl et al. (2006, 2007) and Warneke et al. (2009)

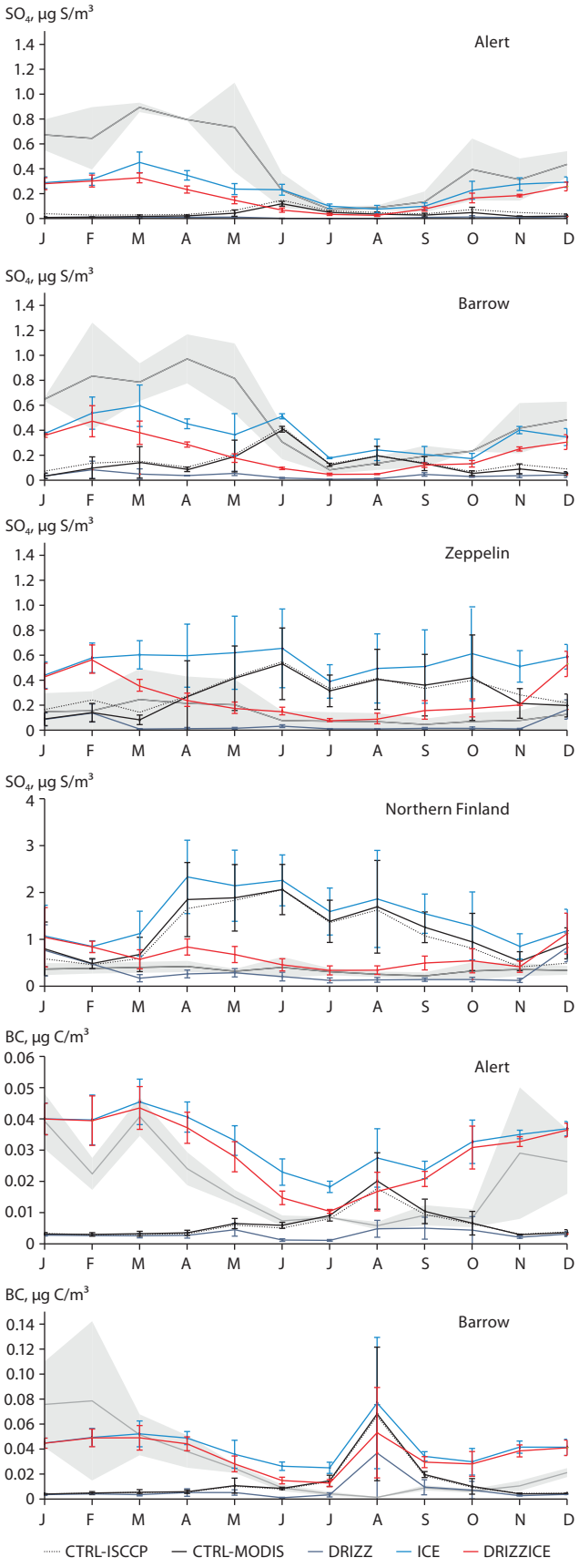

Figure 6.5 Monthly mean sulfate and black carbon (BC) surface mass concentration at three Arctic ground stations averaged over 2000–2002 (Browse et al. 2012). Observations are shown in grey with the monthly interannual standard deviation indicated by light grey shading. Observed sulfate and BC mass concentrations are compared with two control runs (CTRL) based on different low-level cloud information as well as with model simulations allowing scavenging by drizzle (DRIZZ), preventing scavenging in ice clouds below -15°C (ICE) and a combination of the two (DRIZZICE).

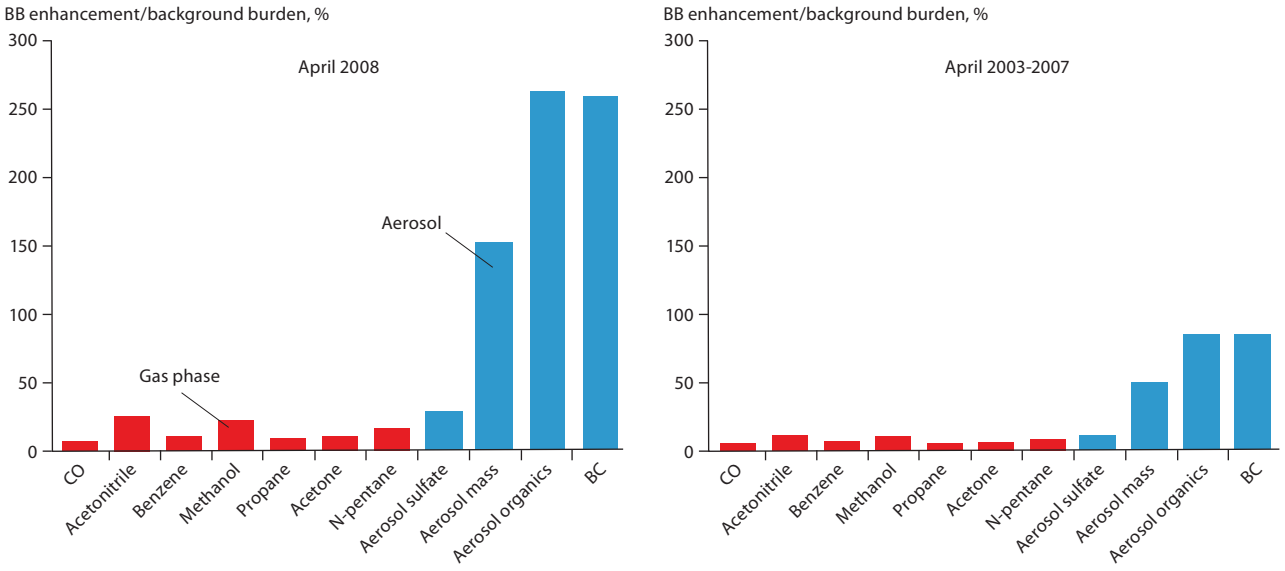

Figure 6.6 Average trace gas and aerosol enhancements due to biomass burning (BB) from emissions within the previous 20 days compared to the determined atmospheric background burden in the Arctic (north of 70°N). Average for April 2008 (left) and April 2003–2007 (right). Source: Warneke et al. (2010).

attributed large enhancements of Arctic BC levels in summer 2004, spring 2006 and spring 2008 to boreal forest fires in North America, agricultural fires in Europe and agricultural/boreal fires in Kazakhstan/Russia, respectively. Warneke et al. (2010) generalized case study results by combining the relative enhancements over the Arctic background level measured in biomass burning plumes during an aircraft campaign in April 2008 (Warneke et al. 2009) with a multi-year transport climatology for a passive CO tracer to estimate the average Arctic burden of various species measured by the aircraft. The results show that episodic biomass burning plumes make a relatively small contribution to the Arctic burden for all investigated gas-phase substances, which have relatively long atmospheric residence times (Fig. 6.6, left). However, for organic carbon (OC) and BC aerosols the episodic biomass burning plumes in April 2008 more than doubled the (mainly anthropogenic) Arctic background burden. While biomass burning in spring 2008 was unusually strong, the contribution of biomass burning averaged over all April months between 2003 and 2007 was still almost 100% of the contribution from background aerosol loading (Fig. 6.6, right), showing the great importance of biomass burning for Arctic aerosol concentrations. Matsui et al. (2011) also showed that biomass burning in Russia was the primary source of all aerosol types observed during an airborne campaign in spring 2008, whereas East Asian anthropogenic sources had a negligible effect on accumulation-mode aerosols during this campaign because of effective scavenging. This is in clear contrast to the dominant contribution of Asian anthropogenic sources to the Arctic CO burden during the same campaign (Fisher et al. 2010). For the longer-lived CO, which has a more uniform distribution in the troposphere, transport barriers such as the Arctic front are less effective and CO is not affected by wet scavenging.

Joint analysis (using, for example, chemical mass balance or factor analysis) of measurements of tracers for particular source types can enable the identification of contributions from different source types. For instance, von Schneidemesser et al. (2009) quantified the contributions of biomass burning, vegetative detritus and fossil fuel combustion to OC levels observed at Summit, Greenland. However, they could not attribute 96% of the observed OC and concluded that it must be of secondary origin. Hegg et al. (2009) used positive matrix factorization on data from pan-Arctic snow samples and concluded that open biomass burning (agricultural burning and boreal fires) was the dominant source of BC throughout the year. This is not fully consistent with results from modeling studies (see Ch. 11). However, the biomass-burning contribution to Arctic BC depends strongly on how exactly the Arctic is defined, as biomass-burning emissions between about 60°N and 67°N can have a strong local impact. Yttri et al. (2014) used a one-year data record of the biomass-burning tracer levoglucosan to estimate biomass-burning contributions to BC observed at the Zeppelin station (Ny-Ålesund, Svalbard). Minimum contributions were 9% in winter (mainly from domestic biomass burning) and 6% in summer (mainly from open fires); however, maximum contributions of 31–45% in winter and 65% in summer seemed possible, depending on assumptions of the rate of levoglucosan degradation by hydroxyl radicals.

McConnell et al. (2007) analyzed BC mass concentrations in an ice core from Greenland and found a strong correlation between BC and a tracer for conifer burning in pre-industrial times, suggesting that boreal forest fires (probably mainly in North America) drove BC levels in Greenland before industrialization. During industrial times, BC levels were higher than during the pre-industrial period and the correlation with the conifer burning tracer was much weaker, suggesting a dominant anthropogenic contribution to BC levels during the 20th century. During the last few decades of the 20th century, BC levels decreased due to reductions in anthropogenic emissions which means that the relative importance of biomass burning could now be more important again. Indeed, Keegan et al. (2014) concluded that widespread surface melt of the Greenland Ice Sheet in 2012 was due to higher temperatures combined with the deposition of BC from northern hemisphere forest fires.

A large number of studies have performed a statistical analysis of trajectory or other transport model calculations combined with atmospheric measurement data. In principle, these methods try to identify the source regions from which high measured concentrations are coming. However, sufficient measurement data for using this method are available only from surface

stations. For instance, Polissar et al. (2001) and Sharma et al. (2004, 2006) studied the source regions of BC measured at Barrow (Alaska) and Alert (Canada) using trajectory statistics. Eleftheriadis et al. (2009) used a similar method for BC measured at Zeppelin station on Svalbard. Huang et al. (2010b) performed a cluster analysis of trajectories arriving at Alert. The studies all attributed the highest measured BC mass concentrations to Eurasian sources and none of the stations appear to be strongly influenced by emissions from North America or southern Asia. For instance, Huang et al. (2010b) estimated that 67% of the BC at Alert in the Canadian High Arctic originated from the former Soviet Union, 18% from the European Union, and only 15% from North America during a 16-year period.

Hirdman et al. (2010b) combined measured concentrations of BC, sulfate and O_3 at Alert, Barrow, Summit and Zeppelin with backward-in-time calculations using an adjoint dispersion model. For the highest 10% of the measured BC values, northern Eurasia was again identified as the main source region for all stations, especially in winter/spring, and some evidence was found for biomass-burning influence from North America in summer (see Fig. 6.7 for Barrow). An even clearer attribution to northern Eurasia throughout the year (probably with a large contribution from Norilsk) was obtained for non-sea-salt sulfate measured at Alert, Barrow and Zeppelin (see Fig. 6.8 for Zeppelin). Applying the same method to O_3 (Fig. 6.9), transport from Eurasia is related to low O_3 concentrations in winter (due to titration of O_3 with nitric oxide) but high O_3 concentrations in summer (due to photochemical O_3 formation). Transport across the Arctic Ocean is associated with decreased O_3 concentrations in spring (and partly in summer), due to halogen-related O_3 depletion events. On the other hand, Hirdman et al. (2010b) found a correlation between surface O_3 and transport from the stratosphere, indicating that stratospheric influx is an important source of O_3 even at the surface.

Above 5 km altitude, air of stratospheric origin was found frequently during both spring and summer airborne campaigns in the Arctic although its contribution to the O_3 budget only appears to be important in the upper troposphere in spring (Emmons et al. 2003; Wespes et al. 2012). It is not only an important direct source of O_3, but may also act as a radical source leading to enhanced O_3 destruction (Arnold et al. 2014) and/or a source of reactive nitrogen leading to net photochemical O_3 formation in the Arctic upper troposphere (Liang et al. 2011). Further quantification of the flux of stratospheric O_3 and its impact on tropospheric O_3 photochemistry is still required.

Finally, chemistry transport models in direct and inverse modes have been used to quantify the SLCF contributions from different source regions and/or source types (Hirdman et al. 2010b; Baklanov et al. 2012; Penenko et al. 2012). The validity of the results depends on the emission data used by the model and the skill of the model in simulating transport, processing and removal of SLCFs and their precursors. This is discussed in more detail in Ch. 11, with particular emphasis on the AMAP models used in this assessment. However, one seeming contradiction to observation-based studies is that most models suggest that Asian emissions are the greatest contributor to the Arctic BC burdens. Whether the much

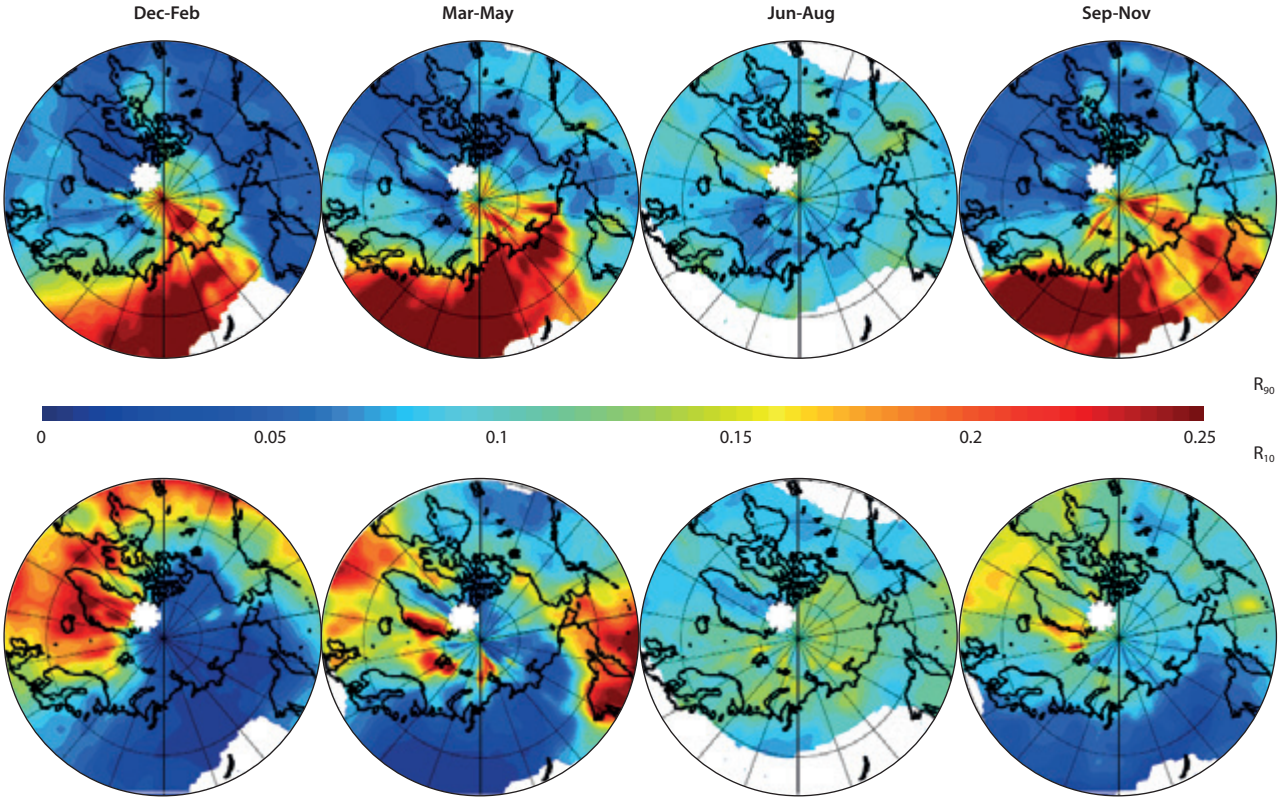

Figure 6.7 Source regions for black carbon (BC) measured at Barrow (Alaska) during the years 2002–2007, for winter (DJF), spring (MAM), summer (JJA) and autumn (SON). Results are based on a statistical analysis of BC measurements at the station combined with 20-day backward calculations using a Lagrangian particle dispersion model. The upper panels show the source region for the highest 10% of measured BC and the lower panels the source region for lowest 10% of measured BC. Source regions are shown as surface emission sensitivities for the selected subset divided by the emission sensitivities for the whole data set, in relative units. Barrow is marked by a white asterisk. White areas were excluded from the analyses due to insufficient data coverage. Source: Hirdman et al. (2010b).

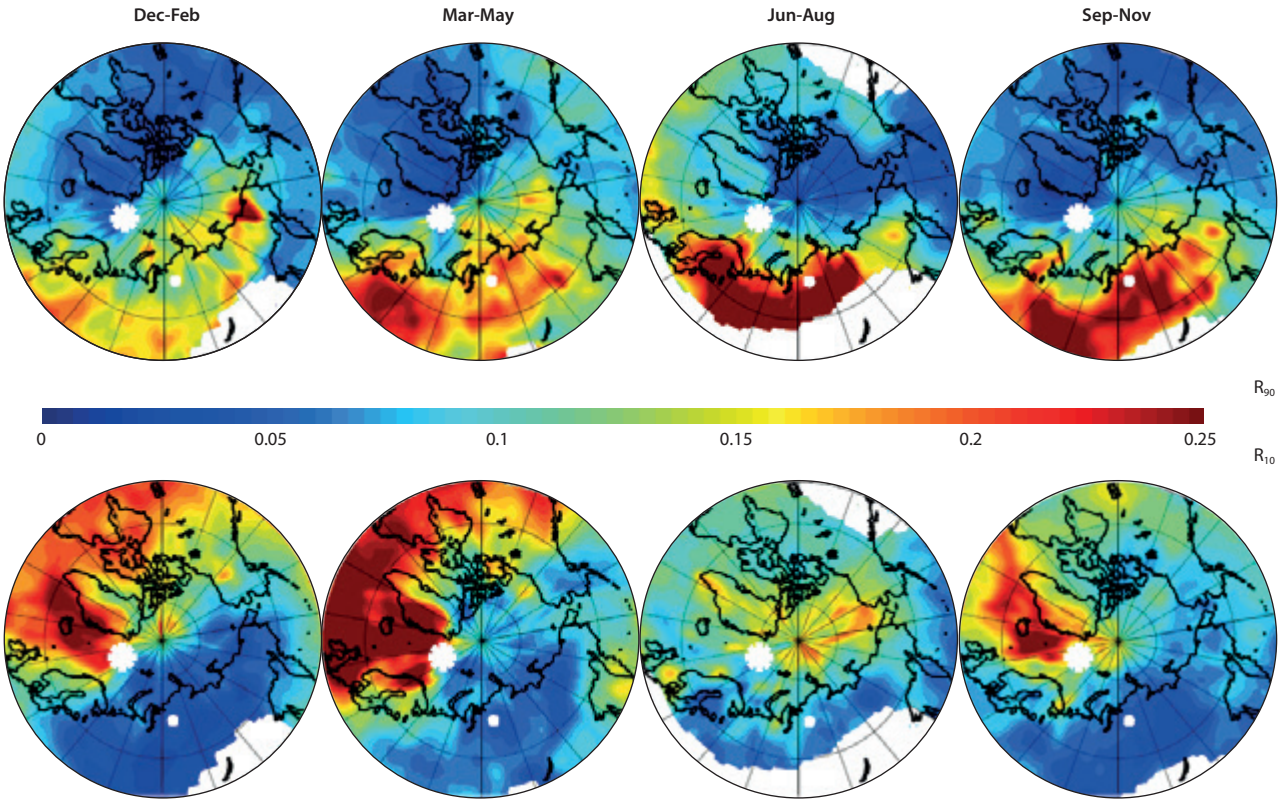

Figure 6.8 Source regions for non-sea-salt sulfate (nss) measured at Zeppelin (Ny-Ålesund, Svalbard) during the years 2002–2007, for winter (DJF), spring (MAM), summer (JJA) and autumn (SON). Results are based on a statistical analysis of nss measurements at the station combined with 20-day backward calculations using a Lagrangian particle dispersion model. The upper panels show the source region for the highest 10% of measured nss and the lower panels the source region for lowest 10% of measured nss. Zeppelin is marked by a white asterisk. White areas were excluded from the analyses due to insufficient data coverage. The white point marks the location of Norilsk. Source: Hirdman et al. (2010b).

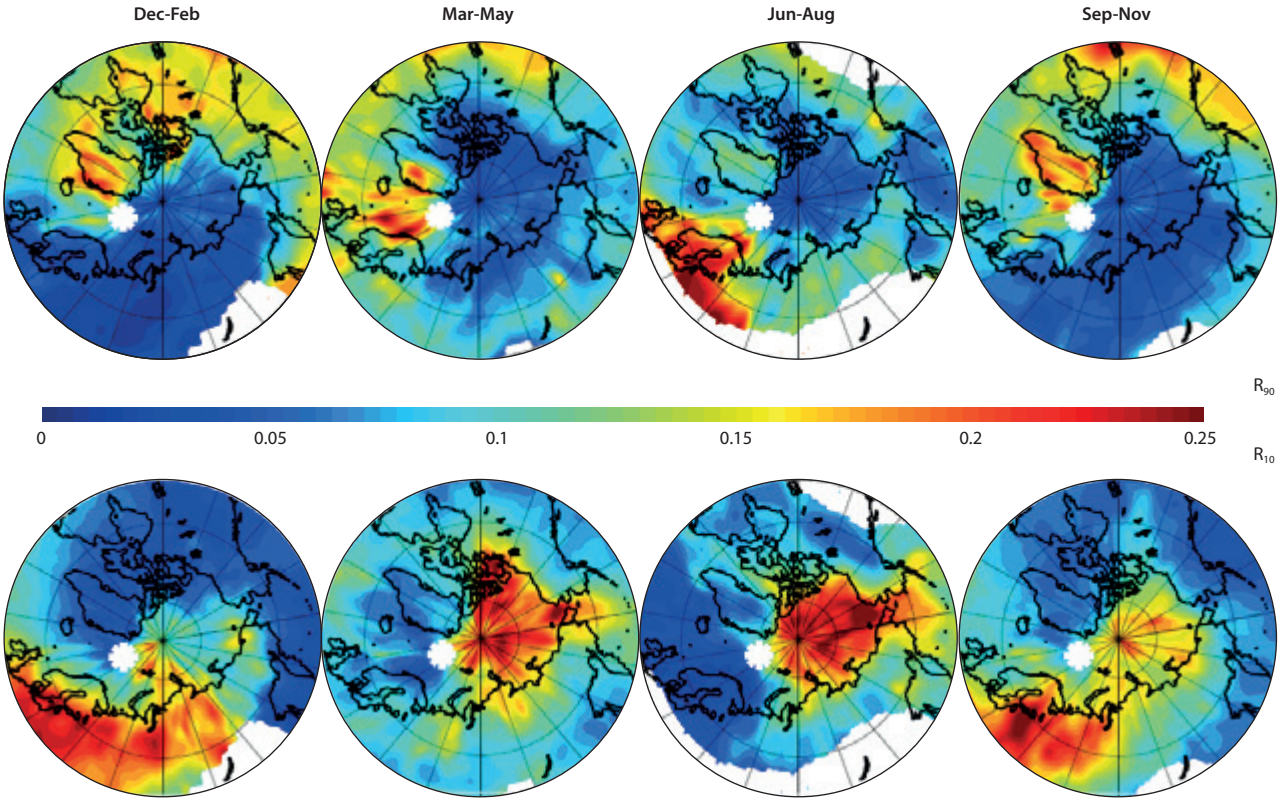

Figure 6.9 Source regions for ozone (O_3) measured at Zeppelin (Ny-Ålesund, Svalbard) during the years 2002–2007, for winter (DJF), spring (MAM), summer (JJA) and autumn (SON). Results are based on a statistical analysis of O_3 measurements at the station combined with 20-day backward calculations using a Lagrangian particle dispersion model. The upper panels show the source region for the highest 10% of measured O_3 and the lower panels the source region for lowest 10% of measured O_3. Zeppelin is marked by a white asterisk. White areas were excluded from the analyses due to insufficient data coverage. Source: Hirdman et al. (2010b).

larger role of Asian emissions in the model studies is due to the often coarse resolution of the models, their definition of the Arctic (which typically includes large areas south of the Arctic measurement stations), or the focus on burdens rather than surface concentrations is still not completely resolved.

While the discussion in this chapter has primarily focused on substances which have anthropogenic sources, it is worth noting that for some important short-lived species natural sources are dominating. For instance, dust, sea salt (Rahn et al. 1977; Quinn et al. 2002) and episodic emissions by volcanic eruptions (Hoffmann et al. 2010) are important natural components of the Arctic aerosol.

6.5 Conclusions

This chapter has outlined the transport and removal processes determining Arctic SLCF concentrations. The most important characteristic of the Arctic atmosphere is its strong stratification with globally the lowest potential temperatures, which leads to the formation of a polar dome isolating the Arctic lower troposphere from the rest of the atmosphere. Atmospheric transport into the dome is not efficient but can involve a number of different pathways, each with different efficiency of wet scavenging. Some of these pathways involve frontal transport, whereas others involve radiative cooling in shallow atmospheric layers. This poses a challenge to global chemistry transport models or climate models, which lack the resolution to correctly simulate these phenomena and this may lead to model biases in simulated Arctic SLCF concentrations. It may also partly explain why the main aerosol source region obtained in observation-focussed studies is high-latitude Eurasia, while model simulations tend to give much larger contributions from sources further south.

7. Modeling methods for studies of short-lived climate forcer effects on Arctic climate

Authors: Alexander Baklanov, Maria Sand, Mark Flanner, Knut von Salzen, Joakim Langner

7.1 Introduction

Different types and complexities of models are used for simulating atmospheric transport, chemical transformations, and radiative forcing of short-lived climate forcers (SLCFs), and they have specific requirements for application in the Arctic. This chapter describes the main modeling approaches for studying SLCFs and their effects on Arctic climate, in particular specifying model setups and new features and processes realized in the models used in this study.

Comprehensive global and regional models are required for an integrated evaluation of forcings, impacts and climate response to SLCFs. The models need to include realistic transport of SLCFs to the Arctic, atmospheric chemistry and aerosol dynamics, forcing mechanisms, the main chains of climate response processes, and depositional losses during transport to and within the Arctic. The models should also take into account the ongoing warming in the Arctic and the associated changes taking place within the cryosphere, on the various SLCF forcing mechanisms.

In general, the models can be separated into regional and global Chemistry Transport models (CTMs) and Chemistry Climate models (CCMs), which as referred to here also include General Circulation models and Earth System models (ESMs). Offline CTMs consider only equations of atmospheric transport, dispersion, deposition and transformation of gaseous and particulate chemical species. CCMs solve all main equations of atmospheric dynamics and atmospheric composition on the model's time step. Offline CTMs are driven by meteorological data while online coupled CTMs generate their own internal meteorology including possible aerosol feedbacks (Zhang et al. 2012a,b). The output from such models can be compared directly with observational data (e.g. Shindell et al. 2008). When coupled with a radiative transfer model, offline CTMs can also calculate radiative forcing. Both CTMs and CCMs use detailed emission information (see Ch. 5) and explicitly treat chemical processes such as changes in aerosol hygroscopicity, state of mixture (external versus internal) with other aerosol components, and removal from the atmosphere. The level of detail in the treatment of these processes varies between models. For ozone (O_3) impact studies, the models consider more comprehensive chemistry mechanisms including photochemistry, emissions of O_3 precursors and radiative forcing due to the direct effect. For O_3 modeling, in particular, natural emissions, including biogenic emissions from different forest/land-classes driven by temperature, precipitation and light, marine emissions of dimethlysulfide, and emissions from volcanoes, are included. Photolysis rates are important for O_3 precursor photochemistry, so cloud optical depths and cloud altitudes are usually used in the photolysis calculations. Photolysis rates are included in CTMs using generated meteorology fields, and in CCMs directly by coupling the photolysis rates and chemical reactions with meteorological conditions at each model time step.

Unlike CTMs, CCMs generate their own climate and calculate the climate response to forcing, such as that associated with human-caused emissions of greenhouse gases and aerosols. CCMs provide different degrees of coupling between the calculated chemical state of the atmosphere and the climate. The emissions, transport, mixing and deposition of species are linked to the physical state of the atmosphere. For example, wet deposition is controlled by 4D structure of clouds and precipitation while dry deposition of aerosols is controlled by turbulence in the boundary layer and surface characteristics. CCMs can be 'nudged' toward observed meteorological data and, thus, be used in a manner similar to CTMs but, in that case, they lose their ability to simulate the climate response. In addition to CCMs, a new generation of ESMs provide coupling between the atmosphere, ocean, sea ice and land surface, and can explicitly represent biogeochemical processes (Flato 2011).

Owing to computational time requirements, there is a limit to the horizontal and vertical resolution of the models, as well as the number of processes treated and the level of detail incorporated (see Table 7.1). This is a critical issue especially in the Arctic where the high static stability produces fine-scale atmospheric structure. The boundary layer height during very stable conditions can be only a few tens of meters and cannot be accurately resolved by current models having lower vertical resolution within the boundary layer. Although regional models can typically be run at higher resolution than global models, they are also unable to resolve the very stable boundary layer over the Arctic, especially during the polar night.

7.2 Models used in this assessment

Different types of model with varying degrees of complexity and resolution were used in this study to calculate species burdens, radiative forcing and the Arctic temperature response to the forcing. Table 7.2 describes the experimental set-up for the models listed in Table 7.1. In contrast to the previous AMAP assessment, which included results from one CCM and one CTM (AMAP 2011), this study is based on the results of three CCMs and five CTMs. The two models used in the previous AMAP assessment were also substantially improved for the current study (see Ch. 8). In particular, the current models generate seasonal cycles of black carbon (BC) in the Arctic that agree much better with observations. In the previous assessment, radiative forcing was calculated for the direct effect of BC and the BC-snow/ice effect only. Here, cloud indirect forcing is also included. Importantly, this study also estimates Arctic climate impacts from forcing exerted outside the Arctic. In addition, this study includes the effect of several additional SLCFs including O_3 and its precursors, sulfate and organic carbon (OC)-containing aerosols. The

Table 7.1 Description and configuration of the models used in this study. CAM5.2, CanAM4.2, NorESM are Chemistry Climate models (CCMs) and run as Chemistry Transport models (CTMs) to calculate radiative forcing of black carbon (BC), organic carbon (OC) and sulfate (SO_4) from sectors/regions. Oslo-CTM2, SMHI-MATCH, WRF-Chem, EMEP and DEHM are global and regional CTMs. Oslo-CTM2 has been used to calculate ozone (O_3) forcing. SMHI-MATCH has also been used to calculate BC/OC/SO_4/O_3 forcing. WRF-Chem, EMEP and DEHM were not calculating radiative forcing.

Model	Configuration	Resolution	References
CESM1 (CAM5.2)	2006–2010 interannually-varying prescribed SSTs. Meteorology generated by the model Aerosols simulated with the Modal Aerosol Model (MAM7)	1.9°×2.5° and 0.9°×1.25°; 30 vertical levels	Flanner et al. 2009; Liu et al. 2012; Wang et al. 2013
CanAM4.2	2006–2010 interannually-varying prescribed SSTs and sea ice. Meteorology generated by the model, with nudging of winds and temperature towards a free control run PLA Aerosol model (PAM)	T63; 49 vertical levels	von Salzen 2006; Ma and von Salzen 2008; Peng and von Salzen 2012; von Salzen et al. 2013
DEHM	Meteorology nudged with NCEP global re-analyses on 1°×1° resolution as input Bulk aerosol scheme	Two domains coupled by two-way nesting: (1) hemispheric with 150km at 60°N and (2) North Atlantic, whole Arctic with 50km; 29 vertical levels	Christensen 1997; Brandt et al. 2012
ECHAM6	ECMWF reanalysis, 2009 Aerosols simulated with the M7 model	1.8°×1.8°; 31 vertical levels	Zhang et al. 2012c; Stevens et al. 2013
EMEP/MSC rv4	ECMWF IFS meteorology EMEP chemistry scheme	1°×1°; 20 vertical levels	Simpson et al. 2012
FLEXPART (LPDM)	3-hourly operational ECMWF analyses	1°×1° meteorological input data, 0.5°×0.5° emission data	Stohl et al. 2005
NorESM	2006–2010 interannually-varying prescribed SSTs. Meteorology generated by the model CAM4-Oslo aerosols	1.9°×2.5°; 26 vertical levels	Bentsen et al. 2013; Iversen et al. 2013; Kirkevåg et al. 2013
Oslo-CTM2	ECMWF reanalysis from the Integrated Forecast System (IFS) model for year 2008 and 2009 Bulk aerosols	T42; 60 vertical levels	Myhre et al. 2009; Skeie et al. 2011b
SMHI-MATCH	ECMWF ERA-Interim reanalysis meteorology EMEP chemistry Ammonium-nitrate-sulfate equilibrium Bulk aerosols (internally mixed)	0.75°×0.75°, 20–90°N; 38 levels	Robertson et al. 1999; Andersson et al. 2007
TM4	ECMWF ERA-Interim reanalysis meteorology, 2008, 2009, 24h	2°×3°; 34 levels	Myriokefalitakis et al. 2011; Kanakidou et al. 2012; Daskalakis et al. 2014
WRF-Chem 3.5	Meteorology nudged with NCEP global re-analyses on 1°×1° resolution as input MOSAIC aerosol scheme (8 bins with aqueous chemistry) CBMZ gas phase chemistry Model run from March–July 2008	100 km × 100 km, 25–90°N; 50 vertical levels Lower latitude boundary conditions from MOZART	Zaveri and Peters 1999; Zaveri et al. 2008; Grell et al. 2005; Marelle et al. 2014

Table 7.2 Description of the model simulations.

Experiment	Emission dataset	Sectors	Regions	Simulation length
Black carbon / organic carbon / sulfate / ozone forcing by sector/region	ECLIPSE v4a 2010 with monthly weights on domestic sources Monthly-varying biomass burning 2007–2010 emissions from GFEDv3.1	Energy+Industrial+Waste (EIW) Flaring (FLR) Transport (TRA) Domestic (DOM) Agricultural fires (AGR) Grass and forest fires (FIR) Shipping (SHP)	Canada (CANA) Nordic countries (NORD) Russia (RUSS) United States (USAM) Rest-of-Europe (OEUR) South Asia, east Asia, and southeast Asia (ASIA) Rest-of-world (ROW)	2007–2010 (2006 spin-up)
Transient climate response	IIASA MFR and CLE v5			2005–2050
Baseline (used for model evaluation in Ch. 8).	ECLIPSE v4a	All sectors	Global	2008–2009

models that calculate BC burden and radiative forcing include prognostic calculation of BC lifetime and treat both internally and externally mixed BC (except SMHI-MATCH). Monthly-varying sea-surface temperatures (SSTs), greenhouse gases, volcanic ash, and solar forcings were specified for the period 2007–2010, with one additional year of spin-up. More details about the radiative forcing calculations in the different models are provided in Sect. 7.3.

7.3 Radiative forcing calculations

The types of radiative forcing reported in Ch. 11 include direct radiative forcing, cloud radiative forcing, snow and sea-ice radiative forcing, and total radiative forcing. All forcings represent annual averages of top-of-atmosphere (TOA) changes in net radiative flux associated with the total presence of each component (rather than, for example, industrial-era changes in each component). Forcings for each component are decomposed into contributions from a variety of sources and sectors, listed in Table 7.2. Flexibility was granted to each modeling group to derive forcing components using their own methods, which differ especially for estimation of cloud indirect and snow effects. This design choice may increase the spread in model results, but reflects the challenges and ambiguity in defining and decomposing radiative forcing. Table 7.1 indicates the types of radiative forcing diagnosed within each model.

7.3.1 CESM1 (CAM5.2 atmosphere model)

Simulations conducted with the Community Earth System Model (CESM) utilize the CAM5.2 atmospheric model with modal aerosol treatment (Liu et al. 2012), including important modifications to the aerosol code that result in substantially more aerosol transport to the Arctic (Wang et al. 2013). In CESM, direct radiative forcing from atmospheric constituents are diagnosed from parallel radiative transfer calculations, conducted each time-step with and without each species of interest. The forcings represent the mean change in instantaneous TOA shortwave+longwave radiative flux caused by the immediate presence of the agent. Independent simulations were conducted for each emissions tag (Ch. 5 and Table 7.2) and meteorology was generated by the model in response to prescribed 2006–2010 SSTs. Use of a nudged meteorology framework (i.e. with re-analysis data) would have been preferable for forcing calculations, both to minimize variability between simulations and to enable cloud indirect radiative forcing calculations, but was not feasible with the version of the model applied here. However, Wang et al. (2014b) constrained a different version of the CAM5 model with re-analysis data (1995–2005) and showed that the global and Arctic annual mean BC direct radiative forcings have minimal interannual variability. Furthermore, the 10-year mean forcing estimate of Wang et al. (2014b) is very close to that of the present study (see Ch. 10 and 11).

Sensitivity studies showed that forcings generated through subtraction of each tag (see Ch. 5) from an all-aerosol emission source produced forcing estimates that were unrealistically noisy. Hence, forcings were calculated relative to base states with no anthropogenic aerosols. This approach produces a slightly higher direct forcing estimate than one with a reference state with all anthropogenic aerosols, but the difference is not large because radiative forcing scales nearly linearly with aerosol burden when the burden is modest. Radiative forcing from BC deposited to land-based snow was calculated interactively in the land component (CLM) of CESM from parallel radiative transfer calculations conducted each time-step of snow albedo with and without BC (Flanner et al. 2007). The calculations were conducted within each coupled atmosphere-land simulation, using prognostic aerosol deposition fluxes that were consistent with the precipitation fluxes. The sea-ice model is not active when SSTs are prescribed, so forcing from BC deposited to sea ice must be achieved with offline calculations. Monthly-mean aerosol deposition fluxes produced from each tagged aerosol run were used to drive offline simulations with the CICE4 sea-ice component of CESM, forced with 2006–2010 meteorology. As for the land model, the forcings were calculated using parallel radiative transfer calculations of sea-ice albedo with and without BC (Holland et al. 2012). Chapter 11 reports combined land and sea-ice radiative forcing. Simulated land snow BC concentrations are not subject to the bias described by Doherty et al. (2014a), which results when temporally inconsistent aerosol wet deposition and precipitation fluxes are used to drive offline simulations. Sea-ice forcings, however, are likely to be subject to this bias, which was found to be a factor of 1.5–2.5 (high) for land snow, but which has not been quantified for sea ice.

7.3.2 CanAM4.2

In simulations with CanAM4.2, total radiative forcing (F_{tot}) is diagnosed using the nudged radiative flux perturbation method (Kooperman et al. 2012). Forcings for each chemical aerosol species are given as the difference in TOA net radiation (shortwave+longwave) between experiments with perturbed (no) ECPLISE V4a emissions of the species and a control simulation with ECLIPSE V4a emissions. Winds and temperatures in the control simulation and experiments were nudged to a free (un-nudged) simulation with CanAM4.2 using 6-hourly model data and a nudging time scale of 24 hours.

To diagnose indirect forcings, an additional control simulation and experiments were conducted with specified monthly cloud droplet number concentrations (CDNC) in the cloud scheme in order to determine total species forcings for specified cloud droplet numbers (F_{noind}) using the nudged radiative flux perturbation method and the same free simulation that was used to diagnose F_{tot}. Indirect species forcings (F_{ind}) were determined as the difference in TOA net radiation from fully interactive and fixed-CDNC simulations: $F_{ind} = F_{tot} - F_{noind}$. Direct ($F_{dir}$) and snow ($F_{snow}$) species radiative forcings were calculated from differences between instantaneous net (shortwave+longwave) forcings at the TOA between the experiments and control simulation.

Forcings for each regional and sectoral tag were derived by scaling each species forcing component (F_{tot}, F_{ind}, F_{dir}, F_{snow}) by changes in aerosol burden for each tag, for example:

$$F_{tot,tag} = (F_{tot} / b) \times b_{tag} \qquad \text{Eq. 7.1}$$

where b and F_{tot} are, respectively, differences in burden and TOA net radiation between experiments and the control simulations.

b_{tag} is the difference in burden between a nudged regional/sectorial experiment (i.e. without emissions from a specific tag) and the control simulation. Scaling calculations are done separately for each grid cell and then averaged over the region of interest (e.g. 60–90°N) to obtain mean forcings. The main motivation for this approach was to diagnose indirect (first and second) forcings in the model. Kooperman et al. (2012) demonstrated that their method yields an efficient approach that does not require unreasonably long model integrations or a large number of model ensembles to diagnose radiative forcing of aerosols. However, simulation results for aerosol concentrations and radiative fluxes are affected by internal spatio-temporal variability in amounts and properties of clouds and snow in the simulations, which are not subject to nudging. This substantially limits the statistical robustness of forcing estimates for small changes in emissions in CanAM (i.e. the signal to noise ratio in forcings can be poor for individual tags), which motivated the choice to scale the forcings using burden perturbations from the individual experiments with perturbed emissions from individual regions and sectors, as described in Eq. 7.1. With nudging, burden perturbations can be more robustly diagnosed than forcing perturbations when emission perturbations are small. This approach will be appropriate if forcings are a linear function of burdens, which is a good approximation with regard to direct radiative effects of BC. The approach was tested for BC emissions from Asia and good agreement was found between scaled and directly diagnosed radiative fluxes. However, model results are typically more strongly affected by variability than results diagnosed from CTMs and other methods which do not account for aerosol indirect effects. The 95% confidence uncertainty ranges for Arctic BC burdens and direct radiative forcing estimated based on seven ensemble members of the control simulation are ±241 Mg C and ±16.1 mW/m^2, respectively. These are comparable to diagnosed BC burdens and forcings for tags associated with the Nordic countries, Canada, and the United States (see Ch. 11). In contrast, uncertainties are relatively small for tags associated with Asia and Russia.

7.3.3 SMHI-MATCH

In the SMHI-MATCH simulations the PORT tool (Conley et al. 2013) was used to diagnose direct radiative forcing of O_3, BC, OC and sulfate contributions from different sector-region combinations. The calculations were performed in two steps. First, the MATCH CTM was run with 20% reduction of the emissions in each sector-region combination. This was done in one run for O_3 precursors and sulfur emissions and one run for BC and OC. The total change in each component for each sector-region combination was then estimated by taking the difference between the perturbation run and a baseline run with no reduction of emissions and scaling by a factor of five. This procedure was adopted to minimize numerical errors resulting from steep gradients in emissions in the perturbation runs. Simulations were carried out for a five-month spin-up period in 2007 and for the whole of 2008. Second, PORT was set up following Conley et al. (2013). This involved running CESM 1.2 for a validated present-day simulation over 16 months with fixed SST and sea ice, storing the necessary output. This simulation used archived monthly 3D trace gas and aerosol distributions for estimating their radiative effects. Using output from this run it was then possible to diagnose the radiation fluxes in the simulation using PORT with good accuracy. To calculate the radiative forcing due to emissions from each sector-region combination the monthly 3D contribution to the concentration of each species simulated with MATCH was deducted from the monthly 3D fields used in the CESM simulation. PORT was then rerun using these perturbed concentration fields as input. The radiative forcing was diagnosed as the difference with and without perturbation. This was done separately for each chemical component diagnosed involving four different PORT runs for each sector-region combination.

7.3.4 NorESM

The direct and indirect aerosol effects in NorESM were estimated by interpolating the optical and physical properties of the aerosols with pre-existing values in look-up tables (Kirkevåg et al. 2013). The input to the look-up tables are aerosol mass concentrations that are tagged according to production mechanisms in cloudy and clear air, and ambient relative humidity. The output of the look-up tables are spectrally-resolved optical parameters to estimate the direct aerosol effect in the radiative transfer code, and aerosol modal size parameters to calculate the activation of cloud condensation nuclei (CCN-activation) and aerosol indirect effects (in liquid clouds). The main advantage of this method is that the degree of internal versus external mixing can be estimated based on physicochemical processes.

7.4 Equilibrium temperature change

Radiative forcings from SLCFs are translated into equilibrium temperature changes through the use of regional climate sensitivity parameters. Because the local surface temperature response to BC forcing in the Arctic and elsewhere depends strongly on the altitude of BC forcing (Ban-Weiss et al. 2011; Flanner 2013; Sand et al. 2013a), a technique was devised to derive vertically-resolved radiative forcings by BC in the Arctic and apply these in combination with vertical climate sensitivity parameters derived by Flanner (2013).

Vertically-resolved direct radiative forcing from BC can be approximated using: modeled TOA forcing at each grid cell g and month m ($F_{BC}(g,m)$) (units W/m^2); modeled burdens of BC in each vertical layer z (B(g,m,z)) (units kg/m^2); and a mean radiative efficiency profile for Arctic BC, defined at each model layer midpoint (E(z)) (units W/kg), which serves as a weighting function. A profile of Arctic annual-mean E(z) derived by Samset et al. (2013) from the Oslo-CTM2 model was applied in this study (see Fig. 7.1). The following preliminary step provides an intermediate forcing term (units W/m^2) defined at each grid cell, month, and layer:

$$F_{tmp}(g, m, z) = B(g, m, z) \times E(z) \qquad \text{Eq. 7.2}$$

This is followed by a normalization procedure to conserve the modeled TOA forcing ($F_{BC}(g,m)$), which varies strongly with season:

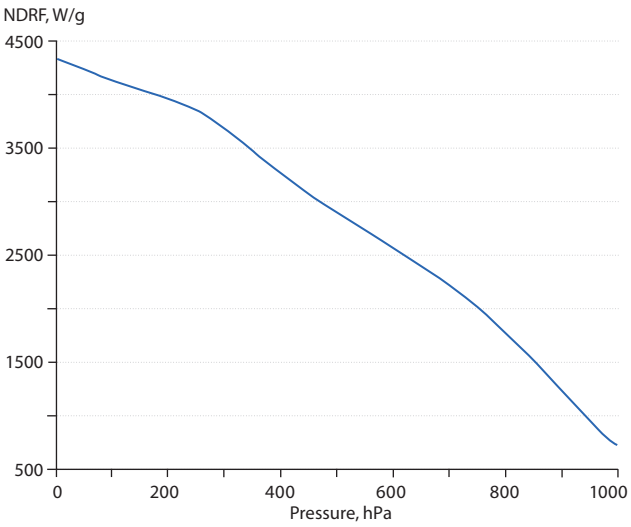

Figure 7.1 Vertical profile of annual-mean normalized direct radiative forcing (NDRF, or radiative efficiency) of black carbon (BC) in the Arctic, derived from Oslo-CTM2 calculations (Samset et al. 2013).

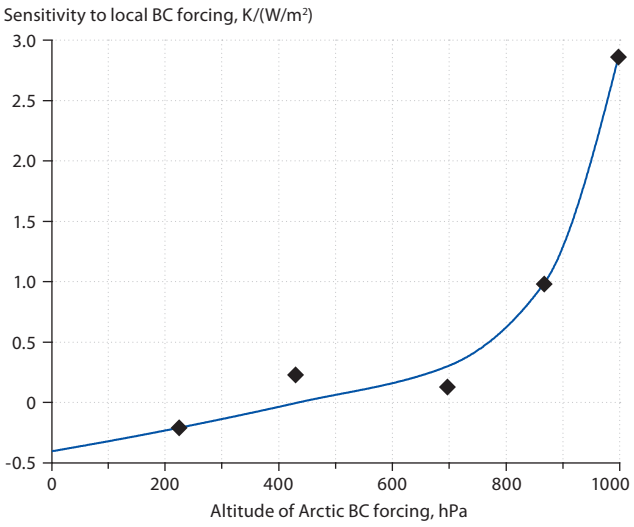

Figure 7.2 Arctic surface temperature response to black carbon (BC) radiative forcings exerted at different altitudes in the Arctic, derived from simulations described by Flanner (2013).

$$F_{BC}(g, m, z) = F_{tmp}(g, m, z) \times \frac{F_{BC}(g, m)}{\sum_{z=1}^{z=N} F_{tmp}(g, m, z)} \quad \text{Eq. 7.3}$$

where the summation is conducted over all N model layers.

These equations can be combined into the following unified expression, providing vertically-resolved forcing that is weighted by modeled layer burden and radiative efficiency, and which conserves modeled TOA direct forcing:

$$F_{BC}(g, m, z) = B(g, m, z)\, E(z) \frac{F_{BC}(g, m)}{\sum_{z=1}^{z=N} B(g, m, z)\, E(z)} \quad \text{Eq. 7.4}$$

This quantity is then averaged annually and horizontally over the Arctic (60–90°N) to obtain an annual-mean vertically-resolved Arctic forcing, $F_{BC,Arc}(z)$, which has units of W/m²/layer. For model intercomparisons, this quantity was divided by the Arctic annual-mean difference in pressure between model layer interfaces, yielding a forcing term with units of W/m²/hPa.

With vertical radiative forcing defined, Arctic equilibrium surface temperature change is quantified in terms of vertical atmospheric BC forcing ($F_{BC,Arc}(z)$), and any combination of other regional forcings exerted by other species (F(i,j)), for example:

$$\Delta T_{Arc,eq} = \sum_{z=1}^{z=N} [F_{BC,Arc}(z)\, \lambda_{BC,Arc}(z)] + \sum_{i=1}^{S} \sum_{j=1}^{R} F(i, j)\, \lambda_{Arc}(i, j) \quad \text{Eq. 7.5}$$

Here, $\lambda_{BC,Arc}(z)$ represents the Arctic surface temperature response to a unit of BC radiative forcing exerted in layer z, defined by a midpoint pressure. Vertical profiles of $\lambda_{BC,Arc}$ are derived from sensitivity studies described by Flanner (2013) and are shown in Fig. 7.2.

Each $\lambda_{i,j}$ refers to an Arctic climate sensitivity (units K/(W/m²)) with respect to a radiative forcing (F(i,j)) exerted by species *i* in region *j*. The parameters and forcing regions applied in this study are listed in Table 7.3.

Note that the parameters listed in Table 7.3 have units of Kelvins per unit of radiative forcing averaged horizontally over the specified domain (rather than averaged globally). The sensitivity parameters originate from Shindell and Faluvegi (2009), and are partially reproduced by Collins et al. (2013a). The parameters were derived from equilibrium climate change simulations with idealized forcings from different species imposed in different regions. These parameters seem to reproduce modeled climate sensitivity to global forcings reasonably well, although they originate from only one model and uncertainty in these parameters has not been quantified. The parameters for BC in

Table 7.3 Arctic climate sensitivity factors (K/(W/m²)).

Forcing location	Forcing component			
	Atmospheric black carbon	Ozone	Scattering aerosol	Black carbon in snow and ice
90–28°S	0.06	0.06	0.06	0.18
28°S – 28°N	0.31	0.13	0.16	0.93
28–60°N	0.15	0.05	0.17	0.45
60–90°N	VR[a]	0.07	0.31	1.46

[a]VR: use of vertically-resolved forcing (see Sect. 7.4).

snow and ice were added for this study. The Arctic BC-in-snow sensitivity term is from Flanner (2013) while the values for other regions are the atmospheric BC parameter multiplied by 3 – loosely representing the efficacy factor of ~3 found in previous studies for this forcing mechanism (Flanner et al. 2007; Hansen et al. 2007). In the present study, the sulfate and OC forcings are assigned to the 'scattering aerosol' sensitivity factors, and direct forcings are only used in the temperature change calculation.

7.5 Conclusions

There are several new features in the modeling approaches realized in the current assessment. First, the models have been substantially improved over the past four years. The current models simulate improved seasonal cycles of near-surface SLCFs, but still underestimate the amplitude of the seasonal cycle of BC in the Arctic (see Ch. 8). In the previous AMAP assessment, only one CCM and one CTM were used to calculate radiative forcing values, and only the atmospheric direct effect of BC and OC and the BC-snow/ice effect were considered. In this study, three CCMs and five CTMs were used. In addition to direct forcing by atmospheric BC, the effects of several additional SLCF species were included, including O_3 and its precursors, OC, sulfate, and BC in snow and ice. In addition, cloud indirect effects from both BC and scattering aerosols were assessed. The previous AMAP assessment cited studies which found that the local surface temperature response to BC forcing in the Arctic depends strongly on the altitude of that forcing, but the modeling analysis did not include those effects. For this assessment, a technique was devised to derive vertically-resolved radiative forcings by BC in the Arctic. These were then applied in combination with vertical climate sensitivity parameters to determine equilibrium surface temperature changes. Finally, this assessment quantified Arctic temperature changes due to radiative forcing exerted both within and outside the Arctic.

8. Modeled and measured distribution and seasonality of short-lived climate forcers in the Arctic

Coordinating lead authors: Sabine Eckhardt, Kathy Law, Steve Arnold

Lead authors: Mark Flanner, Joakim Langner, Sarah Monks, Maria Sand, Andreas Stohl

Co-authors: Boris Quennehen, Chaoyi Jiao, Terje Berntsen, Ribu Cherian, Jesper Christensen, Nikos Daskalakis, Chris Heyes, Øivind Hodnebrog, Maria Kanakidou, Zbigniew Klimont, Ulrik Korsholm, Marianne Lund, Gunnar Myhre, Stelios Myriokefalitakis, Dirk Olivie, Johannes Quaas, Jean-Christophe Raut, Knut von Salzen, Bjørn Samset, Michael Schulz, Ragnhild Skeie

Data provided by: Gerard Ancellet, Hans Schlager, Anke Roiger, Nis Jepsen, Bo Christiansen

8.1 Introduction

This chapter describes the observed distribution and seasonality of short-lived climate forcers (SLCFs) in the Arctic, and uses these data in model evaluation. Given that the radiative forcing and Arctic climate response calculations presented in Ch. 11 are based on model calculations, evaluating the ability of the models to reproduce the seasonality and distribution of SLCFs in the Arctic is extremely important.

This chapter reports in-situ measurements of SLCFs at several Arctic surface sites for the years 2008–2009, as well as aircraft measurements obtained mainly from campaigns during the International Polar Year. For ozone (O_3), some profile information is available from ozonesondes. This study also uses measurements of black carbon (BC) in snow sampled throughout the Arctic. Model results are from the suite of AMAP and ECLIPSE (www.eclipse.no) models (see Ch. 7), and were used to perform simulations for the years 2008–2009 using a consistent set of emission inventories (ECLIPSE V4a). This means that inter-model differences in the simulated distributions of gases and aerosols are almost entirely due to differences in meteorological input data (or modeled climate realization in case of free-running climate models), resolution, numerical schemes and model physics and chemistry. Very small differences may also result from slightly different emission heights used in the different models, and from different treatment of some natural emissions (such as dimethyl sulfide) not included in the ECLIPSE emission data set. It is important to note that models using different sets of emission data would probably show a greater spread in their results than is documented here. It is also important to note that the measurements used here are point measurements, whereas the modeled values are grid-box averages. Therefore, extreme values are less likely to occur in the models than in the measurements.

8.2 Aerosols

8.2.1 Measurement data

In this study, aerosol analysis is focused on BC and sulfate, for which measurement data are available from several Arctic surface stations and aircraft campaigns. BC model results are compared (later in this chapter) with measurements of aerosol light absorption (converted to equivalent BC, eBC) from four sites in different parts of the Arctic: Barrow (Alaska), Alert (Canada), Pallas (Finland) and Zeppelin (Svalbard). The locations are shown in Fig. 8.1 with

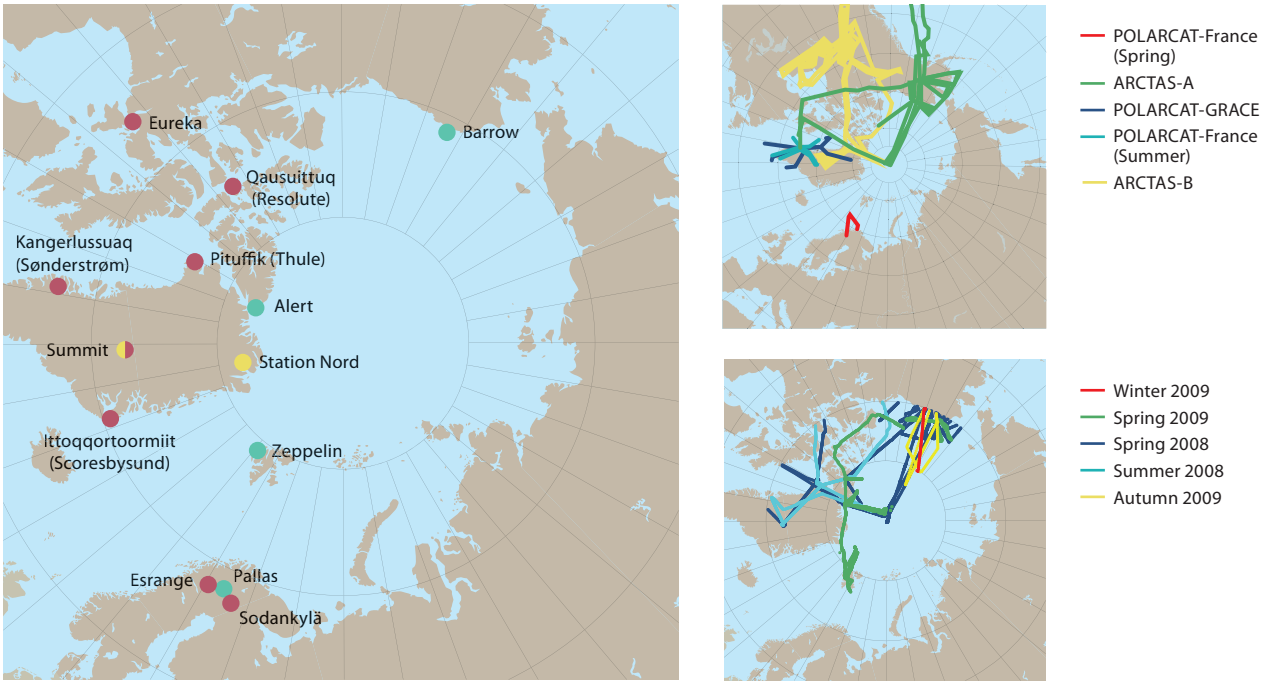

Figure 8.1 Location of measurement stations (left) and flight tracks north of 70°N (right) used in this study. Dot colors indicate measurement types available (green=aerosol plus gas-phase; yellow=aerosol only; magenta=gas-phase only).

Table 8.1 Long-term systematic aerosol observations in the Arctic (north of 60°N) contributing to the analyses discussed in this study (see Ch. 2, 8 and 9).

Site	Location	Elevation, m asl	Physical properties		Optical properties		Chemical inorganic speciation		Direct carbon[a]
			Number concentration	Number size distribution	Light absorption	Light scattering	Integrated filter	Continuous	
Alert	82.45°N, 62.52°W	210	✓		✓	✓	Elements; SO_4^{2-}; NO_3^-; NH_4^+;		
Barrow	71.32°N, 156.6°W	11	✓	✓	✓	✓	Fine; Coarse		
Summit, Greenland	72.60°N, 38.42°W	3208			✓		DRUM Sampling		
Zeppelin (Ny Ålesund)	78.91°N, 11.88°E	474	✓	✓	✓	✓	SO_4^{2-}		
Pallas	67.97°N, 24.12°E	560	✓	✓	✓	✓			
Station Nord	81°36'N,16°39'W	25	✓	✓	✓		Elements; SO_4^{2-}; NO_3^-; NH_4^+;	O_3; NO_X; CO, CO_2; H_2	Weekly EC/OC

[a]For example, the use of integrated filter measurements for elemental carbon (EC) and organic carbon (OC) via thermal evolution techniques.

information on measurements undertaken at the stations provided in Table 8.1. Various instruments were used at the sites: different types of particle soot absorption photometer (PSAP) at Barrow, Alert and Zeppelin, and a multi-angle absorption photometer at Pallas (Hyvärinen et al. 2011). These devices all measure the particle light absorption coefficient (σ_{ap}), each at its own specific wavelength (typically around 530–550 nm) and for different size fractions of the aerosol (typically particles smaller than 1.0, 2.5 or 10 µm). Conversion of σ_{ap} to eBC mass concentration is not straightforward and requires certain assumptions (see Ch. 2). The mass absorption efficiency used for conversion is site-, instrument- and wavelength-specific and has an uncertainty of at least a factor of two (see Ch. 2 for more details). In this study, the measured light absorption was converted to eBC mass concentration using a mass absorption efficiency of 10 m^2/g, typical of aged BC aerosol (Bond and Bergstrom 2006). Sharma et al. (2013) used an even higher value of 19 m^2/g for Barrow and Alert data. The converted light absorption values are referred to as eBC in this study to reflect the uncertainties in this conversion, as well as other uncertainties resulting, for instance, from the use of different cut-off sizes for the different instruments.

Monitoring data from Barrow and Alert are routinely 'cleaned', that is, the influence of local sources is removed. Zeppelin monitoring data are generally not strongly influenced by local emissions, although summer values are enhanced by about 11% due to local cruise ship emissions (Eckhardt et al. 2013).

Sulfate measurements were available from Pallas, Zeppelin, Barrow, Station Nord, and Alert. Aerosol particles were collected on open face filters and major inorganic cations and anions were quantified by ion chromatography. Non-sea salt (nss) sulfate concentrations were obtained by subtracting the sea salt contribution via analysis of sodium (Na^+) and chlorine (Cl^-) data, thus making the sulfate data directly comparable to the modeled values which also report nss-sulfate. For Station Nord, the contribution from sea salt is minor (Heidam et al. 2004), so no correction was applied. Samples were taken with daily to weekly resolution, depending on station and season. Organic carbon (OC) data are not covered in this chapter because OC is not monitored at most stations, and not all models reported OC concentrations.

Aircraft data were obtained from two ARCTAS campaigns mainly covering the North American Arctic (Jacob et al. 2010) in April and June/July 2008, the ARCPAC campaign conducted together with ARCTAS in spring 2008 (Brock et al. 2011), the PAMARCMIP campaign covering the central Arctic in April 2009 (Stone et al. 2010), and the HIPPO campaign (Schwarz et al. 2010, 2013b; Wofsy 2011) during January and October 2009. The flight tracks of all aircraft campaigns are shown in Fig. 8.1. Refractory BC (rBC) was measured during these campaigns with single particle soot photometer instruments (see Ch. 2 and Schwarz et al. 2006). Observations of submicrometer sulfate aerosol mass during ARCTAS were made with the SAGA instrumentation package (Dibb et al. 2003) using a mist chamber/ion chromatograph and during ARCPAC with a compact time-of-flight aerosol mass spectrometer (Bahreini et al. 2008). No sulfate data were available from PAMARCMIP and HIPPO.

While ARCTAS and ARCPAC, in addition to sampling the background Arctic atmosphere, also specifically targeted pollution plumes, PAMARCMIP and HIPPO sampled the Arctic atmosphere without intentionally targeting pollution plumes. However, a low sampling bias for these campaigns may occur because they purposefully targeted only remote regions of the Arctic. During April 2008, biomass burning influence was widespread throughout the Arctic (Warneke et al. 2010; Brock et al. 2011). Thus, the higher mean BC concentrations found during ARCTAS and ARCPAC than during PAMARCMIP a year later are not only caused by the different sampling strategies of these campaigns, but also by the early start to the biomass burning season in 2008. Even though all available BC and sulfate data from several campaigns were used for model evaluation, data coverage was still poor and perhaps not fully representative of the regions and seasons in which the campaigns were conducted.

8.2.2 Seasonality at measurement stations

Measurements throughout the Arctic have repeatedly shown that aerosol concentrations (including BC and sulfate) near the surface, peak in winter/early spring – the phenomenon is known as Arctic Haze – and are lowest in early autumn (e.g. Sharma et al. 2006; Quinn et al. 2007). This seasonality was discussed in detail by AMAP (2011) and is not repeated here. At the four sites with continuous eBC monitoring, eBC concentrations are comparable, with monthly median values of about 20–80 ng/m^3 in late winter/early spring and <10 ng/m^3 in summer/early autumn (see Fig. 8.2). Seasonality is least strong at the southernmost site, Pallas, where the summer concentrations are about twice as high as at the other sites, reflecting a decrease in the seasonal minimum with latitude. While aerosol concentrations in the Arctic during late winter/early spring are comparable to those at remote regions further south, concentrations in summer/early autumn are lower owing to the effective 'cleansing' of the atmosphere (see Ch. 6). The timing of the highest eBC concentrations varied by site (January at Alert, February at Barrow, March at Pallas, and April at Zeppelin), but with no clear relationship between the timing of the peak concentration and latitude; although the maximum occurred earlier at the two North American sites compared to the other sites.

The models used in this study are described in Ch. 7 (see Table 7.1 for a summary). They capture the Arctic BC concentrations with variable success (Fig. 8.2). Nevertheless, there is clear progress since earlier studies (e.g. Shindell et al. 2008; AMAP 2011), when the seasonality generated by most models was incorrect and many models systematically underestimated Arctic Haze

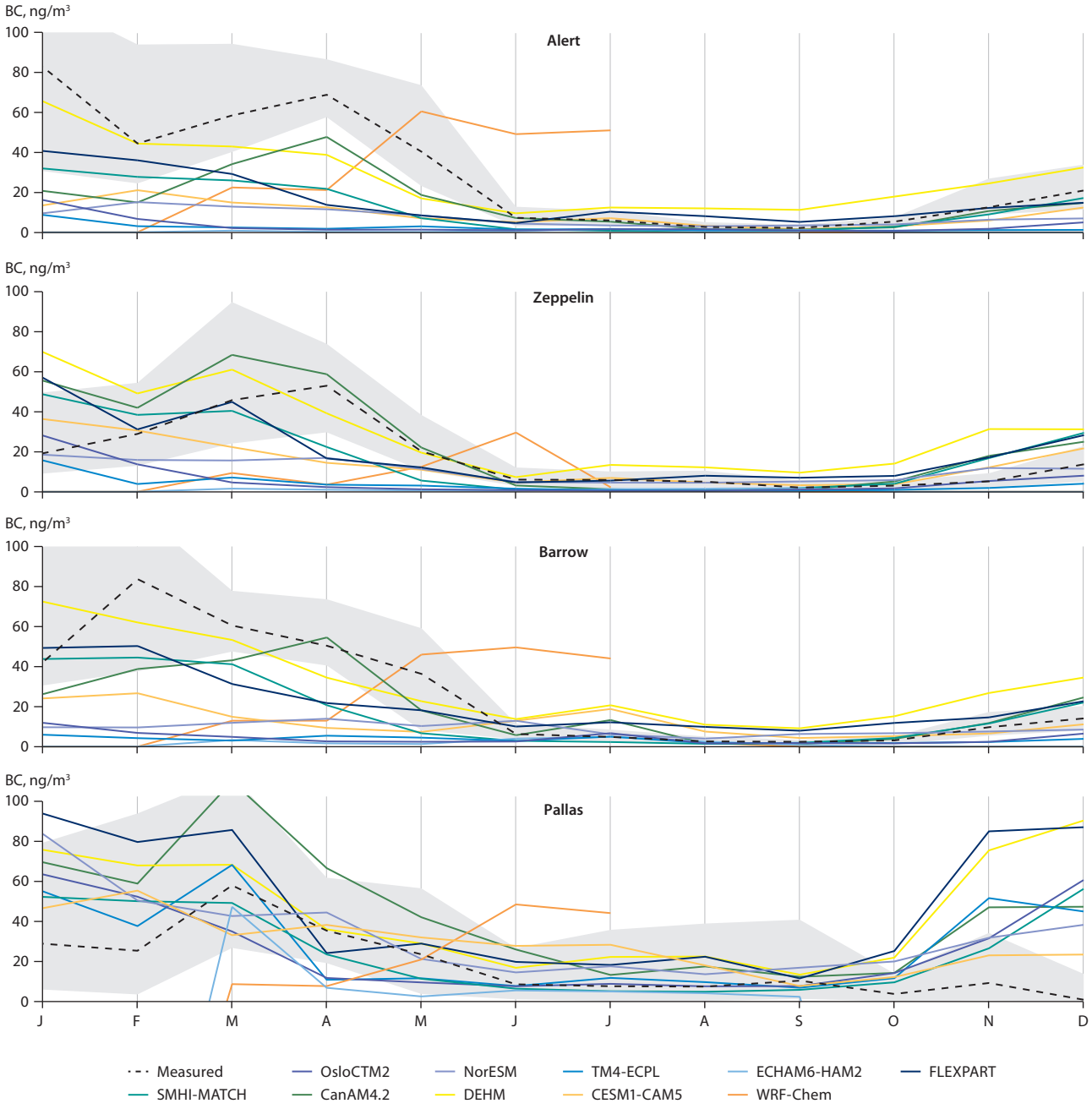

Figure 8.2 Seasonal variation in observed and modeled equivalent black carbon (eBC) concentrations for the years 2008 and 2009 at four stations. The black dashed line is the observed median, the light shaded area indicates the range between the 25th and 75th percentiles. Different colored lines show the modeled monthly median values.

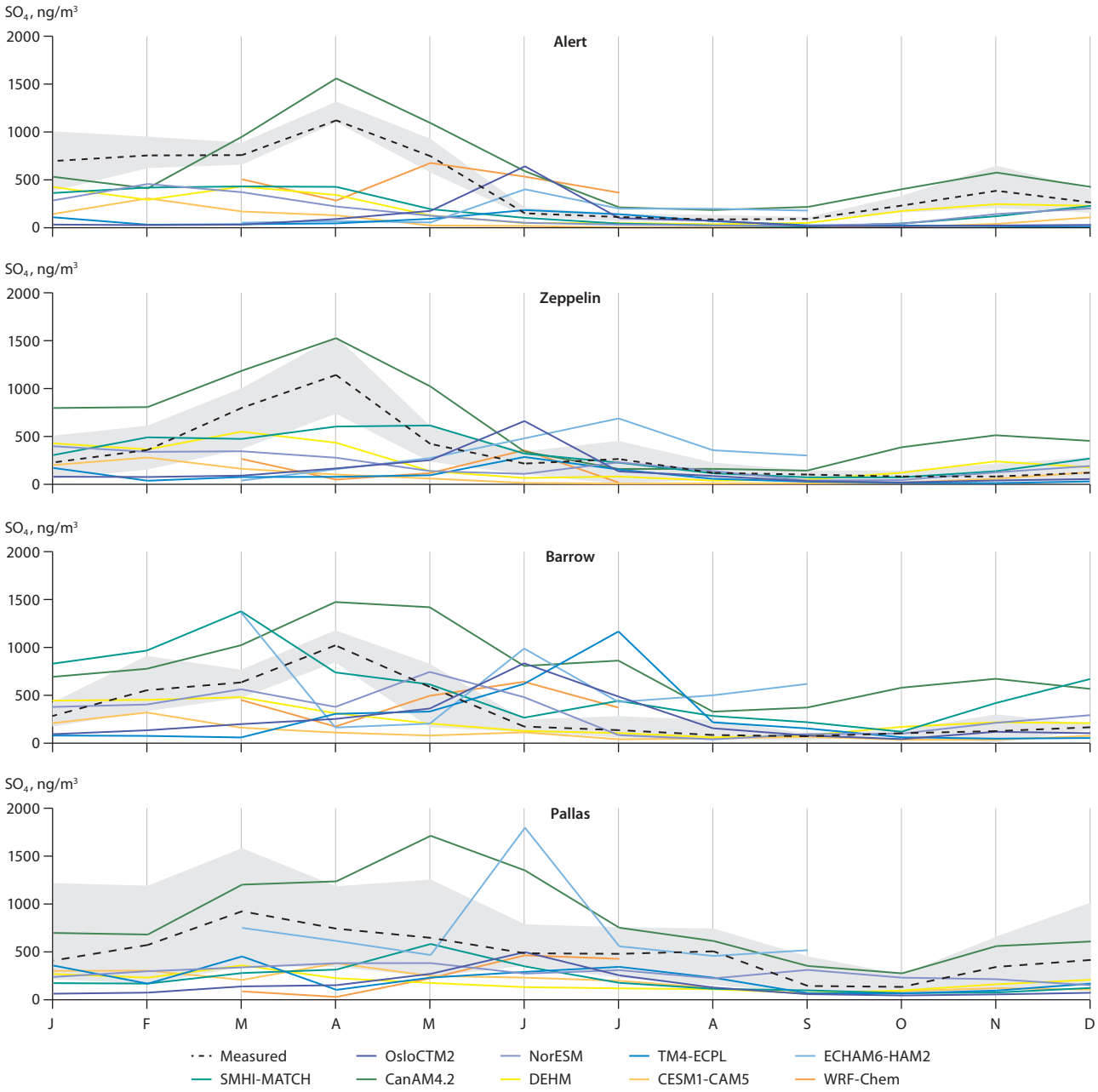

Figure 8.3 Seasonal variation in observed and modeled sulfate (SO_4) concentrations for four stations for 2008 and 2009. The black dashed line is the observed median, the light shaded area indicates the range between the 25th and the 75th percentiles. Different colored lines show the modeled monthly median values.

concentrations. In this study, most models capture the much higher concentrations in winter/spring compared to summer/autumn, and some can approximately reproduce concentrations reached during the Arctic Haze season (see also Breider et al. 2014). However, there is still much variability between individual models, with seasonal median values varying by about an order of magnitude both in spring and summer even when excluding the most extreme models (see Table 8.2). Some models still underestimate the high eBC concentrations observed during the Arctic Haze season and overestimate the low eBC concentrations observed in summer. The model discrepancies also increase with increasing latitude. At the northernmost site, Alert (82.5°N), all models underestimate eBC concentrations for the full duration of the Arctic Haze season (January until April). It is also clear that the model underestimates for spring 2008 and 2009 were of similar magnitude.

Sulfate is the dominant component of Arctic aerosol (Quinn et al. 2007). The seasonal sulfate (SO_4) cycle at the monitoring stations is similar to that of BC, with a clear maximum during the Arctic Haze season and a minimum in summer/early autumn (Fig. 8.3). However, the seasonal SO_4 cycle at the northernmost stations is weaker than for BC, with a factor of 5.4 difference between winter/spring and summer, compared to 15 for BC (Table 8.2). This is likely to be due to the influence of biogenic SO_4 sources in summer (Quinn et al. 2002).

The models have similar difficulties capturing the SO_4 seasonality as for BC, with up to about an order of magnitude difference between simulated seasonal median concentrations for different models, both in summer and in winter (Table 8.2). In fact, model variability for SO_4 in summer is even greater than for BC, probably due to different treatments for biogenic sources. In contrast to BC, where modeled concentrations

Table 8.2 Median observed equivalent black carbon (eBC) and modeled BC mass concentrations and median observed and modeled sulfate (SO_4) concentrations for the stations Zeppelin (Svalbard), Barrow (Alaska) and Alert (Canada) during winter/spring (January to March) and summer (July to September). The data are for 2008 and 2009, but a few models did not simulate the full period (see Table 7.1).

Observations/Model	eBC, ng/m^3		SO_4, ng/m^3	
	Winter/Spring	Summer	Winter/Spring	Summer
Measured data	49.4	3.3	561.0	103.2
Model mean	22.1	6.8	388.1	163.4
FLEXPART	40.2	7.7		
OsloCTM	8.4	1.3	90.2	109.7
NorESM	13.0	4.4	394.2	70.8
TM4	5.4	1.3	71.3	149.7
ECHAM6[a]	1.9	2.1	488.7	388.9
SMHI-MATCH	38.6	1.1	603.3	151.1
CanAM4.2	38.8	1.6	791.3	270.9
DEHM	57.1	11.6	434.6	61.1
CAM5	21.3	5.1	210.5	21.9
WRF-Chem	14.9	32.3	408.8	246.6

[a]Model data incomplete.

at Pallas are too high, here most models overestimate SO_4 concentrations at the lowest latitude site (Pallas) and the northernmost station (Alert).

8.2.3 Vertical profiles

The radiative effects of aerosols depend strongly on the altitude of the aerosol layer (Samset and Myhre 2011; Samset et al. 2013), so it is very important to know not only the total column loading but also the vertical distribution of aerosols. This is particularly important in the Arctic (Flanner et al. 2013; Sand et al. 2013a).

8.2.3.1 Black carbon

Figure 8.4 summarizes all rBC data from the ARCTAS and ARCPAC spring 2008 aircraft campaigns. Median concentrations are shown as a function of latitude (binned into 10° intervals) both for lower (<3 km) and higher (>3 km) altitudes, and as a function of altitude both for the High Arctic (>70°N) and lower latitudes. The models were sampled at the grid box closest to the locations and times of the measurements and were subsequently binned in the same way as the measurement data to allow a direct comparison.

For the low-altitude (below 3 km) bin, the highest median rBC values were observed at 30°N and 50°N, with a substantial drop in concentration towards higher latitudes. For the high-altitude (above 3 km) bin, the highest median concentrations were slightly further north, at 60°N, and concentrations dropped less strongly towards the North Pole than at lower altitude. All models except CanAM4.2, systematically underestimate the measured values substantially for both altitude bins and for all latitudes. This contrasts with the situation for measurements mainly outside the Arctic where most models strongly overestimate rBC values, especially at high altitudes (Hodnebrog et al. 2014). When plotted as a function of altitude, the measured values peak near 5 km, both for sub-Arctic and Arctic latitudes. All models, except CanAM4.2, underestimate the measured median values throughout the entire depth of the profile. Some of the models, mainly those driven by observed meteorology, capture the BC maximum near 5 km in the Arctic. However, the lower-latitude maximum observed around 4–5 km is hardly captured by any of the models. One reason for this discrepancy between the model results and the observations could be the strong influence of biomass burning during spring 2008 (Warneke et al. 2010; Brock et al. 2011). Even though the emission data used in the models should capture the strong biomass burning events in 2008, it cannot be excluded that the emission data are underestimated or that the emission altitudes used in the models are incorrect. However, it is likely that the models also underestimate the contributions of other BC sources, because the median measured rBC concentration should be much less affected than the mean and higher percentiles by the biomass burning plumes, which were only sampled during parts of the campaigns.

Figure 8.5 shows similar comparisons for the HIPPO campaigns in winter and autumn 2009, the ARCTAS/ARCPAC campaign in spring, the ARCTAS campaign in summer 2008, and the PAMARCMIP campaign in spring 2009. For brevity, the results show only data for latitudes north of 70°N and for median values above and below 3 km in altitude. For spring 2008, the aggregate plots for BC show even more clearly than in Fig. 8.4 that all models except CanAM4.2 at low altitudes underestimate the measured rBC concentrations, some substantially (by up to factors of 50 and 260). For summer 2008, results are mixed. Measured concentrations in summer are much lower than in spring, both at low and high altitudes, and the majority of models overestimate measured concentrations, especially below 3 km. This picture of substantial model underestimates in spring and a tendency towards overestimates in summer is consistent with the previous findings based on intercomparisons between model estimates and observations at surface sites (see Sect. 8.2.2). The

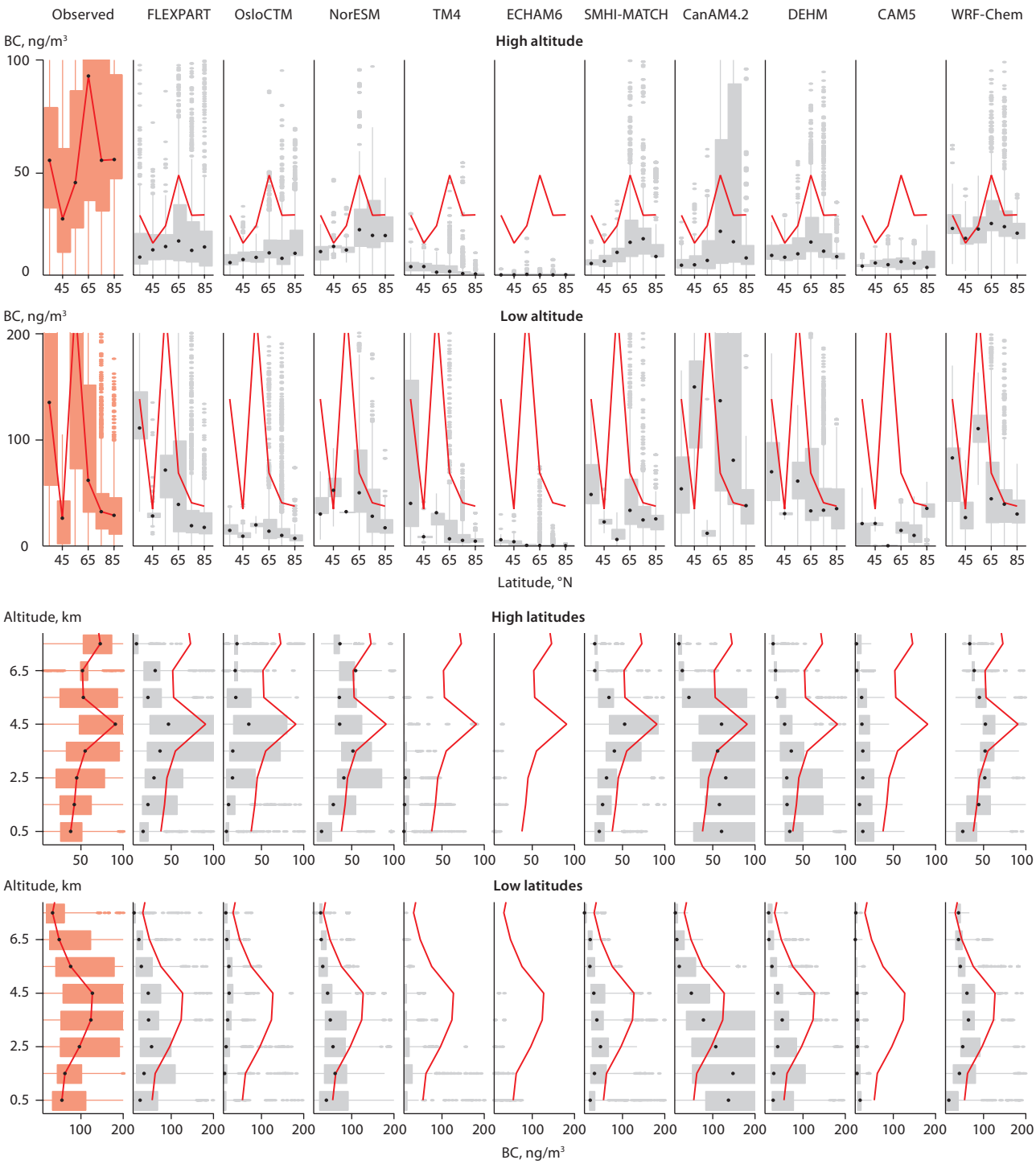

Figure 8.4 Comparison of modeled black carbon (BC) concentrations with observations of refractory BC (rBC) from the ARCTAS-spring and ARCPAC aircraft campaigns in spring 2008. The first column shows box and whisker plots of observed rBC concentrations in ng/m³. The black dots and red line represent the median, the boxes extend from the 25th to the 75th percentiles and the red dots represent outliers. The other columns show the modeled BC concentrations for a range of models. The two upper rows show BC concentrations binned into 10° latitude bands from 30–40°N to 80–90°N, and for altitudes above/below 3 km asl. The two lower rows show BC concentrations binned into 1-km height intervals for latitudes above/below 70°N.

seasonality in the low-altitude bin from the aircraft campaigns is consistent with that measured at the surface sites.

The spring 2009 PAMARCMIP campaign shows a slightly different picture. This campaign had little influence from biomass burning. The measured median rBC concentrations at low (high) altitudes were about a factor of two (four) lower than for the spring 2008 campaigns. Most model results show the same tendency, also simulating lower median concentrations than a year earlier. However, while there is a significant difference between the measurements for spring 2009 (little influence from biomass burning) and spring 2008 (strong influence from biomass burning), the difference between the two sets of simulated concentrations was much less and the simulated concentrations fit better the measured median values in spring 2009. The vertical gradient of measured rBC also differed between 2008 and 2009. In spring 2008, concentrations above 3 km were higher than those below, owing to the strong biomass burning influence aloft, while the opposite was true in

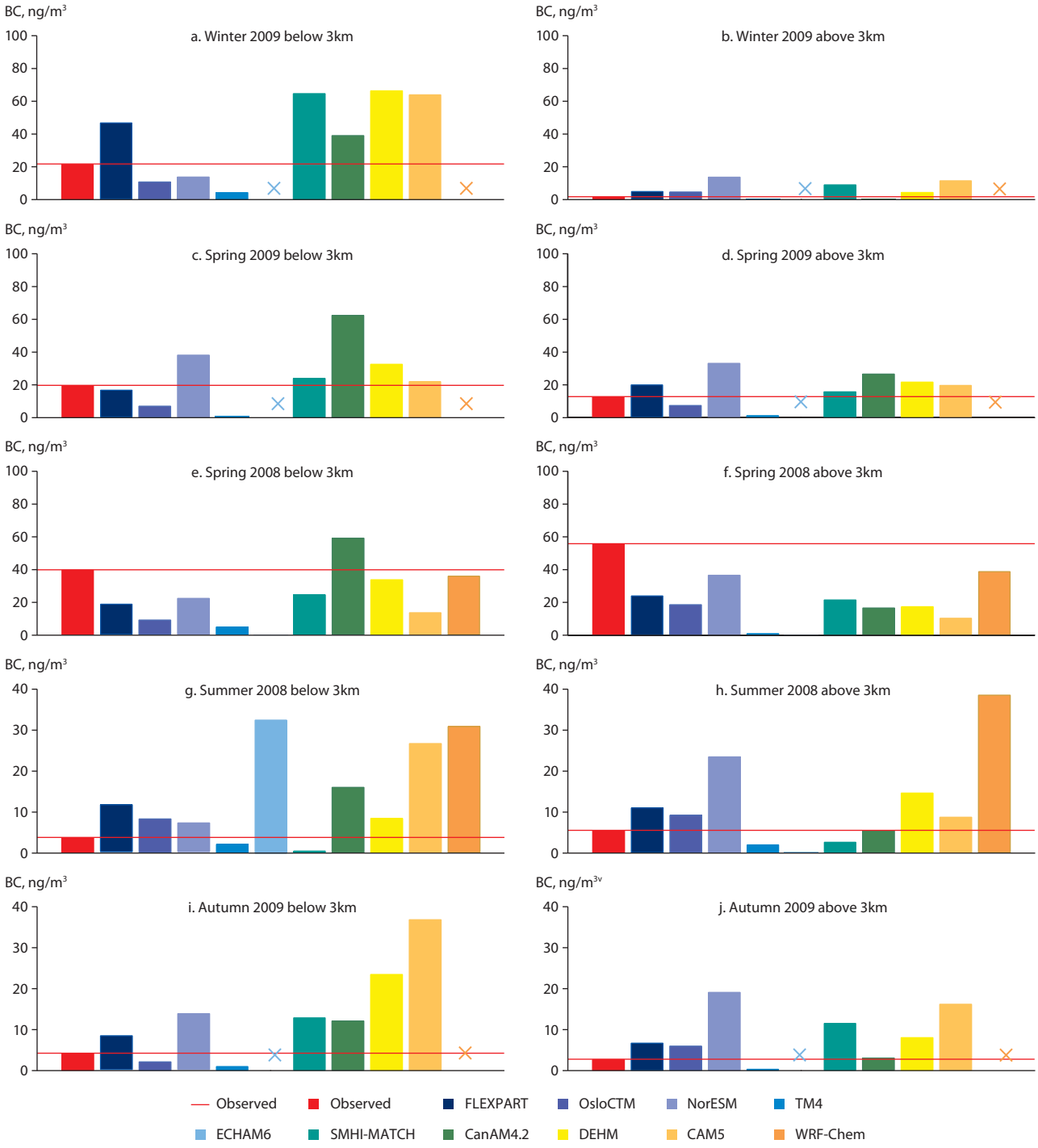

Figure 8.5 Median black carbon (BC) concentrations north of 70°N for various aircraft campaigns during the International Polar Year. Winter 2009, HIPPO (a, b), spring 2009 PAMARCMIP (c, d) and spring 2008 ARCTAS/ARCPAC (e, f), summer 2008 ARCTAS (g, h) and autumn 2009 HIPPO (i, j). The red bar and red line show observed concentrations and the colored bars show model results. Missing model results are marked by a cross. The analysis is performed for measurements below 3 km (left panels) and above 3 km (right panels) in altitude. Note: scales on the y-axes vary.

spring 2009 when there was little biomass burning influence. This change in the vertical distribution of rBC over the two years is not well captured by the models. It is noteworthy that despite the differences in the aircraft measurements, the median concentrations measured at the surface stations were nearly identical in April 2008 and April 2009.

The HIPPO campaign in autumn 2009 was conducted about one month after the seasonal minimum at most surface sites and measured very low rBC concentrations, which are consistent with surface observations. Most of the models overestimated the measured concentrations, both above and below 3 km. The HIPPO campaign in winter (January) 2009 measured strong vertical differences: moderately high rBC concentrations below 3 km, but the lowest concentrations of all campaigns above 3km. This feature is very well captured by the models.

Overall, the aircraft measurements confirm the BC seasonality measured at the surface stations. They also confirm that most models underestimate BC concentrations in spring, while many

overestimate concentrations in summer and autumn. Plus, the BC seasonality generated by the models is too weak to properly represent changes measured at the surface (Fig. 8.2), or vertically through the troposphere.

8.2.3.2 Sulfate

Measured median SO_4 concentrations in the Arctic during spring 2008 were lower above 3 km than below 3 km (see Fig. 8.6). Below 3 km, the median measured SO_4 concentration (1200 ng/m^3) was higher than measured at the surface during winter/spring (413 ng/m^3; Table 8.2), consistent with a strong vertical gradient measured in the lowest 1 km during spring 2008 (Brock et al. 2011). All models, except CanAM4.2, strongly underestimate the measured SO_4 concentrations, some models by more than an order of magnitude. Also, the models vary in their vertical distribution of SO_4, with some models correctly simulating lower concentrations above 3 km than below, while others show the opposite.

During summer 2008, the measured median SO_4 concentrations were about a factor of 4–6 lower than in spring 2008, consistent with the seasonality measured at surface sites. Median concentrations above and below 3 km are very similar. Two-thirds of the models underestimate the summer SO_4 concentrations above 3 km, and large overestimates and underestimates occur below 3 km. Given the large differences in rBC measured between spring 2008 and spring 2009, the representativity of the 2008 SO_4 measurements may be limited, even though biomass burning is a much less important source of SO_4 than for BC. However, it does seem that the models underestimate SO_4 seasonality not only at the surface (see Fig. 8.3) but also higher in the troposphere.

8.2.4 Black carbon in snow

Modeled impacts of BC on snow albedo are best evaluated using direct measurements of BC in the snowpack and sea ice. In this study, simulated distributions of BC in snow were evaluated against measurements by Doherty et al. (2010). This observation dataset comprises hundreds of samples collected during an extensive survey of the Arctic in 2006–2009. Most of the measurements were made in the top 5 cm of snow. The model outputs evaluated were the CESM1.1.1 and CanAM4.2 simulations that apply all global BC emissions (Ch. 11) and are driven with interannually-varying sea-surface temperatures (SSTs) during the period of measurements. The land component of CESM simulates BC in the surface layer of the snowpack (on average ~2 cm thick), which is dependent on wet and dry aerosol deposition fluxes, precipitation, snow sublimation, melt removal, and snow layer combinations and divisions (e.g. Flanner et al. 2007). In CanAM4.2, the temporal evolution of BC in surface snow on bare ground and sea ice is calculated based on a simplified mass budget, which accounts for aerosol deposition and melting of snow. Increases in BC concentration in snow from BC deposition are represented as an adjustment of the BC concentration towards instantaneous values at the snow surface. The adjustment occurs over a timescale that is inversely related to the snowfall deposition flux and proportional to the depth of the surface snow layer, which is assumed to be 20 cm. In both models, BC becomes more highly concentrated in the surface snow layer when snow melts and meltwater drains out of the surface snow layer. This process is parameterized in terms of the meltwater flux out of the snow layer and assumptions about the hygroscopicity of BC particles. A shallower surface layer in the CESM model means that the 'surface layer' is more strongly influenced by dry deposition of BC and the effects of

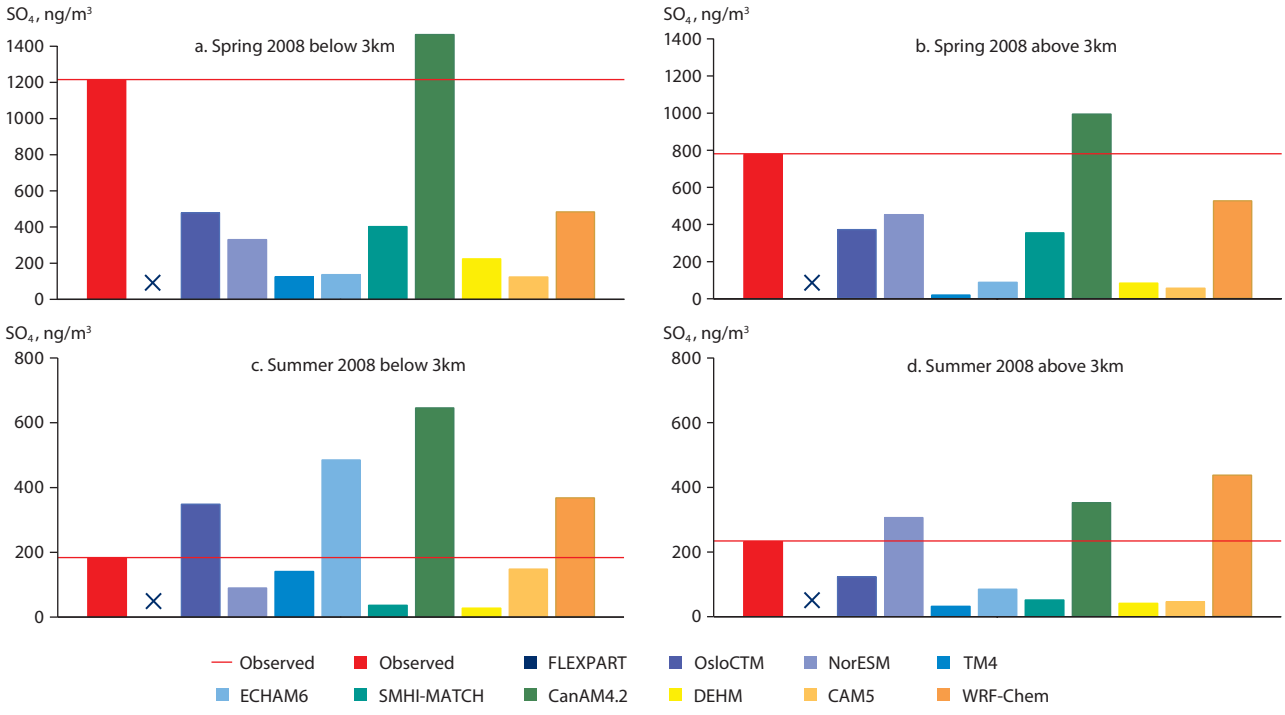

Figure 8.6 Median sulfate (SO_4) concentrations north of 70°N for the spring 2008 ARCTAS and ARCPAC aircraft campaigns and the summer 2008 ARCTAS campaign. The red bar and red line show observed concentrations and the colored bars show model results. Missing model results are marked by a cross. The analysis is performed for measurements below 3 km (left panels) and above 3 km (right panels) in altitude. Note: scales on the y-axes vary.

melting on near-surface BC, both of which will lead to higher surface layer BC concentrations in the CESM model than in the CanAm model.

Monthly-mean values from the same grid cell, year, and month of measurement are used for the comparison, following procedures similar to those adopted by Jiao et al. (2014). To avoid ambiguities associated with matching model snow layers and depth profiles of samples, the comparisons are restricted to measurements collected within the surface layer (top 2 cm) of land-based snow. Measurements within the same model grid cell are averaged and evaluated as a single sample, and samples coinciding with grid cells that have no snow cover are discarded from the analysis. It should be noted that simulated BC-in-snow concentrations applied here are not subject to the bias described by Doherty et al. (2014c), which results when temporally inconsistent aerosol wet deposition and precipitation fluxes are used to drive offline simulations.

Figure 8.7 shows scatterplots of measured and simulated values from the two models. Mean observed and modeled BC concentrations averaged over all points used in the CESM evaluation are 20.1 and 12.0 ng/g, respectively. The correlation coefficient (r) is only 0.15, but rises to 0.41 with the removal of two outlier points from Greenland. Observed and modeled mean values derived from the CanAM4.2 analysis are 20.9 and 6.2 ng/g respectively, with r=0.46. CESM captures much of the low and moderate concentrations of BC in snow, but overestimates BC in snow over parts of Greenland, especially in melt-affected grid cells. Neither model captures the very high concentrations measured in Russia. CanAM4.2 has a higher correlation coefficient than CESM, but tends to underestimate surface-layer BC in all regions. The CanAM4.2 evaluation may also be affected by the different thickness thresholds assumed for surface snow in the model and measurements. It is interesting that CESM tends to underestimate BC in the near-surface Arctic atmosphere (Sect. 8.2.2) while simulating reasonable concentrations of BC in Arctic snow. CanAM4.2, on the other hand, tends to simulate better near-surface atmospheric concentrations while underestimating BC in snow. Future investigations into the roles of Arctic aerosol deposition processes, melt-induced impurity accumulation, sublimation, and discretization of snow layers should help identify the reasons for these differences.

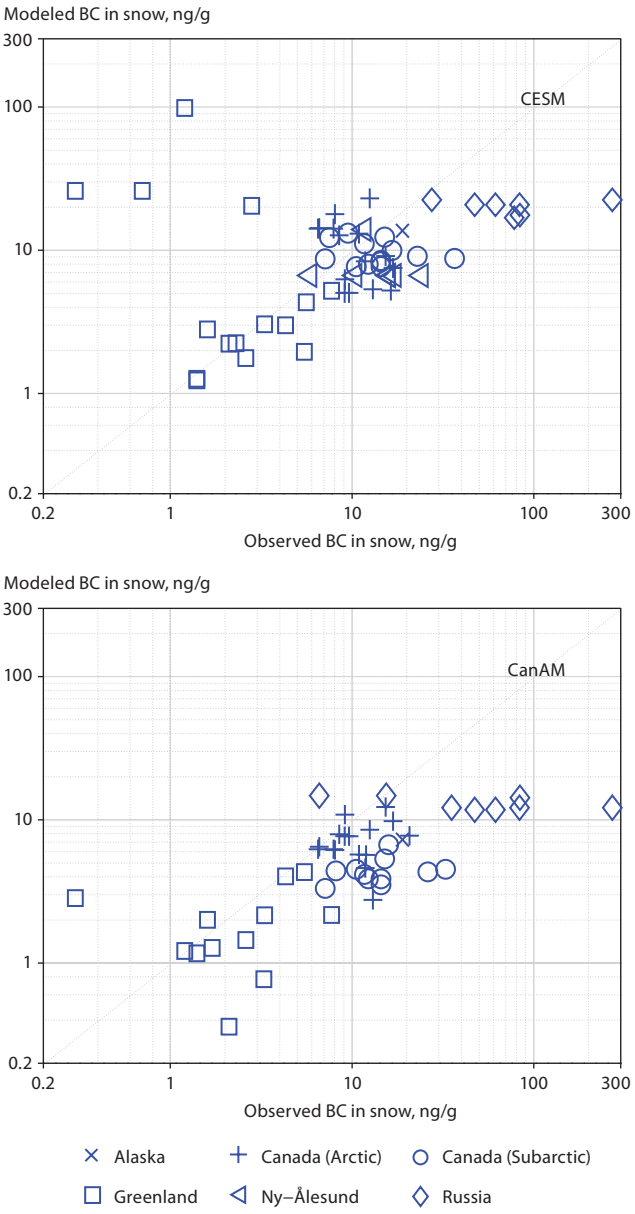

Figure 8.7 Comparison of simulated black carbon (BC) concentrations in surface snow from the CESM1.1.1 model (upper) and the CanAM4.2 model (lower) versus BC measurements by Doherty et al. (2010).

8.2.5 Conclusions (aerosols)

Sulfate and BC concentrations measured at Arctic surface sites show a clear maximum in winter and early spring during the Arctic Haze season and a minimum in summer and early autumn. Model simulations of seasonality have improved and BC concentrations in Arctic Haze are underestimated to a lesser extent than with earlier models (AMAP 2011). However, the monthly median concentrations of BC and SO_4 generated by models still show much scatter and deviate from measurements by up to an order of magnitude, or even more in some cases. Despite improvements, most models still underestimate BC and SO_4 concentrations at the highest-latitude stations in spring. For an aircraft campaign in spring 2008, a season with pronounced biomass burning influence, the underestimates extend through the full depth of the troposphere, whereas for a campaign in spring 2009, which had less biomass burning influence, some models overestimate the much lower BC concentrations measured. For the surface stations, however, consistent underestimates are found in 2008 and 2009. It is unclear whether the different results obtained for the different aircraft campaigns reflect differences in the measurement strategies (e.g. 'plume hunting' vs. background measurements) or the measurement instruments used, or whether they reflect real atmospheric variability. There is currently insufficient vertical profile information available for BC in the Arctic atmosphere to enable comprehensive model validation. Summer concentrations of BC and SO_4 at the surface and through the troposphere are overestimated by some models and underestimated by others, with large differences between individual models. Overall, the simulated seasonality of BC within the troposphere seems too weak in most models. Simulated concentrations of BC in land-based Arctic snow are biased low, on average, by factors of 1.7 and 3.4 in two models, with the most severe underestimates occurring in Russia.

8.3 Trace gases

This section evaluates the performance of the AMAP and ECLIPSE models in the Arctic region for trace gases. The main focus is on tropospheric O_3 and its precursors, notably carbon monoxide (CO) and nitrogen oxides (NO_X), as well as important NO_X reservoir species such as peroxyacetyl nitrate (PAN) (see Ch. 3). The results presented here build on previous analyses where global and regional chemical transport and chemistry-climate models were evaluated against observations in the Arctic and over anthropogenic and boreal fire emission regions for the year 2008. In particular, the POLARCAT Model Intercomparison Project (POLMIP) recently evaluated eight global models and one regional model against POLARCAT aircraft data, surface measurements and satellite data. Results from POLMIP were reported by Arnold et al. (2015), Emmons et al. (2015) and Monks et al. (2015). The models also simulated year 2008, but using POLMIP-specific emissions data (see Emmons et al. 2015). Several models took part in both POLMIP and AMAP model comparison exercises, allowing some indication of the sensitivity of simulated O_3 and precursor distributions to input emissions. ECLIPSE model results are also included in the present analysis.

8.3.1 Measurement data

The models were evaluated using a variety of measurement data. They were compared to O_3 and CO observations at several surface sites (see Table 8.3): Barrow (Alaska); Alert (Canada); Zeppelin (Svalbard); Pallas (Finland); and Summit (Greenland). It should be noted that local pollution events are removed from CO data at Barrow and Alert. The models were also compared to ozonesonde vertical profile data collected as part of the Network for the Detection of Atmospheric Composition Change (NDACC, www.ndsc.ncep.noaa.gov): Eureka (Canada), Summit, Ittoqqortoormiit (Greenland), Ny Ålesund and Sodankylä (Finland) (see also Ch. 3). Extensive trace gas measurements were collected in spring and summer 2008 as part of POLARCAT (see Law et al. 2014 and references therein). The present study compares the new AMAP model output to 2008 aircraft data collected during ARCTAS-A (Alaska, April), POLARCAT-France (northern Sweden, April), ARCTAS-B (Canada, June-July), and POLARCAT-France/POLARCAT-GRACE (Greenland, June-July) (Adam de Villers et al. 2010; Jacob et al. 2010; Brock et al. 2011; Roiger et al. 2011). See Fig. 8.1 for station locations and flight tracks and Table 8.3 for further information on measurements.

8.3.2 Seasonal cycles at surface sites

Figure 8.8 compares observed and modeled surface CO concentrations at Barrow (Alaska) and Zeppelin (Svalbard). The models capture the observed seasonal cycle with a maximum at both locations in late winter / early spring and a minimum in summer, but underestimate the winter and spring concentrations, as shown by the mean seasonal model biases. Similar features are also found at Pallas (Finland) and Alert (Canada). This discrepancy is a very common feature in global chemical models and has been reported previously based on models run with different anthropogenic emission datasets (Shindell et al. 2008). The more recent POLMIP results also show some underestimation (Monks et al. 2015) but to a lesser extent than for the AMAP model results. Model variability in POLMIP was attributed to differences in model oxidative capacity (i.e. the ability to destroy CO by chemical reaction with the hydroxyl radical, OH) and differences in export of pollutants from emission regions (Monks et al. 2015). Differences in boreal fire emissions used in the two studies (GFEDv3 in AMAP and FINN in POLMIP) may also explain some of the differences.

The MATCH model was used in both the POLMIP and AMAP studies. The only difference between the simulations submitted to POLMIP and AMAP was in the emission data, thereby showing

Table 8.3 Long-term systematic ozone and carbon monoxide observations in the Arctic (north of 60°N) contributing to the analyses discussed in this study (see Ch. 2, 8 and 9).

Site	Location	Elevation, m asl	Ozone (O_3)		Carbon monoxide (CO)
			Surface	Sondes	Surface
Alert	82.45°N, 62.52°W	210		✓	
Barrow	71.32°N, 156.6°W	11	✓	✓	✓
Zeppelin (Ny Ålesund)	78.91°N, 11.88°E	474	✓		✓
Pallas	67.97°N, 24.12°E	560	✓		✓
Eureka	80.05°N, 86.42°W	610		✓	
Qausuittuq (Resolute)	74.72°N, 94.98°W	68		✓	
Sodankylä	67.37°N, 26.65°E	100		✓	✓
Summit	72.60°N, 38.42°W	3208	✓		✓
Ittoqqortoormiit (Scoresbysund)	70.48°N, 21.97°W	68		✓	
Pituffik (Thule)	76.52°N, 68.77°W	200		✓	
Kangerlussuaq (Sønderstrøm)	67.00°N, 50.98°W	150		Total column	
Esrange	67.89°N, 21.11°E		✓		

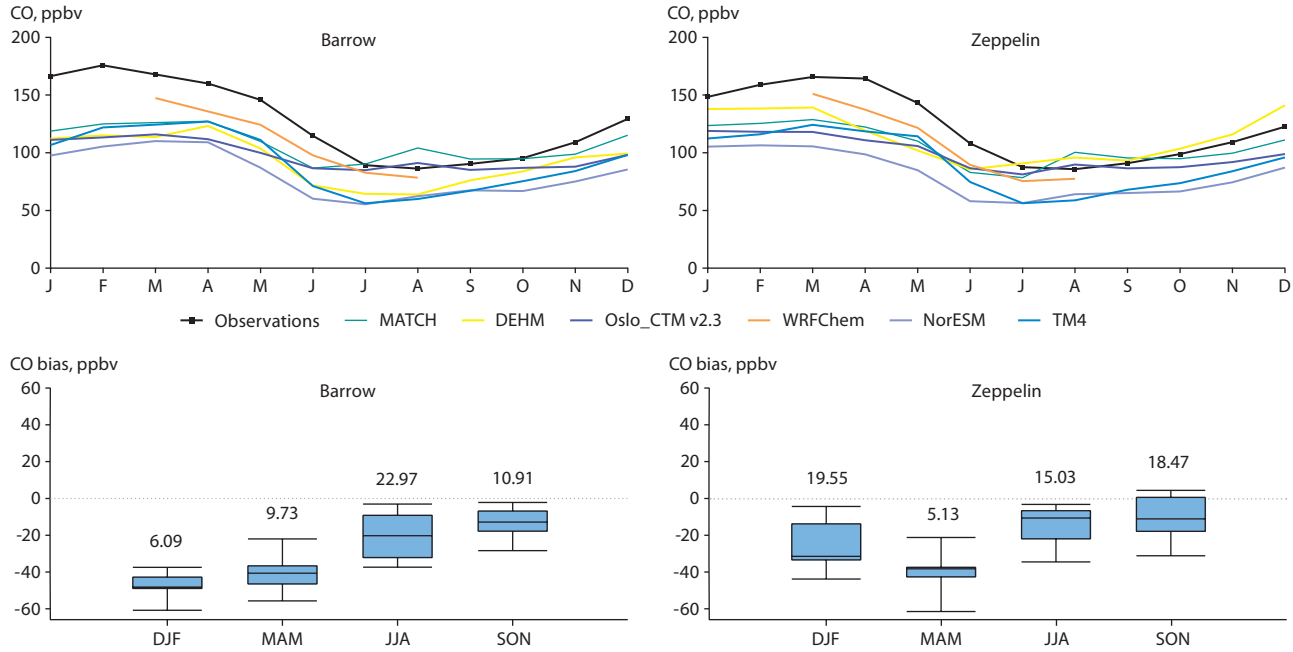

Figure 8.8 Seasonal variation in measured and modeled carbon monoxide (CO) concentrations in the Arctic in 2008. Observed (black lines/symbols) and modeled (colored lines) monthly mean CO concentrations at Barrow (left) and Zeppelin (right) and seasonal mean biases of models-observations in winter (December/January/February), spring (March/April/May), summer (June/July/August) and autumn (September/October/November) 2008. The box and whisker plots show minimum, 25th percentile, median, 75th percentile and maximum values for each set of model data. The interquartile range, IQR (75th to 25th percentiles) represents the spread in the model results, the numbers show the absolute IQR.

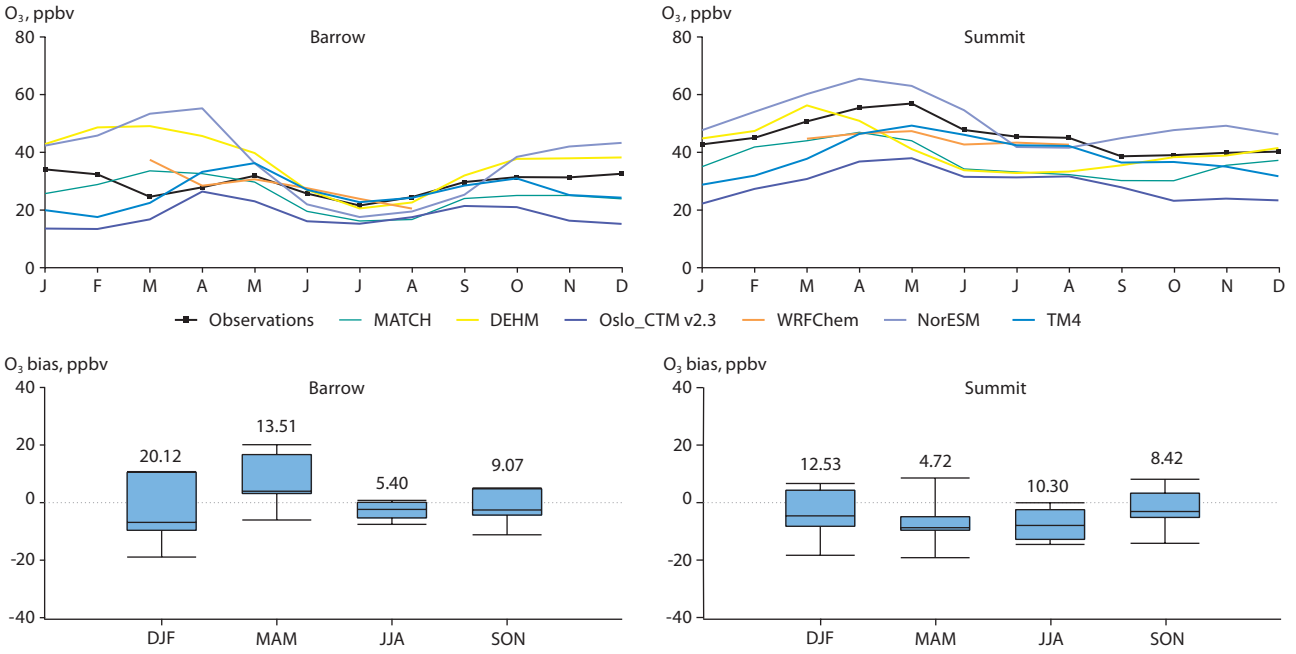

Figure 8.9 Seasonal variation in measured and modeled nitrogen oxide (NO_X) concentrations in the Arctic in 2008. Observed (black lines/symbols) and modeled (colored lines) monthly mean NO_X concentrations at Barrow (left) and Summit (right). Seasonal mean biases of models-observations in winter (December/January/February), spring (March/April/May), summer (June/July/August) and autumn (September/October/November) 2008. The box and whisker plots show minimum, 25th percentile, median, 75th percentile and maximum values for each set of model data. The interquartile range, IQR (75th to 25th percentiles) represents the spread in the model results, the numbers show the absolute IQR.

the effect of different emissions data on simulation of Arctic atmospheric composition. The simulated seasonal cycles of CO and O_3 at Barrow, Zeppelin, and Summit are very similar while the concentrations of CO are 10–20 ppb greater year-round in POLMIP, resulting in overestimates in the period June–November (not shown). CO simulated during spring is still lower when using POLMIP emissions, but closer to the observations than using AMAP emissions. It seems likely that similar differences in CO concentration would be simulated if the same multi-emission experiment was repeated with other models.

Figure 8.9 compares modeled and observed O_3 concentrations at Barrow (Alaska) and Summit (Greenland). As discussed in Ch. 3, sites on the coast of the Arctic Ocean often show low O_3

concentrations in spring attributed to halogen destruction due to reactions involving bromine. None of the AMAP models consider bromine chemistry, and all have problems simulating the seasonal O_3 cycle at surface sites such as Barrow, which are influenced by air masses crossing the Arctic Ocean / sea ice. Three models (NorESM, Oslo, DEHM) also largely overestimate winter concentrations. This leads to significant mean model biases in the winter and spring. On the other hand, models are generally able to capture the summer minimum at Barrow. The picture is different at Summit, which is at 3 km elevation in central Greenland. This site receives air masses from mid-latitude continental regions, primarily from North America but also from Europe and Asia. Lower biases are found between model results and observations at this site with the main discrepancies being an underestimation during summer and autumn. This could be due to lack of O_3 production in air masses originating from anthropogenic and fire emissions (e.g. Thomas et al. 2013; Arnold et al. 2015). Due to the stability of air masses over the Greenland Ice Sheet, local photochemistry leading to net O_3 production in summer may also play a role very close to the surface (Thomas et al. 2012). It is important to quantify model biases at surface locations in the Arctic given that, as discussed in Ch. 4, O_3 radiative forcing is more sensitive to changes in shortwave radiation absorption due to O_3 perturbations in the lower troposphere than previously appreciated.

8.3.3 Vertical profiles

Vertical profile data includes ozonesonde data collected at several Arctic sites as well as trace gas data, including O_3 and precursors, collected during the POLARCAT aircraft campaigns in spring and summer 2008. Although the relative importance of shortwave radiative forcing in the lower troposphere is greater in the Arctic, it is important to evaluate model behavior over the depth of the troposphere since both short- and longwave O_3 radiative forcing, driven by anthropogenic perturbations, are very sensitive to changes in O_3 at different altitudes.

8.3.3.1 Ozonesondes

A comparison of model results and ozonesonde data at five Arctic locations for late spring and summer (May-July) 2008 when NDACC observations were available is shown in Fig. 8.10. Ozone data from sondes, typically launched on a weekly basis during this period, were binned into 50 hPa layers, averaged and compared to model output averaged for the same dates. The models capture well the general increase in O_3 concentrations with altitude seen at all sites. However, model biases are particularly large in the upper troposphere, for example at Ny Ålesund and Summit, and probably due to differences in transport of air masses from the stratosphere. None of the models simulate stratospheric O_3 chemistry and so use different approaches for specifying O_3 upper boundary conditions, which may also help to explain some of the differences. The models tend to underestimate O_3 in the mid-troposphere at Ny Ålesund. Some models (MATCH, DEHM) also underestimate O_3 in the mid-troposphere at other locations (Ittoqqortoormiit, Sodankylä). MATCH also shows a tendency to underestimate O_3 concentrations in the lower troposphere, consistent with the results from the surface sites.

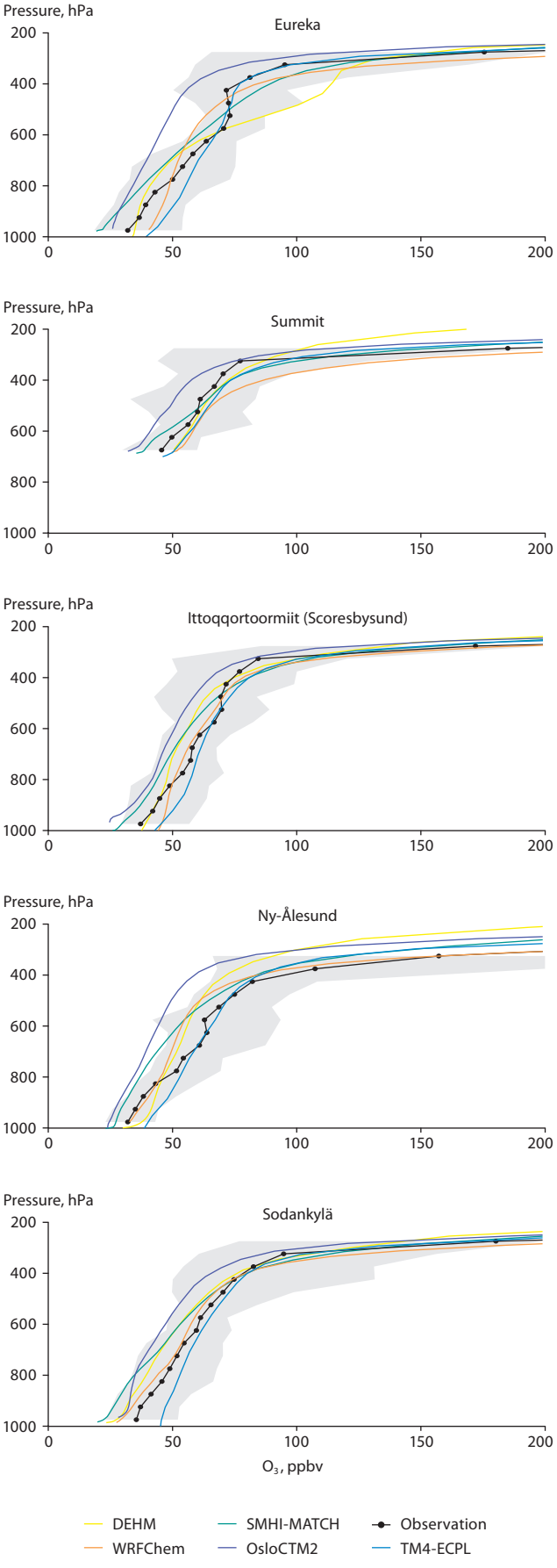

Figure 8.10. Comparison of AMAP model results and ozonesonde data at five Arctic measurement sites for May-July 2008. Observations were binned into 50 hPa layers and then averaged. Horizontal bars for observations indicate the total range between days in the observations. The number of profiles were 11 (Eureka), 23 (Summit), 13 (Scorebysund), 13 (Ny-Ålesund) and 14 (Sodankylä).

8.3.3.2 Aircraft data

Aircraft data from the POLARCAT aircraft experiments allow an evaluation of O_3 and its precursors from the AMAP model simulations through the full depth of the troposphere for spring and summer 2008. This evaluation is important for establishing confidence in simulated O_3 radiative effects at times of year when solar radiation is at its maximum. To illustrate model performance Fig 8.11 compares model results with data collected during ARCTAS-A in spring 2008 (Jacob et al. 2010) and Fig. 8.12 compares model results with summer POLARCAT-GRACE data collected over Greenland (Roiger et al. 2011). Model–observation differences are summarized in Fig. 8.13, which shows model biases compared to data from several POLARCAT airborne campaigns.

Spring

Several model discrepancies are apparent in the spring, in particular, the large underestimation in CO concentrations through the depth of the troposphere in all models. This feature was also found in POLMIP although discrepancies were smaller for flights sampling air masses influenced by Siberian fires (Emmons et al. 2015). It is worth noting that the ARCTAS-A data shown in Fig 8.11 includes air masses influenced by boreal fires, which were prevalent in April 2008 over Siberia and eastern Europe / Russia as well as air masses carrying anthropogenic emissions from Asia. Analysis of POLARCAT data has shown that models have significant difficulties reproducing oxygenated volatile organic compounds (VOCs), such as formaldehyde or acetone, which also act as important sources of hydroxyl radicals ($OH + HO_2 = HO_X$) (Law et al. 2014; Emmons et al. 2015). As noted previously, analysis of POLMIP results highlighted differences in CO destruction by OH as a major source of uncertainty (Emmons et al. 2015; Monks et al. 2015). New photochemistry, involving the loss of HO_2 radicals on aerosols, has also been proposed to resolve the negative CO model bias (Mao et al. 2013).

The models overestimate PAN compared to the ARCTAS spring data. But it should be noted that the MATCH model (and other models) compare better with ARCPAC data, also from flights flown in April 2008, which primarily targeted air masses influenced by boreal fires (Emmons et al. 2015). However, simulated CO is still too low. The overestimation of PAN, an important NO_X reservoir, may be due to general overproduction from (anthropogenic) emissions or due to temperature biases in models enhancing PAN stability (the main loss of PAN is via thermal decomposition). Potentially coupled to this, NO_X species (NO, NO_2) are underestimated compared to ARCTAS-A data in the mid-troposphere (4–8km) (see Fig. 8.11). Previous studies have already shown that photochemical production of O_3 is important in the free troposphere in the spring months and an important contributor to the observed maximum at this time of year in the Arctic (Wespes et al. 2012; Emmons et al. 2015). Discrepancies between model and observed NO_X and NO_X reservoirs as well as other trace species, such as HO_X and oxygenated VOCs, point to gaps in knowledge leading to uncertainties in the ability to simulate the tropospheric O_3

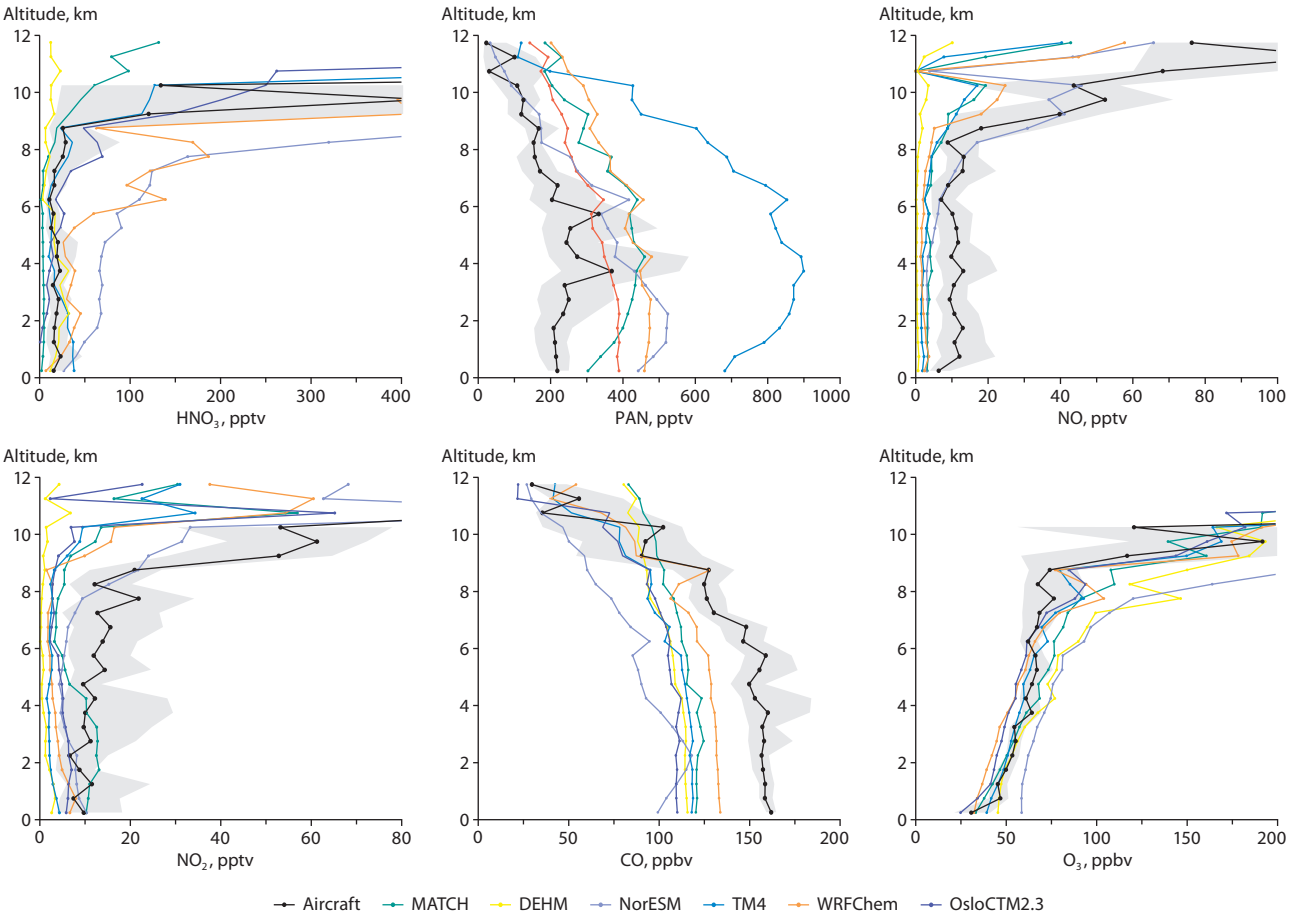

Figure 8.11 Comparison of AMAP models against NASA DC-8 aircraft data collected as part of the ARCTAS-A spring campaign in April 2008. Observed medians are shown in black together with 25th/75th percentiles. Model median results are shown by the different color lines. Data are plotted for nitric acid (HNO_3), peroxyacetyl nitrate (PAN), nitrogen oxide (NO), nitrogen dioxide (NO_2), carbon monoxide (CO), and ozone (O_3).

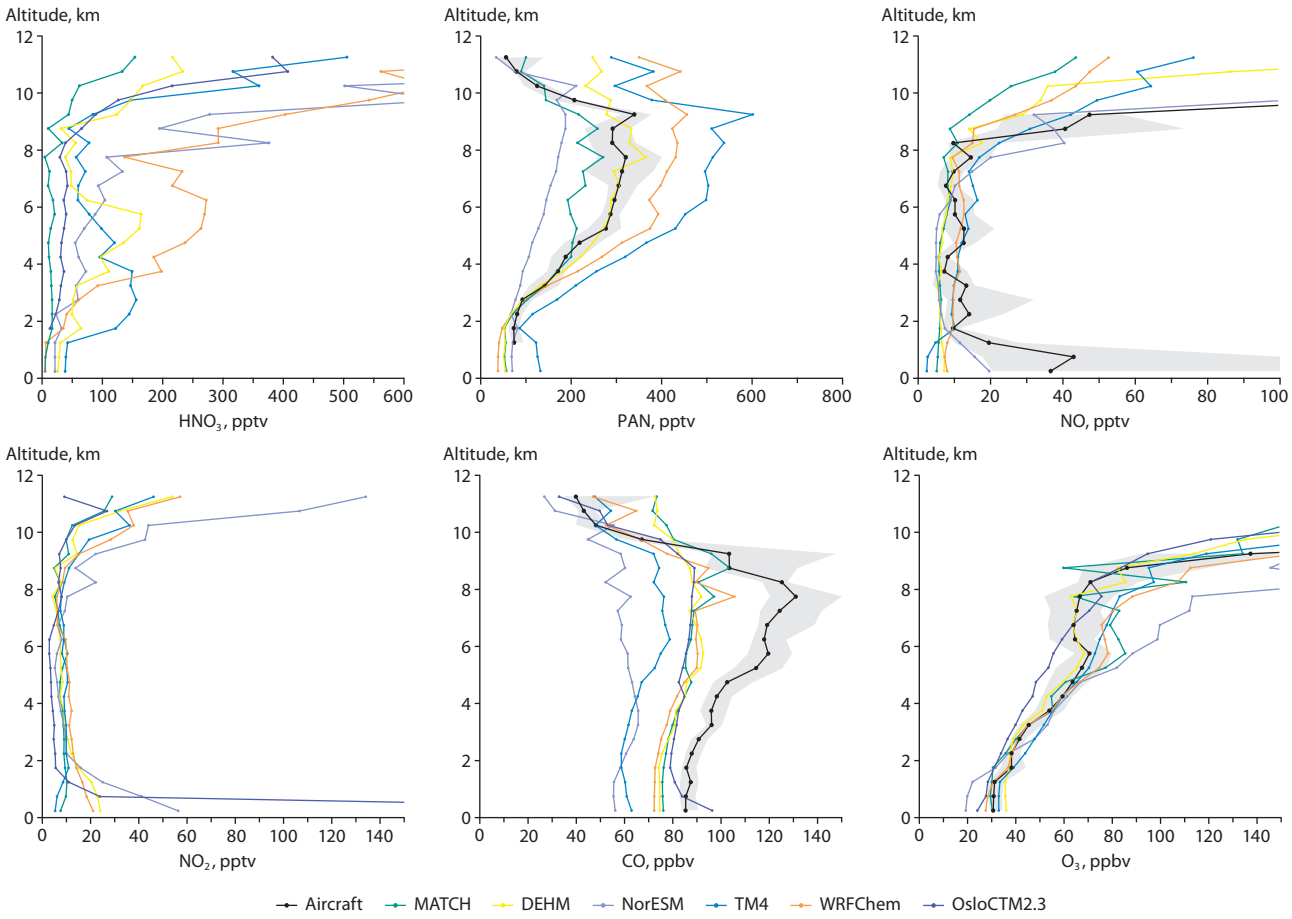

Figure 8.12 Comparison of AMAP models against DLR-Falcon aircraft data collected as part of the POLARCAT-GRACE campaign in June/July 2008. Observed medians are shown in black together with 25th/75th percentiles. Model median results are shown by the different color lines. Data are plotted for nitric acid (HNO_3), peroxyacetyl nitrate (PAN), nitrogen oxide (NO), nitrogen dioxide (NO_2), carbon monoxide (CO), and ozone (O_3). HNO_3 and NO_2 were not observed by the aircraft but are plotted to show model results only.

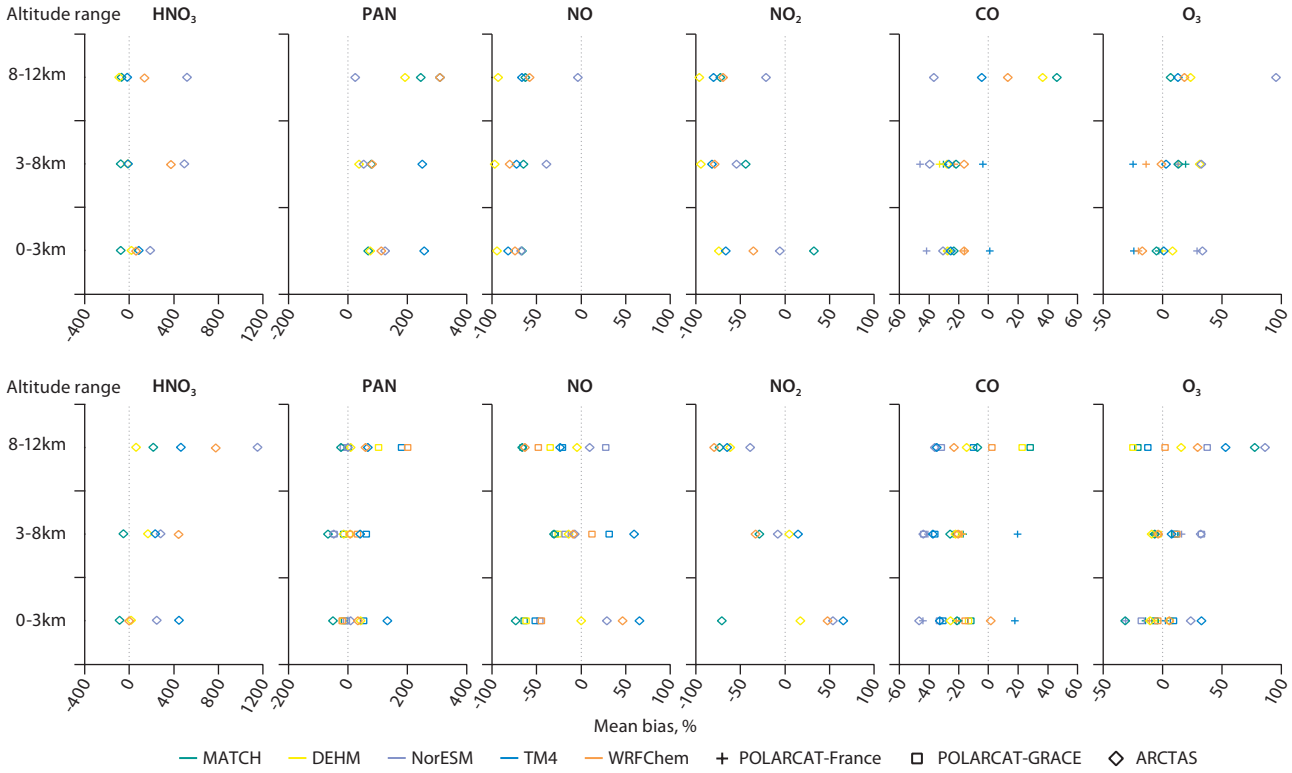

Figure 8.13 Model mean biases binned over three altitude ranges. The upper panels show results for April 2008 compared to data from the POLARCAT-France and ARCTAS-A campaigns. The lower panels show results for July 2008 using data from POLARCAT-France/GRACE and ARCTAS-B. Different models are shown by different colors and biases compared to the different campaigns by different symbols. Results are plotted for nitric acid (HNO_3), peroxyacetyl nitrate (PAN), nitrogen oxide (NO), nitrogen dioxide (NO_2), carbon monoxide (CO), and ozone (O_3).

budget. However, model biases in O_3 (Fig. 8.13) are generally positive. In contrast to the ozonesonde comparisons, the more detailed evaluation along flight tracks as illustrated in Figs. 8.11 and 8.12, suggests that models have too much O_3 transported from the stratosphere rather than too much photochemical production. These biases are larger in the summer (see next section). Since stratospheric O_3 is also a source of HO_X radicals in the troposphere, these biases may also lead to modeled chemical regimes favoring O_3 destruction (and CO, VOC oxidation) rather than O_3 production.

Summer

Comparison of the AMAP models against summer 2008 aircraft data shows that, in general, the models do not simulate enhancements in CO observed through the majority of the depth of the troposphere (Fig 8.13). Many of the ARCTAS-B flights targeted fresh highly concentrated fire plumes over Canada, resulting in a CO maximum observed in the lowermost 2 km. Such plumes are challenging to simulate in large-scale global models. Nevertheless, the AMAP models perform less well in this regard than the POLMIP models, which were evaluated with the same data by Monks et al. (2015). This difference is likely to be due to the use of different fire emission data between the studies. Estimates of fire-emitted CO in this region from the GFEDv3 emissions used by AMAP are lower than those from the FINN inventory used in POLMIP.

As noted in the comparison against ozonesondes, there are large inter-model differences and biases against observations for O_3 in the upper troposphere. These partly result from different treatments of stratospheric O_3 in the models and different efficiencies of transport of stratospheric air across the tropopause. The AMAP models tend to overestimate O_3 and underestimate CO in the upper troposphere and lower stratosphere (Fig. 8.13) suggesting a displacement in the simulated position of the tropopause even if certain models agree reasonably well with O_3 data measured by the DLR-Falcon over Greenland (see Fig. 8.12). This picture is consistent with a more diffuse tropopause in the models than observed and has important implications for the diagnosis of O_3 radiative forcing from anthropogenic emission perturbations. Models importing too much stratospheric O_3 are likely to simulate an O_3-loss dominated chemical regime in the upper troposphere, such that any anthropogenic in-situ photochemical O_3 production may be swamped by an overestimated stratospheric signal.

The AMAP models underestimate enhancements in summertime free-tropospheric CO observed remote from source regions by the French ATR- and DLR-Falcon aircraft over Greenland, and over the Canadian Arctic during ARCTAS-B (as shown by biases in Fig. 8.13). This is also shown in Fig. 8.12, which shows mean modeled and observed vertical profiles compared to the DLR-Falcon data collected over Greenland during June–July 2008. Comparison with observed O_3 / CO relationships from the DLR-Falcon aircraft (not shown), suggests that O_3 enhancements in tropospheric air masses are underestimated. This is may indicate missing photochemically produced O_3 in simulated air masses imported from mid-latitude source regions. This could result from underestimated emissions of O_3 precursors over source regions, a poor representation of poleward transport in the models, missing photochemical processes, or a combination of these factors. For example, Thomas et al. (2013) demonstrated that errors in the simulated transport of fire plumes in this region resulted in the WRF-Chem model underestimating CO along the DLR flights over Greenland.

Evaluation of simulated Arctic NO_Y (sum of NO_X plus reservoirs, HNO_3, PAN etc.) with vertical profile observations from aircraft in summer 2008 shows large diversity in model performance. In particular, partitioning of NO_Y between HNO_3 and PAN shows large variation between models, with a large diversity in model bias against observations. Compared with DLR-Falcon data, the DEHM model produces the most skilled simulation of PAN vertical profiles. There is some evidence of compensation between overestimated PAN and underestimated HNO_3. Several models (DEHM, MATCH and WRF-Chem) simulate some enhancement in PAN in imported polluted air masses observed by the DLR-Falcon between 5 and 8 km over Greenland (Fig 8.12). However, there remains a substantial underestimate in simulated CO in these air masses. Since both PAN and CO are primarily emitted or formed close to emission regions (fire and anthropogenic) these results suggest CO lifetimes, governed by OH loss, may be too short in models, in contrast to PAN which is lost by thermal decomposition and to a lesser extent photolysis, during transport to the Arctic. It could also point to more efficient formation of PAN over source regions in these models compared to emission, transport and photochemical loss of CO. Figure 8.13 indicates that simulated NO enhancements in the polluted air masses may be inversely related to the amount of PAN simulated, with implications for photochemical O_3 formation during transport to the Arctic.

8.3.4 Modeled pollutant export to the Arctic

In order to evaluate model differences in the export efficiency of O_3 precursors to the Arctic, it is also useful to examine simulated PAN:CO ratios. PAN has been shown to be a key precursor for tropospheric O_3 production at high latitudes (Walker et al. 2012). The efficiency with which PAN is transported relative to CO from mid-latitude source regions to the Arctic is influenced by photochemical processes that influence both modeled organic chemistry and NO_Y partitioning, as well as simulated vertical transport, which controls the formation efficiency and stability of PAN through variations in temperature. Figure 8.14 shows maps of PAN:CO ratios from the AMAP model simulations for July at approximately 500 hPa, and aircraft profile comparisons of simulated PAN:CO ratios compared with those measured by the DLR-Falcon aircraft over Greenland in summer 2008. There is large spread in the simulated PAN abundance relative to CO at high latitudes. This spread is also evident in differences in PAN export efficiency over mid-latitude source regions. The TM4 model in particular exports much larger amounts of PAN relative to CO compared with other models, and the MATCH model exports the least. Compared with aircraft measurements, the MATCH and NorESM models best reproduce the profile of observed PAN:CO ratios. The DEHM and WRF-Chem models also overestimate this ratio in the mid- and upper troposphere. Differences in large-scale PAN:CO ratios between models in the POLMIP study were attributed to differences in simulated vertical transport efficiency over source regions (Arnold et al. 2015). Organic chemistry differences may also play a role, through controlling the abundance of PAN precursors.

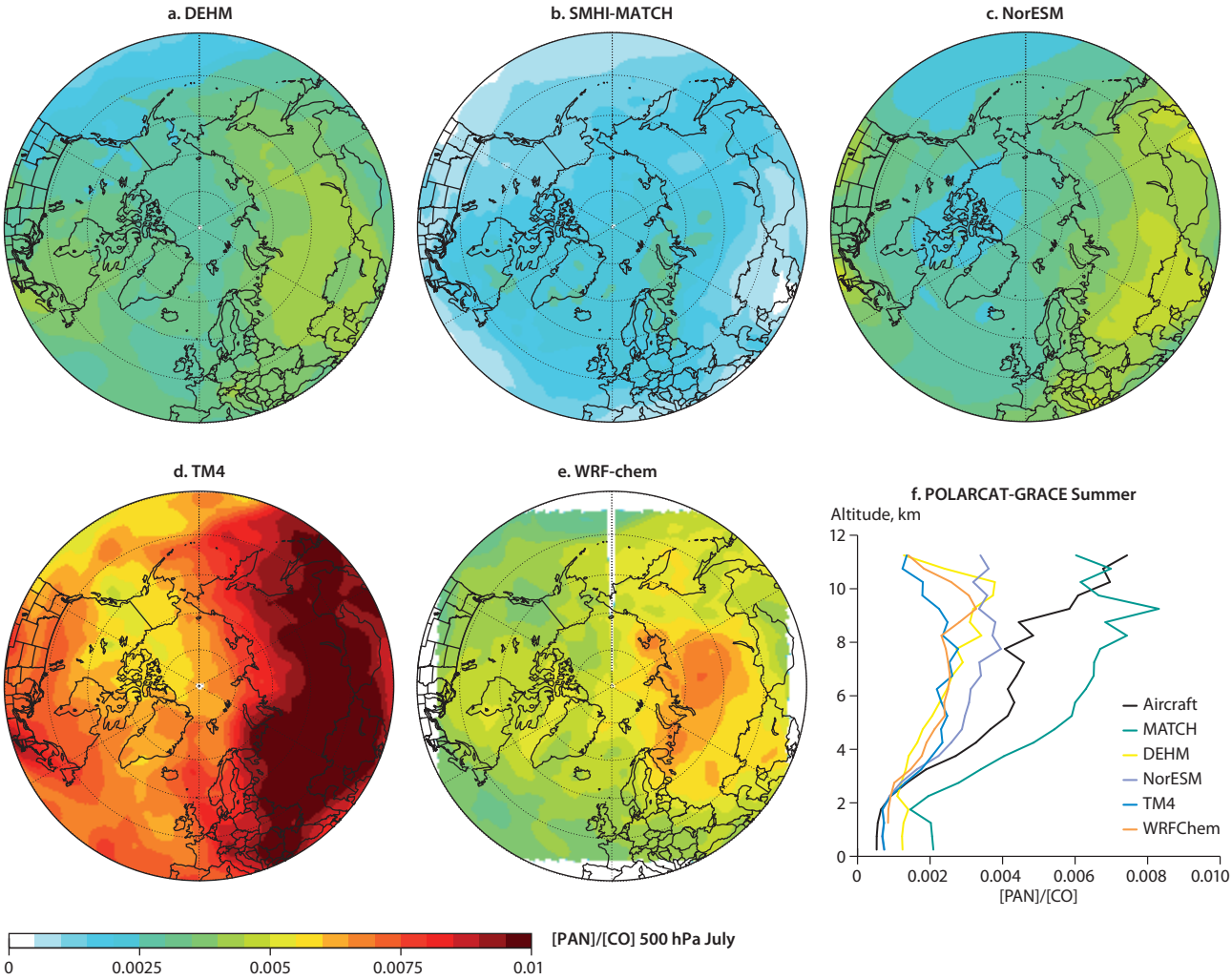

Figure 8.14 Simulated PAN:CO ratios for July at approximately 500 hPa (a-e) from AMAP models, and profiles of model PAN:CO ratios compared with POLARCAT-GRACE aircraft observations over Greenland in summer 2008 (f).

8.3.5 Conclusions (trace gases)

Available surface observations of CO in the Arctic exhibit a clear seasonal cycle with a maximum in spring and a minimum in summer. This is also the case for the European sector of the Arctic (i.e. at Zeppelin, Svalbard), and to a certain extent at Summit (Greenland) where the summer minimum is less evident. The seasonal O_3 variation in the western Arctic shows a winter maximum and a broad spring-summer minimum.

Models are able to simulate gross features of observed seasonal and vertical distributions of O_3 and important precursors in the Arctic troposphere. However, mean biases are substantial for both O_3 and precursor concentrations, with large differences also occurring between models.

All models underestimate CO at Arctic surface stations, particularly in winter and spring, and through the depth of the Arctic troposphere in spring and summer. The underestimate is greater than in previous studies, and may be related to deficiencies in emission data, modeled oxidants and/or chemical processing.

Several models appear to overestimate the amount of O_3 transported from the stratosphere into the Arctic troposphere, especially in summer. This may lead to an overestimate of HO_X radicals which could lead to simulated O_3 destruction rather than O_3 production from imported anthropogenic precursors, with implications for the modeled response to perturbations in anthropogenic emissions and radiative forcing. In addition, AMAP models demonstrate lower than observed enhancements in both CO and O_3 in air masses imported from anthropogenic and fire sources during summer also pointing to an underestimation in simulated photochemical O_3 production in the Arctic free troposphere.

This may be linked to speciation of nitrogen-containing compounds (NO_Y) which show large diversity between models. There are substantial differences in the efficiencies of PAN export from source regions and its import into the Arctic. Aircraft data comparisons suggest that this may have implications for NO abundances simulated in the Arctic, and hence photochemical O_3 production.

Acknowledgments

The research leading to these results received partial funding from the European Union Seventh Framework Programme (FP7/2007-2013) under grant agreement no 282688 – ECLIPSE. Environment Canada (Sangeeta Sharma) provided the EBC and sulfate data from Alert. For Station Nord data, we acknowledge

the Aarhus University, Department of Environmental Science (ENVS). NOAA/ESRL/GMD, EMEP (http://ebas.nilu.no) and WMO GAW network are acknowledged for Barrow and Zeppelin observational datasets. We thank ECMWF for providing meteorological data, and all contributors to the ARCTAS, ARCPAC, POLARCAT-France, POLARCAT-GRACE and PAMARCMIP campaigns. We also acknowledge the use of HIPPO data products downloaded from http://hippo.ornl.gov/dataaccess. Contributions by SMHI were funded by the Swedish Environmental Protection Agency under contract NV-09414-12 and through the Swedish Climate and Clean Air Research program, SCAC. LATMOS also acknowledges partial funding support from the French ANR project Climate Impacts of Short-lived Pollutants and Methane in the Arctic (CLIMSLIP) and the EU Arctic Climate Change, Economy and Society (ACCESS) project under grant agreement n° 265863.

9. Trends in concentrations of short-lived climate forcers in the Arctic

Lead author: Patricia K. Quinn
Contributing authors: Andreas Herber, Joakim Langner, Kathy Law, Kaarle Kupiainen, Julia Schmale, Sangeeta Sharma

9.1 Introduction

This chapter summarizes trends in black carbon (BC) and co-emitted species as well as tropospheric ozone (O_3). Historical trends are presented based on published emission inventories and long-term trends from observations at Arctic monitoring stations. The measured trends are compared with those simulated from two global models.

9.2 Historical trends

The gridded emissions presented by Lamarque et al. (2010) indicate historical trends in anthropogenic and biomass burning global emissions between 1850 and 2000 for black carbon, organic carbon (OC), sulfur dioxide (SO_2), and the ozone precursors nitrogen oxides (NO_X) and non-methane volatile organic compounds (nmVOCs) (Fig. 9.1). Global anthropogenic emissions of all species increased almost linearly between 1850 and 1980. After about 1980, emissions of SO_2, NO_X, and nmVOCs decreased due to efforts to reduce air quality pollutants (e.g. McConnell et al. 2007; Smith et al. 2011). As a result, according to ice core records, sulfate (SO_4^{2-}) aerosol deposited on the Greenland Ice Sheet underwent a slow decline between the late 1970s and 1992, followed by a sharp decrease to almost pre-industrial levels by 2002 (McConnell et al. 2007).

Fyfe et al. (2013) compared the observed SO_4^{2-} deposition over Greenland derived from ice core records (McConnell et al. 2007) with that simulated by global climate models that participated in the Coupled Model Intercomparison Project Phase 5 (CMIP5), these being the models with available wet and dry SO_4^{2-} deposition rates. All models simulate increased SO_4^{2-} deposition during the period 1900–1970 and decreased SO_4^{2-} deposition at the end of the 20th century (see Fig. 9.2), consistent with the observations and a maximum in global sulfur emissions around 1980 (Lamarque et al. 2010). However, large differences in total deposition rates exist, due to the differing treatments of aerosols, clouds, and chemical processing in the models.

Unlike SO_4^{2-}, emissions of BC and OC continued to rise after 1980. Source contributions to emissions of anthropogenic BC between 1850 and 2000 varied (Bond et al. 2007; Smith and Bond 2014): biofuel combustion accounted for half of all anthropogenic BC emissions until 1890, coal combustion then dominated anthropogenic BC emissions between 1890 and 1975, after which biofuel combustion dominated between 1975 and 1990, followed by diesel emissions from 1990 onwards.

Although global emissions can be used to describe general trends, regional emissions must be considered when assessing the impact of different sources of short-lived climate forcers (SLCFs) on Arctic climate. Regional contributions to total anthropogenic global emissions have changed substantially over the period 1850 to 2000 (Bond et al. 2007; Skeie et al. 2011a). North America and Europe were the regions of highest anthropogenic BC emission up until about 1950 when combustion technology was improved and the use of lower emission fuels was implemented. BC emissions from the former Soviet Union decreased in the late 20th century due to an economic collapse while, over roughly the same period, emissions from China and the rest of Asia increased significantly.

Lamarque et al. (2010) held biomass burning emissions between 1850 and 1900 constant due to a lack of information for the species considered here. Ice-core and charcoal records indicate

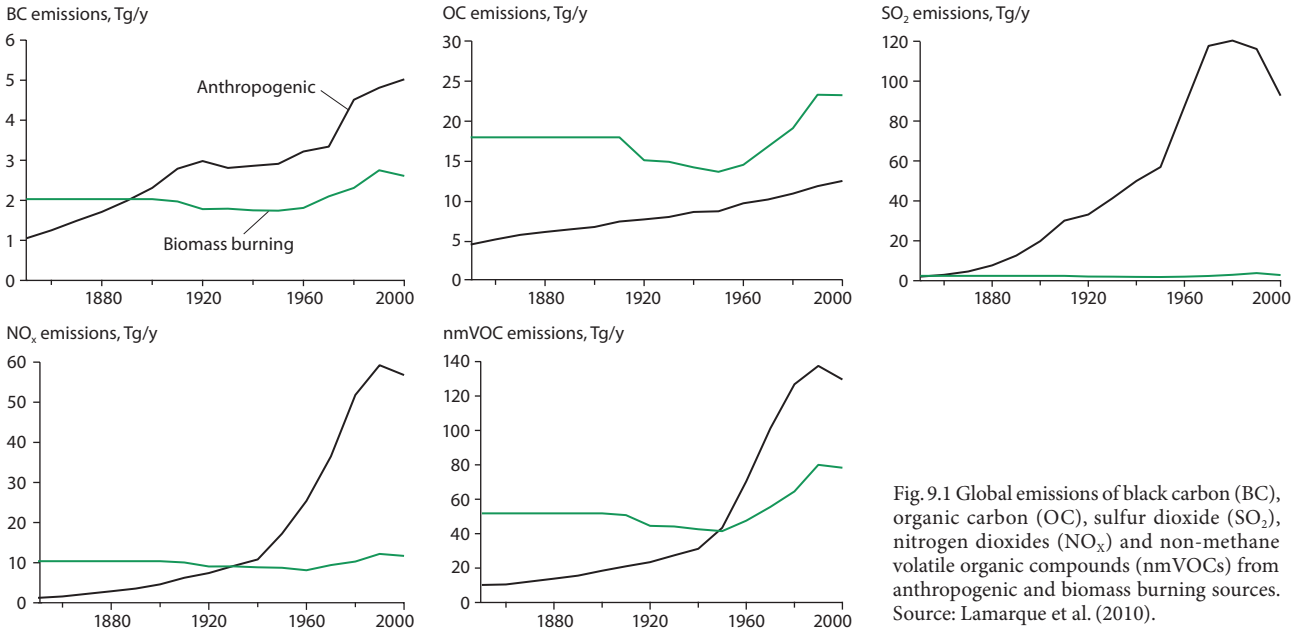

Fig. 9.1 Global emissions of black carbon (BC), organic carbon (OC), sulfur dioxide (SO_2), nitrogen dioxides (NO_X) and non-methane volatile organic compounds (nmVOCs) from anthropogenic and biomass burning sources. Source: Lamarque et al. (2010).

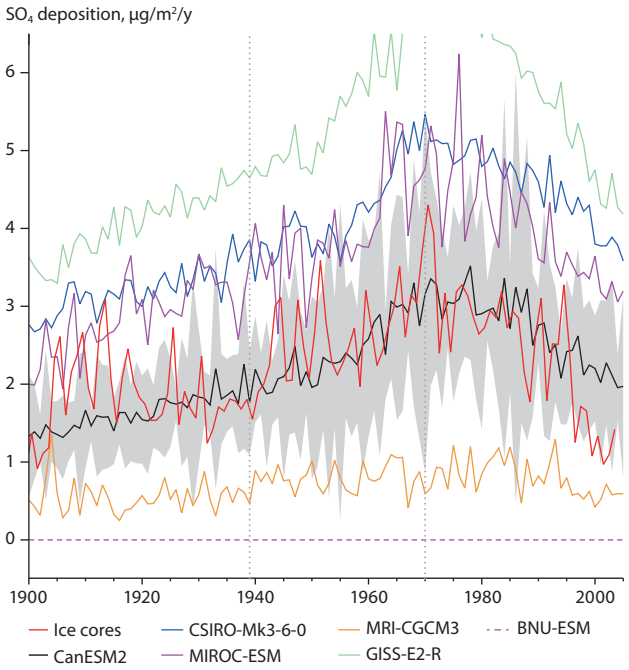

Fig. 9.2 Annual-average sulfate (SO_4^{2-}) deposition over Greenland. The red curve shows observed rate of SO_4^{2-} deposition averaged over ice core records at the Act2 (66.0°N, 45.2°W), D4 (71.4°N, 43.9°W), Humboldt (78.5°N, 56.8°W), and Summit_2010 (72.6°N, 38.3°W) sites. The other curves are simulated deposition rates averaged over 66.0–78.5°N and 56.8–38.3°W in CMIP5 models. The grey shading represents 2.5–97.5% ranges of CanESM2 values. Adapted from Fyfe et al. (2013).

the occurrence of interannual variability in emissions during this period but no significant long-term trends (McConnell et al. 2007; Marlon et al. 2008). Emissions decreased after 1900 with a decrease in forest clearing in the mid-latitude and boreal regions. On a regional basis, emissions around 30°N have decreased since the early 20th century while emissions from 50–60°N increased significantly between 1990 and 2000. The zonal distribution of BC emissions between 1750 and 2000 is shown in Fig. 9.3.

9.3 Long-term observations available for trend analyses

Long-term, continuous records of equivalent black carbon (eBC) concentrations in the Arctic atmosphere, based on measurements of aerosol light absorption, are available at four locations including Alert (Canada), Barrow (Alaska), Zeppelin (Ny-Ålesund, Svalbard), and Summit (Greenland). The longest records are from Barrow and Alert, where measurements began in 1988 and 1989, respectively. Measurements at Zeppelin and Summit began in the late 1990s. Long-term, continuous surface observations of non-sea salt (nss) SO_4^{2-} are available for Alert (1981–present), Barrow (1997–present), and Zeppelin (1993–present).

Surface observations of tropospheric O_3 in the Arctic are available at Barrow since 1973, Zeppelin since 1990, Esrange (Sweden) since 1991, and Alert since 1992. Shorter-term data sets are available from Stórhöfði (Iceland, 1993–2009), Pallas (Finland, 1995–2012) and Summit (2001–2010). In addition, ozonesonde data are available for Qausuittuq (Resolute, Canada) since 1979, Alert since 1987, Ny-Ålesund since 1990, Pituffik (Thule, Greenland) since 1991, and Ittoqqortoormiit (Scoresbysund, Greenland) since 1989. Locations of long-term measurements of eBC (light absorption), nss-SO_4^{2-}, and O_3 along with the years of observation and measurement methods are listed in Table 9.1.

9.4 Observed trends in black carbon

The first trend analysis for Arctic aerosol did not focus on measurements of BC or aerosol light absorption but on light scattering by particles and aerosol optical depth (AOD), measured at Barrow since 1977 (Bodhaine and Dutton 1993) and at Ny-Ålesund since 1991 (Stone et al. 2014). AOD is a measure of the fraction of solar radiation removed through the scattering and absorption of light by aerosol over the atmospheric path length of the measurement. It is not specific to BC but, unlike measurements of aerosol absorption at

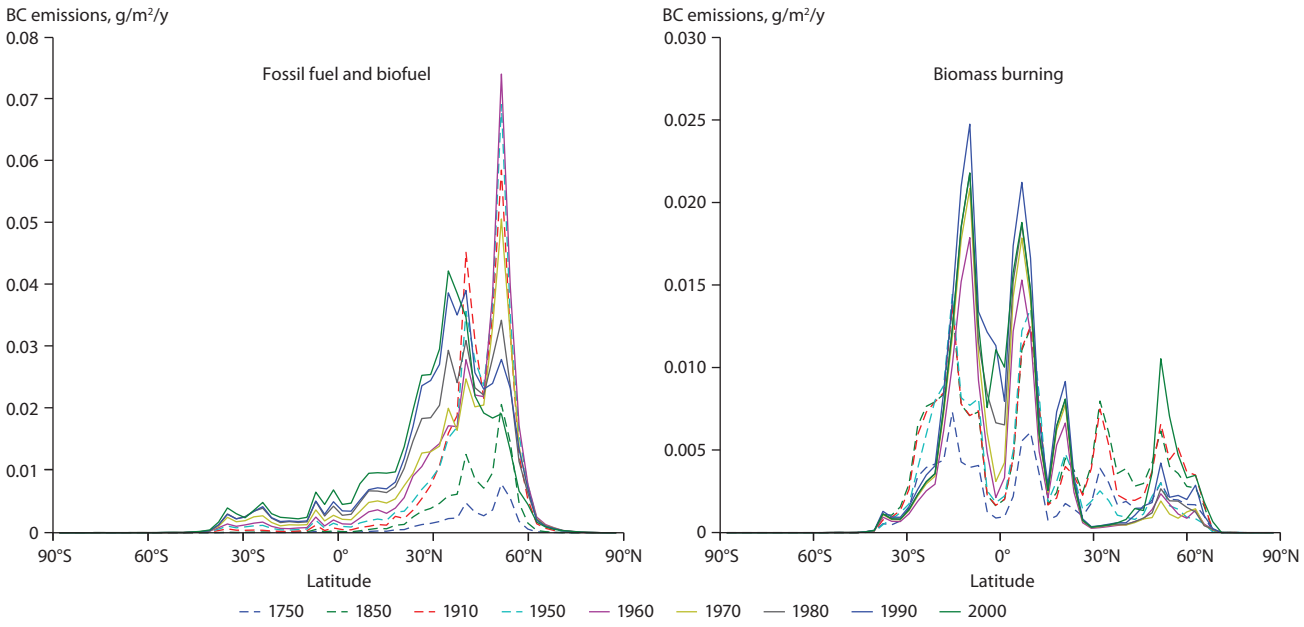

Fig. 9.3 Zonal annual mean emissions of black carbon (BC) from fossil fuel and biofuel (left) and biomass burning (right) for selected years. Source: Skeie et al. (2011a).

Table 9.1 Locations of long-term measurements of black carbon, non-sea salt sulfate, and ozone (see Fig. 8.1 for a map of site locations).

Site	Years	Method	Measured parameter
Alert (82.5°N, 62.2°W)	1989–present	Aethalometer, model AE-6	Light absorption. Specific absorption of 19 m^2/g used to convert absorption to eBC
	1981–present	Hi-volume filter, Ion chromatography	Sulfate mass concentration
	1992–present	Surface observations, ultraviolet absorption	Ozone partial pressure
	1987	Ozonesonde	Ozone partial pressure
Barrow (71.3°N, 156°W)	1988–2003	Aethalometer, model AE-8	Light absorption. Specific absorption of 19 m^2/g used to convert absorption to eBC
	1997–present	Particle soot absorption photometer	Light absorption
	1977–present	Sunphotometer	Aerosol Optical Depth
	1997–present	Impactor sub- and supermicron, Ion chromatography	Sulfate mass concentration
	1973–present	Surface observations, ultraviolet absorption	Ozone partial pressure
Pituffik (Thule) (76.5°N, 68.8°W)	1991–present	Ozonesonde	Ozone partial pressure
	1990–present	Total ozone column, SAOZ spectrometer	Total ozone column
	1996–2003	Surface observations; API	Ozone partial pressure
Ittoqqortoormiit (Scoresbysund) (70.5°N, 22°W)	1989–present	Ozonesonde	Ozone partial pressure
	2007–present	Total ozone column, SAOZ spectrometer	Total ozone column
Kangerlussuaq (Sønderstrøm) (67°N, 59.7°W)	1990–present	Total ozone column, Brewer Spectrometer	Total ozone column
Ny-Ålesund (78.9°N, 12°E), Zeppelin	1998–present	Aethalometer, model AE-31	Light absorption. Specific absorption of 19 m^2/g used to convert absorption to eBC
	1991–present	Sunphotometer	Aerosol Optical Depth
	1993–present	Filter, Ion chromatography	Sulfate mass concentration
	1990–present	Ozonesonde	Ozone partial pressure
	1990–2012	Surface observation, ultraviolet absorption	Ozone partial pressure
Esrange (68°N, 21°E)	1991–2012	Surface observation, ultraviolet absorption	Ozone partial pressure
Summit (72.6°N, 38.5°W)	1998–present	Particle soot absorption photometer	Light absorption
	2001–2010	Surface observations, ultraviolet absorption	Ozone partial pressure
Pallas (68°N, 24°E)	1995–2012	Surface observations, ultraviolet absorption	Ozone partial pressure
Qausuittuq (Resolute) (75°N, 94.8°W)	1981–2010	Ozonesonde	Ozone partial pressure
Stórhöfði (64°N, 16.7°E)	1993–2009	Surface observations, ultraviolet absorption	Ozone partial pressure

surface sites, it reveals information about trends in aerosol concentrations over the entire atmospheric column.

Between 1977 and 1993, both AOD and light scattering measured during the springtime Arctic Haze period at Barrow peaked in 1982 followed by a factor of two decrease between 1982 and 1993 (Bodhaine and Dutton 1993). It was hypothesized that the observed decrease was due to reductions in emissions from the former Soviet Union resulting from economic factors and from Europe due to stricter pollution controls. Stone et al. (2014) examined the trend in AOD measured at Barrow, Alert, and Ny-Ålesund and found an increase between 2001 and 2012, primarily due to high aerosol loadings during the springs of 2008 and 2009. The high 2008 loadings were a result of biomass burning smoke from Asia that was distributed throughout the lower atmosphere from the surface up to higher than 6.5 km (Warneke et al. 2009; Brock et al. 2011). Atmospheric circulation patterns during spring 2009 resulted in the transport of haze and dust into the central Arctic (Stone et al. 2010). Tomasi et al. (2012) assessed the long-term variation in the seasonal mean for Arctic Haze conditions at Ny-Ålesund (1991–2010) and Barrow (1977–2010) and found large episodic fluctuations in AOD but no well-defined trends. During summertime, background conditions, AOD was found to increase at both Barrow and Ny-Ålesund over these periods. Tomasi et al. (2012) attributed the increase at Ny-Ålesund to enhanced aerosol loading in the stratosphere due to minor volcanic eruptions. Their analysis for Barrow indicates additional contributions from Eurasian emissions and/or coal burning in China.

Studies focused on Arctic trends in aerosol light absorption and eBC measured at surface sites found a 61% decrease for

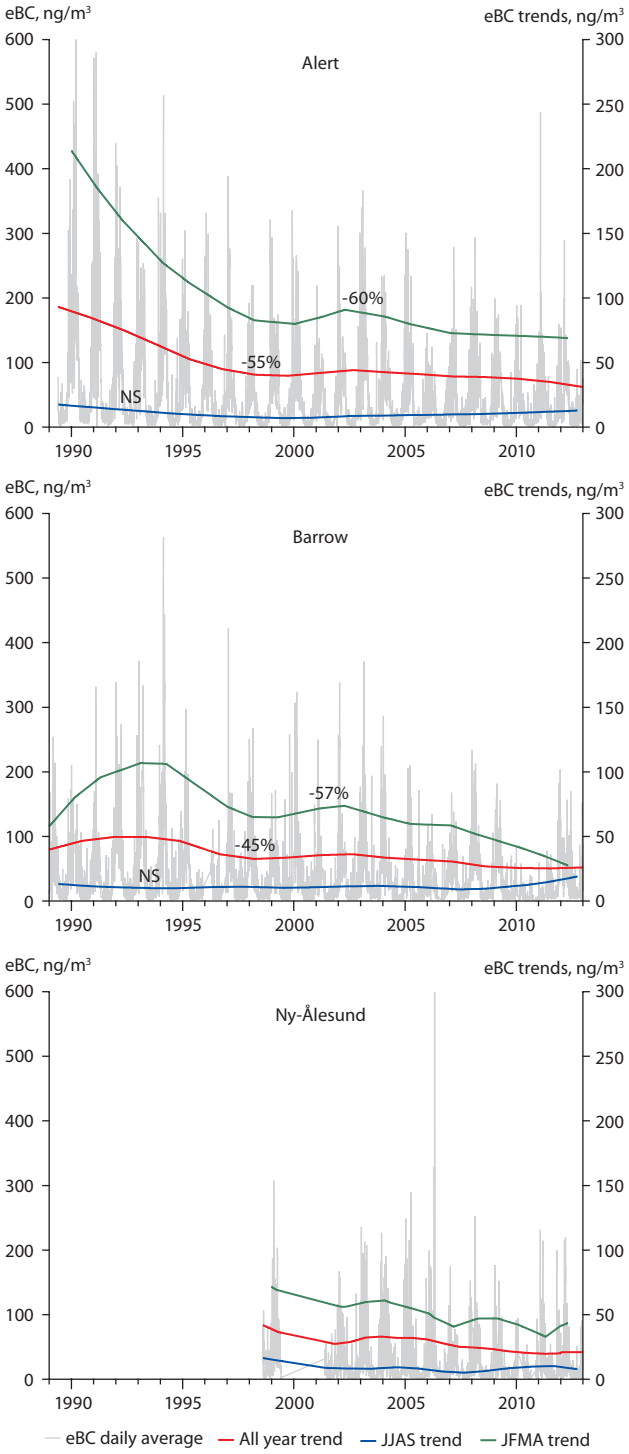

Fig. 9.4 Daily average surface equivalent black carbon (eBC) at Alert (Canada), Barrow (Alaska), and Zeppelin (Svalbard). Trend lines were based on the LOWESS technique (Locally Weighted Exponentially Scatterplot Smoothing). The red line represents the trend for all data, the green line is the winter–spring average (January to April), and the blue line is the summer average (June to September). Source: Sharma et al. (2013).

the March monthly average between 1988 and 2006 at Barrow (Quinn et al. 2007) and a 49% and 33% decrease in wintertime eBC concentrations between 1989 and 2003 at Alert and Barrow, respectively (Sharma et al. 2006). Sharma et al. (2013) and Stone et al. (2014) updated the trend analyses for Barrow, Alert, and Zeppelin and found an overall decline of 40% in eBC during the winter between 1990 and 2009 with most of the change occurring during the early 1990s (Fig. 9.4). Coupling a model analysis with the observations indicated that the maximum contribution to surface BC concentrations at Alert, Barrow, and Zeppelin was from the combined former Soviet Union and European Union regions and that trends in wintertime BC are primarily due to changes in emissions in the former Soviet Union (Sharma et al. 2013).

There are no monitoring programs that provide regular, systematic vertical profile information for BC. In addition, the aircraft campaigns that have taken place since the early 1980s have been conducted in different parts of the Arctic and employed different measurement techniques so that direct comparison of the observations is problematic. That said, as shown in Fig. 9.5, a compilation of averaged eBC and refractory black carbon (rBC) vertical profiles measured between 1983 and 2011 provides evidence that concentrations have decreased throughout the atmospheric column over this period (Stone et al. 2014). The large eBC concentrations measured during the Arctic Gas and Aerosol Sampling Program (AGASP) in 1983 and 1986 are consistent with higher AOD values also observed during the experiments (Bodhaine 1989; Dutton et al. 1989). The decrease in concentrations throughout subsequent years is consistent with the downward trends in eBC measured at Barrow, Alert, and Ny-Ålesund surface sites. However, a slight increase in AOD (which includes all aerosol, not just BC) was observed in the Arctic between 2000 and 2011 and has been attributed to changing emissions of natural aerosols, including biomass smoke and volcanic aerosols (Stone et al. 2014).

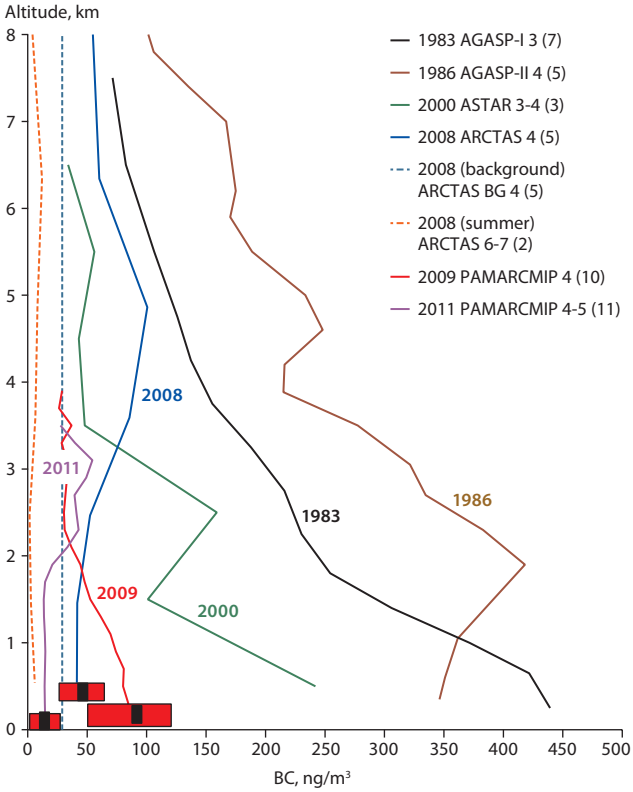

Fig. 9.5 Averaged profiles of black carbon (BC) concentrations from Arctic aircraft campaigns conducted between 1983 and 2011. The number of flights included in each average profile is given in parentheses. The grey dashed line represents clean background values measured in the Alaskan Arctic during April 2008. The yellow dashed line is for the summer of 2008. Climatological means (±1 std dev) of equivalent black carbon (eBC) measured during April at Barrow (Alaska), Alert (Canada), and Zeppelin (Svalbard) (shown by altitude of site; Barrow is lowest at 11m above sea level, Alert is at 210 m, and Zeppelin is at 474 m) are indicated by black symbols and red bars. Source: Stone et al. (2014).

In addition to the lack of routine vertical profile measurements, there is no routine monitoring of deposition or concentrations of BC in Arctic snow but sporadic campaigns have provided data for assessment of long-term behavior. Since 1983, over 1200 snow samples have been collected for BC analysis. Summarizing the results, Doherty et al. (2010) concluded that over all of the Arctic, concentrations decreased between 1983 and 2009. The decrease in BC snow concentration observed over 1983/84 to 2009 in Alaska (-40%), the Canadian Arctic (-62%), and on Svalbard (-36%) is on the same order as the decrease in atmospheric eBC observed in the surface atmosphere at Barrow, Alert, and Zeppelin (Stone et al. 2014).

Overall, for regions where repeat measurements have been made, there appears to be a downward trend in atmospheric BC at the surface and aloft as well as in snow.

9.5 Observed trends in organic carbon and sulfate

There are no published long-term records of particulate OC concentrations for the Arctic. Sporadic measurements have been made but are too infrequent to reveal anything about trends in Arctic aerosol OC. Long-term records of nss-SO_4^{2-} concentrations are available for Alert, Barrow, and Zeppelin. Hirdman et al. (2010a) performed a trend analysis based on annual geometric mean concentrations and found a decrease at Alert between 1985 and 2006 of 64%. At Zeppelin, nss-SO_4^{2-} was found to decrease by 21.5% between 1990 and 2008. No significant trend was found for Barrow over the 1997 to 2006 period. The lack of a trend was attributed to the limited period of available data. The Alert and Zeppelin data show the steepest decline in nss-SO_4^{2-} to be during the early 1990s, which was not captured by the later start of the Barrow observations.

9.6 Observed trends in ozone

Long-term changes in tropospheric O_3 in the Arctic will be driven by changes in transport processes such as the flux from the stratosphere (affecting upper tropospheric O_3) and transport of O_3 and O_3 precursors from mid-latitudes, including both methane and nmVOCs. Increased emissions of O_3 precursors at mid-latitudes followed by photochemical production will increase the amount of O_3 transported to the Arctic. Mid-latitude trends in emissions are the likely cause of increasing O_3 observed at these latitudes, at least until the 2000s over North America and Europe (Parrish et al. 2012a; Cooper et al. 2014). Ozone is still increasing over and downwind of Asia. Ozone trends have also been attributed to changes in the flux of O_3 from the stratosphere (Pausata et al. 2012). Nevertheless, the network of global O_3 measurements is sparse and does not represent broad regions of the world.

There is evidence that O_3 concentrations in the Arctic lower troposphere are also increasing. A 38-year record at Barrow (1973–2010) reveals an increase of 0.09±0.03 ppb/y (Oltmans et al. 2013) (Fig. 9.6). Concentrations during the intervening years indicate decadal-scale variability. Over the entire 30-year record of ozonesondes at Qausuittuq (Resolute) (1981–2010), there is an overall negative trend (-0.09±0.06 ppbv/y) in O_3 concentrations measured between the surface and 850 hPa. Observations over the last two decades indicate an increase of 0.21±0.08 ppbv/y. Records starting in the early 1990s are available in EBAS (http://ebas.nilu.no/) for Zeppelin and Esrange and from 1995 for Pallas. Concentrations at Zeppelin increased by 0.14±0.09 ppb/y (95% confidence level, CL) while there was a less significant trend for Esrange, 0.073±0.14 ppb/y (95% CL). The record for Pallas over 1995–2012 shows a significant negative trend, -0.21±0.17 ppb/y (95% CL). Shorter-term records are available for Stórhöfði (Iceland) and Summit (Greenland) (Cooper et al. 2014). Concentrations at Stórhöfði

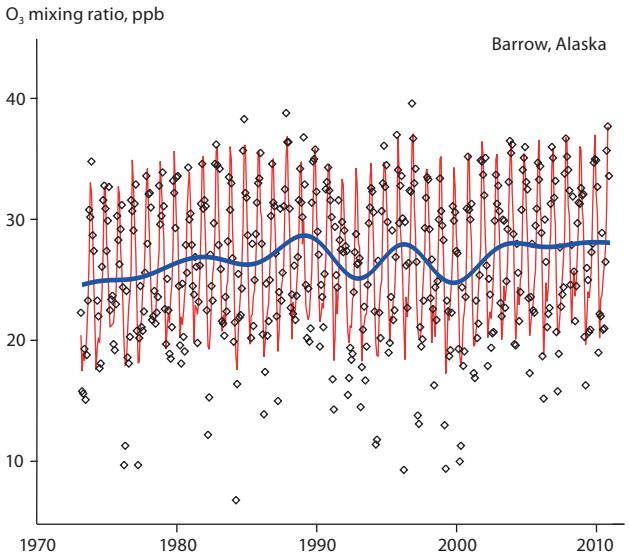

Fig. 9.6 Monthly measured mean ozone (O_3) mixing ratios (black markers), model fit (red line), and smooth trend curve (blue line) for Barrow based on surface observations. Source: Oltmans et al. (2013).

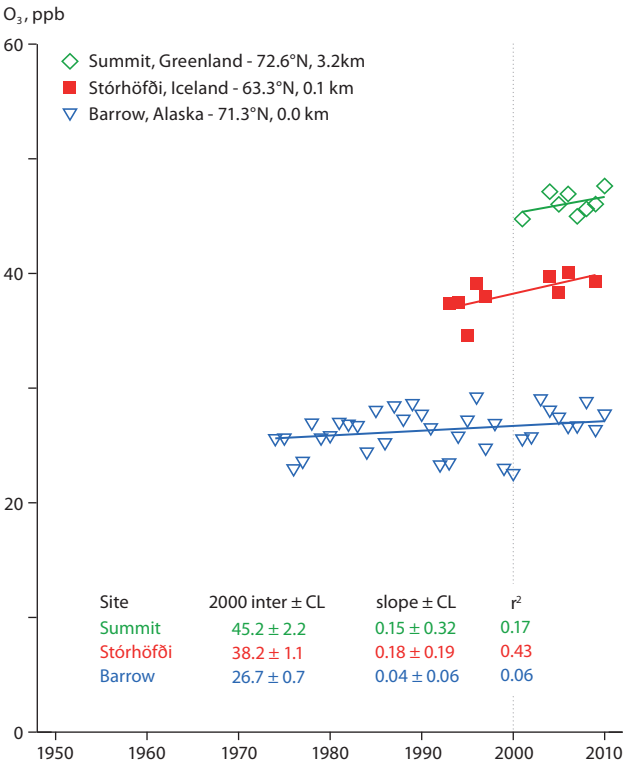

Fig. 9.7 Surface ozone (O_3) time series for Summit (Greenland), Stórhöfði (Iceland) and Barrow (Alaska). Trend lines are fitted through the annual average O_3 values using the least-square regression method. Figure courtesy of D. Parrish (NOAA) (see Parrish et al. 2012a, for details of method).

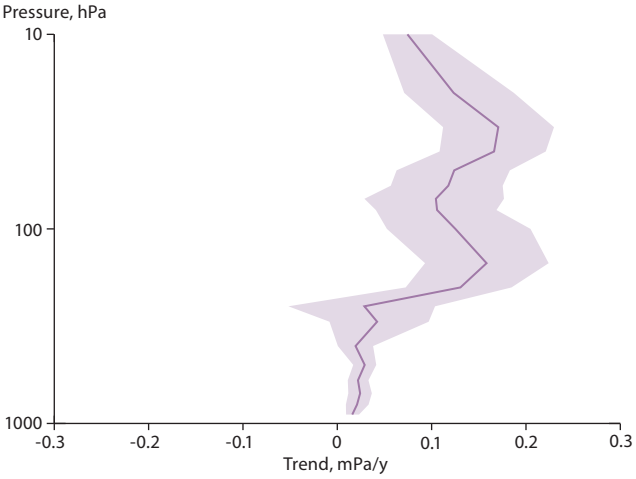

Fig. 9.8 Linear trend for the ozonesonde station at Ittoqqortoormiit (Scoresbysund) in Greenland (full curve) with 95% confidence limits indicated by shading. Trends based on fitting a nonlinear model to weekly ozone values from 1989 to 2013. Source: (Christiansen et al. 2015).

increased by 0.18±0.19 ppbv/y between 1993 and 2009 while those at Summit increased by 0.15±0.32 ppbv/y between 2001 and 2010 (see Fig. 9.7). For higher altitudes, Hess and Zbinden (2011) reported an increasing trend in the European Arctic middle troposphere (500 hPa) of 0.36±0.23 ppb/y from ozonesonde measurements over the period 1996–2010.

Long-term monitoring data from the Ittoqqortoormiit (Scoresbysund) station in Greenland (Christiansen et al. 2015) revealed a significant increasing linear trend at both 500 hPa and higher levels (see Fig. 9.8). The trend was strongest around 200 hPa with a value of 0.14±0.09 mPa/y. However, second- and third-order polynomials were also significant leading to a nonlinear time evolution of the O_3 concentration with a maximum in 2007.

9.7 Comparison of models and measurements for long-term trends

Two Climate Chemistry Models, CESM1 (CAM5.2) and CanAM, were used to calculate long-term trends in BC, nss-SO_4^{2-}, and O_3 for comparison to values measured at Zeppelin, Alert, and Barrow. Details of the two models can be found in Ch. 7. For this purpose, CESM simulations were conducted from 1990 to 2015 using ECLIPSE Version 5 (1990–2009) emissions (see Ch. 5 for more details on ECLIPSE emissions) interpolated to annual resolution. Data after 2010 were generated from emissions that were interpolated between estimates of actual 2010 emissions and projected emissions for 2015. The model was driven with climatological (annually repeating) sea surface temperatures (SSTs). The MAM3 aerosol model was used with MOZART chemistry. MAM7 aerosols were used in the forcing runs described in Ch. 11. The MAM7 aerosol model produces more BC transport to the Arctic than MAM3.

CanAM simulations were conducted over the period of the measurements at each monitoring site using emissions from ECLIPSE V5 (1990–2009) and monthly vegetation fire emissions from GFED V3.1 (1997–2009) merged with emissions from CMIP for the RCP4.5 scenario. Emissions were linearly interpolated in time to obtain a continuous time series during the period of the simulation. The model was driven with monthly varying SSTs. Monthly mean aerosol concentrations were calculated based on a simulation with specified boundary conditions for the period 1950–2009. SSTs and sea-ice concentrations from CMIP5 were used.

For both the model simulations and observations, concentrations were averaged over the months of January through April to capture the Arctic Haze season and to remove seasonality from the trend analysis. Reported concentrations of eBC were derived from measured absorption coefficients and an assumed mass absorption coefficient of 16, 19, and 19 m^2/g, respectively for Zeppelin, Alert, and Barrow. Results of the comparisons are shown in Figs. 9.9 (BC), 9.10 (nss-SO_4^{2-}), and 9.11 (O_3). In addition, modeled and measured values of percentage change in concentration per year for each species and station are listed in Table 9.2 for all available data.

As previously stated, based on observations, concentrations of nss-SO_4^{2-} and BC have decreased during the haze season over the period of measurement at Alert, Barrow, and Zeppelin. In most cases, but not all, observations of nss-SO_4^{2-} and BC indicate a stronger decrease in concentration over the measurement period than simulated by the models. Observations at Alert and Zeppelin indicate a statistically significant increase in O_3 during the Arctic Haze season. For all three stations, the modeled and observed changes in O_3 concentration agree well.

Determining reasons for discrepancies in measured and modeled long-term trends in BC and nss-SO_4^{2-} may help improve historic emission inventories and model parameterizations controlling aerosol transport and deposition. Future work should include sensitivity tests with the models to evaluate how emissions from different regions and source sectors affect concentration trends in the Arctic.

9.8 Conclusions

In summary, the trend analyses based on long-term measurements at ground sites show significant decreases in eBC and nss-SO_4^{2-} mass concentrations over the period of observation. Measurements of O_3 at several ground sites in the Arctic also indicate an increasing trend in the lower and upper troposphere. A compilation of averaged eBC and rBC vertical profiles from aircraft flights conducted between 1983 and 2011 provide evidence that concentrations have decreased throughout the atmospheric column over this period. Measurements of BC in snow have been conducted sporadically since 1983. These data indicate a decrease in BC snow concentration on the same order as the decrease in atmospheric eBC.

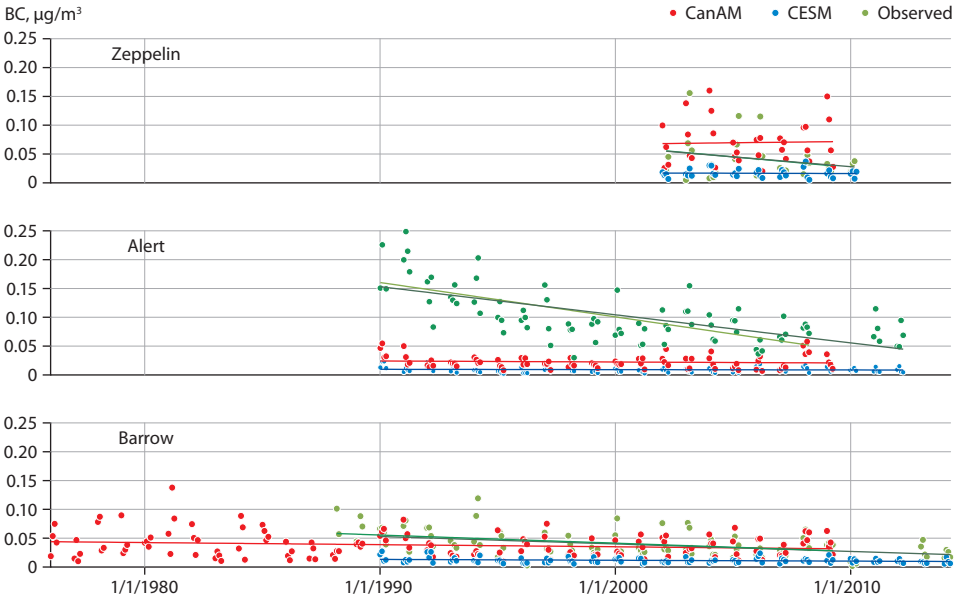

Fig. 9.9 Comparison of measured and model simulated linear trends in black carbon (BC) averaged over the Arctic Haze months (January to April) at Zeppelin (Svalbard), Alert (Canada), and Barrow (Alaska).

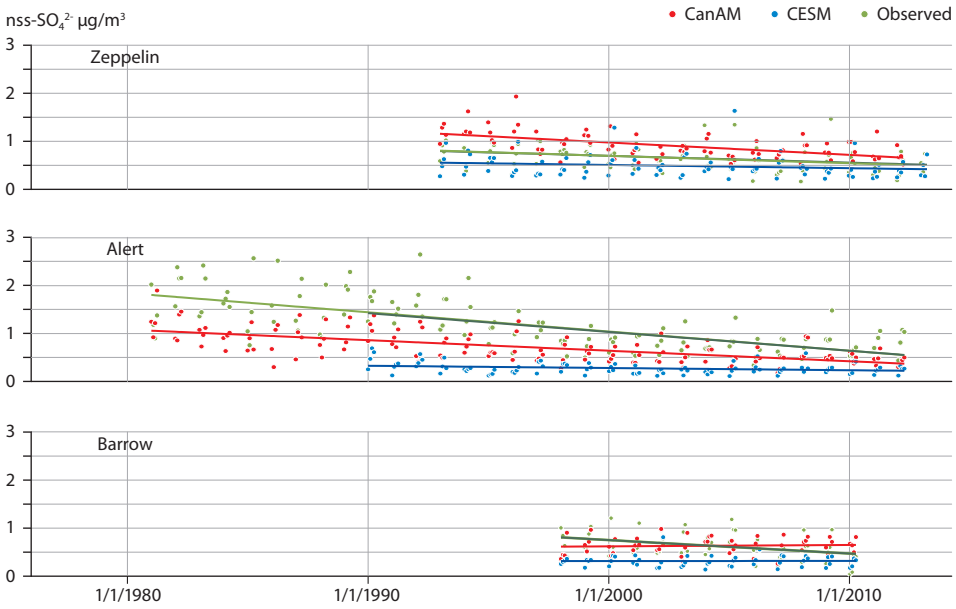

Fig. 9.10 Comparison of measured and model simulated linear trends in non-sea salt sulfate (nss-SO_4^{2-}) averaged over the Arctic Haze months (January to April) at Zeppelin (Svalbard), Alert, and Barrow.

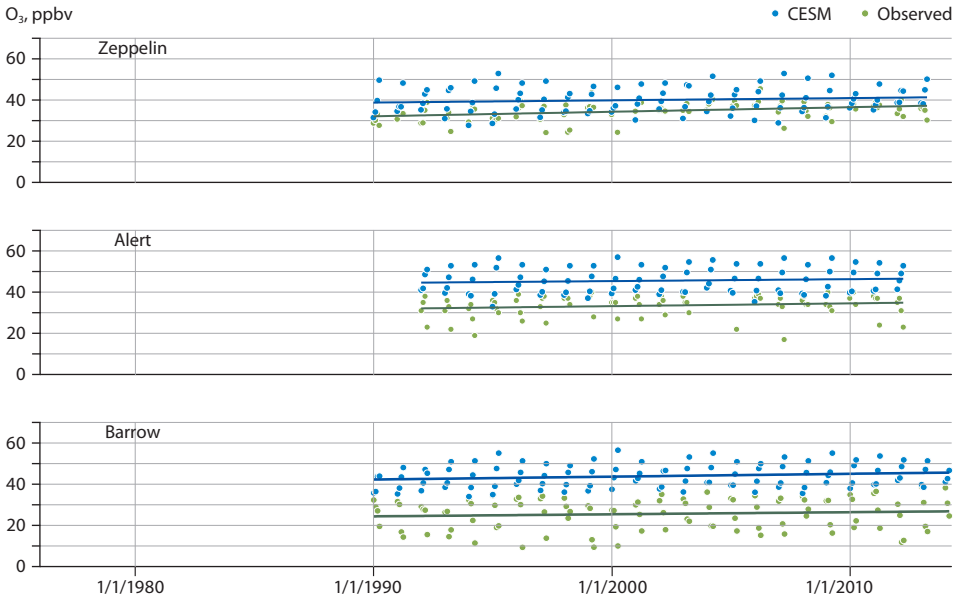

Fig. 9.11 Comparison of measured and model simulated linear trends in ozone (O_3) averaged over the Arctic Haze months (January to April) at Zeppelin (Svalbard), Alert (Canada), and Barrow (Alaska).

Table 9.2. Modeled and measured percentage change per year in non-sea salt sulfate, black carbon and ozone at Alert, Barrow, and Zeppelin over the indicated time period. *p* Value indicates the significance level of a trend such that 0.001 indicates a 0.1% probability of no trend. No values indicates a significant level >0.1.

Model	Station	Start date	End date	Source	Percentage change per year	*p* value
Non-sea salt sulfate						
CanAM	Alert (Canada)	1 Jan 1981	1 Apr 2012	Modeled	-2.02	< 0.01
				Observed	-2.22	< 0.01
	Barrow (Alaska)	1 Jan 1998	1 Apr 2010	Modeled	1.17	
				Observed	-3.49	
	Zeppelin (Svalbard)	1 Jan 1993	1 Apr 2012	Modeled	-2.20	< 0.001
				Observed	-2.12	< 0.001
CESM	Alert (Canada)	1 Jan 1990	1 Apr 2012	Modeled	-1.10	< 0.01
				Observed	-2.64	< 0.001
	Barrow (Alaska)	1 Jan 1998	1 Apr 2010	Modeled	0.37	
				Observed	-3.49	< 0.05
	Zeppelin (Svalbard)	1 Jan 1993	1 Apr 2013	Modeled	-1.08	
				Observed	-1.91	< 0.001
Black carbon						
CanAM	Alert (Canada)	1 Jan 1990	1 Apr 2009	Modeled	-1.30	< 0.1
				Observed	-3.56	< 0.001
	Barrow (Alaska)	1 Jan 1976	1 Apr 2009	Modeled	-0.52	
				Observed	-1.89	< 0.01
	Zeppelin (Svalbard)	1 Jan 2002	1 Apr 2009	Modeled	-0.27	
				Observed	-3.17	
CESM	Alert (Canada)	1 Jan 1990	1 Apr 2012	Modeled	-0.41	
				Observed	-3.01	< 0.001
	Barrow (Alaska)	1 Jan 1990	1 Apr 2014	Modeled	-0.85	
				Observed	-2.47	< 0.001
	Zeppelin (Svalbard)	1 Jan 2002	1 Apr 2010	Modeled	-2.25	
				Observed	-2.70	
Ozone						
CESM	Alert (Canada)	1 Jan 1992	1 Apr 2012	Modeled	0.22	
				Observed	0.33	< 0.1
	Barrow (Alaska)	1 Jan 1990	1 Mar 2014	Modeled	0.41	< 0.05
				Observed	0.32	
	Zeppelin (Svalbard)	1 Jan 1990	1 Apr 2013	Modeled	0.42	
				Observed	0.66	< 0.001

10. Arctic radiative forcing and climate response: Literature review

Lead authors: Mark Flanner, Terje Berntsen, Kaarle Kupiainen, Joakim Langner, Knut von Salzen
Contributing authors: Hailong Wang

10.1 Introduction

This chapter presents an overview of previous studies that have quantified Arctic radiative forcing associated with aerosols and ozone (O_3), and the Arctic climate response to forcing by short-lived climate forcers (SLCFs). The material is organized into sections describing forcing by black carbon (BC) in snow and sea ice, forcing by atmospheric aerosols and O_3, and the Arctic climate response to SLCFs. Although this assessment has focused on BC and O_3, as described elsewhere in this report aerosol species that are co-emitted with BC and O_3 precursors, including organic carbon (OC) and sulfur dioxide (SO_2), often exert a global cooling effect. Any realistic assessment of climate mitigation must therefore consider the effects of all co-emitted species associated with the actions of interest. Chapter 11 presents modeling results for Arctic climate impacts associated with numerous co-emitted species, thus offering a more complete picture of the net climate impacts of SLCFs from specific regions and sectors.

10.2 Forcing from black carbon in snow and sea ice

10.2.1 Arctic forcing

This section describes recent studies that report Arctic radiative forcings from BC deposition to snow and sea ice. Table 10.1 summarizes these recent estimates of Arctic-mean radiative forcings from both atmospheric and snow-deposited BC. Jiao et al. (2014) applied BC deposition fields simulated by 25 models contributing to two phases of the AeroCom (Aerosol Comparisons between Observations and Models) project to calculate vertically-resolved BC-in-snow concentrations, accomplished by prescribing deposition fields in offline land and sea-ice simulations. They evaluated these simulated distributions of BC in snow against the Arctic survey of Doherty et al. (2010) (see Ch. 8 for a similar comparison), and then scaled the distributions in different regions to derive a measurement-corrected estimate of the Arctic radiative forcing. The multi-model mean corrected Arctic (60–90°N) radiative forcing from all sources of BC in snow and ice was 0.17 W/m^2. Unless otherwise noted, forcings reported in this chapter are direct forcings (either instantaneous or adjusted) that do not account for the high efficacy of snow forcing, which leads to an effective forcing that is greater by a factor of 2–4 (Flanner et al. 2007; Hansen et al. 2007). Prior to applying measurement-based scaling factors, Jiao et al. (2014) derived uncorrected ranges of Arctic forcing from AeroCom Phase I and Phase II models of, respectively, 0.07–0.25 and 0.06–0.28 W/m^2. These uncorrected estimates, however, may provide unrealistically large estimates of forcing associated with each model's deposition fields because of a bias identified by Doherty et al. (2014a) that occurs when temporally inconsistent aerosol deposition and precipitation fluxes are used to drive offline land and sea-ice simulations. The magnitude of the bias in surface-layer BC concentrations was found to vary regionally from a factor of 1.5–2.5.

Table 10.1 Estimates of Arctic annual-mean radiative forcing from black carbon (BC) in the cryosphere and atmosphere.

Reference	Arctic forcing, W/m^2	Domain	Notes
BC in snow and sea ice			
Flanner et al. 2009	0.28	60–90°N	CAM3.1 model, all BC sources
Koch et al. 2009a	0.03	64–90°N	GISS ModelE, 1890–1995 change, all BC sources
AMAP 2011	0.13	60–90°N	CCSM4 model, all BC sources
Zhou et al. 2012	0.11–0.13	66.5–90°N	IMPACT model, all BC sources, two sets of meteorology
Dou et al. 2012	0.7–1.1*	66–90°N	GISS-E2-PUCCINI model, 2007-2009, *spring season only
Jiao et al. 2014	0.17	60–90°N	Observation-corrected average from 25 AeroCom models
BC in atmosphere			
Koch and Hansen 2005	0.63	60–90°N	GISS ModelE, all sources of BC+OC
Flanner et al. 2009	0.55	60–90°N	CAM3.1 model, all sources of BC+OM
Bond et al. 2011	0.40	60–90°N	CAM3.5 model, all sources of BC+OC
AMAP 2011	0.12, 0.14	60–90°N	CCSM4 and Oslo-CTM models, all sources of BC
Samset et al. 2013	0.38±0.30	70–90°N	Multi-model mean from 15 AeroCom models, all BC sources
	0.07–1.19	70–90°N	Full range from 15 AeroCom models, all BC sources
Wang et al. 2014b	0.21	60–90°N	CAM5.1 model with 3-mode aerosol module, all BC sources
	0.72	60–90°N	Same as above but with 7-mode aerosol module (slower BC aging treatment)

Flanner et al. (2009), using the CAM3.1 model, estimated an all-source Arctic (60–90°N) radiative forcing of 0.28 W/m^2, with contributions of 0.14 W/m^2 each from snow on land and sea ice. While their study applied prognostic aerosol deposition fluxes and was therefore not afflicted by the bias identified by Doherty et al. (2014a), no corrections were applied to account for biases with respect to measurements. Koch et al. (2009a) used the GISS ModelE to quantify an 1890–1995 change in Arctic (64–90°N) radiative forcing of 0.03 W/m^2 due to changes in BC deposition. Dou et al. (2012) applied the GISS-PUCCINI model to assess snow albedo changes from BC deposition, and provide springtime Arctic (66–90°N) surface radiative forcing estimates of 0.7, 1.1, and 1.0 W/m^2 for 2007, 2008, and 2009, respectively, indicating that there is substantial interannual variability in forcing associated with differences in aerosol emissions and transport. Simulations conducted with CCSM4 for the previous AMAP assessment on the impact of BC on Arctic climate (AMAP 2011) produced an Arctic-mean BC-in-snow forcing of 0.13 W/m^2, with respective contributions of 0.10 and 0.03 W/m^2 from land snow and sea ice. Zhou et al. (2012) estimated Arctic-mean forcings of 0.11–0.13 W/m^2, using deposition fluxes simulated with the IMPACT model combined with offline land and sea-ice model calculations, as reported by Jiao et al. (2014).

10.2.2 Global forcing

Other studies have derived global BC-in-snow radiative forcings without specifying Arctic averages. Because much of the forcing operates at high latitudes, however, these studies also offer some indication of the spread in model-derived Arctic forcing. Furthermore, forcing operating outside the Arctic also influences Arctic climate (see Ch. 11). Bond et al. (2013) applied global radiative forcing fields from Flanner et al. (2009) and Koch et al. (2009a), corrected using data from Doherty et al. (2010), to derive global-mean all-source adjusted forcings of 0.040 W/m^2 from BC in land snow and 0.012 W/m^2 from BC in sea ice. The industrial-era (change between 1750 and 2005) adjusted radiative forcings from BC in land snow and sea ice were estimated to be, respectively, 0.035 and 0.011 W/m^2. These estimates were largely adopted by the Intergovernmental Panel on Climate Change in its Fifth Assessment Report (IPCC AR5; Myhre et al. 2013b), which documents a combined snow and sea-ice anthropogenic radiative forcing of 0.04 W/m^2 with a 95% confidence interval of 0.02–0.09 W/m^2, and notes that the effective forcing is a factor of 2–4 times greater than these estimates. Lee et al. (2013) used aerosol deposition fields from eight models contributing to the Atmospheric Chemistry and Climate Model Intercomparison Project (ACCMIP), combined with the offline technique adopted by Jiao et al. (2014), to derive forcing estimates for different time slices. The all-BC radiative forcing in year 2000 ranged from 0.024 to 0.037 W/m^2 in this study. Relative to 1850, radiative forcings ranged from about 0.008–0.020 W/m^2 in year 1930, about 0.010–0.035 W/m^2 in year 1980 and about 0.008–0.021 W/m^2 in year 2000. Hence, one important conclusion from the study was that BC-in-snow forcing was greater in 1980 than in 2000. All models contributing to this exercise applied the same BC emission inventory from Lamarque et al. (2010). Skeie et al. (2011a), using the Oslo-CTM2 model along with BC emissions from Bond et al. (2007), simulated the largest Arctic BC burden and deposition fluxes occurring during the 1960s, and estimated year 2000 radiative forcing (relative to 1750) of 0.016 W/m^2, due to fossil fuel and biofuel BC sources only (i.e. excluding open burning). Similarly, Bauer and Menon (2012) simulated 1850–2000 radiative forcing from global BC-in-snow of 0.016 W/m^2, using the GISS-MATRIX model and emissions from Lamarque et al. (2010). They found a much greater increase (0.11 W/m^2) in the net top-of-atmosphere (TOA) shortwave flux, however, after allowing the climate to adjust to the forcing, caused largely by reduced high-latitude cloud cover. Zhou et al. (2012), using the IMPACT model with modified emissions from Ito and Penner (2005) and offline snow/ice calculations, simulated a global all-source BC-in-snow radiative forcing of 0.020–0.022 W/m^2. An estimate of the all-source global BC in snow and sea-ice forcing from Jacobson (2004) is 0.06 W/m^2, as cited by Bond et al. (2013). Koch et al. (2009a), using the GISS ModelE, simulated 1890–1995 instantaneous direct global and Arctic-mean radiative forcings of 0.01 and 0.03 W/m^2, respectively, where the Arctic average was over 64–90°N. The 1995 radiative effect from all sources of BC was 0.03 W/m^2 in this study.

Finally, Lin et al. (2014) also applied the IMPACT model to derive the first global estimates of radiative forcing from light-absorbing organic aerosol ('brown carbon') in snow. Large uncertainty in these estimates arises from uncertainty in both the formation of secondary organic aerosol and the absorptivity of OC. The 1870–2000 radiative forcing by OC in snow and ice (originating from both primary emissions and secondary formation) simulated across multiple sensitivity studies was found to be 0.0011–0.0031 W/m^2 in this study, with contributions of 0.0009–0.0025 W/m^2 from land snow and 0.00016–0.00055 W/m^2 from sea ice. However, it should be noted that the Zhou et al. (2012), Lee et al. (2013), and Lin et al. (2014) estimates of snow and ice forcing may be biased high (perhaps by a factor of 2) owing to inconsistency between precipitation and aerosol deposition (Doherty et al. 2014a). Uncorrected estimates from Jiao et al. (2014) are also affected by this issue, while the measurement-corrected estimates are not.

10.3 Forcing from atmospheric aerosols and ozone

10.3.1 Arctic forcing

Numerous studies have derived global radiative forcing estimates for atmospheric aerosols and O_3. This section summarizes only those studies that report Arctic-averaged forcings (see also Table 10.1).

The Arctic-mean TOA direct radiative forcing from all sources of atmospheric BC was calculated to be 0.12 and 0.14 W/m^2 in the previous AMAP (2011) report, as simulated with the CCSM4 and Oslo-CTM models, respectively. Earlier studies, however, simulated much greater Arctic BC burdens and forcings. For example, simulations with GISS ModelE, described by Koch and Hansen (2005), produced an Arctic direct forcing of 0.54 W/m^2 from all fossil fuel and biofuel BC+OC, and 0.09 W/m^2 from biomass burning BC+OC, as reported by AMAP (2011). Similarly, Flanner et al. (2009) produced an all-source Arctic

BC+OM (organic matter) radiative forcing of 0.55 W/m^2 using the CAM3.1 model. Using a version of CAM3.5 nudged with re-analysis winds, Bond et al. (2011) simulated all-source BC+OC Arctic radiative forcing of 0.40 W/m^2. The AMAP (2011) report showed that the models applied in that assessment (CCSM4 and Oslo-CTM) substantially underestimated BC in the Arctic atmosphere. Recent work has led to improved physical parameterizations of aerosol transport, wet scavenging, and BC aging in CESM (the successor to CCSM4) and other models that result in much greater Arctic burdens and radiative forcing (e.g. Wang et al. 2013). In particular, Wang et al. (2014b) showed that slower BC aging treatment in CESM can significantly increase the global atmospheric BC lifetime (from 4.7 to 7.4 days), the efficiency of BC transport to the Arctic, and Arctic BC direct forcing (from 0.21 to 0.72 W/m^2). Consequently, forcing results presented in Ch. 11 are similar to, or even greater than, those reported in the earlier studies of Koch and Hansen (2005) and Flanner et al. (2009).

More recently, Samset et al. (2013) analyzed BC fields from 15 AeroCom models and quantified radiative forcing and mass-normalized radiative forcing (or radiative efficiency), including an assessment of variability attributable to different vertical distributions and co-location with clouds. Averaged over the Arctic, defined as 70–90°N in that study, the TOA all-source BC radiative forcing varied from 0.07–1.19 W/m^2, with a mean and standard deviation of 0.38±0.30 W/m^2. (BC forcing averaged over 70–90°N differs by only 3% from forcing averaged over 60–90°N in the all-source CESM simulation conducted for the present assessment.) Samset et al. (2013) also showed that the multi-model mean normalized direct radiative forcing for Arctic BC was 3792±328 W/g. Their study led to the conclusion that at least 20% of the uncertainty in modeled forcing by BC is attributable to diversity in simulated vertical profiles of BC.

There have been many studies presenting estimates of radiative forcing due to O_3 changes, but few have reported radiative forcing averaged over the Arctic region. Collins et al. (2013a) estimated radiative forcing due to the O_3 precursors nitrogen oxides (NO_X), volatile organic compounds (VOCs) and carbon monoxide (CO) based on the HTAP multi-model ensemble of chemical transport models. The radiative forcing was estimated based on offline radiation calculations accounting for the effects on methane (CH_4) through changes in the hydroxyl radical (OH). Their estimated emission-normalized radiative forcings for the Arctic are 1.2, 0.42 and 0.07 mW/m^2/Tg (from their figure 7) for emissions of NO_X, VOCs and CO from four emission regions in the northern hemisphere: North America, Europe, East Asia and South Asia. Assuming total anthropogenic emissions from these regions of 75 Tg NO_X, 90 Tg VOC, and 330 Tg CO yields a combined radiative forcing in the Arctic of 0.15 W/m^2.

10.3.2 Global forcing

Recent major assessments of global radiative forcing from BC include those of Bond et al. (2013), Shindell et al. (2013), Myhre et al. (2013a), and the IPCC AR5 (Myhre et al. 2013b). Key findings only are summarized here and readers are referred to those assessments, and to Bond et al. (2013) in particular, for more details on the state of science of global BC forcing. Bond et al. (2013) estimated present-day direct radiative forcing from all sources of BC to be 0.88 (0.17–2.1) W/m^2, where the bracketed values indicate a 90% uncertainty range. They estimated industrial-era (change from 1750 to 2005) direct radiative forcing and adjusted forcing of 0.71 (0.08–1.27) and 1.1 (0.17–2.1) W/m^2, respectively. The latter includes fast feedbacks (mostly associated with clouds) and forcing via all mechanisms, including snow and ice deposition. These forcing estimates are larger than those reported in previous modeling studies because models incorporated by Bond et al. (2013) were adjusted for substantial underestimation of aerosol absorption optical depth (AAOD). One of the more uncertain aspects of this correction is associated with isolating the contribution of BC to observed AAOD. Shindell et al. (2013) applied five model contributions to the ACCMIP project to derive 1850–2000 direct radiative forcing from fossil fuel and biofuel BC sources of 0.24±0.09 W/m^2 (multi-model mean and standard deviation). The multi-model mean (from 10 models) all-aerosol direct and effective radiative forcings in this study were found to be -0.26±0.14 and -1.17±0.29 W/m^2, respectively. Notably, their study showed that the all-aerosol 1850–2000 effective forcing exceeds +0.5 W/m^2 over much of the Arctic Ocean despite this forcing being negative in the global mean. Myhre et al. (2013a) applied the AeroCom Phase II archive of model simulations (with contributions from 16 models) to estimate global direct forcing from atmospheric BC associated with fossil fuel and biofuel emissions of 0.18±0.07 W/m^2, with a full range of 0.05 to 0.37 W/m^2. Inclusion of biomass burning emissions would elevate the BC forcing estimates of Shindell et al. (2013) and Myhre et al. (2013a), but not to the level of Bond et al. (2013). Finally, the IPCC AR5 took into account all of these studies to suggest a direct radiative forcing from anthropogenic fossil fuel and biofuel BC sources of 0.40 (0.05–0.80) W/m^2, and a 1750–2011 direct radiative forcing from all BC sources (including biomass burning) of 0.64 W/m^2 (Myhre et al. 2013b). The forcing from global biomass burning BC, however, is almost entirely offset by cooling from co-emitted OC in this estimate. Forcing from fossil fuel and biofuel BC is offset to varying degrees by co-emitted species, depending on the source. Bond et al. (2013), for example, showed that BC-rich sources such as on-road diesel exert strong mass-normalized warming because they emit large proportions of BC, while other sources, such as biofuel cooking, exert more of a climate neutral forcing because they coincidentally emit large fractions of non-BC species. The IPCC AR5 estimates a global direct radiative forcing of -0.40 W/m^2 from all anthropogenic sources of sulfate (SO_4), an estimate that is unchanged with respect to the previous three IPCC assessment reports. Sulfate forcing over the Arctic is much less than in the global mean because of smaller burdens and more reflective underlying surfaces. Much of the SO_4 forcing also originates from sources that emit little BC, implying widely varying consequences of emissions reductions, as described quantitatively in Ch. 11.

Stevenson et al. (2013) presented a comprehensive assessment of radiative forcing from changes in tropospheric O_3, simulated by 17 models contributing to the ACCMIP project. They calculated 1850–2000 multi-model mean (± one standard deviation) global radiative forcing of 0.36±0.06 W/m^2 or 0.38±0.07 W/m^2, depending on the tropopause definition, with longwave forcing dominating globally over shortwave forcing. Extrapolating these estimates to the 1750–2010 timeframe, they estimated a

radiative forcing of 0.41 W/m^2 with an overall uncertainty range of 30%. Shindell et al. (2013) also reported multi-model mean (from six models) 1850–2000 O_3 radiative forcing of 0.33±0.11 W/m^2. Unlike aerosol forcing, the spatial pattern of O_3 forcing, described in both studies, shows that it is substantially less positive over the Arctic than over northern mid-latitudes. This is because temperature inversions and cloud cover within the Arctic reduce longwave forcing by greenhouse gases relative to those in other regions. Based on attribution experiments using six models, Stevenson et al. (2013) also reported contributions from CH_4, NO_X, VOCs and CO to 1850–2000 global mean O_3 radiative forcing of 0.166, 0.119, 0.058 and 0.035 W/m^2, respectively, summing to 0.38 W/m^2.

10.4 Arctic climate response to short-lived climate forcers

This section briefly summarizes studies that have explicitly isolated and reported estimates of Arctic temperature response due to forcing by BC and other short-lived pollutants. Early studies incorporating snow darkening from BC reported global temperature changes and showed that northern high latitude and Arctic temperature responses were substantially greater than the global mean response. Such studies include those by Jacobson (2004) and Hansen et al. (2005). Jacobson (2004) simulated 10-year global surface warming of 0.27 K from fossil fuel and biofuel sources of BC and OM operating in the atmosphere, snow and sea ice (or 0.20 K when BC+OM operates only in the atmosphere). Hansen et al. (2005) simulated a global surface temperature change of 0.21 K in response to all fossil fuel and biofuel BC (derived here by dividing the reported 0.42 K response to doubled BC by a factor of 2), and global warming of 0.065 K in response to 1880–2000 changes in snow albedo from BC.

Flanner et al. (2007) simulated equilibrium global and Arctic surface warming of 0.10–0.15 K and 0.50–1.61 K, respectively, in response to snow darkening from global emissions of all BC. Flanner et al. (2009) quantified equilibrium global and Arctic warming of 0.07 K and 0.58 K, respectively, in response to all fossil fuel and biofuel emissions of BC and OM, operating both in the atmosphere and in snow. Jacobson (2010) simulated 15-year reductions in Arctic (66–90°N) warming of roughly 1.2, 1.7, and 0.9 K resulting from the elimination of all fossil-fuel soot, fossil-fuel + biofuel soot and gases, and CH_4, respectively. (These Arctic temperature changes compare with respective global temperature changes of 0.3–0.5, 0.4–0.7, and 0.2–0.4 K.) Goldenson et al. (2012), using CESM1 (a successor to CAM3), simulated equilibrium 70–90°N warming of about 1 K in response to BC and dust deposition from all sources, with roughly equal contributions from each species. Notably, they found that Arctic surface temperature and sea ice responded more strongly to aerosol deposition on land snow than to deposition on sea ice.

Other studies have explored the transient response of Arctic climate to forcing by SLCFs. For example, Koch et al. (2009a) simulated Arctic (64–90°N) temperature change between 1890 and 1995 of -0.33 K in response to direct aerosol forcing from all species, -2.2 K in response to aerosol-cloud indirect forcing, and +0.5 K in response to BC deposition to snow and sea ice. Fyfe et al. (2013) found that aerosol changes are mainly responsible for the observed cooling of the Arctic in the mid-20th century (i.e. -0.26 K per decade for 1939–1970). During the period from 1900 to 2005, cooling from aerosols substantially reduced the warming rate from increased greenhouse gas concentrations in simulations with global climate models in the Coupled Model Intercomparison Project Phase 5 (CMIP5). An analysis of results from one of these models did not produce any evidence for strong contributions of BC to overall Arctic temperature trends during the 20th century. Koch et al. (2011) used transient chemistry-climate simulations to attribute roughly 20% of the Arctic warming and loss of Arctic snow and ice during the 20th century to BC in snow and ice, although reduced BC near the end of the century actually contributed to Arctic cooling, contrary to observations and therefore suggesting that other effects have dominated the recent Arctic response. Yang et al. (2014) modeled transient climate change due to direct forcing by changing aerosol emissions over 1975–2005 and found cooling in some parts of the Arctic and warming in others, with strong warming (+1.8 K) over the European Arctic during this period. They attributed about two-thirds of this warming to decreased SO_4 aerosols from Europe and about one-third to changes in BC.

The UNEP/WMO (2011) assessment and subsequent work of Shindell et al. (2012) explored potential climate benefits associated with reduced emissions of short-lived pollutants. The UNEP/WMO assessment found that the impacts on Arctic climate between 2005 and 2030 of reference scenario (i.e. business as usual) emissions of non-CH_4 SLCFs, SLCFs+CH_4, and SLCFs+CH_4+LLGHGs (long-lived greenhouse gases) would be, respectively, -0.04, -0.01, and +0.73 K. Under one set of aggressive measures to reduce CH_4 emissions, Arctic warming between 2005 and 2070 could be reduced by 0.37 K, and under two separate sets of measures to reduce BC emissions Arctic warming could be reduced by 0.21 and 0.14 K. Shindell et al. (2012) found that aggressive measures to reduce emissions of BC and CH_4 could mitigate projected warming in the Arctic over the next three decades by two-thirds, relative to the amount of warming that would occur in the absence of such measures. The measures applied in their study targeted sources rich in BC and CH_4, but the simulated climate was also affected by co-emitted species including OC and SO_4. Smith and Mizrahi (2013), however, applied a simplified global change model and concluded that aggressive BC and CH_4 measures would reduce the amount of global warming occurring by 2050 by only about 0.16 K (including impacts of co-generated OC, SO_4, O_3, and carbon dioxide, CO_2, associated with the measures). This lower estimate originates largely from the use of a baseline scenario that assumes more substantial reductions in emissions than the baseline scenario applied by Shindell et al. (2012), illustrating that there is substantial uncertainty in both the likelihood of future emissions trajectories and the climate response to short-lived climate forcing agents.

Four recent studies conducted idealized climate simulations to better characterize the sensitivity of Arctic temperature to radiative forcings exerted in different locations. Shindell and Faluvegi (2009) quantified Arctic climate sensitivities of about -0.08 K (W/m^2)$^{-1}$ in response to forcing exerted by BC in the Arctic atmosphere. This result was surprising because it indicated that the Arctic surface may cool in response to heating

by BC in the Arctic atmosphere. Subsequent work by Flanner (2013) demonstrated that this may be true for BC forcing in the upper Arctic atmosphere, above roughly 430 hPa, but BC lower in the Arctic troposphere and deposited to snow and ice can cause very powerful Arctic warming, with local sensitivities of 1.5–2.8 K/(W/m^2). Shindell and Faluvegi (2009) also showed that Arctic forcings by CO_2 and SO_4 exert similar sensitivities of roughly +0.35 K/(W/m^2), while O_3 forcing triggers much smaller temperature responses of about +0.07 K/(W/m^2). The latter may result from the fact that the shortwave component of O_3 forcing within the Arctic is a relatively large fraction of its total forcing, and the Arctic surface temperature response to the shortwave component of O_3 forcing may be similar to that of BC forcing, as hypothesized in Ch. 4. Shindell and Faluvegi (2009) also showed that forcing by BC exerted outside the Arctic can warm the Arctic. This topic was explored in more detail by Sand et al. (2013a), who concluded that BC forcing occurring outside the Arctic may have a greater impact on Arctic climate than BC forcing within the Arctic, and who also showed that Arctic surface cooling may result from Arctic atmospheric BC because of reduced poleward heat flux and surface dimming. Building on these studies, Sand et al. (2013b) showed that a mass of BC emitted within the Arctic causes about five times more Arctic surface warming than an equal mass of BC emitted from mid-latitudes. One important component of this result was the inclusion of snow darkening from BC. As described in Ch. 7, regional sensitivity parameters derived from Shindell and Faluvegi (2009) and Flanner (2013) are applied in Ch. 11 to determine Arctic temperature changes.

While this section has focused on Arctic temperature, other states of the Arctic climate system are important for societal well-being. One example is the mass balance of the Greenland Ice Sheet, which drives sea-level change. A recent study by Keegan et al. (2014) implicated BC deposition from boreal forest fires in the widespread surface melt that occurred on the Greenland Ice Sheet in summer 2012. Enhanced snow metamorphism from higher temperatures was found to be a critical process operating in combination with BC-induced darkening. Historically, forest fires have been shown to be an infrequent, but sometimes very large, source of BC deposition to Greenland (e.g. McConnell et al. 2007). Keegan et al. (2014) speculated that in a warming climate, BC from forest fires would become a more frequent trigger of widespread melt on the Greenland Ice Sheet. A more consistent source of BC deposition to Greenland is fossil fuel combustion, although ice cores indicate that this source of BC deposition to central Greenland peaked in the early 20th century and has since declined steadily (McConnell et al. 2007). Dumont et al. (2014) applied remote sensing observations to show that the surface albedo of the Greenland Ice Sheet has been declining since 2009. They argued that light-absorbing impurities are the likely source of this decline because much of the albedo change has occurred within the visible spectrum. They speculated that increased dust, associated with more snow-free land area, and not BC, is the impurity that is likely to be responsible for this observation. More work is needed, however, to identify the sources of observed albedo decreases on the Greenland Ice Sheet.

10.5 Conclusions

Several studies published since the AMAP (2011) report have helped advance understanding of Arctic climate impacts from SLCFs. The most comprehensive estimate of Arctic-mean direct radiative forcing from all sources of BC in snow is likely to be the multi-model, measurement-corrected estimate of 0.17 W/m^2 provided by Jiao et al. (2014). Taken together with studies from Doherty et al. (2014a) and others, this assessment by Jiao and co-workers also suggests that most global aerosol models tend to deposit too little BC within the Arctic. Samset et al. (2013) also applied a multi-model assessment to estimate Arctic-mean radiative forcing from all atmospheric BC of 0.38±0.30 W/m^2. The Arctic forcing from atmospheric BC is similar to the global-mean forcing, with offsetting effects of lower Arctic burdens and higher Arctic reflectance. Since the global-mean BC forcing found in this assessment is substantially less than measurement-based estimates (e.g. Bond et al. 2013), it is possible that Arctic forcing from atmospheric BC is greater than the multi-model estimate of Samset et al. (2013). An estimate of Arctic-mean radiative forcing from anthropogenic changes in tropospheric O_3 is 0.15 W/m^2, based on work from Collins et al. (2013a). This is substantially less than global-mean estimates (0.41±0.12 W/m^2; Stevenson et al. 2013) because it does not include the effect of increased CH_4 emissions and because more stable atmospheric conditions and increased cloudiness in the Arctic reduce the local longwave forcing. Owing to low burdens and high surface reflectance, Arctic direct forcing from anthropogenic SO_4 is also substantially less than the global-mean estimate of -0.40 W/m^2 (Myhre et al. 2013b).

Simulations exploring potential Arctic temperature impacts associated with short-lived pollutants indicate that Arctic warming over the next several decades could be reduced by as much as two-thirds with aggressive measures that reduce emissions of BC and CH_4 (Shindell et al. 2012), although this result is sensitive to assumptions of both baseline and mitigation emissions scenarios (Smith and Mizrahi 2013). Recent studies (Shindell and Faluvegi 2009; Flanner 2013; Sand et al. 2013a,b) exploring Arctic equilibrium climate sensitivity to different forcings collectively indicate that Arctic surface temperature:

- responds weakly and perhaps even cools in response to solar heating by BC, and probably O_3, residing at higher altitudes in the Arctic
- warms strongly in response to BC at lower altitudes or within Arctic snow
- warms more because of total BC forcing exerted outside the Arctic than within the Arctic
- cools in response to negative SO_4 forcing within the Arctic.

Transient simulations of historical Arctic temperature suggest that aerosols, particularly increased burdens of SO_4, may have played a dominant role in the mid-20th century cooling of Arctic climate (Koch et al. 2009a; Fyfe et al. 2013).

11. Linking sources to Arctic radiative forcing and climate response

Lead author: Maria Sand
Contributing authors: Mark Flanner, Knut von Salzen, Joakim Langner, Terje Berntsen

11.1 Introduction

In this study, a multi-model ensemble was used to estimate the contributions of emissions of black carbon (BC), other aerosol species (organic carbon, OC; and sulfate, SO_4), and ozone (O_3) precursors from different geographical regions and source sectors, to changes in Arctic climate. Emissions from Canada (CANA), United States (USAM), Nordic countries (NORD), Russia (RUSS), non-Arctic Europe (OEUR) (other Europe, without Turkey), Asia (ASIA) that includes China, India, Japan, Singapore, South Korea (without Central Asian countries), and the Rest of the world (ROW, mostly comprising the southern hemisphere) are considered. Emissions are expressed by emission sector: Domestic, Energy+Industry+Waste, Transport, Agricultural fires, Grass+Forest fires (natural+anthropogenic) and Flaring. Chapter 5 gives greater details on emissions and geographical regions. Chapter 7 describes the models and methods used in this chapter in more detail.

The impacts of emissions from different geographical regions and emission sectors on Arctic climate are first evaluated in terms of direct, indirect and snow/ice radiative forcing (RF) in the Arctic (defined here as the area north of 60°N), and then in terms of the Arctic surface temperature response. The forcing values reported here are due to all emissions (natural+anthropogenic), if not otherwise specified. As discussed in the previous report from the expert group (AMAP 2011) and Ch. 4 of the present report, RF outside the Arctic and the resulting changes in heat import can contribute significantly to warming in the Arctic, and the surface temperature response to RF from different forcing mechanisms can be quite different (e.g. Shindell and Faluvegi 2009). To account for this, a modified version of the regional temperature potential (RTP) concept of Shindell and Faluvegi (2009) was used in this study to estimate the contribution of RF in different geographical regions to Arctic surface temperature change, including the impact of RF at lower latitudes (Ch. 7 and Sect. 11.4).

To facilitate an evaluation of the cost-effectiveness of regional emission mitigation options, the normalized impacts (i.e. impacts per unit emission from each region and sector) are also presented. Note that for the O_3 precursors (nitrogen oxides, NO_X; carbon monoxide, CO; and volatile organic compounds, VOCs) this was not possible because the simulations for the sectors and regions were done by changing all three components simultaneously.

11.2 Contribution of source regions and sectors to changes in burdens of black carbon and tropospheric ozone

11.2.1 Black carbon

The contributions of different geographic regions to BC burdens in the Arctic as simulated in four models using the same emissions are shown in Fig. 11.1. A further breakdown of the results in this figure into contributions from different emission sectors is shown in Fig. 11.2. Differences in results from different models reflect inherent uncertainties in modeling and diagnostic approaches, as described in Ch. 7.

Emissions from East+South Asia and Russia are the largest contributors to BC burdens in the Arctic in all the models, with mean contributions of 43% and 21%, respectively. Total BC emissions from Asia are substantially higher than emissions from the other individual regions (Ch. 5), but comparable to emissions from ROW. The Nordic countries contribute less to Arctic BC burdens than any other region, in accordance with the lower emissions in that region.

Owing to the geographic location of sources, emissions from Russia, Canada, and the Nordic countries are more efficiently transported to the Arctic than emissions from regions at lower latitudes (Ch. 6). Current emissions from Russia are substantially lower than emissions from non-Arctic Europe but contribute more to Arctic BC burdens. Owing to their magnitude and geographic location, Russian emissions from

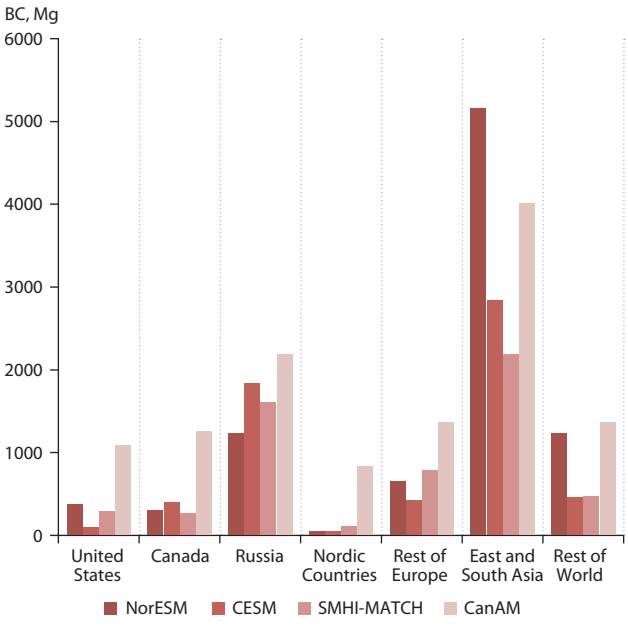

Figure 11.1 Contribution of different emission regions to black carbon (BC) burdens in the Arctic as simulated by four models using the same emissions for 2010.

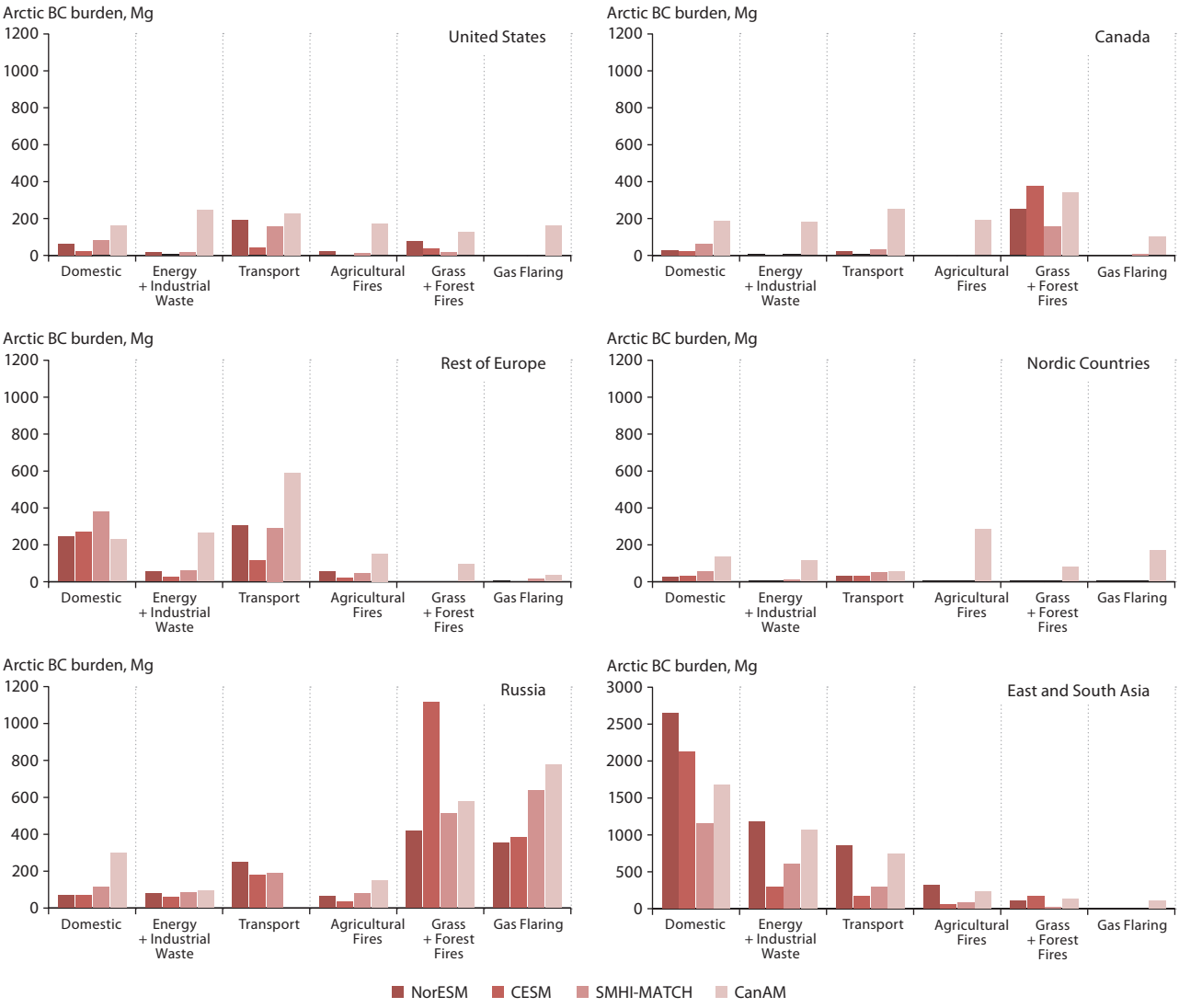

Figure 11.2 Contribution of different sectors within emission regions to black carbon (BC) burdens in the Arctic as simulated in four models using the same emissions for 2010. Note different scale for Asia relative to the other world regions.

Flaring have particularly large impacts on Arctic BC burdens (Fig. 11.2). While BC burden correlates well with the direct RF, BC burden may be less relevant to indirect cloud RF and deposition of BC (snow-ice RF), which are driven by BC in the atmospheric boundary layer. Figure 4.3 depicts how emissions at low latitudes contribute to higher-altitude BC concentrations in the Arctic, while emissions at high latitudes contribute to lower-altitude BC concentrations in the Arctic.

11.2.2 Ozone

Two chemical transport models (CTMs), the Oslo-CTM and SMHI-MATCH, were used to derive contributions from source regions and sectors to O_3 burdens and RF. Emissions from open burning (Grass+Forest) were included in SMHI-MATCH CTM but not Oslo-CTM. Note that in the present study, methane (CH_4) emissions are kept constant, and it is only changes in NO_X, CO and VOC that contribute to changes in O_3 burden. This approach was used due to the long atmospheric lifetime of CH_4 (8 to 10 years), which leads to an approximately equal contribution per unit CH_4 emission from all regions. The report from the AMAP Expert Group on Methane (Gauss et al. 2015) presents simulations of changes in O_3 burden due to global changes in emissions of CH_4, NO_X, CO and VOCs for different scenarios.

The largest contributions to the annual Arctic O_3 budget are from Asia, the United States and Russia in SMHI-MATCH while for Oslo-CTM the order is Asia, the United States and ROW (Fig. 11.3). This result is in line with the magnitude of emissions of the main O_3 precursors (NO_X, VOCs and CO) from these regions (see Ch. 5). The difference for the ROW region is because the SMHI-MATCH model domain is not global but only covers the area north of 20°N so emissions from lower latitudes are not fully accounted for. The Energy+Industry+Waste and Transport sectors dominate generally in both models, but for the SMHI-MATCH model emissions from Grass+Forest fires in Canada and Russia are the dominant source. Note that Oslo-CTM did not simulate the effect of open biomass burning (Grass+Forest) emissions. Overall Oslo-CTM simulates an Arctic burden, excluding the contribution from ROW, which is 20% larger than that simulated by SMHI-MATCH. The fact that Oslo-CTM is a global model will lead to higher contributions to Arctic O_3, particularly for source regions at more southerly latitudes.

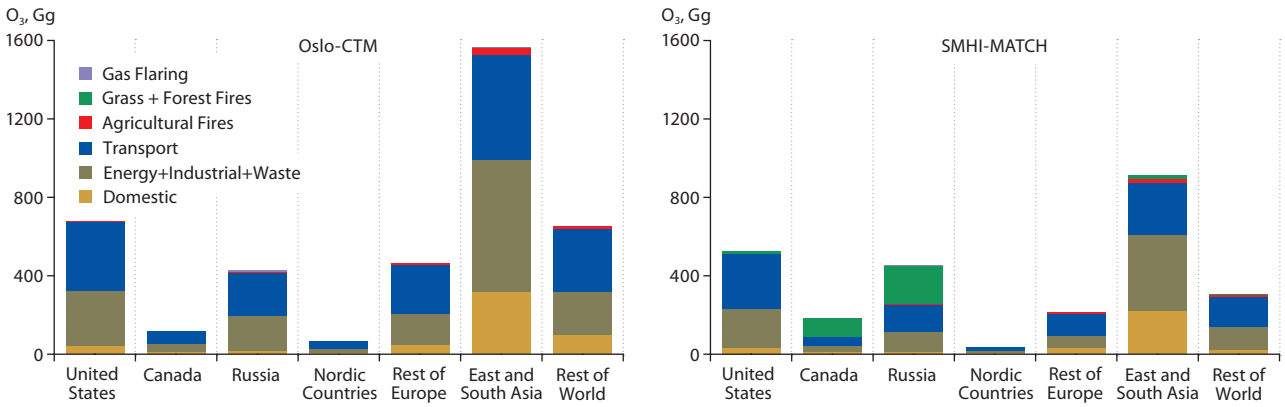

Figure 11.3 Arctic annual ozone (O_3) burden from different source regions and emission sectors as simulated by two chemical transport models. The SMHI-MATCH models includes anthropogenic emissions and emissions from Grass+Forest fires, the Oslo-CTM model includes anthropogenic emissions only.

11.3 Contribution of source regions and sectors to radiative forcing

11.3.1 Forcing within the Arctic

11.3.1.1 Black carbon forcing

The Arctic direct RF of BC, a measure of the heating of the atmosphere by absorption of solar radiation by BC (Ch. 4), is shown in Fig. 11.4. Emissions from Asia and Russia are the largest contributors to the BC direct RF in the Arctic, with multi-model mean contributions of 280 and 140 mW/m^2, respectively. The Nordic countries contribute less to Arctic BC direct RF than any other region. Overall, the impact of emissions on direct RF is well correlated with changes in BC burden (see Sect. 11.2), indicating that radiative effects are strongly related to concentrations of BC in the atmosphere. Differences in simulated RF estimates arise from differences in simulated burdens and the vertical distribution of BC, cloud distributions, and uncertainties in treatments of radiative processes in the models. The BC direct RF in the Arctic is 640 mW/m^2 averaged over all models.

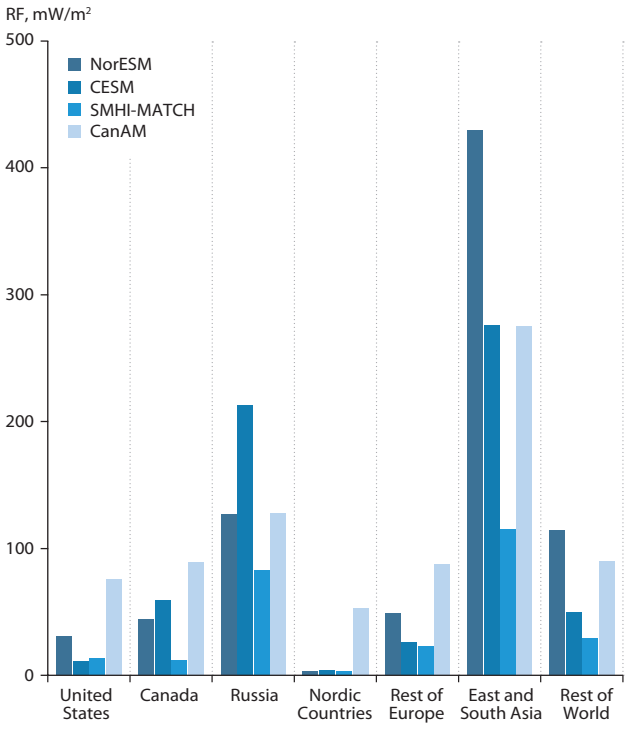

Figure 11.4 Arctic annual mean direct radiative forcing (RF) of black carbon for each emission region as simulated by four models.

Globally, the Domestic sector produces the largest BC direct RF in the Arctic, followed by Grass+Forest fires and Transport. Emissions from Asia from Domestic sources, Energy+Industry+Waste, and Transport produce the largest regional/sectorial contributions to BC direct RF in the Arctic, with mean contributions of 140, 63 and 41 mW/m^2, respectively (Fig. 11.5). The mean contribution of emissions from Russian Flaring is 26 mW/m^2.

The BC snow/ice RF, a measure of the heating of snow and ice by absorption of solar radiation by BC in snow and ice, is shown in Fig. 11.6. The greatest contribution is from Russian Flaring emissions and from East+South Asia Domestic emissions, 53 and 29 mW/m^2 respectively. The total model mean snow/ice forcing is 180 mW/m^2, about 30% of the atmospheric BC direct RF. Note, however, that the surface warming by the snow/albedo effect is greater than the surface warming caused by the same amount of heat added higher in the atmosphere through the direct effect (see Sect. 11.4 for estimates of surface warming).

The BC cloud (indirect) RF, a measure of the heating of the atmosphere by changes in cloud droplet size and cloud lifetime, is shown is Fig. 11.7. NorESM and CanAM produce positive cloud RFs for each emission region, with greater RF in CanAM. Similar to direct and snow/ice RF, emissions from Asia are particularly important compared to emissions from other regions. Impacts of Grass+Forest fire emissions are more important in NorESM than CanAM, which reflects inherent uncertainties in simulations of cloud RF in the models. The total model mean BC cloud forcing for all regions/sectors combined is 270 mW/m^2, which is less than BC direct RF. However, it is notable that this indirect forcing is positive, unlike that of SO_4 which is negative. Cloud RF is calculated for warm liquid clouds only, and it should be noted that the impact of BC acting as ice nuclei in cold clouds could also be important (Bond et al. 2013).

11.3.1.2 Forcing by ozone precursors

Emissions of NO_X, CO and VOCs lead to changes in the concentration of O_3 as well as to changes in the oxidizing capacity of the atmosphere through changes in the concentration of hydroxyl radical (OH). The latter process leads to changes in

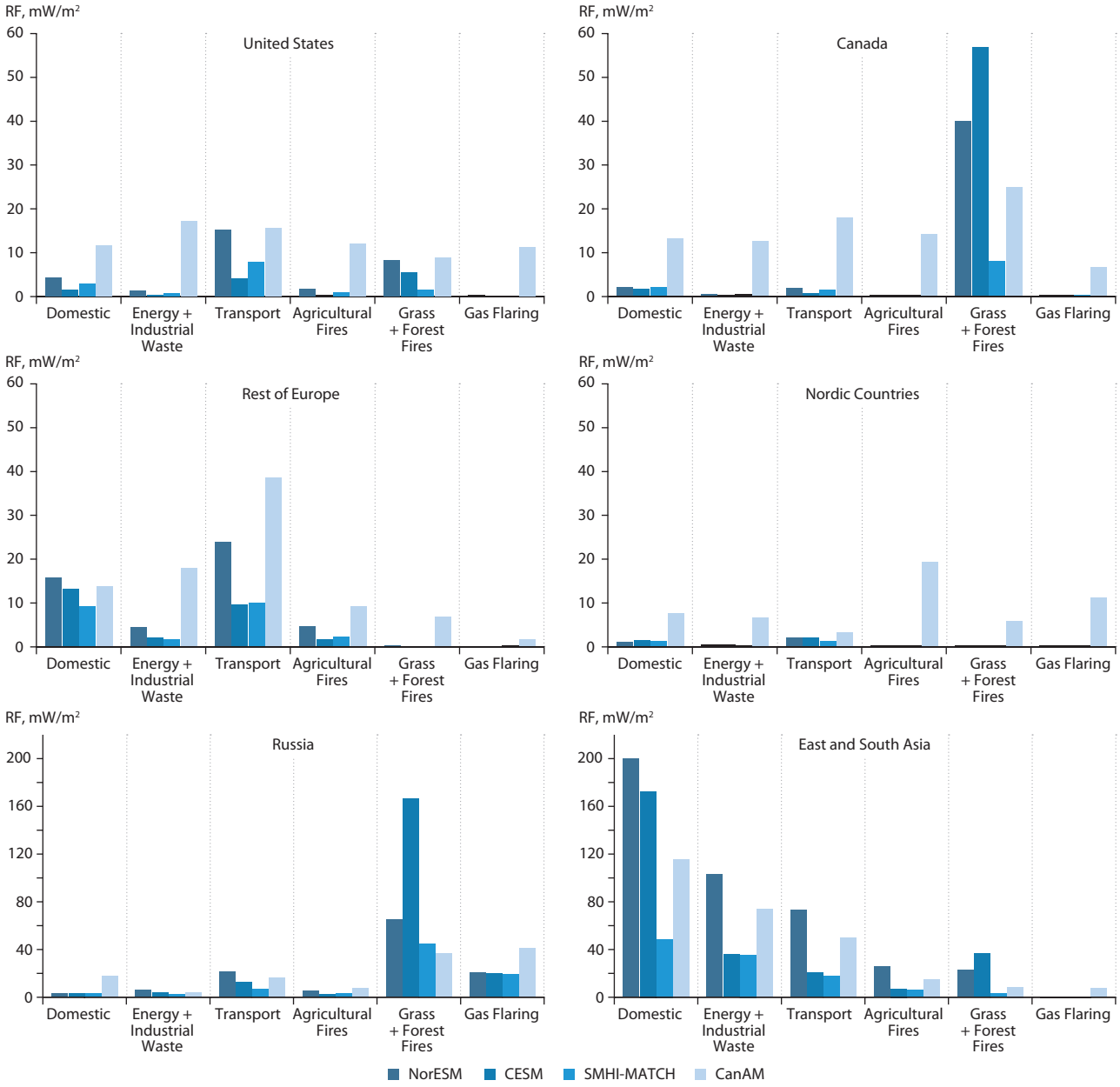

Figure 11.5 Annual mean black carbon (BC) direct radiative forcing in the Arctic for each emission region and sector as simulated by four models. Note use of different scale for Russia and Asia relative to the other world regions.

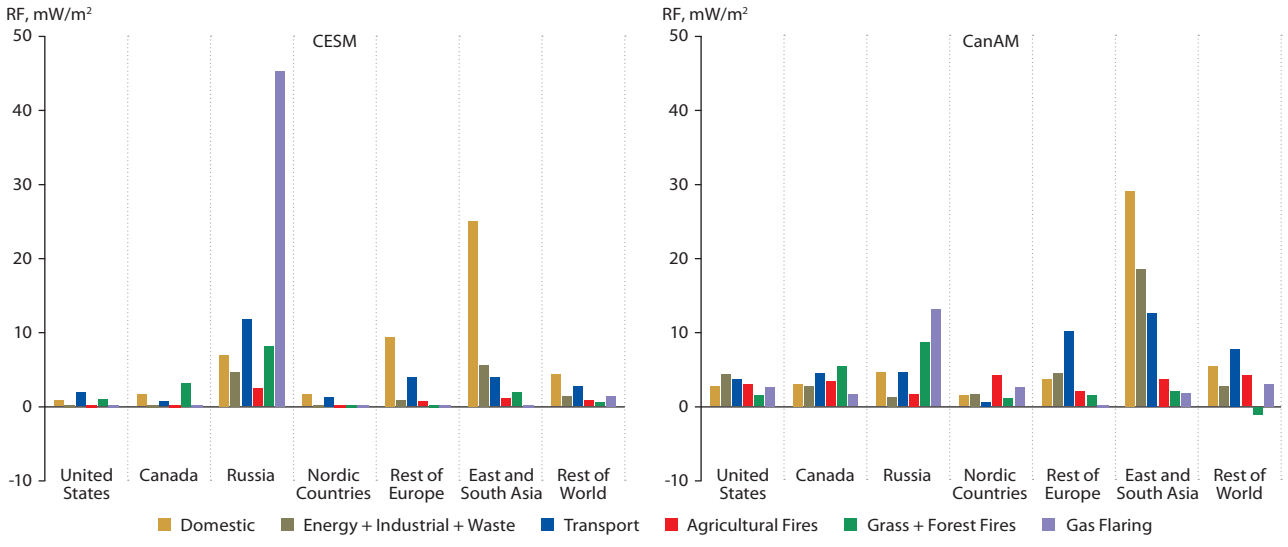

Figure 11.6 Annual mean Arctic black carbon (BC) snow/ice radiative forcing (RF) for all emission sectors and source regions as simulated by two models.

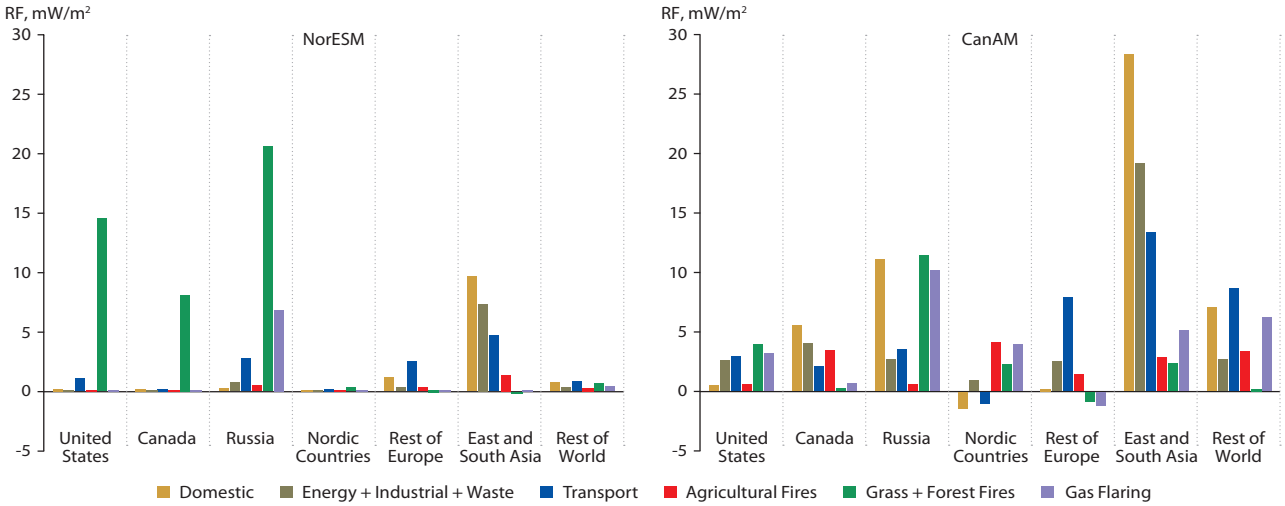

Figure 11.7 Annual mean Arctic cloud (indirect) radiative forcing (RF) due to black carbon (BC) for all emission sectors and source regions as simulated by two models.

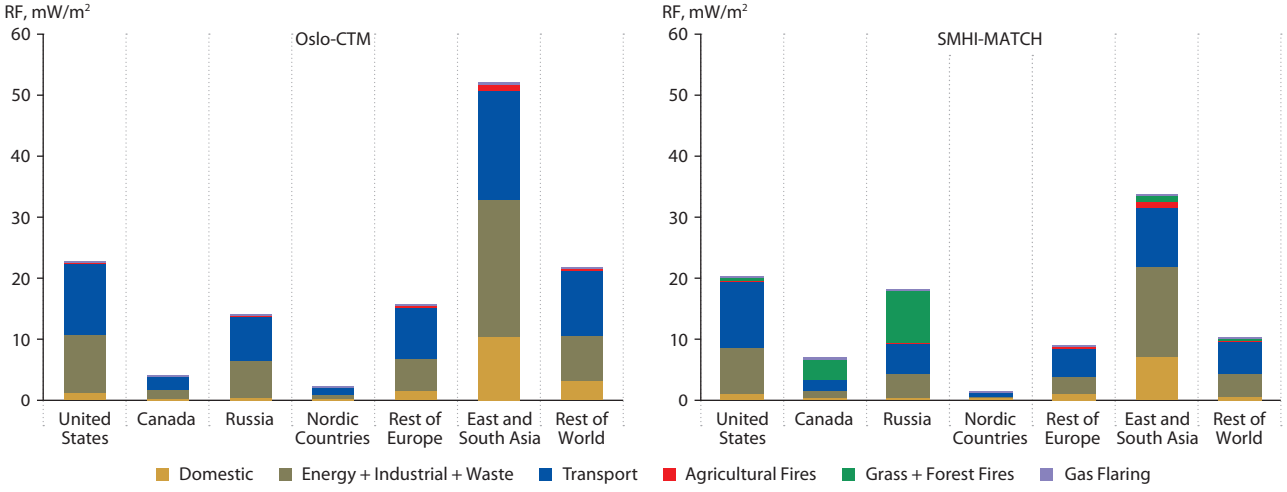

Figure 11.8 Simulated Arctic annual mean radiative forcing of ozone (O_3) from different source regions and emission sectors. The SMHI-MATCH model includes anthropogenic emissions and emissions from Grass+Forest fires, the Oslo-CTM model includes anthropogenic emissions only.

the lifetime and concentration of CH_4 and thus a RF. While all three precursors tend to increase O_3, NO_X emissions enhance OH and thus reduce CH_4 concentrations. Emissions of CO and VOCs on the other hand cause a reduction in OH and thus an increase in CH_4. Figure 11.8 shows the contributions from different sectors and regions to the RF of O_3 north of 60°N. The relative contributions are similar to the O_3 burden contributions, again with the largest contributions from Asia, the United States and Russia and with the main contributions from the Energy+Industry+Waste, Transport, and Grass+Forest fire sectors. The total RF from O_3 north of 60°N from anthropogenic emissions and Grass+Forest fires is estimated to be 98 mW/m² in SMHI-MATCH (110 mW/m² including shipping). In Oslo-CTM the anthropogenic contribution is 130 mW/m². The overall contribution from shortwave and longwave RF is 57% and 43% respectively for SMHI-MATCH. The shortwave contribution is higher for high-latitude sources, reaching 64% for Canada and 74% for the Nordic countries in SMHI-MATCH. This is because more northerly emissions primarily contribute to O_3 in the lower troposphere in the Arctic while more distant sources contribute more at higher altitudes.

The RF by CH_4 concentration changes and CH_4-induced global O_3 changes due to emissions of NO_X, CO and VOCs (often

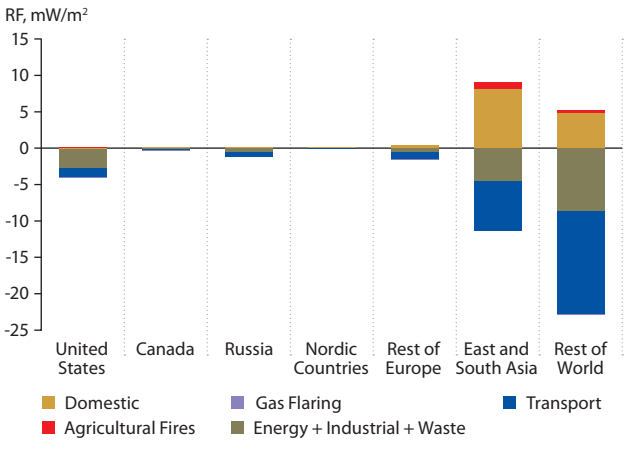

Figure 11.9 Simulated Arctic annual mean radiative forcing (RF) of methane (CH_4) and CH_4-induced ozone (O_3) from different source regions and emission sectors (excludes emissions from Grass+Forest fires).

also called primary-mode O_3) is calculated by the Oslo-CTM based on diagnosed changes in global mean CH_4 lifetime from the separate simulations of sectors and regions. The change in CH_4 and CH_4-induced O_3 were calculated following the procedure described by Berntsen et al. (2005). Figure 11.9 shows the estimated Arctic mean RF by changes in CH_4 and

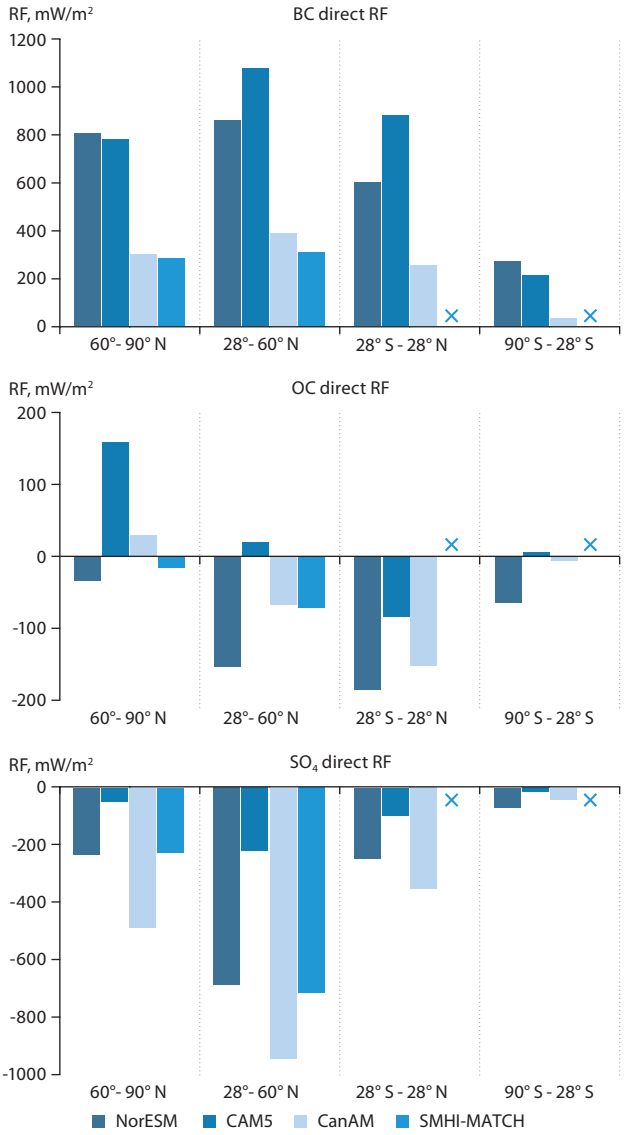

Figure 11.10 Annual mean direct radiative forcing (RF) due to global emissions of black carbon (BC), organic carbon (OC) and sulfur dioxide (SO_2) separated by latitude band (Arctic, mid-latitudes, tropics and southern hemisphere) for four models. Note that SMHI-MATCH is a regional model (20–90°N), while the other three models are global.

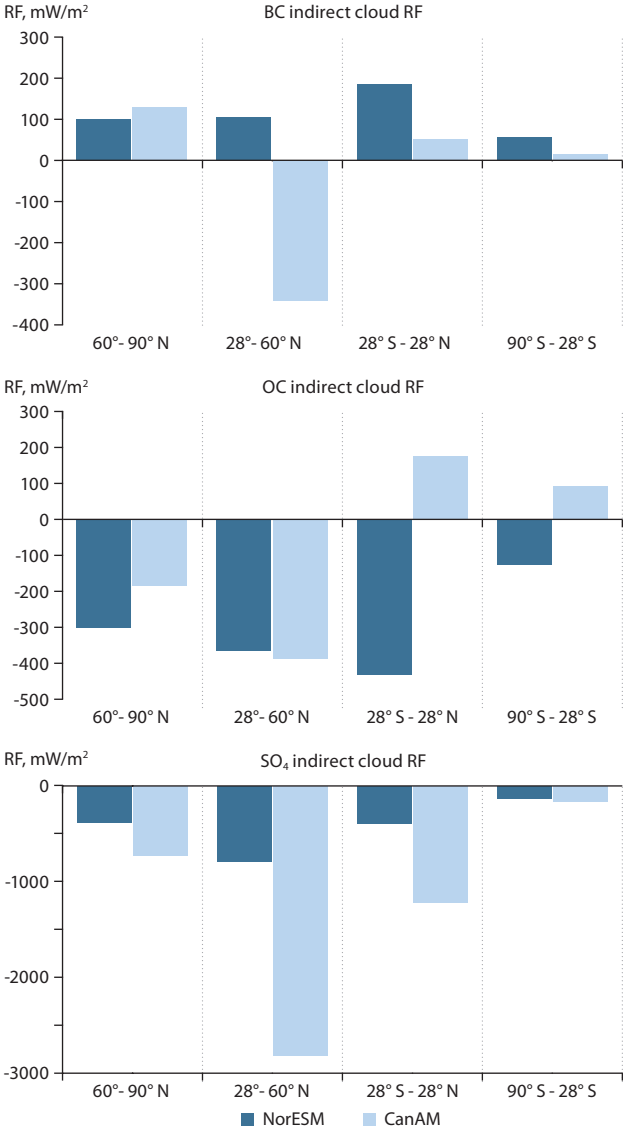

Figure 11.11 Annual mean cloud indirect radiative forcing (RF, mW/m^2) due to global emissions of black carbon (BC), organic carbon (OC) and sulfur dioxide (SO_2) by latitude band for the models NorESM and CanAM.

CH_4-induced O_3. Note the difference in sign between the NO_X-rich sources (Transport, and Energy+Industry+Waste) versus the CO- and VOC-rich sources from Domestic combustion and Agricultural waste burning. The net effect on Arctic RF from these CH_4 and CH_4-induced O_3 changes is -25 mW/m^2.

11.3.1.3 Forcing from other aerosols

To evaluate the effects of mitigation of BC emissions on Arctic climate, co-emitted species must also be taken into account. To apply the RTP concept, the RF in separate latitude bands is required. Figure 11.10 shows the RF for BC, OC and SO_4 due to global emissions for four latitude bands (Arctic, mid-latitudes, tropics and southern hemisphere) used for RTP-based temperature estimates (see Sect. 11.4). OC forcing (for the global emissions) is generally negative, but for two of the models is positive in the Arctic. CESM has a much smaller SO_4 forcing than the other three models.

For comparison, the cloud indirect RF for the same components and latitude bands is shown in Fig. 11.11. Simulations with NorESM and CanAM indicate that indirect effects of OC and SO_4 cause negative radiative forcings in the Arctic. The cloud indirect RF is highly uncertain and has not been included in the RTP-based temperature estimates. However, according to results from all models considered in this study, it is very likely that reductions in sulfur emissions would at least partially counteract the effects of reduced BC and O_3 precursor emissions on Arctic climate, which may limit the effectiveness of mitigation actions.

11.3.1.4 Forcing from shipping emissions

Emissions from shipping, both within the Arctic and outside the Arctic, induce Arctic RF (see Fig. 11.2). The total Arctic RF for all forcing agents is 18 mW/m^2 for extra-Arctic shipping and 0.26 mW/m^2 for within-Arctic shipping. For BC, the Arctic direct RF from shipping is 3% of the Arctic RF due to non-shipping sources. Figure 11.12 shows only the direct RF from shipping emissions (indirect effects on clouds are not included). The figure excludes the indirect chemical effects of O_3 precursors (primarily NO_X from shipping) on CH_4 because only the regional model MATCH was used for the O_3

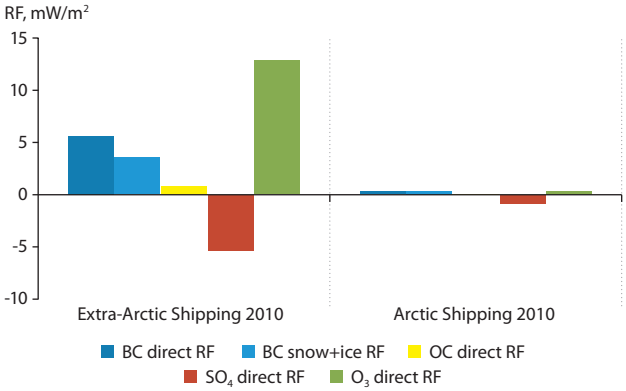

Figure 11.12 Arctic radiative forcing due to black carbon (BC) in the atmosphere and in snow+ice, and to organic carbon (OC), sulfate (SO_4) and ozone (O_3) (mW/m²) from shipping emissions within and outside the Arctic. Model-mean (CESM and SMHI-MATCH).

simulations. Previous studies on the climate impact of emissions from shipping (e.g. Eyring et al. 2010 and references therein) have shown that on a global scale the indirect cloud effects are potentially large, this is because the SO_2 emissions occur in clean background conditions where the concentration of cloud condensation nuclei (CCN) is relatively low. Previous studies have also shown that the negative RF (on a global scale) of NO_X-induced CH_4 changes tends to be of a similar magnitude to the positive RF from direct O_3 forcing (Fuglestvedt et al. 1999).

11.4 Equilibrium climate response due to forcing by black carbon and tropospheric ozone

Arctic climate forcing is not a suitable metric for diagnosing the Arctic climate response, in terms of surface temperature change, for three reasons. First, because species absorbing solar radiation (BC and partly O_3) in the upper Arctic troposphere may actually cool the surface despite exerting a positive RF (Shindell and Faluvegi 2009; Sand et al. 2013a). Second, forcing by BC or O_3 outside the Arctic can cause substantial Arctic warming by increasing the poleward heat flux. Third, forcing by the snow/albedo effect triggers strong local feedbacks enhancing the regional warming. As a more suitable proxy for the impacts of BC and O_3 on Arctic climate, this study estimated the equilibrium temperature response to emission perturbations through the use of RTPs (Shindell and Faluvegi 2009; Shindell 2012; Collins et al. 2013a).

The equilibrium surface temperature response was calculated by translating the RFs through the use of regional climate sensitivity parameters defined in four latitude bands (see Table 7.3). In this way, both regional and remote contributions to changes in Arctic temperature are taken into account. For BC in the Arctic, vertically-resolved RFs were derived and applied in combination with vertical climate sensitivity parameters (Flanner 2013). These temperature estimates do not include the effect of cloud indirect forcing, because there are no established RTP coefficients for the indirect effect. Details are given in Sect. 7.4.

The Arctic equilibrium surface temperature response is shown in Fig. 11.13. The net surface temperature response for all components averaged over all models is 0.35°C, where 0.40°C is from BC in the atmosphere, 0.22°C is from BC in snow, -0.04°C is from OC and -0.23°C is from SO_4. SMHI-MATCH only covers 20–90°N meaning that contributions south of 20°N were not accounted for. Therefore, the model-mean for latitudes south of 20°N were added to these results.

In terms of the Arctic equilibrium surface temperature response for each sector and source region for BC, OC, SO_4 and O_3 (Fig. 11.14), the largest contributions to warming in the Arctic come from East+South Asia Domestic emissions, Russian Fires and Flaring emissions, and Domestic and Fire emissions from ROW.

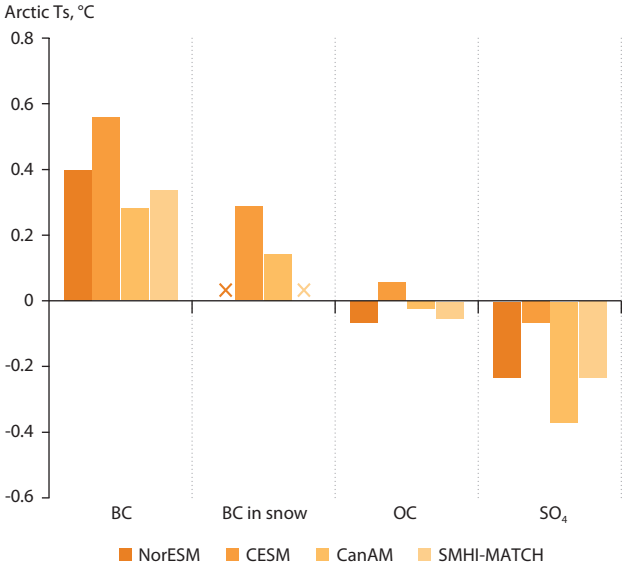

Figure 11.13 Global (total) contributions to annual-mean Arctic equilibrium surface temperature response due to black carbon (BC), organic carbon (OC) and sulfate (SO_4) direct forcing and due to BC in snow. The models NorESM and SMHI-MATCH do not include BC in snow. SMHI-MATCH does not include contributions from south of 20°N, so the model mean was added for 90°S–20°N. Temperature changes were derived by translating the radiative forcings with the use of climate sensitivity parameters (see Sect. 7.4 for details).

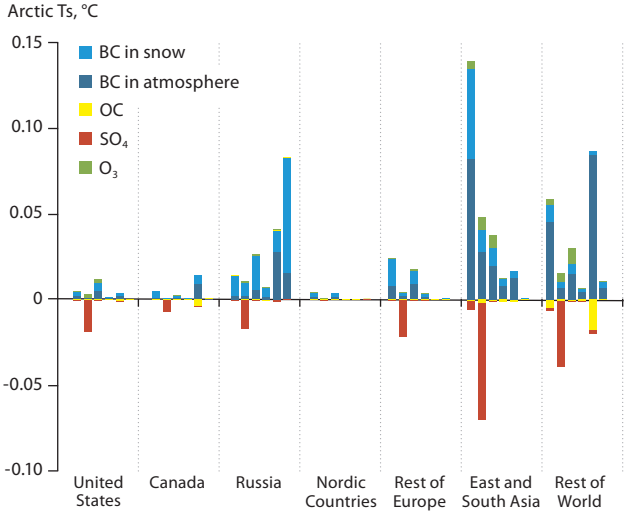

Figure 11.14 Arctic equilibrium surface temperature response due to direct forcing by black carbon (BC), organic carbon (OC), sulfate (SO_4) and ozone (O_3) averaged over the models CESM, NorESM, SMHI-MATCH and Oslo-CTM. Each bar represents the different emission sectors for each source region specified on the X-axis. The sectors for each emission region are 1) Domestic, 2) Energy+Industry+Waste, 3) Transport, 4) Agricultural waste burning, 5) Forest fires and, 6) Flaring. The temperature changes were derived by translating the radiative forcings with the use of climate sensitivity parameters (see Sect. 7.4 for details).

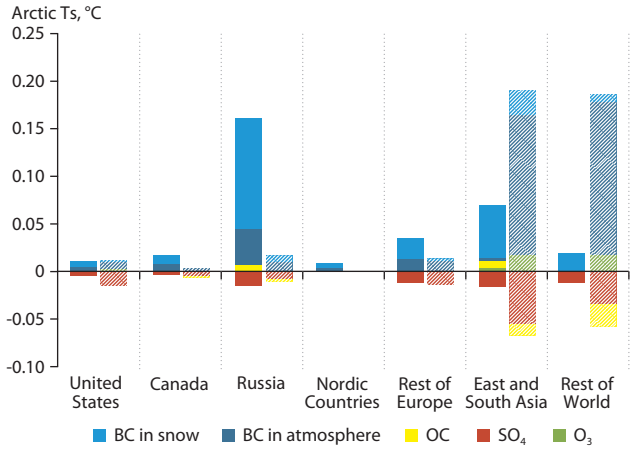

Figure 11.15 Arctic equilibrium surface temperature response due to direct forcing by black carbon (BC), organic carbon (OC), sulfate (SO_4) and ozone (O_3) averaged over the models CESM, NorESM, SMHI-MATCH and Oslo-CTM from each emission region. The Arctic response is divided into contributions from radiative forcing (RF) within the Arctic (solid fill) and outside the Arctic (pattern fill).

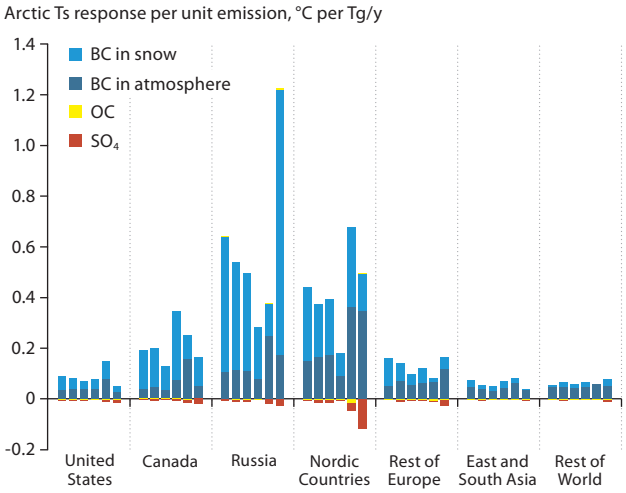

Figure 11.16 Arctic equilibrium surface temperature response per emissions due to direct forcing of black carbon (BC), BC in snow, organic carbon (OC) and sulfate (SO_4) averaged over the models CESM, NorESM, SMHI-MATCH and Oslo-CTM. The sectors for each emission region are (from left to right): 1) Domestic, 2) Energy+Industry+Waste, 3) Transport, 4) Agricultural waste burning, 5) Forest fires and, 6) Flaring. The temperature changes were derived by translating the radiative forcings with the use of climate sensitivity parameters (see Sect. 7.4 for details).

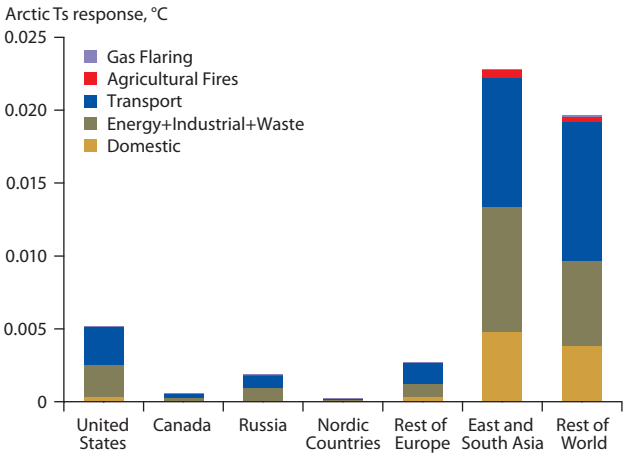

Figure 11.17 Arctic equilibrium surface temperature response due to ozone (O_3) averaged over the models SMHI-MATCH and Oslo-CTM. The temperature changes were derived by translating the radiative forcings with the use of climate sensitivity parameters (see Sect. 7.4 for details).

The Arctic temperature response to all emissions from each source region is shown in Fig. 11.15, with the response shown for contributions from RF exerted from emissions within and outside the Arctic. For East+South Asia emissions the greatest contribution to BC warming in the Arctic comes from BC forcing exerted outside the Arctic, while for Russia and OEUR a greater proportion of the warming is from BC within the Arctic.

Exactly how the different emissions affect the Arctic can be separated into (i) the magnitude of the emissions and the fraction transported into the Arctic and (ii) the sensitivity of the Arctic temperature response to the forcing in the different regions and by different forcing mechanisms. While Figs. 11.13 to 11.15 show the absolute contributions, Fig. 11.16 shows the Arctic sensitivity per unit emission to source sectors within each region. Here the temperature response is normalized to the magnitude of the emissions for each region and sector. In this way the effectiveness of regional emission mitigation options can be evaluated. Flaring emissions from Russia have the highest temperature response per unit emission. The Arctic is also sensitive to Nordic emissions and even if the emissions from the Nordic countries are small, the large specific temperature response associated with these emissions implies that Arctic climate change abatement through reductions of these emissions could be cost-effective. The absolute contribution from Asian emissions is large, but normalized to per unit emission the contribution is relatively small.

RTPs can only be used to calculate annual mean temperature changes even though the seasonal variation of underlying processes was accounted for in the estimates of the annual mean RTPs. Previous studies of the impact of BC on surface temperatures in the Arctic (Flanner 2013; Sand et al. 2013a) show complex responses with significant warming even during winter (when the local RF is virtually zero) due to changes in sea-ice cover. Further research is required to assess the seasonality of climate responses.

11.4.1 Ozone

The estimated warming due to O_3 from emissions of NO_X, non-methane volatile organic compounds (nmVOCs) and CO in the Arctic is much smaller than for BC, with a total warming of 0.05°C based on two models (see Fig. 11.17).

The Arctic temperature response to the simulated O_3 changes is generally higher for the Oslo-CTM model than for the SMHI-MATCH model, even if the RF within the Arctic is quite similar (see Sect. 11.3). The difference between the two models is greater for the low latitude sources (Asia and ROW). The Oslo-CTM, being a global model, is also able to capture the impact of O_3 changes in the tropics and in the southern hemisphere. The forcing at these latitudes also contributes to Arctic warming, here estimated through the RTP coefficients. The sensitivity for O_3 (as given by the RTP coefficients) is quite low for the Arctic temperature response to RF within the Arctic. For O_3, a significant part of the RF in the Arctic is due to absorption of shortwave radiation (similar to BC), while at lower latitudes the greenhouse effect of O_3 (absorption of longwave radiation) dominates.

11.4.2 Net Arctic warming by emissions of ozone precursors

As discussed in Sect. 11.3 and shown in Fig. 11.9, the accompanying changes in CH_4 and CH_4-induced O_3 substantially change the net RF caused by emissions of NO_X, nmVOCs and CO. Figure 11.18 shows the estimated Arctic temperature change when all these forcing mechanisms are included. The same methodology using the RTPs is applied in this estimate. Note that the Arctic climate sensitivity (°C/Wm^{-2}) to changes in CH_4 is substantially higher than for O_3 due to the impact of O_3 on shortwave radiation (see Sect. 7.4).

The relative impacts of emissions in the different regions do not change dramatically. However, the relative importance of the Domestic combustion sector increases substantially. This source is rich in CO and VOC relative to NO_X compared with the other sectors. Thus there is a positive RF for both O_3 and CH_4 changes. For some regions and sectors (most notably the Energy+Industry+Waste and Transport emissions from ROW) the net impact of emissions of O_3 precursors on Arctic temperatures is estimated to be a cooling.

Methane emissions also lead to increased O_3 formation. Neither of the AMAP Expert Groups performed model simulations to quantify the Arctic warming that is due only to O_3 formed from anthropogenic CH_4 emissions. To give an estimate of this effect, this study has used simulations of O_3 changes due to current anthropogenic emissions of all O_3 precursors (NO_X, CO, nmVOCs and CH_4) in the ACCMIP experiment (Lamarque et al. 2013). Using PORT (see Sect. 7.3.3) the tropospheric RF from O_3 was estimated for two models participating in ACCMIP, NCAR-CAM3.5 and OsloCTM2. The resulting global-mean annual mean RF for year 1850-2000 change in tropospheric O_3 was 415 and 401 mW/m^2 for the two models, respectively. These values are close to those reported by Stevenson et al. (2013) for the same models using 150 ppbv as the tropopause definition and slightly higher than the average over 17 models of 377±65 mW/m^2. Using the average RF over the four broad latitude bands (see Sect. 7.4) for NCAR-CAM3.5 and OsloCTM2 and the RTP approach, this study estimated a total Arctic warming due to O_3 RF of 0.12°C. Assuming that the difference between this value and the warming derived from O_3 changes due to the precursors NO_X, CO and nmVOCs given above (Sect. 11.4.2, Fig. 11.18) can be assigned to O_3 produced from CH_4, it may be concluded that O_3 produced by current CH_4 oxidation gives an equilibrium Arctic warming of about 0.07°C. This crude estimate neglects non-linear chemical effects and has substantial uncertainty arising from the RTP coefficients for O_3 which, to date, have only been calculated by the GISS model.

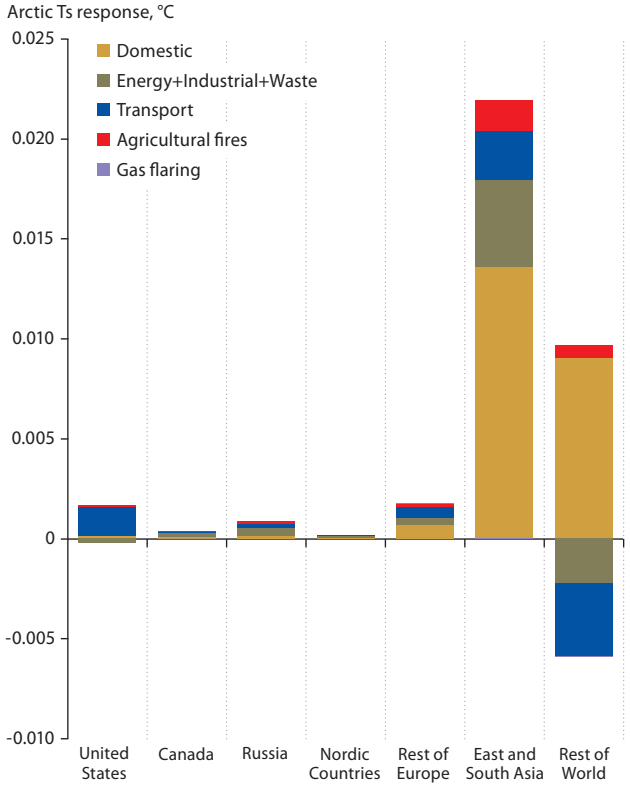

Figure 11.18 Arctic equilibrium surface temperature response due to the net impact of emission of ozone (O_3) precursors in the Oslo-CTM model. The temperature changes were derived by translating the radiative forcings with the use of climate sensitivity parameters (see Sect. 7.4 for details).

11.5 Climate response to mitigation scenarios (IIASA scenarios)

The equilibrium climate response to total emissions of non-methane SLCFs was simulated in the preceding sections. This climate response represents the upper limit because a 100% reduction in emissions is unrealistic and it would take a very long time for the climate system to reach a new equilibrium. A more relevant question for policymakers is what might be the transient response to a more realistic mitigation of non-methane SLCFs. Due to the high cost of running simulations with global climate models (including a full ocean) there is a very limited capacity to make online simulations for realistic emissions reduction scenarios. Nevertheless the following section reports the results from one such experiment.

11.5.1 Transient climate simulations

The analysis presented earlier of equilibrium climate change relies on the use of RTPs (e.g. Shindell 2012) to translate very small radiative forcings into regional temperature changes. This approach is needed because the explicit simulation of temperature change in response to small perturbations requires very long climate integrations or a large number of ensemble members, both of which incur excessive computational costs. This section briefly considers results from a set of fully-coupled transient climate simulations designed to explore potential climate benefits associated with aggressive reductions in global emissions of SLCFs.

The CESM v1.1.1 model is applied with fully coupled atmosphere, ocean, land, and sea-ice components, initialized to year 2001 conditions. The model was configured with modal aerosol (MAM3) treatment (Liu et al. 2012) and MOZART chemistry (Emmons et al. 2010). Simulations were carried out to 2050, with four ensemble members representing a current legislation scenario ('BASELINE'), and four ensemble members representing an experiment with aggressive changes in emissions of aerosols, CH_4, and O_3 precursors beginning in year 2016 ('MITIGATE'). These emissions scenarios are described in Ch. 5. Global annual emissions of BC, CH_4, and NO_X applied in the BASELINE and MITIGATE simulations are shown in Fig. 11.19. The emissions

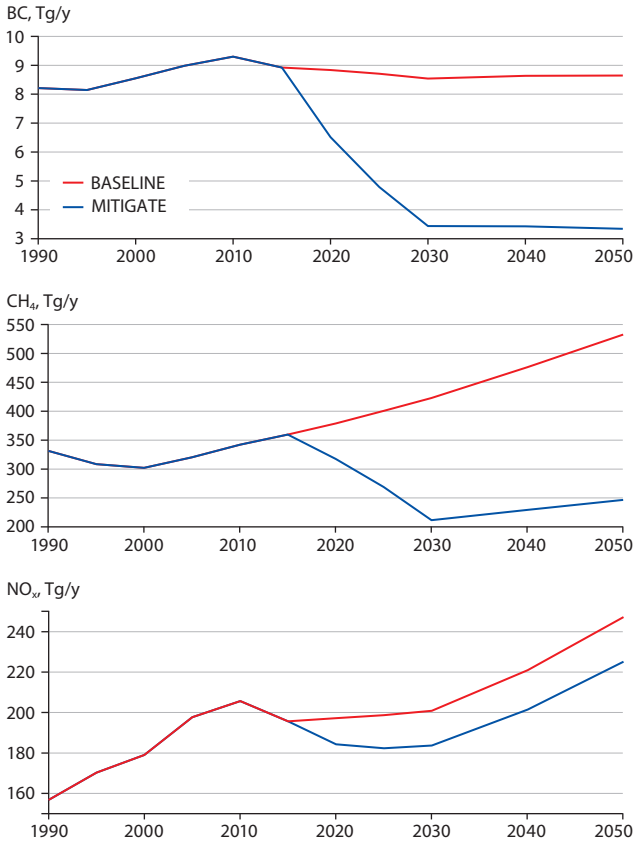

Figure 11.19 Global annual-mean emissions of black carbon (BC), methane (CH_4), and nitrogen oxides (NO_X expressed as NO_2) applied in the BASELINE and MITIGATE sets of transient simulations.

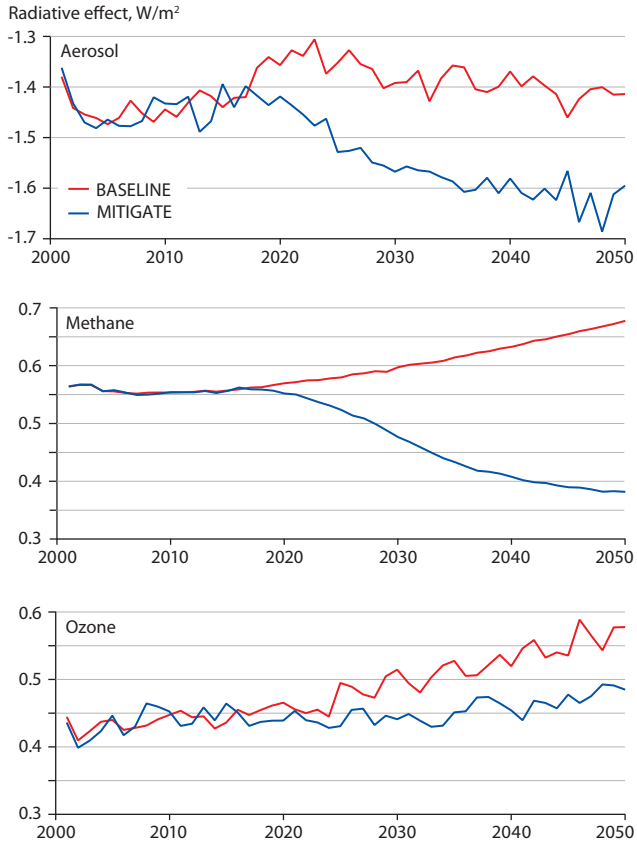

Figure 11.20 Global annual-mean direct radiative effect (shortwave + longwave) of all atmospheric aerosols (aerosols in snow and sea ice excluded), methane (CH_4), and ozone (O_3) diagnosed in a single ensemble member each of the BASELINE and MITIGATE sets of simulations.

differences between the scenarios are designed to be large enough to cause a significant signal in climate response within a small number of ensemble members.

Time series of the instantaneous radiative effects of SLCFs (diagnosed in one ensemble member each of BASELINE and MITIGATE) indicate that the MITIGATE scenario provides substantial benefit in direct radiative forcing (Fig. 11.20). The differences (MITIGATE – BASELINE) in global-mean radiative effect of all atmospheric aerosols, land snow-deposited aerosols, CH_4, and O_3 averaged over 2041–2050 are, respectively, -0.21, -0.01, -0.27, and -0.08 W/m^2. Averaged only over the Arctic (60–90°N), these changes are: -0.12, -0.07, -0.19, and -0.04 W/m^2 (for reference, the change in global carbon dioxide (CO_2) forcing between 2015 and 2050 under the RCP6.0 scenario is 0.96 W/m^2).

The benefit to Arctic climate associated with this reduced radiative forcing is shown in Table 11.1. Here results from three additional models (NorESM CESM (CAM4) and HadGEM) from the ECLIPSE project are included. The numbers are the differences (MITIGATE – BASELINE) in ensemble-mean Arctic and global climate states averaged over 2041–2050. In the MITIGATE scenario, Arctic surface air temperature is reduced by 0.3–0.6°C relative to BASELINE conditions, and the area of annual-mean sea ice within the Arctic is 1.6×10^5 – 2.9×10^5 km^2 greater. The global surface air temperature is reduced by 0.2–0.3°C (CESM CAM5 shows an increase in global temperature of 0.05°C, but it is not significant at the 95% confidence level).

Reasons for the damped global climate response in CESM (CAM5) can be partially traced to cloud changes, which largely offset the radiative benefit associated with direct forcing. However, it should be noted that cloud indirect effects vary substantially between models and are challenging to represent in global climate models (e.g. Stevens and Boucher 2012). It is also important to keep in mind that the response time of the fully-coupled climate system is very long (of the order of 100 years), and hence the system has only partially responded by 2050 to the forcing changes, which begin in 2016 and ramp up thereafter (Fig. 11.20).

11.5.1.1 Transient climate response with the RTP-based method

The transient Arctic surface temperature response following the ECLIPSE mitigation scenario of SLCFs can also be calculated with an RTP-based method using the results described in Sect. 11.4. For BC, OC and SO_2, equilibrium Arctic RTPs have been calculated for seven regions and six emission sectors (see Fig. 11.16). In the ECLIPSE emission mitigation scenarios, emissions are reduced from 2015 for all sectors, regions and species. For these species, the reduction in Arctic warming in year t ($\Delta T_A(t)$) can then be estimated by:

$$\Delta T_A(t) = \sum_{r,s,k} \int_{t_e=2015}^{t} E_{r,s,k}(t_e) \times RTP_{r,s,k} \times IRF(t - t_e) dt_e \qquad \text{Eq. 11.1}$$

where $E_{r,s,k}(t_e)$ is emission reduction year t_e from region r, sector s and component k. The global climate response function (IRF, here taken from Boucher and Reddy (2008)), accounts for the inertia of the climate system.

Table 11.1 Differences in the ensemble-mean climate states (MITIGATE – BASELINE) averaged over 2041–2050. Changes significant at p=0.05 are shown in bold.

	Model	Direct forcing from aerosols+CH_4+O_3 (W/m^2)	Surface air temperature (°C)	Sea-ice area (km^2)	Net cloud radiative effect (W/m^2)
Global	CESM (CAM5)	**-0.57**[a]	+0.05	+8.8×10^4	**+0.60**
	NorESM		**-0.20**	**+4.4×10^5**	
	CESM (CAM4)		**-0.24**	**+5.0×10^5**	
	HadGEM		**-0.29**	**+9.5×10^5**	
Arctic (60–90°N)	CESM (CAM5)	**-0.40**[b]	**-0.29**	**+1.6×10^5**	**+0.60**
	NorESM		**-0.42**	**+2.3×10^5**	
	CESM (CAM4)		**-0.58**	**+2.8×10^5**	
	HadGEM		**-0.49**	**+2.9×10^5**	

[a] Includes -0.014 W/m^2 change from aerosols (BC, OC, and dust) deposited to land snow. Forcing from sea-ice deposited aerosols was not diagnosed;
[b] includes -0.066 W/m^2 change from aerosols (BC, OC, and dust) deposited to land snow. Forcing from sea-ice deposited aerosols was not diagnosed.

The model simulations described in Sect. 11.4 calculated the RTPs only for the combined effect of NO_X, CO and nmVOCs. While this is very useful for identifying the potential net effects of mitigation from regions and sectors, it cannot be used for a scenario where NO_X, CO and VOCs are reduced at different rates, as in the ECLIPSE scenario. This study therefore used RTP values from the literature (Collins et al. 2013a) for these components. These RTP values include impact on O_3 and indirect effects on CH_4 through changes in the oxidizing capacity of the atmosphere. To make a complete estimate of the reduced Arctic warming due to the mitigation in the ECLIPSE scenarios, the impact of CH_4 reductions has also been simulated with the RTP-based method. For CH_4, a simple box simulation was done to calculate the net global radiative forcing over time following the emission perturbation in year t_e ($RF(t, t_e)$). RTP_A coefficients for the Arctic adopted from Collins et al. (2013a) were then used and the Arctic temperature response was estimated by convolution according to Eq. 11.2

$$\Delta T_{methane}(t) = \sum_{t_e=2015}^{t} \int_{t'=t_e}^{t} RTP_A \times RF(t', t_e) \times IRF(t-t')dt' \quad \text{Eq. 11.2}$$

Following the procedure outlined above, the transient Arctic surface temperature response (avoided warming due to the ECLIPSE mitigation scenario) can now be calculated. Figure 11.21 shows the net response to individual components (as a sum over all sectors and regions), as well as the total net response. The total net response averaged over the 2040–2050 period is -0.40°C (-0.23°C from BC and -0.17°C from CH_4). The corresponding net average for the four Earth System Models (ESMs) reported in Table 11.1 is -0.45°C.

The agreement between the RTP-based estimate and the ESM estimates is quite good. The ESM results have the benefit that geographical and seasonal distributions can be diagnosed, and impacts on other parameters such as wind, precipitation, and sea-ice coverage are also given. The RTP-based estimate only gives the annual mean temperature response for the whole Arctic region, although the contribution from individual regions, sectors and components are readily available. Also, the impact of many different emission mitigation scenarios can be easily calculated.

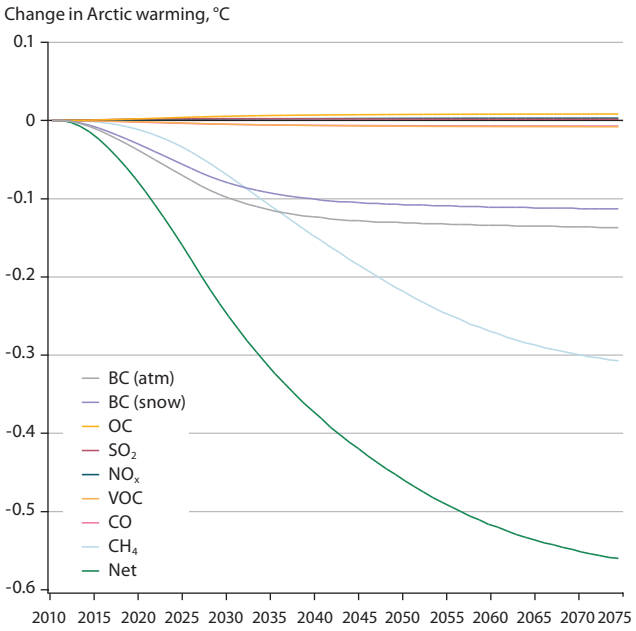

Figure 11.21 RTP-based estimate of reduced warming in the Arctic in response to ECLIPSE mitigation scenario.

11.6 Role of carbon dioxide mitigation in a short-term perspective

Carbon dioxide is the most important anthropogenic greenhouse gas and any long-term mitigation strategy must have CO_2 reductions as the primary objective. The removal of CO_2 from the atmosphere occurs through uptake in the terrestrial biosphere, in the upper mixed layer of the ocean and on the longer term in the deeper ocean. Due to these multiple removal processes there are multiple time constants for the removal of CO_2. In particular, the time constant for CO_2 uptake in the upper ocean is of the order of five years (Joos et al. 2013). The impulse response function for CO_2 removal from the atmosphere according to Joos et al. (2013) indicates that 28% of the CO_2 pulse is removed with a time constant of 4.3 years. Thus, in addition to its well-known long-term effect, CO_2 also has a short-term effect and so should be included in mitigation policies with a focus on the near term (e.g. 20-year timescale).

Based on global forcing calculations from ECLIPSE (Belloin N., University of Reading, UK, pers. comm. 2014; Aamaas B., CICERO, Norway, pers. comm. 2014, see Fig. 4.5), a reduction in emissions of BC ramped up to 1 kg/y after 15 years (see Fig. 11.19) gives the equivalent global mean temperature reduction after 20 years of a 4000 kg/y reduction in CO_2 emissions. In other words, an equal decrease in global temperature 20 years after the start of the mitigation resulting from a reduction of BC emission of 5 Tg/y, would require a reduction in CO_2 emissions of 20 Pg CO_2/y (or 60% of current (2010) fossil CO_2 emission, http://cdiac.ornl.gov/). On a longer timescale the benefit of the CO_2 reductions would be greater than for the BC reduction. It should be noted that this estimate does not include change in emissions of other species (e.g. SO_2 and OC) that are co-emitted with either BC or CO_2. As a result, the reduction in CO_2 emissions needed to equal (on a 20-year time horizon) the impact of SLCF reductions is uncertain and may be smaller than 20 Pg/y.

11.7 Conclusions

The impact of emissions of SLCFs in different regions and sectors on Arctic burden, radiative forcing and equilibrium surface temperature has been estimated. The estimates of equilibrium surface temperature changes include direct effects and effects of BC on snow, but do not include cloud indirect effects.

- Emissions from East+South Asia and Russia are the largest contributors to BC burdens in the Arctic in all the models, with mean contributions of 43% and 21%, respectively.
- The impact of BC emissions on direct RFs is well correlated with changes in BC burdens, indicating that radiative effects are strongly related to concentrations of BC in the atmosphere. The BC direct RF in the Arctic is 640 mW/m^2 averaged over all models.
- Arctic radiative forcing is not a good metric for Arctic response. The equilibrium temperature response to emission perturbations, estimated here through a scaling method using regional radiative forcings from this report and pre-calculated regional climate sensitivities (RTPs), is a much more accurate way of quantifying impact although uncertainties in RTPs are substantial. Separate Arctic temperature responses due to emissions of four short-lived species for 44 emission categories/source regions derived in this report from four different models can be used to design mitigation scenarios.
- The best estimate of total Arctic equilibrium surface temperature response due to the direct effect of current global BC, OC and sulfur emissions is 0.35°C, where 0.40°C is from BC in atmosphere, 0.22°C is from BC in snow, -0.04°C is from OC and -0.23°C is from SO_4.
- For non-methane SLCFs, emissions from the Domestic sector from East+South Asia have the largest warming effect in the Arctic of all sector/region combinations studied here. The Energy+Industry+Waste sector from Asia has the largest cooling effect.
- Emissions from Russia, Asia and ROW contribute to about equal warming in the Arctic. For East+South Asia and ROW, more than half of this warming comes from forcing exerted outside the Arctic.
- Per unit emission, the Arctic surface temperature is most sensitive to Russian Flaring emissions. A large part of this temperature increase is due to BC in snow. In general, Russian and Nordic emissions have the highest temperature response per unit emitted mass.
- Two models that include estimates of indirect effects, indicate that cooling effects by SO_4 in particular and OC emissions could be substantial. The large uncertainty in the indirect effects of aerosols on clouds precludes an assessment of the net effect of aerosols, but according to results from all models considered here, it is very likely that reductions in sulfur emissions would at least partially counteract effects of reduced BC and O_3 precursor emissions on Arctic climate, which may limit the effectiveness of mitigation action.
- Fully-coupled model runs with aggressive mitigation measures from year 2016 onwards showed reduced Arctic warming by 0.3–0.6°C by 2050.
- The RTP-based method indicated that CH_4 and BC reductions both contributed about 50% to this reduction in Arctic warming.
- Emissions of non-methane O_3 precursors contribute to both warming and cooling, in the Arctic and globally.
- Tropospheric O_3 produced from NO_X, nmVOC and CO emissions is estimated to produce an equilibrium temperature response of 0.05°C in the Arctic, while the response estimated for O_3 produced from CH_4 oxidation is estimated to be 0.07°C.
- Sources high in CO and VOCs relative to NO_X (i.e. biomass burning sources) are more effective in causing Arctic warming by O_3 and induced CH_4 changes. Domestic combustion in East+South Asia and ROW are the two largest anthropogenic sources of O_3 precursors.

12. Key findings and recommendations

Reductions in the emission of carbon dioxide (CO_2) are the backbone of any meaningful effort to mitigate climate change. The limited focus of this assessment on short-lived climate forcers (SLCFs) is not meant to detract from primary efforts on CO_2 reduction or redirect climate mitigation action toward a focus on SLCFs.

Model results indicate that fast and substantial reductions in CO_2 emissions can be effective in slowing climate warming on a short time scale, in addition to also leading to long-term climate benefits. A crude estimate indicates that, in terms of the effect on global annual average temperature on a 20-year time horizon, a sustained reduction in black carbon (BC) emissions of 1 Tg/y is approximately equivalent to a 4 Pg/y CO_2 reduction (about 10% of current global CO_2 emissions). But as this climate impact estimate for BC reduction does not include the change in emission of co-emitted species that would accompany BC mitigation, the reduction in CO_2 emissions needed to equal (on a 20-year time horizon) the impact of SLCF reductions may even be less than 4 Pg/y. Thus, targeted SLCF mitigation is not the only way of reducing the rate of warming in the near-term.

Sulfur emission reductions implemented to improve air quality are enhancing climate warming. This is because sulfate (SO_4) aerosols formed from sulfur emissions scatter solar radiation and influence clouds, both of which cause climate cooling. Any reduction in sulfur emissions will therefore reduce the potential for cooling through SO_4 formation, and thus enhance warming. However, a mitigation strategy which also reduces the emissions of those SLCF components that actively warm the climate, especially methane (CH_4) and BC, could help offset warming induced by decreasing sulfur emissions, especially in the Arctic.

12.1 Key findings

12.1.1 SLCF emissions and Arctic climate change

- Black carbon and SO_4 concentrations near the surface and in ice cores have declined in the Arctic over the past few decades. In contrast, surface and ozonesonde measurements show that tropospheric ozone (O_3) concentrations have increased.
- Sulfate and BC concentrations measured at Arctic surface sites show a clear maximum in winter and early spring during the Arctic Haze season and a minimum in summer and early autumn.
- The contribution of anthropogenic emissions in the ECLIPSE inventory from Arctic Council nations to global totals is about 10% for BC and ranges from 5% for organic carbon (OC) to 23% for nitrogen oxides (NO_X). All other co-emitted aerosol and O_3 precursors fall within this range.
- A mitigation case study indicates that there is still considerable potential for reducing Arctic Council SLCF emissions beyond the current legislation.
- The best estimate, based on four models, of the total Arctic equilibrium surface temperature response due to the direct effect of current global combustion-derived BC, OC and sulfur emissions is +0.35 K (multi-model range +0.03 to +0.84 K), where +0.40 K (+0.28 K to +0.56 K) is from BC in atmosphere, +0.22 K (+0.15 to +0.29 K) is from BC in snow, -0.04 K (-0.14 to +0.06 K) is from OC and -0.23 K (-0.37 to + 0.07 K) is from SO_4. Two models that calculated the indirect effect of aerosols on clouds indicate that the warming by aerosols would be less when this effect is included. A significant fraction of the warming is caused by forcing exerted outside the Arctic (Fig. 11.14).
- Emissions of non-methane O_3 precursors (nmOPs) contribute to warming via production of tropospheric O_3 (carbon monoxide, CO; volatile organic compounds, VOCs; NO_X) and cooling via reduction of the CH_4 lifetime (i.e. NO_X). The net effect on Arctic warming is slightly positive (+0.05 K from one model). However, this does not include a larger contribution to warming from tropospheric O_3 produced by CH_4 oxidation.
- Non-CH_4 SLCF emissions from the domestic sector in East+South Asia have the greatest warming effect in the Arctic of all sector/region combinations studied here. The Energy+Industry+Waste sector from Asia has the greatest cooling effect. Emissions from Russia, Asia and the Rest-of-World (ROW) contribute roughly equally to warming in the Arctic (see Fig. 11.14).
- A recent study suggests that emissions of SLCFs by flaring of gas associated with oil production are potentially very large in and near the Arctic, but the uncertainties for this source are high, as neither flaring volumes nor emission factors are well known. This assessment confirms the findings of the previous study that the flaring emissions have a large impact on Arctic BC concentrations.
- Per unit emission, Arctic surface temperature is most sensitive to Russian flaring emissions. A large part of this temperature increase is due to BC in snow. In general, Russian and Nordic emissions have the highest temperature response per unit emitted mass (see Fig. 11.16).
- The contributions of Arctic Council countries to Arctic warming by BC is 32% of the total BC warming and occurs primarily via within-Arctic forcing, whereas the contributions from other countries occur mainly through forcing outside the Arctic. Warming from forcing exerted outside the Arctic is associated with increased heat transport to the Arctic (see Fig. 11.15).
- Temperature changes from even substantial SLCF (including CH_4) emission changes are difficult to detect with statistical significance in transient climate model simulations, unless a large number of ensemble members and long periods are simulated. Two climate models simulating transient climate change associated with deep SLCF mitigation measures (including reductions in emissions of BC, OC, and CH_4 but

not SO_2 – see Fig. 11.19) showed reduced Arctic warming of 0.3 and 0.5 K, respectively, by 2050. Aerosol-induced cloud changes counteracted the benefits of reduced direct forcing. In the BASELINE scenario (i.e. current emissions legislation) of one model, 2.2 million km^2 of Arctic sea ice area was lost by 2050, whereas in the MITIGATION scenario (i.e. aggressive changes in emissions of aerosols, CH_4, and O_3 precursors beginning in year 2016) the loss was reduced by 7%.

- The vertical distribution of SLCFs, not only their total tropospheric burden, is very important for climate response. For instance, BC at higher altitudes in the Arctic may result in cooling at the surface whereas BC in the Arctic atmospheric boundary layer and deposited to snow and sea ice is likely to cause strong mass-normalized surface warming. Therefore, Arctic forcing is not a good metric for Arctic temperature response. Using equilibrium temperature response to emission perturbations through the use of regional temperature potentials is a much more accurate way of quantifying SLCF climate impact.
- Model processes that control the vertical distribution of BC/O_3 and aerosol-cloud indirect and semi-direct effects are the greatest sources of uncertainty in simulations of the impacts of mitigation measures on the Arctic climate.

12.1.2 Transport to the Arctic

- High-latitude anthropogenic emissions from Eurasia dominate the near-surface pollutant concentrations (such as those for SO_4 and BC) in the Arctic, whereas anthropogenic emissions from East+South Asia contribute substantially to pollution in the Arctic upper troposphere.
- Surface measurements of O_3 show clear effects of air mass transport from emission source regions. Episodes with enhanced O_3 in summer due to photochemical formation and depleted O_3 in winter due to titration (i.e. O_3 removal by emissions of nitric oxide, NO) are observed. There is also strong evidence of reduced O_3 concentrations after transport across the Arctic Ocean in spring, a result of halogen-induced O_3 depletion events.
- Biomass burning plumes lead to strong enhancements of aerosol concentrations in the Arctic with a significant impact on the mean concentrations in summer. Boreal fires also impact trace gas distributions and O_3 formation.

12.1.3 Modeling methods

- Black carbon transport models have improved considerably since the previous AMAP assessment on the impact of BC on Arctic climate, due to the inclusion of more sophisticated treatments of BC ageing and scavenging processes. In contrast to the previous assessment, some models used here now quantify aerosol-cloud indirect effects.
- Including seasonally varying emissions and emissions from gas flaring have substantially improved the simulation of BC in the Arctic.

12.1.4 Model-measurement comparisons

- The present study has involved a more thorough evaluation of model performance in the Arctic compared to the previous AMAP assessment.
- Even though model performance has improved substantially, monthly median concentrations of BC and SO_4 at the surface from different models still differ by up to about one order of magnitude and even more in some cases. Models still tend to underestimate the seasonal cycle of BC and SO_4 in the Arctic, mostly due to low simulated concentrations in late winter/early spring compared to observations. In addition, most models are unable to accurately simulate observed vertical profiles of BC. For an aircraft campaign in spring 2008, model underestimates of BC extended throughout the depth of the troposphere. In contrast, models overestimated low BC concentrations measured during a 2009 spring campaign both near the surface and higher in the troposphere. These conflicting results may be due to the emission inventory that was used and particularly the emissions due to biomass burning, emission injection height, and/or the parameterization of loss processes.
- Simulated concentrations of BC in land-based Arctic snow are biased low, on average, by factors of 1.7 and 3.4 in two models, with the most severe underestimations occurring in Russia.
- All models underestimate CO at Arctic surface stations in winter and spring, and throughout the depth of the Arctic troposphere in spring and summer. However, there is some indication that models run at higher spatial resolution perform better.
- Most models overestimate the amount of O_3 transported from the stratosphere into the Arctic troposphere, especially in spring. This may alter simulated photochemical O_3 enhancements resulting from import of O_3 precursors, with possible implications for modeled O_3 responses to different emission sources.
- Speciation of reactive nitrogen (NO_Y) shows large diversity between models, and there are substantial differences in the efficiencies of peroxyacetyl nitrate (PAN) export from source regions into the Arctic. Aircraft data comparisons show models with overestimated PAN have low NO_X in the Arctic which may be limiting photochemical O_3 production from anthropogenic and fire emissions in models.

12.1.5 Arctic radiative forcing and climate response

- Emissions from East+South Asia and Russia are the largest contributors to BC burdens in the Arctic in all the models, with mean contributions of 43% and 21%, respectively.
- The impact of emissions on direct radiative forcing (RF) is well correlated with changes in BC burdens, indicating that radiative effects are strongly related to concentrations of BC in the atmosphere. The direct RF of atmospheric BC in the Arctic is 640 mW/m^2 averaged over all models. The RF of BC in snow is 180 m/m^2.

- Equilibrium temperature response to emission perturbations is, in this study, estimated through the use of regional temperature potentials (RTPs). Temperature changes due to four species and 44 emission source regions and sectors were calculated for this study using four different models. This has resulted in emissions-normalized temperature changes that can be used to design mitigation scenarios.

12.2 Recommendations

12.2.1 SLCF observations

- Long-term monitoring of atmospheric composition at existing stations needs to be continued and integrated into a Pan-Arctic observation network building, for example, on IASOA (International Arctic Systems for Observing the Atmosphere) and WMO GAW (World Meteorological Organization - Global Atmosphere Watch). This should include information on the SLCF vertical distribution (e.g. using tethered balloons, additional ozonesondes, unmanned aerial vehicles, and aircraft). There is a particular lack of SLCF measurements in the eastern part of the Arctic. Satellite retrievals of SLCFs for Arctic regions should also be improved.
- An open access policy and common archiving/formatting, including relevant metadata, for Arctic measurement data are needed.
- Intercomparisons of different methods to measure BC and OC in the atmosphere and snow are urgently needed. Currently, measurements made with different instrument types do not measure exactly the same quantity, they have systematic biases, and it is not straightforward to use the data for identifying model biases.
- The choice of a BC monitoring method in the Arctic should be made carefully and should take into account efforts to establish harmonized BC measurements within the European Union, ongoing discussions within the International Marine Organization, and methods that are already in use for long-term Arctic monitoring.
- When reporting BC data and metadata, the value actually reported should be specified (such as elemental carbon, EC; equivalent black carbon, eBC; or refractory black carbon, rBC) and the measurement method stated. Deviations of the method used from other BC measurement methods should be provided if available.
- There are only a few sites where O_3 and its precursors, primarily CO, are continuously monitored in the Arctic. The network can be expanded especially in the eastern Arctic and Arctic Ocean. Measurements of NO_X, VOCs, PAN and halogenated species are also needed to allow better source characterization. Few vertical profiles measured during airborne campaigns are available. Further measurements of NO_Y species as well as VOCs including oxygenated VOCs (OVOCs) and halogens are needed in the Arctic free troposphere and lower stratosphere.

12.2.2 Model development, evaluation and application

- Model features that govern the vertical distribution and lifetimes of SLCFs in the Arctic atmosphere should be identified and improved.
- A multi-model exercise to calculate RTPs for different SLCFs is needed.
- Future efforts should ensure consistency between RTPs and forcing definitions, especially for those associated with cloud indirect effects.
- Diagnosing small forcing contributions is a substantial challenge. Techniques for quantifying radiative forcing associated with small emission perturbations should therefore be explored.
- Precipitation responses to SLCF mitigation have not been quantified in this assessment but should be considered in future studies because aerosols especially are expected to influence precipitation in the Arctic and elsewhere.

12.2.3 SLCF emission inventories in an Arctic context

- A comparison of several global emission inventories has shown that relative uncertainties in the total emissions per latitude band increase with latitude and are largest in the Arctic. The global inventories thus need improvement, especially at high latitudes. This could be achieved by including information from regional and Arctic Council national inventories.
- Further analysis of observed and modeled historical trends of SLCFs should be made.
- Future work should develop emission scenarios that describe a strong increase in anthropogenic activities within the Arctic and quantify the projected impacts these activities would have on the Arctic climate and environment.

Annex: Modeling the climate response – A summary

Authors: Terje K. Berntsen, Michael Gauss

A1 Introduction

This Annex is a common contribution to the AMAP assessments on methane (AMAP 2015) and black carbon and ozone (the present report) and has been produced to facilitate an integrated understanding of the separate climate modeling exercises undertaken by the two AMAP expert groups on short-lived climate forcers (SLCFs).

The objective for modeling studies in the two expert groups has been to quantify the potential reduction in global and Arctic warming by mitigation of methane (CH_4), black carbon (BC) or non-methane ozone precursors (nmOP). The nmOP include nitrogen oxides (NO_X), carbon monoxide (CO) and non-methane volatile organic carbons (nmVOC).

To address this objective, the two expert groups chose different modeling strategies due to the different nature of methane versus BC/nmOP. Although these species are commonly referred to as short-lived climate forcers it is important to distinguish two different interpretations of the term 'short-lived'.

1. *Short-lived* in the sense that the residence time is shorter than the typical mixing time in the atmosphere on a hemispheric scale (i.e. shorter than about one month). Only BC/nmOP is short-lived in this context. With this short lifetime, the location and seasonal cycle of emissions can have direct effect on the climate response in the Arctic, so that sources and regions must be treated individually. These compounds are denoted here as very-SLCFs (VSLCF).
2. *Short-lived* in the sense that the residence time is shorter than for typical long-lived greenhouse gases (such as carbon dioxide, CO_2; nitrous oxide, N_2O; or sulfur hexafluoride, SF_6) and that the compound is amenable to mitigation for which a climate response would be evident in the near term (decades). Both methane and BC/nmOP are short-lived in this context.

A2 Modeling approach

Coupled chemistry-climate models (CCMs) are now available, so the ideal approach for estimating the effect of reductions in both methane and BC/OP emissions would be through fully coupled transient CCM simulations. However, for BC/nmOP emissions (including co-emitted species like organic carbon, OC, and sulfur dioxide, SO_2) this is not feasible due to the very small forcing signals from individual regions/sources, which would require extremely long simulations (or a very high number of ensembles) to obtain a statistically robust result for the climate response. In the case of methane, due its relatively long lifetime (about nine years) and thus its relatively small spatial variability in the atmosphere, it is common in climate models to prescribe concentrations rather than emissions. For the AMAP methane assessment, methane concentrations were calculated with a box model and a chemical transport model (CTM), and then used in Earth System Models (ESMs) to calculate the climate response.

A2.1 VSLCFs

In the black carbon and ozone assessment the main outcome of the modeling simulations is a quantification of the contribution to Arctic equilibrium warming by *current* emissions from *seven regions, six emission sectors,* and by the *components BC, OC, SO_2, and nmOP.* From each experiment and model the zonally average radiative forcings in broad latitude bands were diagnosed. To obtain an estimate of the Arctic surface air temperature response, the AMAP Black Carbon and Ozone Expert Group used regional temperature potentials (RTPs) pre-calculated by the Goddard Institute for Space Studies Earth System Model (GISS ESM, Shindell and Faluvegi 2010). RTPs relate equilibrium regional temperature response to radiative forcing in different latitude bands and thus offer an efficient way to obtain regional temperature change for a multitude of scenarios.

In parallel to the modeling efforts of the AMAP expert groups, the EU-project ECLIPSE has undertaken similar modeling efforts. ECLIPSE developed and used a global mitigation scenario with focus on optimal BC/nmOP reductions, including all regions and sectors. For this global scenario, transient CCM simulations were performed, and some results are reported in Ch. 11 (Sect. 11.5).

A2.2 SLCFs

For methane the reductions in emissions from all regions and sectors were considered together since the location and annual cycle of the emissions are of minor importance. In addition, since the radiative forcing due to reduction in methane emissions is greater than that for other SLCFs, fewer experiments were needed. Transient simulations performed with three different ESMs (see AMAP 2015: Sect. 8.3) were used to calculate the climate response to reductions in anthropogenic methane emissions, averaged over the 2036–2050 period, with respect to the 2006–2010 period. Methane emissions from the ECLIPSE 2012 data set were used (see AMAP 2015: Fig. 5.9 and Table 8.1), as this was the most recent version at the time.

A3 Summary of main results

Table A1 provides a summary of the potential for reduced warming in the Arctic (and globally) around year 2050 if emissions of SLCFs are reduced according to the mitigation scenario established within the ECLIPSE project. The numbers given are from the AMAP Expert Groups, and from the ECLIPSE project (see Sect. A4.2).

Table A1 Summary of ESM and RTP-based modeling estimates of the potential reduction in Arctic (and global) warming around 2050[a], by mitigation of SLCFs.

	Predicted total warming[b]	Reduction potential by mitigation of SLCF emissions			
Arctic	About 2°C	Net of all SLCFs			
		°C	Model		
		0.40	RTP-based		
		0.29	ECLIPSE, CESM-CAM5		
		0.42	ECLIPSE, NorESM		
		0.54	ECLIPSE, CESM-CAM4		
		0.49	ECLIPSE, HadGCM		
		Non-methane only		Methane only	
		°C	Model	°C	Model
		0.23	RTP-based	0.40±0.14	CanESM2, RCP6.0
		0.14	ECLIPSE, ECHAM[c]	0.35±0.17	CanESM2, RCP8.5
				0.26±0.26	CESM1, RCP6.0
				0.33±0.25	CESM1, RCP8.5
				0.33±0.14	NorESM, RCP6.0
				0.17	RTP-based
Global	About 0.7–1.5°C[d]	Net of all SLCFs		Methane only	
		°C	Model	°C	Model
		-0.05	ECLIPSE, CESM-CAM5	0.27±0.07	CanESM2, RCP6.0
		0.20	ECLIPSE, NorESM	0.26±0.04	CanESM2, RCP8.5
		0.22	ECLIPSE, CESM-CAM4	0.10±0.05	CESM1, RCP6.0
		0.29	ECLIPSE, HadGCM	0.15±0.06	CESM1, RCP8.5
				0.22±0.04	NorESM, RCP6.0

[a]The model results and RTP-based values in this table are given as multi-year averages, representative for the 2040s; [b]with respect to present day; [c]results from ECHAM (an ESM used in the present assessment) are for BC, OC and SO_4 only; ECHAM does not include the impact of BC on snow; [d]Collins et al. (2013b, their figure 12.5).

A4 Results from the Expert Group on Black Carbon and Ozone

To identify the mitigation potential for BC/nmOP, for combinations of regions and sectors, the individual contributions by current emissions to equilibrium Arctic warming were calculated first (see Fig. 11.14). In absolute terms, emissions from domestic combustion (e.g. heating, cooking, waste burning – with BC as the main component) make the largest contribution. The impact of nmOP is relatively small.

While the results shown in Fig. 11.14 provide a tool to identify the potential for impact on Arctic temperature from mitigation by region and sector, the results in Fig. 11.16 provide a basis for estimating the Arctic temperature response for any given combination of compounds, regions and sectors. The numbers in Fig. 11.16 also provide the basis for estimating cost-efficacy if the cost for each source is known.

A4.1 Ozone

Ozone is a secondary gas formed through oxidation of methane, nmVOC, CO and NO_X in the presence of sunlight. For the present assessment, model simulations were performed where the emissions of the three ozone precursors NO_X, CO and nmVOC were removed *simultaneously.* Methane concentrations were kept constant at the 2010 level in all simulations. With this model set-up it was possible to estimate the effect on Arctic temperture from these ozone procursors combined, but not their individual contributions. The CTMs were used to calculate concentration changes and radiative forcings. Emissions of NO_X, CO and nmVOCs do not only change ozone, but also the oxidizing capacity of the atmosphere and thus impact methane concentrations. RTPs were applied to estimate the impact on Arctic temperature as shown in Fig. 11.18, giving a net Arctic warming of about 0.05°C. Note that the net impact of the ozone precursors (NO_X, CO and nmVOCs) is much lower than the impact of aerosols (BC, OC, and SO_4) (Fig. 11.16).

Increased methane emissions also lead to increased ozone formation. Neither of the AMAP expert groups performed model simulations to quantify the Arctic warming that is due only to changes in ozone concentration associated with increases in anthropogenic methane emissions. To derive an estimate of this effect, simulations of ozone changes due to current anthropogenic emissions of all ozone precursors (NO_X, CO, nmVOC and methane) were used in the ACCMIP experiment (Lamarque

et al. 2013). Calculating the radiative forcing and using the RTP approach, resulted in an estimated total Arctic warming by these emissions of 0.12°C. Assuming that the difference can be assigned to ozone produced from methane, it may be concluded that ozone produced by current methane oxidation gives an equilibrium Arctic warming of about 0.07°C . This crude estimate neglects non-linear chemical effects and has substantial uncertainty through the RTP coefficients for ozone which have only been calculated by one model (GISS) so far.

A4.2 Results from the ECLIPSE transient simulations

Within the ECLIPSE project a future emission mitigation scenario of SLCFs has been established, taking into account that mitigation of compounds (e.g. BC) that lead to warming will, to a certain extent, also reduce emissions of cooling compounds (co-emitted species). The scenario assumes that for all sources the emission reductions are phased in linearly over 15 years (2015–2030), and kept constant after that. The scenario includes mitigation of all SLCFs, including methane, OC and SO_2. It should be noted that the total emission reductions in this scenario are quite high. By 2050, according to version 5 of the ECLIPSE data set (in the AMAP methane assessment – AMAP 2015 – referred to as 'ECLIPSE 2014'), the maximum technically feasible reductions with respect to the CLE (Current LEgislation) scenario are 76% or 4.7 Tg/y (BC), 54% or 285 Tg/y (CH_4), 48% or 270 Tg/y (CO) and 63% or 79 Tg/y for VOC. For OC the reduction is 71% (9.8 Tg/y), while for SO_2 it is only 1%.

Transient model simulations for the period 2015–2050 have been performed with four ESMs. The response to the SLCF mitigation scenario mentioned above can also be estimated with an RTP-based approach using the climate sensitivities given in Fig. 11.16 (and from the literature for NO_X, CO, nmVOC and methane). Table A2 summarizes the net global and Arctic responses (averaged over the period 2041–2050) for the ESMs and for the RTP-based method.

Table A2 Effects of maximum technically feasible reduction in all SLCF emissions on ensemble-mean climate states, averaged over 2041–2050, following the ECLIPSE version 5 scenario. Changes significant at p=0.05 are shown in bold.

	Model	Reduction in surface air temperature, °C	Increase in sea-ice area, km^2
Global	CESM-CAM5	-0.05	8.8×10^4
	NorESM	**0.20**	**4.4×10^5**
	CESM-CAM4	**0.22**	**5.0×10^5**
	HadGEM	**0.29**	**9.5×10^5**
Arctic (60–90°N)	CESM-CAM5	**0.29**	**1.6×10^5**
	NorESM	**0.42**	**2.3×10^5**
	CESM-CAM4	**0.54**	2.8×10^5
	HadGEM	**0.49**	**2.9×10^5**
	RTP-based	0.40	

The MITIGATE scenario assumes the full implementation of a portfolio of SLCF measures by 2030 and 2050 designed to achieve large reductions in temperature response in the short term at the global scale. The BASELINE scenario includes all presently agreed legislation and adopted policies affecting air pollutant emissions (see Ch. 5).

The forcing and responses given in Table A2 are for the combined effect of mitigation of all SLFCs. Without additional costly simulations it is not possible to attribute the impacts to individual components. However, this can be done using the more simple RTP-based approach (Shindell and Faluvegi 2010) described in Section A2.1. Using the Arctic RTPs for the aerosols (BC, OC, and SO_4) from Fig. 11.16, and RTPs for the ozone precursors (including methane) from Collins et al. (2013b) it was possible to calculate the transient response to the mitigation scenario. For the 2040–2050 period, methane mitigation accounts for 42% of the signal in the reduced Arctic surface warming. Figure 11.21 shows the contributions from the different components as a function of time using the RTP-based method.

A5 Results from the Expert Group on Methane

The Expert Group on Methane used emissions from the ECLIPSE 2012 data set (see AMAP 2015: Fig. 5.9 and Table 8.1) to calculate the effect of methane emissions mitigation on surface air temperature. It was possible to calculate the effect of methane in isolation from other SLCFs because the methane mitigation measures considered in the ECLIPSE scenario do not affect the emissions of other species to a significant degree. The methane emissions mitigation potential by year 2050 in this version amounts to 205 Tg CH_4/y, compared to year 2005. This is lower than in the more recent ECLIPSE 2014 data set (285 Tg CH_4/y, AMAP 2015: Fig. 5.9), which was used in the present assessment. The reason why ECLIPSE 2012 was used for the methane assessment is because this was the most recent data set at the time the model calculations began.

Three different ESMs (CanESM2, CESM1, NorESM) were used to calculate the climate response to maximum technically feasible reductions (MFR) in anthropogenic methane emissions. The climate response was calculated over the period 2036–2050 as the difference between simulations that used methane concentrations corresponding to the MFR scenario and simulations that used concentrations corresponding to the CLE scenario. In the CLE scenario, the anthropogenic methane emissions continue to increase as the current state of technology prevails and any further emission reductions are limited to those prescribed by currently adopted legislation.

Since the ECLIPSE 2012 data did not contain all climate gases that are needed to run the ESMs, some components (notably CO_2) were taken from the RCP (representative concentration pathways) scenarios used by the Intergovernmental Panel on Climate Change in its Fifth Assessment (IPCC AR5). This approach of blending ECLIPSE and RCP data is explained in Ch. 8 (Box 8.3) of the methane assessment (AMAP 2015). It is important to note that methane emissions used in the present calculation were derived solely from the MFR and CLE scenarios of the ECLIPSE data set. Methane data from the RCP scenarios were not used.

The methane concentrations corresponding to the two emissions scenarios (MFR and CLE) were obtained using two approaches:

Table A3 Summary of results for the *reduction* in global warming for the 2036–2050 period, due to maximum technically feasible reduction in anthropogenic methane emissions, diagnosed as the difference in surface air temperature between the MFR and CLE scenarios, averaged either globally or over the Arctic region. (This table corresponds to Table 8.3 in the methane assessment – AMAP 2015 – but with the RTP-based result added for comparison.)

Model	Background scenario	Reduction in temperature simulated by the model (ΔT), °C		Reduction in temperature after taking into account the associated changes in ozone and stratospheric water vapor ($\Delta T_{O3,H2O}$), °C
		Global	Arctic	Global
CanESM2	RCP6.0	0.18±0.05	0.40±0.14	0.27±0.07
	RCP8.5	0.18±0.03	0.35±0.17	0.26±0.04
CESM1	RCP6.0	0.07±0.04	0.26±0.26	0.10±0.05
	RCP8.5	0.11±0.05	0.33±0.25	0.15±0.06
NorESM	RCP6.0	0.20±0.03	0.33±0.14	0.22±0.04
Mean		-	-	0.20±0.02[a]
RTP-based			0.17	

'Background scenario' refers to the scenario according to which non-methane climate forcers (e.g. CO_2) were specified. ΔT is the result from the ESM simulations, while $\Delta T_{O3,H2O}$ takes into account the effects of changes in ozone and stratospheric water vapor due to changes in methane emissions. The ratio between $\Delta T_{O3,H2O}$ and ΔT depends on the ESM and is calculated based on numbers of radiative forcing given by IPCC AR5 (Myhre et al. 2013a), as described in Box 8.4 in the methane assessment – AMAP 2015).

[a]The error bar of ±0.02°C is the statistical uncertainty of the mean over the five model simulations. It is not representative of the level of scientific understanding, as it does not take into account any systematic errors in the models (model biases, missing processes, etc.) or uncertainties in the emission estimates.

1. A one-box model of atmospheric methane calculated annually-averaged global-mean concentrations of methane and these were used by CanESM2 and CESM1.
2. A chemical transport model calculated monthly-averaged 3-D fields of methane and ozone concentration and these were used by NorESM.

Table A3 summarizes the temperature reduction due to maximum technically feasible reduction in anthropogenic emissions of methane, averaged over the Arctic region and globally, based on 26 simulations. Averaging over the results of all models generates a reduction in global-mean temperature of 0.20°C. The models calculate Arctic temperature reductions of between 0.26 and 0.40°C, which compares well with the ECLIPSE results. Given the different capabilities of the ESMs, the effects of ozone and stratospheric water vapor due to changes in methane emissions are not included in all models. However, the effects of ozone and stratospheric water vapor are accounted for through scaling methods, although only for the *global mean* values. The distribution of *regional* climate response is more complex to calculate and depends on the climate forcer (e.g. Shindell 2007). As methane-induced changes in ozone and stratospheric water vapor are not evenly distributed (see AMAP 2015: Sect. 8.3.2.2), the Arctic climate response (north of 60°N) should not be multiplied by scaling factors derived on the basis of global-mean radiative forcing values.

As seen in Table A3, the spread of calculated reductions for the Arctic is considerable and reflects the uncertainty in modeling climate response over small regions, especially in the Arctic given its inherent climatic variability. This uncertainty should also be kept in mind when estimating temperature change based on RTPs used above, which are derived from one model only (GISS ESM).

References

Abel, S.J., J.M. Haywood, E.J. Highwood, J. Li and P.R. Buseck, 2003. Evolution of biomass burning aerosol properties from an agricultural fire in southern Africa. Geophysical Research Letters, 30:1783, doi:10.1029/2003GL017342.

ACAP, 2014. Reduction of Black Carbon Emissions from Residential Wood Combustion in the Arctic: Black Carbon Inventory, Abatement Instruments and Measures. Arctic Contaminants Action Programme (ACAP).

ACIA, 2005. Arctic Climate Impact Assessment. Cambridge University Press.

Adam de Villers, R., G. Ancellet, J. Pelon, B. Quennehen, A. Schwarzenboeck, J.F. Gayet and K. Law, 2010. Airborne measurements of aerosol optical properties related to early spring transport of mid-latitude sources into the Arctic. Atmospheric Chemistry and Physics, 10:5011-5030.

Allen, R.J. and W. Landuyt, 2014. The vertical distribution of black carbon in CMIP5 models: Comparison to observations and the importance of convective transport. Journal of Geophysical Research: Atmospheres, 119:4808-4835.

Alvarado, M.J., J.A. Logan, J. Mao, E. Apel, D. Riemer, D. Blake, R.C. Cohen, K.E. Min, A.E. Perring, E.C. Browne, P.J. Wooldridge, G.S. Diskin, G.W. Sachse, H. Fuelberg, W.R. Sessions, D.L. Harrigan, G. Huey, J. Liao, A. Case-Hanks, J.L. Jimenez, M.J. Cubison, S.A. Vay, A.J. Weinheimer, D.J. Knapp, D.D. Montzka, F.M. Flocke, I.B. Pollack, P.O. Wennberg, A. Kurten, J. Crounse, J.M. St Clair, A. Wisthaler, T. Mikoviny, R.M. Yantosca, C.C. Carouge and P. Le Sager, 2010. Nitrogen oxides and PAN in plumes from boreal fires during ARCTAS-B and their impact on ozone: an integrated analysis of aircraft and satellite observations. Atmospheric Chemistry and Physics, 10:9739-9760.

Amann, M., I. Bertok, J. Borken-Kleefeld, J. Cofala, C. Heyes, L. Hoeglund-Isaksson, Z. Klimont, B. Nguyen, M. Posch, P. Rafaj, R. Sandler, W. Schoepp, F. Wagner and W. Winiwarter, 2011. Cost-effective control of air quality and greenhouse gases in Europe: modeling and policy applications. Environmental Modelling and Software, 26:1489-1501.

Amann, M., Z. Klimont and F. Wagner, 2013. Regional and global emissions of air pollutants: Recent trends and future scenarios. Annual Review of Environment and Resources, 38:31-55.

AMAP, 1998. AMAP Assessment Report: Arctic Pollution Issues. Arctic Monitoring and Assessment Programme (AMAP), Oslo, Norway.

AMAP, 2007. Arctic Oil and Gas 2007. Arctic Monitoring and Assessment Programme (AMAP), Oslo, Norway.

AMAP, 2011. The Impact of Black Carbon on Arctic Climate. 2011. By P.K. Quinn, A. Stohl, A. Arneth, T. Berntsen, J.F. Burkhart, J.H. Christensen, M.G. Flanner, K. Kupiainen, H. Lihavainen, M. Shepherd, V.P. Shevchenko, H. Skov and V. Vestreng. AMAP Technical Report No. 4. Arctic Monitoring and Assessment Programme (AMAP), Oslo.

AMAP, 2012. Arctic Climate Issues 2011: Changes in Arctic Snow, Water, Ice and Permafrost. Arctic Monitoring and Assessment Programme (AMAP), Oslo, Norway.

AMAP, 2015. AMAP Assessment 2015: Methane as an Arctic Climate Forcer. Arctic Monitoring and Assessment Programme (AMAP), Oslo.

Andersson, C., J. Langner and R. Bergström, 2007. Interannual variation and trends in air pollution over Europe due to climate variability during 1958–2001 simulated with a regional CTM coupled to the ERA40 reanalysis. Tellus B, 59:77-98.

Arctic Council, 2009. Arctic Marine Shipping Assessment 2009 Report. Arctic Council.

Arctic Council, 2011. An Assessment of Emissions and Mitigation Options for Black Carbon for the Arctic Council: Technical Report on Short-Lived Climate Forcers. Arctic Council.

Arnold, S.R., L.K. Emmons, S.A. Monks, K.S. Law, D.A. Ridley, S. Turquety, S. Tilmes, J.L. Thomas, I. Bouarar, J. Flemming, V. Huijnen, J. Mao, B.N. Duncan, S. Steenrod, Y. Yoshida, J. Langner and Y. Long, 2015. Biomass burning influence on high latitude tropospheric ozone and reactive nitrogen in summer 2008: a multi-model analysis based on POLMIP simulations. Atmospheric Chemistry and Physics, 15:6047-6068.

Arnott, W.P., H. Moosmuller and C.F. Rogers, 1997. Photoacoustic spectrometer for measuring light absorption by aerosol: Instrument description. Atmospheric Environment, 33:2845-2852.

Bahreini, R., E.J. Dunlea, B.M. Matthew, C. Simons, K.S. Docherty, P.F. DeCarlo, J. Jimenez, C.A. Brock, and A. Middlebrook, 2008. Design and operation of a pressure-controlled inlet for airborne sampling with an aerodynamic aerosol lens. Aerosol Science and Technology, 42:465-471.

Baklanov, A., A. Mahura, L. Nazarenko, N. Tausnev, A. Kuchin and O. Rigina, 2012. Modelling of Atmospheric Pollution and Climate Change in Northern Latitudes. Russian Academy of Sciences.

Ban-Weiss, G.A., L. Cao, G. Bala and K. Caldeira, 2011. Dependence of climate forcing and response on the altitude of black carbon aerosols. Climate Dynamics, 38:897-911.

Barrie, L.A., 1986. Arctic air pollution – An overview of current knowledge. Atmospheric Environment, 20:643-663.

Barrie, L.A., J.W. Bottenheim, R.C. Schnell, P.J. Crutzen and R.A. Rasmussen, 1988. Ozone destruction and photochemical reactions at polar sunrise in the lower Arctic atmosphere. Nature, 334:138-141.

Bauer, S.E. and S. Menon, 2012. Aerosol direct, indirect, semidirect, and surface albedo effects from sector contributions based on the IPCC AR5 emissions for preindustrial and present-day conditions. Journal of Geophysical Research: Atmospheres, 117:D01206, doi:10.1029/2011JD016816.

Bentsen, M., I. Bethke, J.B. Debernard, T. Iversen, A. Kirkevåg, Ø. Seland, H. Drange, C. Roelandt, I.A. Seierstad, C. Hoose and J.E. Kristjánsson, 2013. The Norwegian Earth System Model, NorESM1-M – Part 1: Description and basic evaluation of the physical climate. Geoscientific Model Development, 6:687-720.

Bergstrom, R.W., 1973. Extinction and absorption coefficients of the atmospheric aerosol as a function of particle size. Beitrage zur Physik der Atmosphare, 46:223-234.

Berntsen, T., I. Isaksen, G. Myhre, J.S. Fuglestvedt, F. Stordal, T.A. Larsen, R.S. Freckleton and K.P. Shine, 1997. Effects of anthropogenic emissions on tropospheric ozone and its radiative forcing. Journal of Geophysical Research: Atmospheres, 102:28101-28126.

Berntsen, T., J.S. Fuglestvedt, M.M. Joshi, K.P. Shine, N. Stuber, M. Ponater, R. Sausen, D.A. Hauglustaine, and L. Li, 2005. Response of climate to regional emissions of ozone precursors: sensitivities and warming potentials. Tellus B, 57:283-304.

Birch, M.E. and R.A. Cary, 1996. Elemental carbon-based method for monitoring occupational exposures to particulate diesel exhaust. Aerosol Science and Technology, 25:221-241.

Bodhaine, B.A., 1989. Barrow surface aerosol: 1976–1986. Atmospheric Environment, 23:2357-2369.

Bodhaine, B.A. and E.G. Dutton, 1993. A long-term decrease in Arctic Haze at Barrow, Alaska. Geophysical Research Letters, 20:947-950.

Bond, T.C. and R.W. Bergstrom, 2006. Light absorption by carbonaceous particles: An investigative review. Aerosol Science and Technology, 40:27-67.

Bond, T.C., T.L. Anderson and D. Campbell, 1999. Calibration and intercomparison of filter-based measurements of visible light absorption by aerosols. Aerosol Science and Technology, 30:582-600.

Bond, T.C., D.G. Streets, K.F. Yarber, S.M. Nelson, J.H. Woo and Z. Klimont, 2004. A technology-based global inventory of black and organic carbon emissions from combustion. Journal of Geophysical Research: Atmospheres, 109:1-43.

Bond, T.C., G. Habib and R.W. Bergstrom, 2006. Limitations in the enhancement of visible light absorption due to mixing state. Journal of Geophysical Research: Atmospheres, 111:D20211, doi:10.1029/2006JD007315.

Bond, T.C., E. Bhardwaj, R. Dong, R. Jogani, S. Jung, C. Roden, D.G. Streets and N.M. Trautmann, 2007. Historical emissions of black and organic carbon aerosol from energy-related combustion, 1850–2000. Global Biogeochemical Cycles, 21:GB2018, doi:10.1029/2006GB002840.

Bond, T.C., C. Zarzycki, M.G. Flanner and D.M. Koch, 2011. Quantifying immediate radiative forcing by black carbon and organic matter with the Specific Forcing Pulse. Atmospheric Chemistry and Physics, 11:1505-1525.

Bond, T.C., S.J. Doherty, D.W. Fahey, P.M. Forster, T. Berntsen, B.J. Deangelo, M.G. Flanner, S. Ghan, B. Kärcher, D. Koch, S. Kinne, Y. Kondo, P.K. Quinn, M.C. Sarofim, M.G. Schultz, M. Schulz, C. Venkataraman, H. Zhang, S. Zhang, N. Bellouin, S.K. Guttikunda, P.K. Hopke, M.Z. Jacobson, J.W. Kaiser, Z. Klimont, U. Lohmann, J.P. Schwarz, D. Shindell, T. Storelvmo, S.G. Warren and C.S. Zender, 2013. Bounding the role of

black carbon in the climate system: A scientific assessment. Journal of Geophysical Research: Atmospheres, 118:5380-5552.

Bottenheim, J.W., S. Netcheva, S. Morin and S.V. Nghiem, 2009. Ozone in the boundary layer air over the Arctic Ocean: measurements during the TARA transpolar drift 2006–2008. Atmospheric Chemistry and Physics, 9:4545-4557.

Boucher, O. and M.S. Reddy, 2008. Climate trade-off between black carbon and carbon dioxide emissions. Energy Policy, 36:193-200.

Bourgeois, Q. and I. Bey, 2011. Pollution transport efficiency toward the Arctic: Sensitivity to aerosol scavenging and source regions. Journal of Geophysical Research: Atmospheres, 116:D08213, doi:10.1029/2010JD015096.

Brandt, J., J.D. Silver, L.M. Frohn, C. Geels, A. Gross, A.B. Hansen, K.M. Hansen, G.B. Hedegaard, C.A. Skjøth, H. Villadsen, A. Zare and J.H. Christensen, 2012. An integrated model study for Europe and North America using the Danish Eulerian Hemispheric Model with focus on intercontinental transport. Atmospheric Environment, 53:156-176.

Breider, T.J., L.J. Mickley, D.J. Jacob, Q. Wang, J.A. Fisher, R.Y.W. Chang and B. Alexander, 2014. Annual distributions and sources of Arctic aerosol components, aerosol optical depth, and aerosol absorption. Journal of Geophysical Research: Atmospheres, 119:4107-4124.

Brock, C.A., J. Cozic, R. Bahreini, K.D. Froyd, A.M. Middlebrook, A. McComiskey, J. Brioude, O.R. Cooper, A. Stohl, K.C. Aikin, J.A. De Gouw, D.W. Fahey, R.A. Ferrare, R.-S. Gao, W. Gore, J. Holloway, G. Hübler, A. Jefferson, D.A. Lack, S. Lance, R.H. Moore, D.M. Murphy, A. Nenes, P.C. Novelli, J.B. Nowak, J.A. Ogren, J. Peischl, R.B. Pierce, P. Pilewskie, P.K. Quinn, T.B. Ryerson, K.S. Schmidt, J.P. Schwarz, H. Sodemann, J.R. Spackman, H. Stark, D.S. Thomson, T. Thornberry, P. Veres, L.A. Watts, C. Warneke and A.G. Wollny, 2011. Characteristics, sources, and transport of aerosols measured in spring 2008 during the aerosol, radiation, and cloud processes affecting Arctic climate (ARCPAC) project. Atmospheric Chemistry and Physics, 11:2423-2453.

Browse, J., K.S. Carslaw, S. Arnold, K.J. Pringle and O. Boucher, 2012. The scavenging processes controlling the seasonal cycle in Arctic sulphate and black carbon aerosol. Atmospheric Chemistry and Physics, 12:6775-6798.

Browse, J., K.S. Carslaw, A. Schmidt and J.J. Corbett, 2013. Impact of future Arctic shipping on high-latitude black carbon deposition. Geophysical Research Letters, 40:4459-4463.

Cappa, C.D., T.B. Onasch, P. Massoli, D.R. Worsnop, T.S. Bates, E.S. Cross, P. Davidovits, J. Hakala, K.L. Hayden and B.T. Jobson, 2012. Radiative absorption enhancements due to the mixing state of atmospheric black carbon. Science, 337:1078-1081.

Carbon Limits, 2013. Evaluering av faklingsstrategi, teknikker for reduksjon av fakling og faklingsutslipp, utslippsfaktorer og metoder for bestemmelse av utslipp til luft fra fakling. [Assessment of flare strategies, techniques for reduction of flaring and associated emissions, emission factors and methods for determination of emissions to air from flaring].

Carlson, T.N., 1981. Speculations on the movement of polluted air to the Arctic. Atmospheric Environment, 15:1473-1477.

Chow, J.C., J.G. Watson, L.C. Pritchett, W.R. Pierson, C.A. Frazier and R.G. Purcell, 1993. The dri thermal/optical reflectance carbon analysis system: Description, evaluation, and applications in U.S. air quality studies. Atmospheric Environment A, 27:1185-1201.

Chow, J.C., J.G. Watson, L.W. Chen, W.P. Arnott and H. Moosmüller, 2004. Equivalence of elemental carbon by thermal/optical reflectance and transmittance with different temperature protocols. Environmental Science and Technology, 38:4414-4422.

Christensen, J.H., 1997. The Danish Eulerian Hemispheric Model – a three-dimensional air pollution model used for the Arctic. Atmospheric Environment, 31:4169-4191.

Christiansen, B., N. Jepsen, R. Kiwi, G.H. Hansen, M. Larsen, and U. Korsholm, 2015. Time series analysis of Arctic tropospheric ozone as a short-lived climate forcer. Nordic Council of Ministers.

Clarke, A.D. and K.J. Noone, 1985. Soot in the Arctic snowpack: a cause for perturbations in radiative transfer. Atmospheric Environment, 19:2045-2053.

Clarke, A.D., Y. Shinozuka, V.N. Kapustin, S.G. Howell, B. Huebert, S.J. Doherty, T.L. Anderson, D.S. Covert, J. Anderson, X. Hua, K.G. Moore, C.S. McNaughton, G. Carmichael and R. Weber, 2004. Size distributions and mixtures of dust and black carbon aerosol in Asian outflow: Physiochemistry and optical properties. Journal of Geophysical Research: Atmospheres, 109:D15S09, doi:10.1029/2003JD004378.

Clarke, L., J. Edmonds, H. Jacoby, H. Pitcher, J. Reilly and R. Richels, 2007. Scenarios of Greenhouse Gas Emissions and Atmospheric Concentrations. Sub-report 2.1A of Synthesis and Assessment Product 2.1 by the U.S. Climate Change Science Program and the Energy, Office of Biological & Environmental Research, Washington DC.

Cofala, J., M. Amann, Z. Klimont, K. Kupiainen and L. Höglund-Isaksson, 2007. Scenarios of global anthropogenic emissions of air pollutants and methane until 2030. Atmospheric Environment, 41:8486-8499.

Collaud Coen, M., E. Weingartner, A. Apituley, D. Ceburnis, R. Fierz-Schmidhauser, H. Flentje, J.S. Henzing, S.G. Jennings, M. Moerman, A. Petzold, O. Schmid and U. Baltensperger, 2010. Minimizing light absorption measurement artifacts of the Aethalometer: evaluation of five correction algorithms. Atmospheric Measurement Techniques, 3:457-474.

Collins, W.J., M.M. Fry, H. Yu, J.S. Fuglestvedt, D. Shindell and J.J. West, 2013a. Global and regional temperature-change potentials for near-term climate forcers. Atmospheric Chemistry and Physics, 13:2471-2485.

Collins, M., R. Knutti, J. Arblaster, J.-L. Dufresne, T. Fichefet, P. Friedlingstein, X. Gao, W.J. Gutowski, T. Johns, G. Krinner, M. Shongwe, C. Tebaldi, A.J. Weaver and M. Wehner, 2013b. Long-term climate change: Projections, commitments and irreversibility. In: Stocker, T.F., D. Qin, G.-K. Plattner, M. Tignor, S.K. Allen, J. Boschung, A. Nauels, Y. Xia, V. Bex and P.M. Midgley (eds.), Climate Change 2013: The Physical Science Basis. Contribution of Working Group I to the Fifth Assessment Report of the Intergovernmental Panel on Climate Change, pp. 1029-1136. Cambridge University Press.

Conley, A., J.F. Lamarque, F. Vitt, W.J. Collins and J. Kiehl, 2013. PORT, a CESM tool for the diagnosis of radiative forcing. Geoscientific Model Development, 6:469-476.

Conway, H., A. Gades and C.F. Raymond, 1996. Albedo of dirty snow during conditions of melt. Water Resources Research, 32:1713-1718.

Cooper, O.R., D.D. Parrish, J. Ziemke, N.V. Balashov, M. Cupeiro, I.E. Galbally, S. Gilge, L. Horowitz, N.R. Jensen, J.-F. Lamarque, V. Naik, S.J. Oltmans, J. Schwab, D.T. Shindell, A.M. Thompson, V. Thouret, Y. Wang, R.M. Zbinden, 2014. Global distribution and trends of tropospheric ozone: An observation-based review. Elementa, 2: 000029 doi: 10.12952/journal.elementa.000029.

Corbett, J.J., D. Lack, J.J. Winebrake, S. Harder, J.A. Silberman and M. Gold, 2010. Arctic shipping emissions inventories and future scenarios. Atmospheric Chemistry and Physics, 10:9689-9704.

Crawford, I., O. Mohler, M. Schnaiter, H. Saathoff, D. Liu, G. McMeeking, C. Linke, M. Flynn, K.N. Bower, P.J. Connolly, M.W. Gallagher and H. Coe, 2011. Studies of propane flame soot acting as heterogeneous ice nuclei in conjunction with single particle soot photometer measurements. Atmospheric Chemistry and Physics, 11:9549-9561.

Cubison, M.J., A.M. Ortega, P.L. Hayes, D.K. Farmer, D.A. Day, M.J. Lechner, W. Brune, E. Apel, G.S. Diskin, J.A. Fisher, H.E. Fuelberg, A. Hecobian, D. Knapp, T. Mikoviny, D.D. Riemer, G. Sachse, W. Sessions, R. Weber, A. Weinheimer, A. Wisthaler and J. Jimenez, 2011. Effects of aging on organic aerosol from open biomass burning smoke in aircraft lab studies. Atmospheric Chemistry and Physics Discussions, 11:12103-12140.

Dahlkötter, F., M. Gysel, D. Sauer, A. Minikin, R. Baumann, P. Seifert, A. Ansmann, M. Fromm, C. Voigt and B. Weinzierl, 2014. The Pagami Creek smoke plume after long-range transport to the upper troposphere over Europe – aerosol properties and black carbon mixing state. Atmospheric Chemistry and Physics, 14:6111-6137.

Dalsøren, S.B., B.H. Samset, G. Myhre, J.J. Corbett, R. Minjares, D. Lack and J.S. Fuglestvedt, 2013. Environmental impacts of shipping in 2030 with a particular focus on the Arctic region. Atmospheric Chemistry and Physics, 13:1941-1955.

Daskalakis, N., S. Myriokefalitakis and M. Kanakidou, 2014. Sensitivity of tropospheric loads and lifetimes of short lived pollutants to fire emissions. Atmospheric Chemistry and Physics Discussions, 14:22639-22676.

DeMott, P.J., Y. Chen, S.M. Kreidenweis, D.C. Rogers and D.E. Sherman, 1999. Ice formation by black carbon particles. Geophysical Research Letters, 26:2429-2432.

Di Pierro, M., L. Jaegle, E.W. Eloranta and S. Sharma, 2013. Spatial and seasonal distribution of Arctic aerosols observed by the CALIOP satellite instrument (2006–2012). Atmospheric Chemistry and Physics, 13:707-7095.

Dibb, J., M. Arsenault, M.C. Peterson and R.E. Honrath, 2002. Fast nitrogen oxide photochemistry in Summit, Greenland snow. Atmospheric Environment, 36:2501-2511.

Dibb, J., R.W. Talbot, E.M. Scheuer, G. Seid, M.A. Avery and H.B. Singh, 2003. Aerosol chemical composition in Asian continental outflow during the TRACE-P campaign: Comparison with PEM-West B. Journal of Geophysical Research: Atmospheres, 108:doi:10.1029/2002JD003111.

DNV, 2013. HFO in the Arctic-Phase 2. DNV Doc. No. Report No. 2013-1542-16G8ZQC-5/1. Det Norske Veritas (DNV).

Doherty, S.J., S.G. Warren, T.C. Grenfell, A.D. Clarke and R.E. Brandt, 2010. Light-absorbing impurities in Arctic snow. Atmospheric Chemistry and Physics, 10:11647-11680.

Doherty, S.J., T.C. Grenfell, S. Forsström, D.L. Hegg, R.E. Brandt and S.G. Warren, 2013. Observed vertical redistribution of black carbon and other insoluble light-absorbing particles in melting snow. Journal of Geophysical Research: Atmospheres, 118:5553-5569.

Doherty, S.J., C.M. Bitz and M.G. Flanner, 2014a. Biases in modeled surface snow BC mixing ratios in prescribed aerosol climate model runs. Atmospheric Chemistry and Physics Discussions, 14:13167-13196.

Doherty, S.J., C.M. Bitz and M.G. Flanner, 2014b. Biases in modeled surface snow BC mixing ratios in prescribed aerosol climate model runs. Atmospheric Chemistry and Physics, 14:11697-11709.

Doherty, S.J., C. Dang, D.A. Hegg, R. Zhang, and S.G. Warren, 2014c. Black carbon and other light-absorbing particles in snow of central North America. Journal of Geophysical Research: Atmospheres, 119:12,807-12,831.

Dou, T., C. Xiao, D.T. Shindell, J. Liu, K. Eleftheriadis, J. Ming and D. Qin, 2012. The distribution of snow black carbon observed in the Arctic and compared to the GISS-PUCCINI model. Atmospheric Chemistry and Physics, 12:7995-8007.

Dumont, M., E. Brun, G. Picard, M. Michou, Q. Libois, J-R. Petit, M. Geyer, S. Morin and B. Josse, 2014. Contribution of light-absorbing impurities in snow to Greenland's darkening since 2009. Nature Geoscience, 7:509-512.

Duncan, B.N. and I. Bey, 2004. A modeling study of the export pathways of pollution from Europe: Seasonal and interannual variations (1987–1997). Journal of Geophysical Research: Atmospheres, 109: D08301, doi:10.1029/2003JD004079.

Dutton, E.G., J.J. Deluisi and G. Herbert, 1989. Shortwave aerosol optical depth of Arctic haze measured on board the NOAA WP-3D during AGASP-II, April 1986. Journal of Atmospheric Chemistry, 9:71-79.

Eckhardt, S., A. Stohl, H. Wernli, P. James, C. Forster and N. Spichtinger, 2004. A 15-year climatology of warm conveyor belts. Journal of Climate, 17:218-237.

Eckhardt, S., J. Hermansen, M. Grythe, M. Fiebig, K. Stebel, M. Cassiani, A. Baecklund and A. Stohl, 2013. The influence of cruise ship emissions on air pollution in Svalbard - a harbinger of a more polluted Arctic? Atmospheric Chemistry and Physics, 13:8401-8409.

Eleftheriadis, K.S., S. Vratolis and S. Nyeki, 2009. Aerosol black carbon in the European Arctic: Measurements at Zeppelin station, Ny-Ålesund, Svalbard from 1998–2007. Geophysical Research Letters, 36:L02809, doi:10.1029/2008GL035741.

Emmons, L.K., P. Hess, A. Klonecki, X. Tie, L. Horowitz, J.F. Lamarque, D. Kinnison, G.P. Brasseur, E. Atlas, E. Browerll, C. Cantrell, F.L. Eisele, R.L. Mauldin, J. Merrill, B. Ridley and R. Shetter, 2003. Budget of tropospheric ozone during TOPSE from two chemical transport models. Journal of Geophysical Research, 108:8372, doi:10.1029/2002JD002665.

Emmons, L.K., S. Walters, P.G. Hess, J.-F. Lamarque, G.G. Pfister, D. Fillmore, C. Granier, A. Guenther, D. Kinnison, T. Laepple, J. Orlando, X. Tie, G. Tyndall, C. Wiedinmyer, S.L. Baughcum and S. Kloster, 2010. Description and evaluation of the Model for Ozone and Related chemical Tracers, version 4 (MOZART-4). Geoscientific Model Development, 3:43-67.

Emmons, L.K., S.R. Arnold, S.A. Monks, V. Huijnen, S. Tilmes, K.S. Law, J.L. Thomas, J.-C. Raut, I. Bouarar, S. Turquety, Y. Long, B. Duncan, S. Steenrod, S. Strode, J. Flemming, J. Mao, J. Langner, A.M. Thompson, D. Tarasick, E.C. Apel, D.R. Blake, R.C. Cohen, J. Dibb, G.S. Diskin, A. Fried, S.R. Hall, L.G. Huey, A.J. Weinheimer, A. Wisthaler, T. Mikoviny, J. Nowak, J. Peischl, J.M. Roberts, T. Ryerson, C. Warneke and D. Helmig, 2015. The POLARCAT Model Intercomparison Project (POLMIP): overview and evaluation with observations. Atmospheric Chemistry and Physics, 15:6721-6744.

Environment Canada, 2013. Canada's Emissions Trends. Environment Canada, En81-18/2013E.

Eyring, V., I.S.A. Isaksen, T. Berntsen, W.J. Collins, J.J. Corbett, O. Endresen, R.G. Grainger, J. Moldanova, H. Schlager and D.S. Stevenson, 2010. Transport impacts on atmosphere and climate: Shipping. Atmospheric Environment, 44:4735-4771.

Fiore, A.M., F. Dentener, O. Wild, C. Cuvelier, M.G. Schultz, P. Hess, C. Textor, M. Schulz, R.M. Doherty, L.W. Horowitz, I.A. MacKenzie, M.G. Sanderson, D.T. Shindell, D.S. Stevenson, S. Szopa, R. Van Dingenen, G. Zeng, C. Atherton, D. Bergmann, I. Bey, G. Carmichael, W.J. Collins, B.N. Duncan, G. Faluvegi, G. Folberth, M. Gauss, S. Gong, D. Hauglustaine, T. Holloway, I.S.A. Isaksen, D.J. Jacob, J.E. Jonson, J.W. Kaminski, T.J. Keating, A. Lupu, E. Marmer, V. Montanaro, R.J. Park, G. Pitari, K.J. Pringle, J.A. Pyle, S. Schroeder, M.G. Vivanco, P. Wind, G. Wojcik, S. Wu and A. Zuber, 2009. Multimodel estimates of intercontinental source–receptor relationships for ozone pollution. Journal of Geophysical Research: Atmospheres, 114:D04301, doi:10.1029/2008JD010816.

Fisher, J.A., D.J. Jacob, M.T. Purdy, M. Kopacz, P. Le Sager, C.C. Carouge, C.D. Holmes, R.M. Yantosca, R.L. Batchelor, K. Strong, G. Diskin, H. Fuelberg, J. Holloway, E.J. Hyer, W.W. McMillan, J. Warner, D. Streets, Q. Zhang, Y. Wang and S. Wu, 2010. Source attribution and interannual variability of Arctic pollution in spring constrained by aircraft (ARCTAS, ARCPAC) and satellite (AIRS) observations of carbon monoxide. Atmospheric Chemistry and Physics, 10:977-996.

Flanner, M.G., 2013. Arctic climate sensitivity to local black carbon. Journal of Geophysical Research: Atmospheres, 118:1840-1851.

Flanner, M.G., C.S. Zender, J.T. Randerson and P.J. Rasch, 2007. Present day climate forcing and response from black carbon in snow. Journal of Geophysical Research: Atmospheres, 112:D11202, doi:10.1029/2006JD008003.

Flanner, M.G., C.S. Zender, P. Hess, N.M. Mahowald, T.H. Painter and V. Ramanathan, 2009. Springtime warming and reduced snow cover from carbonaceous particles. Atmospheric Chemistry and Physics, 9:2481-2497.

Flato, G.M., 2011. Earth system models: an overview. WIREs Climate Change, 2:783-800.

Forsström, S., E. Isaksson, R.B. Skeie, J. Ström, C.A. Pedersen, S.R. Hudson, T.K. Berntsen, H. Lihavainen, F. Godtliebsen and S. Gerland, 2013. Elemental carbon measurements in European Arctic snow packs. Journal of Geophysical Research: Atmospheres, 118:13614-13627.

Forster, P.M. and K.P. Shine, 1997. Radiative forcing and temperature trends from stratospheric ozone changes. Journal of Geophysical Research: Atmospheres, 102:10841-10855.

Forster, P., V. Ramaswamy, P. Artaxo, T. Berntsen, R. Betts, D.W. Fahey, J. Haywood, J. Lean, D.C. Lowe, G. Myhre, J. Nganga, R. Prinn, G. Raga, M. Schulz and R. Van Dorland, 2007. Changes in atmospheric constituents and in radiative forcing. In: Solomon, S., D. Qin, M. Manning, Z. Chen, M. Marquis, K.B. Averyt, M. Tignor and H.L. Miller (eds.), Climate Change 2007: The Physical Science Basis. Contribution of Working Group I to the Fourth Assessment Report of the Intergovernmental Panel on Climate Change. Cambridge University Press.

Fuglestvedt, J.S., T.K. Berntsen, I.S.A. Isaksen, H. Mao, X.Z. Liang and W.C. Wang, 1999. Climatic forcing of nitrogen oxides through changes in tropospheric ozone and methane; global 3D model studies. Atmospheric Environment, 33:961-977.

Fuglestvedt, J.S., T. Berntsen, O. Godal, R. Sausen, K.P. Shine and T. Skodvin, 2003. Metrics of climate change: Assessing radiative forcing and emission indices. Climatic Change, 58:267-331.

Fujino, J., R. Nair, M. Kainuma, T. Masui and Y. Matsuoka, 2006. Multi-gas mitigation analysis on stabilization scenarios using AIM global model. The Energy Journal, SI:Multigas Mitigation and Climate Policy, 343-354.

Fuller, K.A., W.C. Malm and S.M. Kreidenweis, 1999. Effects of mixing on extinction by carbonaceous particles. Journal of Geophysical Research: Atmospheres, 104:15941-15954.

Fyfe, J.C., K. von Salzen, N.P. Gillett, VK. Arora, G.M. Flato and J.R. McConnell, 2013. One hundred years of Arctic surface temperature variation due to anthropogenic influence. Scientific Reports, 3:2645, doi:10.1038/srep02645.

Garrett, T.J. and C. Zhao, 2006. Increased Arctic cloud longwave emissivity associated with pollution from mid-latitudes. Nature, 440:787-789.

Garrett, T.J., C. Zhao, X. Dong, G.G. Mace and P.V. Hobbs, 2004. Effects of varying aerosol regimes on low-level Arctic stratus. Geophysical Research Letters, 31:L17105, doi:10.1029/2004GL019928.

Garrett, T.J., C. Zhao and P.C. Novelli, 2010. Assessing the relative contributions of transport efficiency and scavenging to seasonal variability in Arctic aerosol. Tellus B, 62:190-196.

Garrett, T.J., S. Brattström, S. Sharma, D.E.J. Worthy and P.C. Novelli, 2011. The role of scavenging in the seasonal transport of black carbon and sulfate to the Arctic. Geophysical Research Letters, 38:L16805, doi: 10.1029/2011GL048221.

Gauss, M., V.K. Arora, C.D. Koven, D.J.L. Olivié, O.A. Søvde, L. Höglund-Isaksson, T.R. Christensen, F-J.W. Parmentier and D.A. Plummer, 2015. Modeling the climate response to methane. In: AMAP Assessment 2015: Methane as an Arctic climate forcer. Arctic Monitoring and Assessment Programme (AMAP), Oslo, Norway.

Ghose, M. and S. Majee, 2007. Dust around an Indian surface coal mining area. Environmental Monitoring and Assessment, 130:17-25.

Gilman, J.B., J.F. Burkhart, J. Lerner, E.J. Williams, W.C. Kuster, P.D. Goldan, P.C. Murphy, C. Warneke, C. Fowler, S. Montzka, B.R. Miller, L. Miller, S. Oltmans, T.B. Ryerson, O.R. Cooper, A. Stohl and J. de Gouw, 2010. Ozone variability and halogen oxidation within the Arctic and sub-Arctic springtime boundary layer. Atmospheric Chemistry and Physics, 10:10223-10236.

Glassman, I. and R.A. Yetter, 2008. Combustion. Academic Press.

Goldenson, N., S.J. Doherty, C.M. Bitz, M.M. Holland, B. Light and A.J. Conley, 2012. Arctic climate response to forcing from light-absorbing particles in snow and sea ice in CESM. Atmospheric Chemistry and Physics, 12:7903-7920.

Gong, S.L., T.L. Zhao, S. Sharma, D. Toom-Sauntry, D. Lavoué, X.B. Zhang, W.R. Leaitch and L.A. Barrie, 2010. Identification of trends and interannual variability of sulfate and black carbon in the Canadian High Arctic: 1981–2007. Journal of Geophysical Research: Atmospheres, 115: D07305, doi: 10.1029/2009JD012943.

Gorbunov, B., A. Baklanov, N. Kakutkina, H.L. Windsor and R. Toumi, 2001. Ice nucleation on soot particles. Journal of Aerosol Science, 32:199-215.

Granier, C., U. Niemeier, J.H. Jungclaus, L.K. Emmons, P. Hess, J.F. Lamarque, S. Walters and G.P. Brasseur, 2006. Ozone pollution from future ship traffic in the Arctic northern passages. Geophysical Research Letters, 33:L13807, doi:10.1029/2006GL026180.

Granier, C., B. Bessagnet, T.C. Bond, A. D'Angiola, H. Denier van der Gon, G.J. Frost, A. Heil, J.W. Kaiser, S. Kinne, Z. Klimont, S. Kloster, J.F. Lamarque, C. Liousse, T. Masui, F. Meleux, A. Mieville, T. Ohara, J.C. Raut, K. Riahi, M.G. Schultz, S.J. Smith, A.M. Thompson, J.A. van Aardenne, G.R. van der Werf and D. van Vuuren, 2011. Evolution of anthropogenic and biomass burning emissions of air pollutants at global and regional scales during the 1980-2010 period. Climatic Change, 109:163-190.

Grell, G.A., S.E. Peckham, R. Schmitz, S.A. McKeen, G.J. Frost, W.C. Skamarock and B. Eder, 2005. Fully coupled online chemistry within the WRF model. Atmospheric Environment, 39:6957-6975.

Grenfell, T.C., S.J. Doherty, A.D. Clarke and S.G. Warren, 2011. Light absorption from particulate impurities in snow and ice determined by spectrophotometric analysis of filters. Applied Optics, 50:2037-2048.

Hadley, O.L., E.C. Corrigan, T.W. Kirchstetter, S.S. Cliff and V. Ramanathan, 2010. Measured black carbon deposition on the Sierra Nevada snow pack and implication for snow pack retreat. Atmospheric Chemistry and Physics, 10:7507-7513.

Hansen, A.D.A., H. Rosen and T. Novakov, 1992. Real time measurement of the absorption coefficient of aerosol particles. Applied Optics, 21:3060-3062.

Hansen, J., M. Sato and R. Ruedy, 1997. Radiative forcing and climate response. Journal of Geophysical Research: Atmospheres, 102:6831-6864.

Hansen, J., M. Sato, R. Ruedy, L. Nazarenko, A. Lacis, G.A. Schmidt, G. Russell, I. Aleinov, M. Bauer, S. Bauer, N. Bell, B. Cairns, V. Canuto, M. Chandler, Y. Cheng, A. del Genio, G. Faluvegi, E. Fleming, A. Friend, T. Hall, C. Jackman, M. Kelley, N. Klang, D. Koch, J. Lean, J. Lerner, K. Lo, S. Menon, R. Miller, P. Minnis, T. Novakov, V. Olinas, J. Perlwitz, J. Perlwitz, D. Rind, A. Romanou, D. Shindell, P. Stone, S. Sun, N. Tausnev, D. Thresher, B. Wielicki, T. Wong, M. Yao and S. Zhang, 2005. Efficacy of climate forcings. Journal of Geophysical Research: Atmospheres, 110:D18104, doi:10.1029/2005JD005776.

Hansen, J., M. Sato, R. Ruedy P. Kharecha, A. Lacis, R. Miller, L. Nazarenko, K. Lo, G. A. Schmidt, G. Russell, I. Aleinov, S. Bauer, E. Baum, B. Cairns, V. Canuto, M. Chandler, Y. Cheng, A. Cohen, A. Del Genio, G. Faluvegi, E. Fleming, A. Friend, T. Hall, C. Jackman, J. Jonas, M. Kelley, N. Y. Kiang, D. Koch, G. Labow, J. Lerner, S. Menon, T. Novakov, V. Oinas, Ja. Perlwitz, Ju. Perlwitz, D. Rind, A. Romanou, R. Schmunk, D. Shindell, P. Stone, S. Sun, D. Streets, N. Tausnev, D. Thresher, N. Unger, M. Yao and S. Zhang, 2007. Climate simulations for 1880–2003 with GISS modelE. Climate Dynamics, 29:661-696.

Hansson H.-C., C. Johansson, G. Nyqvist, K. Kindbom, S. Åström and J. Moldanovna, 2011. Black Carbon – Possibilities to Reduce Emissions and Potential Effects. Department of Applied Environmental science, Stockholm University (ITM), ITM Report 202.

Harrigan, D.L., H. Fuelberg, I.J. Simpson, D. Blake, G. Carmichael and G. Diskin, 2011. Anthropogenic emissions during Arctas-A: mean transport characteristics and regional case studies. Atmospheric Chemistry and Physics, 11:8677-8701.

Hegg, D.A., S.G. Warren, T C. Grenfell, S.J. Doherty, T.V. Larson and A.D. Clarke, 2009. Source attribution of black carbon in Arctic snow. Environmental Science and Technology, 43:4016-4021.

Heidam, N.Z., J.H. Christensen, P. Wåhlin and H. Skov, 2004. Arctic atmospheric contaminants in NE Greenland: levels, variations, origins, transport, transformations and trends 1990-2001. Science of the Total Environment, 331:5-28.

Heintzenberg, J., 1982. Size-segregated measurements of particulate elemental carbon and aerosol light absorption at remote arctic locations. Atmospheric Environment, 16:2461-2469.

Heintzenberg, J., T. Tuch, B. Wehner, A. Wiedensohler, H. Wex, A. Ansmann, I. Mattis, M. Müller, M. Wendisch, S. Eckhardt and A. Stohl, 2003. Arctic haze over Central Europe. Tellus B, 55:796-807.

Helmig, D., J. Bottenheim, I.E. Galbally, A. Lewis, M.J.T. Milton, S. Penkett, C. Plass-Duelmer, S. Reimann, P. Tans and S. Thiel, 2009. Volatile organic compounds in the global atmosphere. Eos, Transactions American Geophysical Union, 90:513-514.

Herber, A.B., C. Haas, R.S. Stone, J.W. Bottenheim, P. Liu, S.-M. Li, R.M. Staebler, J.W. Strapp and K. Dethloff, 2012. Regular airborne surveys of Arctic sea ice and atmosphere. Eos, Transactions American Geophysical Union, 93:41-42.

Hess, P.G. and R. Zbinden 2011. Stratospheric impact on tropospheric ozone variability and trends: 1990-2009. Atmospheric Chemistry and Physics, 11:22719-22770.

Hijioka, Y., Y. Matsuoka, H. Nishimoto, M. Masui and M. Kainuma, 2008. Global GHG emissions scenarios under GHG concentration stabilization targets. Journal of Global Environmental Engineering, 13:97-108.

Hirdman, D., J.F. Burkhart, H. Sodemann, S. Eckhardt, A. Jefferson, P.K. Quinn, S. Sharma, J. Ström and A. Stohl, 2010a. Long-term trends of black carbon and sulphate aerosol in the Arctic: changes in atmospheric transport and source region emissions. Atmospheric Chemistry and Physics, 10:9351-9368.

Hirdman, D., H. Sodemann, S. Eckhardt, J.F. Burkhart, A. Jefferson, T. Mefford, P.K. Quinn, S. Sharma, J. Ström and A. Stohl, 2010b. Source identification of short-lived air pollutants in the Arctic using statistical analysis of measurement data and particle dispersion model output. Atmospheric Chemistry and Physics, 10:669-693.

Hodnebrog, Ø., G. Myhre and B.H. Samset, 2014. How shorter black carbon lifetime alters its climate effect. Nature Communications, 5:5065, doi:10.1038/ncomms6065.

Hoffmann, A., C. Ritter, M. Stock, M. Maturilli, S. Eckhardt, A. Herber and R. Neuber, 2010. Lidar measurements of the Kasatochi aerosol plume in August and September 2008 in Ny-Ålesund, Spitsbergen. Journal of Geophysical Research: Atmospheres, 115:D00L12, doi:10.1029/2009JD013039.

Holland, M.M., D.A. Bailey, B.P. Briegleb, B. Light and E. Hunke, 2012. Improved sea ice shortwave radiation physics in CCSM4: The impact of melt ponds and aerosols on Arctic sea ice. Journal of Climate, 25:1413-1430.

Huang, L., S.L. Gong, C.Q. Jia and D. Lavoué, 2010a. Importance of deposition processes in simulating the seasonality of the Arctic black carbon aerosol. Journal of Geophysical Research: Atmospheres, 115: D17207, doi:10.1029/2009JD013478.

Huang, L., S L. Gong, C.Q. Jia and D. Lavoué, 2010b. Relative contributions of anthropogenic emissions to black carbon aerosol in the Arctic. Journal of Geophysical Research: Atmospheres, 115: D19208, doi:10.1029/2009JD013592.

Huntzicker, J.J., R.L. Johnson, J.J. Shah and R.A. Cary, 1982. Analysis of organic and elemental carbon in ambient aerosol by a thermal-optical method. In: Wolff, G.T. and R.L. Klimisch (eds.). Particulate Carbon: Atmospheric Life Cycle. Plenum Press.

Hurrell, J.W., 1995. Decadal trends in the North Atlantic Oscillation: Regional temperatures and precipitation. Science, 269:676-679.

Hyvärinen, A.P., P. Kolmonen, V.-M. Kerminen, A. Virkkula, A. Leskinen, M. Komppula, J. Hatakka, J. Burkhart, A. Stohl, P. Aalto, M. Kulmala, K.E.J. Lehtinen, Y. Viisanen, H. Lihavainen, 2011. Aerosol black carbon at five background measurement sites over Finland, a gateway to the Arctic. Atmospheric Environment, 45:4042-4050.

IEA, 2011. World Energy Outlook 2011. International Energy Agency.

IEA, 2012. Energy Technology Perspectives 2012: Pathways to a Clean Energy System. International Energy Agency.

IMO, 2010. Guidelines for Ships Operating in Polar Waters. 2010 Edition. Electronic Edition. IMO Publication E190E. International Maritime Organization, London.

IPCC, 2013a. Summary for Policymakers. In: Climate Change 2013: The Physical Science Basis. Contribution of Working Group I to the Fifth Assessment Report of the Intergovernmental Panel on Climate

Change. Stocker,T.F., D. Qin, G.-K. Plattner, M. Tignor, S.K. Allen, J. Boschung, A. Nauels, Y. Xia, V. Bex and P.M. Midgley (eds.). Cambridge University Press.

IPCC, 2013b. Contribution of Working Group 1 to the Fifth Assessment Report of the Intergovernmental Panel on Climate Change. Climate Change, 2013: The Physical Science Basis. Stocker, T.F., D. Qin, G.-K. Plattner, M. Tignor, S.K. Allen, J. Boschung, A. Nauels, Y. Xia, V. Bex and P.M. Midgley (eds.). Cambridge University Press.

Ito, A. and J.E. Penner, 2005. Historical emissions of carbonaceous aerosols from biomass and fossil fuel burning for the period 1870–2000. Global Biogeochemical Cycles, 19:GB2028, doi:10.1029/2004GB002374.

Iversen, T., 1984. On the atmospheric transport of pollution to the Arctic. Geophysical Research Letters, 11:457-460.

Iversen, T., 1996. Atmospheric transport pathways for the Arctic. In: E. Wolff and R.C. Bales (eds.). Chemical exchange between the atmosphere and polar snow. Global Environmental Change. NATO ASI Series I, Volume 43, pp. 71-92. Springer-Verlag.

Iversen, T., M. Bentsen, I. Bethke, J.B. Debernard, A. Kirkevåg, Ø. Seland, H. Drange, J.E. Kristjansson, I. Medhaug, M. Sand and I.A. Seierstad, 2013. The Norwegian Earth System Model, NorESM1-M – Part 2: Climate response and scenario projections. Geoscientific Model Development, 6:389-415.

Jacob, D.J., J.H. Crawford, H. Maring, A.D. Clarke, J.E. Dibb, L.K. Emmons, R.A. Ferrare, C.A. Hostetler, P.B. Russell, H.B. Singh, A.M. Thompson, G.E. Shaw, E. McCauley, J.R. Pederson and J.A. Fisher, 2010. The Arctic Research of the Composition of the Troposphere from Aircraft and Satellites (ARCTAS) mission: design, execution, and first results. Atmospheric Chemistry and Physics, 10:5191-5212.

Jacobi, H.- W., S. Morin and J.W. Bottenheim, 2010. Observation of widespread depletion of ozone in the springtime boundary layer of the central Arctic linked to mesoscale synoptic conditions. Journal of Geophysical Research: Atmospheres, 115:D17302, doi:10.1029/2010JD013940.

Jacobson, M.Z., 2004. Climate response of fossil fuel and biofuel soot, accounting for soot's feedback to snow and sea ice albedo and emissivity. Journal of Geophysical Research: Atmospheres, 109:D21201, doi:10.1029/2004JD004945.

Jacobson, M.Z., 2010. Short-term effects of controlling fossil-fuel soot, biofuel soot and gases, and methane on climate, arctic ice, and air pollution health, Journal of Geophysical Research: Atmospheres, 115:D14209, doi:10.1029/2009JD013795.

Jacobson, M.Z., J.T. Wilkerson, S. Balasubramanian, W.W. Cooper Jr., and N. Mohleji, 2012. The effects of rerouting aircraft around the arctic circle on arctic and global climate. Climatic Change, 115:709-724.

Jaffe, D.A. and N.L. Wigder, 2012. Ozone production from wildfires: A critical review. Atmospheric Environment, 51:1-10.

Janssens-Maenhout, G., A.M.R. Petrescu, M. Muntean and V. Blujdea, 2011. Verifying greenhouse gas emissions: Methods to support international climate agreements. Greenhouse Gas Measurement and Management, 1:132-133.

Jiao, C., M.G. Flanner, Y. Balkanski, S.E. Bauer, N. Bellouin, T.K. Berntsen, H. Bian, K.S. Carslaw, M. Chin, N. De Luca, T. Diehl, S.J. Ghan, T. Iversen, A. Kirkevåg, D. Koch, X. Liu, G.W. Mann, J.E. Penner, G. Pitari, M. Schulz, Ø. Seland, R.B. Skeie, S.D. Steenrod, P. Stier, T. Takemura, K. Tsigaridis, T. van Noije, Y. Yun and K. Zhang, 2014. An AeroCom assessment of black carbon in Arctic snow and sea ice. Atmospheric Chemistry and Physics, 14:2399-2417.

Johnson, B.T., K.P. Shine and P.M. Forster, 2004. The semi-direct aerosol effect: Impact of absorbing aerosols on marine stratocumulus. Quarterly Journal of the Royal Meteorological Society, 130:1407-1422.

Joos, F., R. Roth, J.S. Fuglestvedt, G.P. Peters, I.G. Enting, W. von Bloh, V. Brovkin, E.J. Burke, M. Eby, N.R. Edwards, T. Friedrich, T.L. Frölicher, P.R. Halloran, P.B. Holden, C. Jones, T. Kleinen, F.T. Mackenzie, K. Matsumoto, M. Meinshausen, G.-K. Plattner, A. Reisinger, J. Segschneider, G. Shaffer, M. Steinacher, K. Strassmann, K. Tanaka, A. Timmermann and A.J. Weaver, 2013. Carbon dioxide and climate impulse response functions for the computation of greenhouse gas metrics: a multi-model analysis. Atmospheric Chemistry and Physics, 13:2793-2825.

Junker, C. and C. Liousse, 2008. A global emission inventory of carbonaceous aerosol from historic records of fossil fuel and biofuel consumption for the period 1860-1997. Atmospheric Chemistry and Physics, 8:1195-1207.

Kaiser, J.W., A. Heil, M.O. Andreae, A. Benedetti, N. Chubarova, L. Jones, J.J. Morcrette, M. Razinger, M.G. Schultz, M. Suttie and G.R. van der Werf, 2012. Biomass burning emissions estimated with a global fire assimilation system based on observed fire radiative power. Biogeosciences, 9:527-554.

Kanakidou, M., R.A. Duce, J.M. Prospero, A.R. Baker, C. Benitez-Nelson, F.J. Dentener, K.A. Hunter, P.S. Liss, N. Mahowald, G.S. Okin, M. Sarin, K. Tsigaridis, M. Uematsu, L.M. Zamora and T. Zhu, 2012. Atmospheric fluxes of organic N and P to the global ocean. Global Biogeochemical Cycles, 26:GB3026, doi:10.1029/2011GB004277.

Keegan, K.M., M.R. Albert, J.R. McConnell and I. Baker, 2014. Climate change and forest fires synergistically drive widespread melt events of the Greenland Ice Sheet. Proceedings of the National Academy of Sciences, 111:7964-7967.

Kindbom, K. and J. Munthe, 2013. Short-lived Climate Pollutants - method development for emission inventories of Black Carbon. Swedish Environmental Research Institute, IVL report B2099.

Kirkevåg, A., T. Iversen, Ø. Seland, C. Hoose, J.E. Kristjánsson, H. Struthers, A.M.L. Ekman, S. Ghan, J. Griesfeller, E.D. Nilsson and M. Schulz, 2013. Aerosol–climate interactions in the Norwegian Earth System Model – NorESM1-M. Geoscientific Model Development, 6:207-244.

Klimont, Z., C. Heyes, L. Höglund-Isaksson, J. Cofala, P. Rafaj, W. Schöpp, P. Purohit, J. Borken, M. Amann, K. Kupiainen, W. Winiwarter, I. Bertok, R. Sander, B. Zhao and S. Wang, 2015. Global air pollutant and methane emission scenarios 1990-2050 – ECLIPSE. [*In preparation for Atmospheric Chemistry and Physics*]

Klonecki, A., P. Hess, L.K. Emmons, L. Smith, J.J. Orlando and D. Blake, 2003. Seasonal changes in the transport of pollutants into the Arctic troposphere-model study. Journal of Geophysical Research, 108: 8367, doi:10.1029/2002JD002199.

Koch, D. and J. Hansen, 2005. Distant origins of Arctic black carbon: a Goddard Institute for Space Studies ModelE experiment. Journal of Geophysical Research: Atmospheres, 110:D04204, doi: 10.1029/2004JD005296.

Koch, D., S. Menon, A. Del Genio, R. Ruedy, I. Alienov and G.A. Schmidt, 2009a. Distinguishing aerosol impacts on climate over the past century. Journal of Climate, 22:2659-2677.

Koch, D., M. Schulz, S. Kinne, C.S. McNaughton, J.R. Spackman, Y. Balkanski, S. Bauer, T. Berntsen, T.C. Bond, O. Boucher, M. Chin, A.D. Clarke, N. DeLuca, F. Dentener, T. Diehl, O. Dubovik, R. Easter, D.W. Fahey, J. Feichter, D. Fillmore, S. Freitag, S. Ghan, P. Ginoux, S.L. Gong, L. Horowitz, T. Iverson, A. Kirkevåg, Z. Klimont, Y. Kondo, M. Krol, S. Reddy, L. Sahu, H. Sakamoto, G. Schuster, J.P. Schwarz, Ø. Seland, P. Stier, N. Takegawa, T. Takemura, C. Textor, J.A. van Aardenne and Y. Zhao, 2009b. Evaluation of black carbon estimations in global aerosol models. Atmospheric Chemistry and Physics, 9:9001-9026.

Koch, D., S.E. Bauer, A. Del Genio, G. Faluvegi, J.R. McConnell, S. Menon, R.L. Miller, D. Rind, R. Ruedy, G.A. Schmidt and D. Shindell, 2011. Coupled aerosol-chemistry-climate twentieth-century transient model investigation: Trends in short-lived species and climate responses. Journal of Climate, 24:2693-2714.

Koike, M., N. Moteki, P. Khatri, T. Takamura, N. Takegawa, Y. Kondo, H. Hashioka, H. Matsui, A. Shimizu and N. Sugimoto, 2014. Case study of absorption aerosol optical depth closure of black carbon over the East China Sea. Journal of Geophysical Research: Atmospheres, 119:122-136.

Kondo, Y., L. Sahu, N. Moteki, F. Khan, N. Takegawa, X. Liu, M. Koike and T. Miyakawa, 2011. Consistency and traceability of black carbon measurements made by laser-induced incandescence, thermal-optical transmittance, and filter-based photo-absorption techniques. Aerosol Science and Technology, 45:295-312.

Kooperman, G.J., M.S. Pritchard, S. Ghan, M. Wang, R.C.J. Somerville and L.M. Russell, 2012. Constraining the influence of natural variability to improve estimates of global aerosol indirect effects in a nudged version of the Community Atmosphere Model 5. Journal of Geophysical Research: Atmospheres, 117:D23204, doi:10.1029/2012JD018588.

Kupiszewski, P., C. Leck, M. Tjernström, S. Sjogren, J. Sedlar, M. Graus, M. Müller, B. Brooks, E. Sweitlicki, S. Norris and A. Hansel, 2013. Vertical profiling of aerosol particles and trace gases over the central Arctic Ocean during summer. Atmospheric Chemistry and Physics, 13:12405-12431.

Kuwata, M., Y. Kondo, M. Mochida, N. Takegawa and K. Kawamura, 2007. Dependence of CCN activity of less volatile particles on the amount of coating observed in Tokyo. Journal of Geophysical Research: Atmospheres, 112:D11207, doi: 10.1029/2006JD007758.

Laborde, M., M. Schnaiter, C. Linke, H. Saathoff, K.H. Naumann, O. Möhler, S. Berlenz, U. Wagner, J.W. Taylor, D. Liu, M. Flynn, J.D. Allan, H. Coe, K. Heimerl, F. Dahlkötter, B. Weinzierl, A.G. Wollny, M. Zanatta, J. Cozic, P. Laj, R. Hitzenberger, J.P. Schwarz and M. Gysel, 2012. Single Particle Soot Photometer intercomparison at the AIDA chamber. Atmospheric Measurement Techniques, 5:3077-3097.

Lack, D., E.R. Lovejoy, T. Baynard, A. Pettersson and A.R. Ravishankara, 2006. Aerosol absorption measurement using photoacoustic spectroscopy: Sensitivity, calibration, and uncertainty developments. Aerosol Science and Technology, 40:697-708.

Lack, D.A., C.D. Cappa, D.S. Covert, T. Baynard, P. Massoli, B. Sierau, T.S. Bates, P.K. Quinn, E.R. Lovejoy and A.R. Ravishankara, 2008. Bias in filter-based aerosol light absorption measurements due to organic aerosol loading: Evidence from ambient measurements. Aerosol Science and Technology, 42:1033-1041.

Lack, D.A., J.M. Langridge, R. Bahreini, C.D. Cappa, A.M. Middlebrook and J.P. Schwarz, 2012. Brown carbon and internal mixing in biomass burning particles. Proceedings of the National Academy of Sciences, 109:14802-14807.

Lamarque, J.F., T.C. Bond, V. Eyring, C. Granier, A. Heil, Z. Klimont, D. Lee, C. Liousse, A. Mieville, B. Owen, M.G. Schultz, D. Shindell, S.J. Smith, E. Stehfest, J.A. van Aardenne, O.R. Cooper, M. Kainuma, N.M. Mahowald, J.R. McConnell, V. Naik, K. Riahi and D. van Vuuren, 2010. Historical (1850–2000) gridded anthropogenic and biomass burning emissions of reactive gases and aerosols: methodology and application. Atmospheric Chemistry and Physics, 10:7017-7039.

Lamarque, J.-F., D.T. Shindell, B. Josse, P.J. Young, I. Cionni, V. Eyring, D. Bergmann, P. Cameron-Smith, W.J. Collins, R. Doherty, S. Dalsoren, G. Faluvegi, G. Folberth, S.J. Ghan, L.W. Horowitz, Y.H. Lee, I.A. MacKenzie, T. Nagashima, V. Naik, D. Plummer, M. Righi, S.T. Rumbold, M. Schulz, R.B. Skeie, D.S. Stevenson, S. Strode, K. Sudo, S. Szopa, A. Voulgarakis and G. Zeng, 2013. The Atmospheric Chemistry and Climate Model Intercomparison Project (ACCMIP): overview and description of models, simulations and climate diagnostics. Geoscientific Model Development, 6:179-206.

Lathem, T.L., A.J. Beyersdorf, K.L. Thornhill, E.L. Winstead, M.J. Cubison, A. Hecobian, J.L. Jimenez, R.J. Weber, B.E. Anderson and A. Nenes, 2013. Analysis of CCN activity of Arctic aerosol and Canadian biomass burning during summer 2008. Atmospheric Chemistry and Physics, 13:2735-2756.

Law, K., A. Stohl, P.K. Quinn, C.A. Brock, J.F. Burkhart, J.-D. Paris, G. Ancellet, H.B. Singh, A. Roiger, H. Schlager, J. Dibb, D.J. Jacob, S.R. Arnold, J. Pelon, J.L. Thomas, 2014. Arctic Air Pollution: New Insights from POLARCAT-IPY. Bulletin of the American Meteorological Society, 95:1873-1895.

Lee, Y.H., J.-F. Lamarque, M.G. Flanner, C. Jiao, D.T. Shindell, T. Berntsen, M.M. Bisiaux, J. Cao, W.J. Collins, M. Curran, R. Edwards, G. Faluvegi, S. Ghan, L.W. Horowitz, J.R. McConnell, J. Ming, G. Myhre, T. Nagashima, V. Naik, S.T. Rumbold, R.B. Skeie, K. Sudo, T. Takemura, F. Thevenon, B. Xu and J.-H. Yoon, 2013. Evaluation of preindustrial to present-day black carbon and its albedo forcing from Atmospheric Chemistry and Climate Model Intercomparison Project (ACCMIP). Atmospheric Chemistry and Physics, 13:2607-2634.

Levy, H., 1971. Normal atmosphere: large radical and formaldehyde concentrations predicted. Science, 173:141-143.

Levy, J.I., T.J. Carrothers, J.T. Tuomisto, J.K. Hammitt and J.S. Evans, 2001. Assessing the public health benefits of reduced ozone concentrations. Environmental Health Perspectives, 109:1215-1226.

Li, S.M., R.W. Talbot, L.A. Barrie, R.C. Harriss, C.I. Davidson and J.-L. Jaffrezo, 1993. Seasonal and geographical variations of methane sulphanic acid in the Arctic troposphere. Atmospheric Environment, 27A:3011-3024.

Liang, Q., J.N. Rodriquez, A.R. Douglass, J.H. Crawford, J.R. Olson, E. Apel, H. Bian, D. Blake, W. Brune, M. Chin, P.R. Colarco, A. da Silva, G. Diskin, B.N. Duncan, L.G. Huey, D. Knapp, S. Montzka, J.E. Nielsen, S. Pawson, D. Riemer, A. Weinheimer and A. Wisthaler, 2011. Reactive nitrogen, ozone and ozone production in the Arctic troposphere and the impact of stratosphere-troposphere exchange. Atmospheric Chemistry and Physics, 11:13181-13199.

Lim, S., X. Faïn, M. Zanatta, J. Cozic, J.L. Jaffrezo, P. Ginot and P. Laj, 2014. Refractory black carbon mass concentrations in snow and ice: method evaluation and inter-comparison with elemental carbon measurement. Atmospheric Measurement Techniques, 7:3307-3324.

Lin, G., J.E. Penner, M.G. Flanner, S. Sillman, L. Xu and C. Zhou, 2014. Radiative forcing of organic aerosol in the atmosphere and on snow: Effects of SOA and brown carbon. Journal of Geophysical Research: Atmospheres, 119:7453-7476.

Liu, X.H., J.E. Penner and M. Herzog, 2005. Global modeling of aerosol dynamics: Model description, evaluation, and interactions between sulfate and nonsulfate aerosols. Journal of Geophysical Research: Atmospheres, 110:D18206, doi: 10.1029/2004JD005674.

Liu, G., D.W. Tarasick, V.E. Fioletov, C.E. Sioris and Y.J. Rochon, 2009. Ozone correlation lengths and measurement uncertainties from analysis of historical ozonesonde data in North America and Europe. Journal of Geophysical Research: Atmospheres, 114:D04112, doi:10.1029/2008JD010576.

Liu, J., S. Fan, L. Horowitz and H. Levy, 2011. Evaluation of factors controlling long-range transport of black carbon to the Arctic. Journal of Geophysical Research: Atmospheres, 116:D04307, doi:10.1029/2010JD015145.

Liu, X., R.C. Easter, S.J. Ghan, R. Zaveri, P. Rasch, X. Shi, J.-F. Lamarque, A. Gettelman, H. Morrison, F. Vitt, A. Conley, S. Park, R. Neale, C. Hannay, A.M.L. Ekman, P. Hess, N. Mahowald, W. Collins, M.J. Iacono, C.S. Bretherton, M.G. Flanner and D. Mitchell, 2012. Toward a minimal representation of aerosols in climate models: description and evaluation in the Community Atmosphere Model CAM5. Geoscientific Model Development, 5:709-739.

Lund, M.T. and T. Berntsen, 2012. Parameterization of black carbon aging in the OsloCTM2 and implications for regional transport to the Arctic. Atmospheric Chemistry and Physics, 12:6999-7014.

Lund Myhre, C., C. Toledano, G. Myhre, K. Stebel, K.E. Yttri, V. Aaltonen, M. Johnsrud, M. Frioud, V. Cachorro, A. de Frutos, H. Lihavainen, J.R. Campbell, A.P. Chaikovsky, M. Shiobara, E.J. Welton and K. Tørseth, 2007. Regional aerosol optical properties and radiative impact of the extreme smoke event in the European Arctic in spring 2006. Atmospheric Chemistry and Physics, 7:5899-5915.

Ma, X. and K. von Salzen, 2008. Modelling sea salt aerosol and its direct and indirect effects on climate. Atmospheric Chemistry and Physics, 8:1311-1327.

Ma, N., C.S. Zhao, T. Müller, Y.F. Cheng, P.F. Liu, Z.Z. Deng, W.Y. Xu, L. Ran, B. Nekat, D. van Pinxteren, T. Gnauk, K. Müller, H. Herrmann, P. Yan, X.J. Zhou and A. Wiedensohler, 2012. A new method to determine the mixing state of light absorbing carbonaceous using the measured aerosol optical properties and number size distributions. Atmospheric Chemistry and Physics, 12:2381-2397.

Mao, J., S. Fan, D.J. Jacob and K.R. Travis, 2013. Radical loss in the atmosphere from Cu-Fe redox coupling in aerosols. Atmospheric Chemistry and Physics, 13:509-519.

Marelle, L., J.-C. Raut, J.L. Thomas, K.S. Law, B. Quennehen, G. Ancellet, J. Pelon, A. Schwarzenboeck and J.D. Fast, 2014. Transport of anthropogenic and biomass burning aerosols from Europe to the Arctic during spring 2008. Atmospheric Chemistry and Physics Discussions, 14:28333-28384.

Marlon, J.R., P.J. Bartlein, C. Carcaillet, D.G. Gavin, S.P. Harrison, P.E. Higuera, F. Joss, M.J. Power and I.C. Prentice, 2008. Climate and human influences on global biomass burning over the past two millennia. Nature Geoscience, 1:697-702.

Martins, J.V., P.V. Hobbs, R.E. Weiss and P. Artaxo, 1998. Sphericity and morphology of smoke particles from biomass burning in Brazil. Journal of Geophysical Research: Atmospheres, 103:32051-32057.

Matsui, H., Y. Kondo, N. Moteki, N. Takegawa, L. Sahu, Y. Zhao, H. Fuelberg, W. Sessions, G. Diskin, D. Blake, A. Wisthaler and M. Krioke, 2011. Seasonal variation of the transport of black carbon aerosol from the Asian continent to the Arctic during the ARCTAS aircraft campaign. Journal of Geophysical Research: Atmospheres, 116:D05202, doi:10.1029/2010JD015067.

McConnell, J.R., R. Edwards, G.L. Kok, M.G. Flanner, C.S. Zender, E.S. Saltzman, J.R. Banta, D.R. Pasteris, M.M. Carter and J.D. Kahl, 2007. 20th-Century industrial black carbon emissions altered Arctic climate forcing. Science, 317:1381-1384.

McEwen, J.D.N. and M.R. Johnson, 2012. Black carbon particulate matter emission factors for buoyancy driven associated gas flares. Journal of the Air & Waste Management Association, 62:307-321.

McNaughton, C.S., A.D. Clarke, S. Freitag, V.N. Kapustin, Y. Kondo, N. Moteki, L. Sahu, N. Takegawa, J.P. Schwarz, J.R. Spackman, L. Watts, G. Diskin, J. Podolske, J.S. Holloway, A. Wisthaler, T. Mikoviny, J. de Gouw, C. Warneke, J. Jimenez, M. Cubison, S.G. Howell, A. Middlebrook, R. Bahreini, B.E. Anderson, E. Winstead, K.L. Thornhill, D. Lack, J. Cozic and C.A. Brock, 2011. Absorbing aerosol in the troposphere of the Western Arctic during the 2008 ARCTAS/ARCPAC airborne field campaigns. Atmospheric Chemistry and Physics, 11:7561-7582.

Ménégoz, M., G. Krinner, Y. Balkanski, A. Cozic, O. Boucher and P. Ciais, 2013. Boreal and temperate snow cover variations induced by black carbon emissions in the middle of the 21st century. The Cryosphere, 7:537-554.

Mieville, A., C. Granier, C. Liousse, B. Guillaume, F. Mouillot, J.F. Lamarque, J.M. Gregoire and G. Petron, 2010. Emissions of gases and particles from biomass burning during the 20th century using satellite data and an historical reconstruction. Atmospheric Environment, 44:1469-1477.

Ming, J., C. Xiao, H. Cachier, D. Qin, X. Qin, Z. Li and J. Pu, 2009. Black carbon (BC) in the snow of glaciers in west China and its potential effects on albedos. Atmospheric Research, 92:114-123.

Möhler, O., S. Büttner, C. Linke, M. Schnaiter, H. Saathoff, O. Stetzer, R. Wagner, M. Krämer, A. Mangold, V. Ebert and U. Schurath, 2005. Effect of sulfuric acid coating on heterogeneous ice nucleation by soot aerosol particles. Journal of Geophysical Research: Atmospheres, 110:D11210, doi: 10.1029/2004JD005169.

Monks, S.A., S.R Arnold, L.K. Emmons, K.S. Law, S. Turquety, B.N. Duncan, J. Flemming, V. Huijnen, S. Tilmes, J. Langner, J. Mao, Y. Long, J.L. Thomas, S.D. Steenrod, J.C. Raut, C. Wilson, M.P. Chipperfield, G.S. Diskin, A. Weinheimer, H. Schlager and G. Ancellet, 2015. Multi-model study of chemical and physical controls on transport of anthropogenic and biomass burning pollution to the Arctic. Atmospheric Chemistry and Physics, 15:3575-3603.

Myhr, K.A., 2003. Støv i arbeidsmiljø og ytre miljø i Svea 2003. [Indoor and outdoor pollution of particulate matter in Svea 2003.] Faculty of Engineering and Technology, Norwegian University of Science and Technology.

Myhre, G., T.F. Berglen, M. Johnsrud, C.R. Hoyle, T.K. Berntsen, S.A. Christopher, D.W. Fahey, I.S.A. Isaksen, T.A. Jones, R.A. Kahn, N. Loeb, P. Quinn, L. Remer, J.P. Schwarz and K.E. Yttri, 2009. Modelled radiative forcing of the direct aerosol effect with multi-observation evaluation. Atmospheric Chemistry and Physics, 9:1365-1392.

Myhre, G., B.H. Samset, M. Schulz, Y. Balkanski, S. Bauer, T.K. Berntsen, H. Bian, N. Bellouin, M. Chin, T. Diehl, R.C. Easter, J. Feichter, S.J. Ghan, D. Hauglustaine, T. Iversen, S. Kinne, A. Kirkevåg, J.-F. Lamarque, G. Lin, X. Liu, M.T. Lund, G. Luo, X. Ma, T. van Noije, J.E. Penner, P.J. Rasch, A. Ruiz, Ø. Seland, R.B. Skeie, P. Stier, T. Takemura, K. Tsigaridis, P. Wang, Z. Wang, L. Xu, H. Yu, F. Yu, J.-H. Yoon, K. Zhang, H. Zhang and C. Zhou, 2013a. Radiative forcing of the direct aerosol effect from AeroCom Phase II simulations. Atmospheric Chemistry and Physics, 13:1853-1877.

Myhre, G., D. Shindell, F.M. Breon, W.J. Collins, J.S. Fuglestvedt, J. Huang, D. Koch, J.F. Lamarque, D. Lee, B. Mendoza, T. Nakajima, A. Robock, G. Stephens, T. Takemura and H. Zhang, 2013b. Anthropogenic and natural radiative forcing. In: Stocker, T.F., D. Qin, G.-K. Plattner, M. Tignor, S.K. Allen, J. Boschung, A. Nauels, Y. Xia, V. Bex and P.M. Midgley (eds.), Climate Change 2013: The Physical Science Basis. Contribution of Working Group 1 to the Fifth Assessment Report of the Intergovernmental Panel on Climate Change. Cambridge University Press.

Myriokefalitakis, S., K. Tsigaridis, N. Mihalopoulos, J. Sciare, A. Nenes, K. Kawamura, A. Segers and M. Kanakidou, 2011. In-cloud oxalate formation in the global troposphere: a 3-D modeling study. Atmospheric Chemistry and Physics, 11:5761-5782.

Novelli, P.C., K. Masarie and P. Lang, 1998. Distributions and recent changes of carbon monoxide in the lower troposphere. Journal of Geophysical Research: Atmospheres, 103:19015-19033.

Oltmans, S. and H. Levy, 1994. Surface ozone measurements from a global network. Atmospheric Environment, 28:9-24.

Oltmans, S., A.S. Lefohn, D. Shadwick, J.M. Harris, H.E. Scheel, I. Galbally, D.W. Tarasick, B.J. Johnson, E.-G. Brunke, H. Claude, G. Zeng, S. Nichol, F. Schmidlin, J. Davies, E. Cuevas, A. Redondas, H. Naoe, T. Nakano and T. Kawasato, 2013. Recent tropospheric ozone changes – A pattern dominated by slow or no growth. Atmospheric Environment, 67:331-351.

Paris, J.D., A. Stohl, P. Nédélec, M.Y. Arshinov, M.V. Panchenko, V.P. Shmargunov, K.S. Law, B. Belan and P. Ciais, 2009. Wildfire smoke in the Siberian Arctic in summer: source characterization and plume evolution from airborne measurements. Atmospheric Chemistry and Physics, 9:9315-9327.

Paris, J.D., A. Stohl, P. Ciais, P. Nédélec, B.D. Belan, M.Y. Arshinov and M. Ramonet, 2010. Source-receptor relationships for airborne measurements of CO_2, CO and O_3 above Siberia: a cluster-based approach. Atmospheric Chemistry and Physics, 10:1671-1687.

Park, R.J., D.J. Jacob, P.I. Palmer, A.D. Clarke, R.J. Weber, M.A. Zondlo, F.L. Eisele, A.R. Bandy, D.C. Thornton, G.W. Sachse and T.C. Bond, 2005. Export efficiency of black carbon aerosol in continental outflow: global implications. Journal of Geophysical Research: Atmospheres, 110:D11205, doi: 10.1029/2004JD005432.

Parrington, M., P.I. Palmer, D.K. Henze, D.W. Tarasick, E.J. Hyer, R.C. Owen, D. Helmig, C. Clerbaux, K. W. Bowman, M.N. Deeter, E.M. Barratt, P.F. Coheur, D. Hurtmans, Z. Jiang, M. George and J.R. Worden, 2012. The influence of boreal biomass burning emissions on the distribution of tropospheric ozone over North America and the North Atlantic during 2010. Atmospheric Chemistry and Physics, 12:2077-2098.

Parrish, D.D., K. Law, J. Staehelin, R. Derwent, O.R. Cooper, H. Tanimoto, A. Volz-Thomas, S. Gilge, H.E. Scheel, M. Steinbacher and E. Chan, 2012a. Long-term changes in lower tropospheric baseline ozone concentrations at northern mid-latitudes. Atmospheric Chemistry and Physics, 12:11485-11504.

Parrish, D.D., K. Law, J. Staehelin, R. Derwent, O.R. Cooper, H. Tanimoto, A. Volz-Thomas, S. Gilge, H.E. Scheel, M. Steinbacher and E. Chan, 2012b. Long-term changes in lower tropospheric baseline ozone concentrations at northern mid-latitudes. Atmospheric Chemistry and Physics Discussions, 12:13881-13931.

Pausata, F.S.R., L. Pozzoli, E. Vignati and F. Dentener, 2012. North Atlantic Oscillation and tropospheric ozone variability in Europe: model analysis and measurements intercomparison. Atmospheric Chemistry and Physics, 12:6537-6376.

Penenko, V., A. Baklanov, E. Tsvetova and A. Mahura, 2012. Direct and inverse problems in a variational concept of environmental modeling. Pure and Applied Geophysics, 169:447-465.

Peng, Y. and K. von Salzen, 2012. Simulation of mineral dust aerosol with Piecewise Log-normal Approximation (PLA) in CanAM4-PAM. Atmospheric Chemistry and Physics, 12:6891-6914.

Peters, G.P., T.B. Nilssen, L. Lindholt, M.S. Eide, S. Glomsrød, L.I. Eide and J.S. Fuglestvedt, 2011. Future emissions from shipping and petroleum activities in the Arctic. Atmospheric Chemistry and Physics, 11:5305-5320.

Petzold, A., A. Dopelheuer, C.A. Brock and F. Schroder, 1999. In situ observations and model calculations of black carbon emission by aircraft at cruise altitude. Journal of Geophysical Research: Atmospheres, 104:22171-22181.

Petzold, A., J.A. Ogren, M. Fiebig, P. Laj, S.M. Li, U. Baltensperger, T. Holzer-Popp, S. Kinne, G. Pappalardo, N. Sugimoto, C. Wehrli, A. Wiedensohler and X.Y. Zhang, 2013. Recommendations for reporting "black carbon" measurements. Atmospheric Chemistry and Physics, 13:8365-8379.

Polissar, A., P.K. Hopke and J. Harris, 2001. Source regions for atmospheric aerosol measured at Barrow, Alaska. Environmental Science and Technology, 35:4214-4226.

Prather, M., D. Ehhalt, F. Dentener, R. Derwent, E.J. Dlugokencky, E. Holland, I. Isaksen, J. Katima, V. Kirchhoff, P. Matson, P. Midgley and M. Wang, 2001. Atmospheric chemistry and greenhouse gases. In: Climate Change 2001: The Scientific Basis, pp. 239-287. J.T. Houghton (ed.). Cambridge University Press.

Prather, M., M. Gauss, T. Berntsen, I. Isaksen, J. Sundet, I. Bey, G. Brasseur, F. Dentener, R. Derwent, D. Stevenson, L. Grenfell, D. Hauglustaine, L. Horowitz, D. Jacob, L. Mickley, M. Lawrence, R. von Kuhlmann, J. –F. Muller, G. Pitari, H. Rogers, M. Johnson, J. Pyle, K. Law, M. van Weele and O. Wild, 2003. Fresh air in the 21st century? Geophysical Research Letters, 30:1100, doi:10.1029/2002GL016285.

Prinn, R.G., R.E. Weiss, B.R. Miller, J. Huang, F.N. Alyea, D.M. Cunnold, P.J. Fraser, D.E. Hartley and P.G. Simmonds, 1995. Atmospheric trends and lifetime of CH_3CCl_3 and global OH concentrations. Science, 269:187-192.

Quinn, P.K. and T.S. Bates, 2005. Regional Aerosol Properties: Comparisons from ACE 1, ACE 2, Aerosols99, INDOEX, ACE Asia, TARFOX, and NEAQS. Journal of Geophysical Research: Atmospheres, 110:D14202, doi:10.1029/2004JD004755.

Quinn, P.K., T.L. Miller, T.S. Bates, J.A. Ogren, E. Andrews and G.E. Shaw, 2002. A 3-year record of simultaneously measured aerosol chemical and optical properties at Barrow, Alaska. Journal of Geophysical Research: Atmospheres, 107(D11): doi: 10.1029/2001JD001248.

Quinn, P.K., G.E. Shaw, E. Andrews, E.G. Dutton, T. Ruoho-Airola and S.L. Gong, 2007. Arctic Haze: Current trends and knowledge gaps. Tellus B, 59:99-114.

Rahn, K.A., R.D. Borys and G.E. Shaw, 1977. Asian source of Arctic haze bands. Nature, 268:713-715.

Riahi, K., A. Gruebler and N. Nakicenovic, 2007. Scenarios of long-term socio-economic and environmental development under climate stabilization. Technological Forecasting and Social Change, 74:887-935.

Robertson, L., J. Langner and M. Engardt, 1999. An Eulerian limited area atmospheric transport model. Journal of Applied Meteorology, 38:90-210.

Robock, A., L. Oman, G.L. Stenchikov, O.B. Toon, C. Bardeen and R.P. Turco, 2007. Climatic consequences of regional nuclear conflicts. Atmospheric Chemistry and Physics, 7:2003-2012.

Roiger, A., H. Schlager, A. Schäfler, H. Huntrieser, M. Scheibe, H. Aufmhoff, O.R. Cooper, H. Sodemann, A. Stohl, J. Burkhart, M. Lazzara, C. Schiller, K.S. Law and F. Arnold, 2011. In-situ observation of Asian pollution transported into the Arctic lowermost stratosphere. Atmospheric Chemistry and Physics, 11:10975-10994.

Rönkkö, T., A. Virtanen, K. Vaaraslahti, J. Keskinen, L. Pirjola and M. Lappi, 2006. Effect of dilution conditions and driving parameters on nucleation mode particles in diesel exhaust: Laboratory and on-road study. Atmospheric Environment, 40:2893-2901.

Royal Society, 2008. Ground-level Ozone in the 21st Century: Future Trends, Impacts and Policy Implications. RS Policy document 15/08. The Royal Society, London.

Samset, B.H. and G. Myhre, 2011. Vertical dependence of black carbon, sulfate and biomass burning aerosol radiative forcing. Geophysical Research Letters, 38:L24802, doi:10.1029/2011gl049697.

Samset, B.H., G. Myhre, M. Schulz, Y. Balkanski, S. Bauer, T.K. Bernsten, H. Bian, N. Bellouin, T. Diehl, R.C. Easter, S.J. Ghan, T. Iversen, S. Kinne, A. Kirkevåg, J.-F. Lamarque, G. Lin, X. Liu, J. Penner, Ø. Seland, R.B. Skeie, P. Stier, T. Takemura, K. Tsigaridis and K. Zhang, 2013. Black carbon vertical profiles strongly affect its radiative forcing uncertainty. Atmospheric Chemistry and Physics, 13:2423-2434.

Sand, M., T. Berntsen, J.E. Kay, J.F. Lamarque, Ø. Seland and A. Kirkevåg, 2013a. The arctic response to remote and local forcing of black carbon. Atmospheric Chemistry and Physics, 13:211-224.

Sand, M., T. Berntsen, Ø. Seland and J.E. Kristjánsson, 2013b. Arctic surface temperature change to emissions of black carbon within Arctic or midlatitudes. Journal of Geophysical Research: Atmospheres, 118:7788-7798.

Schmale, J., J. Schneider, G. Ancellet, B. Quennehen, A. Stohl, H. Sodemann, J.F. Burkhart, T. Hamburger, S. Arnold, A. Schwarzenboeck, S. Borrmann and K. Law, 2011. Source identification and airborne chemical characterisation of aerosol pollution from long-range transport over Greenland during POLARCAT Summer campaign 2008. Atmospheric Chemistry and Physics, 11:10097-10123.

Schmid, H., L. Laskus, H.J. Abraham, U. Baltensperger, V. Lavanchy, M. Bizjak, P. Burba, H. Cachier, D. Crow, J.C. Chow, T. Gnauk, A. Even, H.M. ten Brink, K.P. Giesen, R. Hitzenberger, C. Hueglin, W. Maenhaut, C. Pio, A. Carvalho, J.P. Putaud, D. Toom-Sauntry and H. Puxbaum, 2001. Results of the "carbon conference" international aerosol carbon round robin test stage I. Atmospheric Environment, 35:2111-2121.

Schnell, R.C., 1984. Arctic haze and the Arctic Gas and Aerosol Sampling Program (AGASP). Geophysical Research Letters, 11:361-364.

Schultz, M.G., A. Heil, J.J. Hoelzemann, A. Spessa, K. Thonicke, J. Goldammer, A.C. Held, J.M. Pereira and M. Van Het Bolscher, 2008. Global wildland fire emissions from 1960 to 2000. Global Biogeochemical Cycles, 22:GB2002, doi: 10.1029/2007GB003031.

Schwarz, J.P., R.S. Gao, D.W. Fahey, D.S. Thomson, L.A. Watts, J.C. Wilson, J.M. Reeves, M. Darbeheshti, D.G. Baumgardner, G.L. Kok, S.H. Chung, M. Schulz, J. Hendricks, A. Lauer, B. Kärcher, J.G. Slowik, K.H. Rosenlof, T.L. Thompson, A.O. Langford, M. Loewenstein and K.C. Aikin, 2006. Single-particle measurement of mid latitude black carbon and light-scattering aerosols from the boundary layer to the lower stratosphere. Journal of Geophysical Research: Atmospheres, 111:D16207, doi:10.1029/2006JD007076.

Schwarz, J.P., R.S. Gao, J.R. Spackman, L. Watts, D.S. Thomson, D.W. Fahey, T.B. Ryerson, J. Peischl, J. Holloway, M. Trainer, G.J. Frost, T. Baynard, D. Lack, J. de Gouw, C. Warneke and L.A. Del Negro, 2008. Measurement of the mixing state, mass, and optical size of individual black carbon particles in urban and biomass burning emissions. Geophysical Research Letters, 35:L13810, doi:10.1029/2008GL033968.

Schwarz, J.P., J.R. Spackman, R.S. Gao, L. Watts, P. Stier, M. Schulz, S.M. Davis, S.C. Wofsy and D.W. Fahey, 2010. Global-scale black carbon profiles observed in the remote atmosphere and compared to model. Geophysical Research Letters, 37:L18812, doi:10.1029/2010gl044372.

Schwarz, J.P., S.J. Doherty, F. Li, S.T. Ruggiero, C.E. Tanner, A.E. Perring, R.S. Gao and D.W. Fahey, 2012. Assessing Single Particle Soot Photometer and Integrating Sphere/Integrating Sandwich Spectrophotometer measurement techniques for quantifying black carbon concentration in snow. Atmospheric Measurement Techniques, 5:2581-2592.

Schwarz, J.P., R.S. Gao, A.E. Perring, J.R. Spackman and D.W. Fahey, 2013a. Black carbon aerosol size in snow. Scientific Reports, 3:1356, doi: 10.1038/srep01356.

Schwarz, J.P., B.H. Samset, A.E. Perring, J.R. Spackman, R.S. Gao, P. Stier, M.G. Schultz, F.L. Moore, E.A. Ray and D.W. Fahey, 2013b. Global-scale seasonally resolved black carbon vertical profiles over the Pacific. Geophysical Research Letters, 40:5542-5547.

Seinfeld, J.H. and S.N. Pandis, 2006. Atmospheric Chemistry and Physics: From Air Pollution to Climate change. 2nd Edition, Wiley.

Shapiro, J.A., T. Hampel and A.J. Krueger, 1987. The Arctic tropopause fold. Monthly Weather Reviews, 115:444-454.

Sharma, S., D. Lavoué, H. Cachier, L.A. Barrie and S.L. Gong, 2004. Long-term trends of the black carbon concentrations in the Canadian Arctic. Journal of Geophysical Research: Atmospheres, 109:D15203, doi:10.1029/2003JD004331.

Sharma, S., E. Andrews, L.A. Barrie, J.A. Ogren and D. Lavoué, 2006. Variations and sources of the equivalent black carbon in the high Arctic revealed by long-term observations at Alert and Barrow: 1989–2003. Journal of Geophysical Research: Atmospheres, 111:D14208, doi:10.1029/2005JD006581.

Sharma, S., M. Ishizawa, D. Chan, D. Lavoué, E. Andrews, K.S. Eleftheriadis and S. Maksyutov, 2013. 16-year simulation of Arctic black carbon: Transport, source contribution, and sensitivity analysis on deposition. Journal of Geophysical Research: Atmospheres, 118:943-964.

Shaw, G.E., 1986. Cloud condensation nuclei associated with Arctic haze. Atmospheric Environment, 20:1453-1456.

Shaw, G.E., 1995. The Arctic haze phenomenon. Bulletin of the American Meteorological Society, 76:2403-2412.

Shaw, G.E. and K. Stamnes, 1980. Arctic haze: perturbation of the polar radiation budget. Annals of the New York Academy of Sciences, 338:533-539.

Shindell, D., 2007. Local and remote contributions to Arctic warming. Geophysical Research Letters, 34:L14704, doi:10.1029/2007GL030221.

Shindell, D., 2012. Evaluation of the absolute regional temperature potential. Atmospheric Chemistry and Physics, 12:7955-7960.

Shindell, D. and G. Faluvegi, 2009. Climate response to regional radiative forcing during the twentieth century. Nature Geoscience, 2:294-300.

Shindell D. and G. Faluvegi, 2010. The net climate impact of coal-fired power plant emissions. Atmospheric Chemistry and Physics, 10:3247-3260.

Shindell, D., G. Faluvegi, A. Lacis, J. Hansen, R. Ruedy and E. Aguilar, 2006. Role of tropospheric ozone increases in 20th-century climate change. Journal of Geophysical Research: Atmospheres, 111:D08302, doi:10.1029/2005JD006348.

Shindell, D., M. Chin, F. Dentener, R.M. Doherty, G. Faluvegi, A.M. Fiore, P. Hess, D. Koch, I.A. Mackenzie, M.G. Sanderson, M.G. Schultz, M. Schulz, D.S. Stevenson, H. Teich, C. Textor, O. Wild, D. Bergmann, I. Bey, H. Bian, C. Cuvelier, B.N. Duncan, G.A. Folberth, L. Horowitz, J. Jonson, J.W. Kaminski, E. Marmer, R.J. Park, K.J. Pringle, S. Schroeder, S. Szopa, T. Takemura, G. Zeng, T.J. Keating and A. Zuber, 2008. A multi-model assessment of pollution transport to the Arctic. Atmospheric Chemistry and Physics, 8:5353-5372.

Shindell, D., J.C.I. Kuylenstierna, E. Vignati, R. van Dingenen, M. Amann, Z. Klimont, S.C. Anenberg, N. Muller, G. Janssens-Maenhout, F. Raes, J.P. Schwarz, G. Faluvegi, L. Pozzoli, K. Kupiainen, L. Höglund-Isaksson, L. Emberson, D. Streets, V. Ramanathan, K. Hicks, N.T.K. Oanh, G. Milly, M. Williams, V. Demkine and D. Fowler, 2012. Simultaneously mitigating near-term climate change and improving human health and food security. Science, 335:183-189.

Shindell, D., J.-F. Lamarque, M. Schulz, M. Flanner, C. Jiao, M. Chin, P.J. Young, Y. H. Lee, L. Rotstayn, N. Mahowald, G. Milly, G. Faluvegi, Y. Balkanski, W.J. Collins, A.J. Conley, S. Dalsoren, R. Easter, S. Ghan, L. Horowitz, X. Liu, G. Myhre, T. Nagashima, V. Naik, S.T. Rumbold, R. Skeie, K. Sudo, S. Szopa, T. Takemura, A. Voulgarakis, J.-H. Yoon and F. Lo, 2013. Radiative forcing in the ACCMIP historical and future climate simulations. Atmospheric Chemistry and Physics, 13:2939-2974.

Shine, K.P, R.G. Derwent, D.J. Wuebbles, J-J. Morcrette, A.J. Apling, J.P. Blanchet, R.J. Charlson, D. Crommelynck, H. Grassl, N. Husson, G.J. Jenkins, I. Karol, M.D. King, V. Ramanathan, H. Rodhe, G-Y. Shi, G. Thomas, W-C. Wang, T.M.L. Wigley and T. Yamanouchi, 1990. Radiative forcing of climate. In: Houghton, J.T., G.J. Jenkins and J.J. Ephraums (eds.), Climate Change: The IPCC Scientific Assessment. Contribution of Working Group I to the First Assessment Report of the Intergovernmental Panel on Climate Change. Cambridge University Press.

Shiraiwa, M., Y. Kondo, N. Moteki, N. Takegawa, L. Sahu, A. Takami, S. Hatakeyama, S. Yonemura and D.R. Blake, 2008. Radiative impact of mixing state of black carbon aerosol in Asian outflow. Journal of Geophysical Research: Atmospheres, 113:D24210, doi:10.1029/2008JD010546.

Simpson, W.R., R. von Glasow, K. Riedel, P. Anderson, P. Ariya, J. Bottenheim, J. Burrows, L.J. Carpenter, U. Frieß, M.E. Goodsite, D. Heard, M. Hutterli, H.-W. Jacobi, L. Kaleschke, B. Neff, J. Plane, U. Platt, A. Richter, H. Roscoe, R. Sander, P. Shepson, J. Sodeau, A. Steffen, T. Wagner and E. Wolff, 2007. Halogens and their role in polar boundary-layer ozone depletion. Atmospheric Chemistry and Physics, 7:4375-4418.

Simpson, D., A. Benedictow, H. Berge, R. Bergström, L.D. Emberson, H. Fagerli, C.R. Flechard, G.D. Hayman, M. Gauss, J.E. Jonson, M.E. Jenkin, A. Nyíri, C. Richter, V.S. Semeena, S. Tsyro, J.-P. Tuovinen, Á. Valdebenito and P. Wind, 2012. The EMEP MSC-W chemical transport model – technical description. Atmospheric Chemistry and Physics, 12:7825-7865.

Singh, H.B. and P.L. Hanst, 1981. Peroxy acetyl nitrate (PAN) in the unpolluted atmosphere – an important reservoir for nitrogen oxides. Geophysical Research Letters, 8:941-944.

Singh, H.B., B.E. Anderson, W. Brune, C. Cai, R.C. Cohen, J.H. Crawford, M. Cubison, E.P. Czech, H.E. Fuelberg, G. Huey, D.J. Jacob, J. Jimenez, A. Kaduwela, Y. Kondo, J. Mao, J.R. Olson, G. Sachse, S.A. Vay, P.O. Wennberg and A. Wisthaler, 2010. Pollution influences on atmospheric composition and chemistry at high northern latitudes: Boreal and California forest fire emissions. Atmospheric Environment, 44:4553-4563.

Sitch, S., P.M. Cox, W.J. Collins and C. Huntingford, 2007. Indirect radiative forcing of climate change through ozone effects on the land-carbon sink. Nature, 448:791-794.

Skeie, R.B., T. Berntsen, G. Myhre, C.A. Pedersen, J. Strom, S. Gerland and J.A. Ogren, 2011a. Black carbon in the atmosphere and snow, from pre-industrial times until present. Atmospheric Chemistry and Physics, 11:7469-7534.

Skeie, R.B., T. Berntsen, G. Myhre, K. Tanaka, M.M. Kvalevåg and C.R. Hoyle, 2011b. Anthropogenic radiative forcing time series from pre-industrial times until 2010. Atmospheric Chemistry and Physics, 11:11827-11857.

Slowik, J.G., K. Stainken, P. Davidovits, L.R. Williams, J.T. Jayne, C.E. Kolb, D.R. Worsnop, Y. Rudich, P.F. DeCarlo and J.L. Jimenez, 2004. Particle morphology and density characterization by combined mobility and aerodynamic diameter measurements. Part 2: Application to combustion-generated soot aerosols as a function of fuel equivalence ratio. Aerosol Science and Technology, 38:1206-1222.

Smith, S.J. and T.C. Bond, 2014. Two hundred fifty years of aerosols and climate: the end of the age of aerosols. Atmospheric Chemistry and Physics, 14:537-549.

Smith, S.J. and A. Mizrahi, 2013. Near-term climate mitigation by short-lived forcers. Proceedings of the National Academy of Sciences, 110:14202-14206.

Smith, S.J. and T.M.L. Wigley, 2006. Multi-gas forcing stabilization with Minicam. Energy Journal (SI), 27:373-391.

Smith, S.J., J. van Aardenne, Z. Klimont, R.J. Andres, A. Volke and S.D. Arias, 2011. Anthropogenic sulfur dioxide emissions: 1850–2005. Atmospheric Chemistry and Physics, 11:1101-1116.

Sodemann, H., M. Pommier, S.R. Arnold, S.A. Monks, K. Stebel, J.F. Burkhart, J.W. Hair, G. Diskin, C. Clerbaux, P.F. Coheur, D. Hurtmans, H. Schlager, A.M. Blechschmidt, J.E. Kristjánsson and A. Stohl, 2011. Episodes of cross-polar transport in the Arctic troposphere during July 2008 as seen from models, satellite, and aircraft observations. Atmospheric Chemistry and Physics, 11:3631-3651.

Sommar, J., M.E. Andersson and H.-W. Jacobi, 2010. Circumpolar measurements of speciated mercury, ozone and carbon monoxide in the boundary layer of the Arctic Ocean. Atmospheric Chemistry and Physics, 10:5031-5045.

Spackman, J.R., R.S. Gao, W.D. Neff, J.P. Schwarz, L. Watts, D.W. Fahey, J. Holloway, T.B. Ryerson, J. Peischl and C.A. Brock, 2010. Aircraft observations of enhancement and depletion of black carbon mass in the springtime Arctic. Atmospheric Chemistry and Physics, 10:9667-9680.

Statistics Norway, 2013. Emissions of Black Carbon and Organic Carbon in Norway 1990-2011. Notater Documents No. 13:2013.

Sterle, K.M., J.R. McConnell, J. Dozier, R. Edwards and M.G. Flanner, 2013. Retention and radiative forcing of black carbon in eastern Sierra Nevada snow. The Cryosphere, 7:365-374.

Stevens, B. and O. Boucher, 2012. Climate science: The aerosol effect. Nature, 490:40-41.

Stevens, B., M. Giorgetta, M. Esch, T. Mauritsen, T. Crueger, S. Rast, M. Salzmann, H. Schmidt, J. Bader, K. Block, R. Brokopf, I. Fast, S. Kinne, L. Kornblueh, U. Lohmann, R. Pincus, T. Reichler and E. Roeckner, 2013. Atmospheric component of the MPI-M Earth System Model: ECHAM6. Journal of Advances in Modelling Earth Systems, 5:146-172.

Stevenson, D.S., P.J. Young, V. Naik, J.-F. Lamarque, D.T. Shindell, A. Voulgarakis, R.B. Skeie, S.B. Dalsoren, G. Myhre, T.K. Berntsen, G.A. Folberth, S.T. Rumbold, W.J. Collins, I.A. MacKenzie, R.M. Doherty, G. Zeng, T.P.C. van Noije, A. Strunk, D. Bergmann, P. Cameron-Smith, D.A. Plummer, S.A. Strode, L. Horowitz, Y.H. Lee, S. Szopa, K. Sudo, T. Nagashima, B. Josse, I. Cionni, M. Righi, V. Eyring, A. Conley, K.W. Bowman, O. Wild and A. Archibald, 2013. Tropospheric ozone changes, radiative forcing and attribution to emissions in the Atmospheric Chemistry and Climate Model Intercomparison Project (ACCMIP). Atmospheric Chemistry and Physics, 13:3063-3085.

Stier, P., J.H. Seinfeld, S. Kinne, J. Feichter and O. Boucher, 2006. Impact of nonabsorbing anthropogenic aerosols on clear-sky atmospheric absorption. Journal of Geophysical Research: Atmospheres, 111:D18201, doi:10.1029/2006JD007147.

Stohl, A., 2006. Characteristics of atmospheric transport into the Arctic troposphere. Journal of Geophysical Research: Atmospheres, 111:D11306, doi:10.1029/2005JD006888.

Stohl, A., C. Forster, A. Frank, P. Seibert and G. Wotawa, 2005. Technical note: The Lagrangian particle dispersion model FLEXPART version 6.2. Atmospheric Chemistry and Physics, 5:2461-2474.

Stohl, A., E. Andrews, J.F. Burkhart, C. Forster, A. Herber, S.W. Hoch, D. Kowal, C. Lunder, T. Mefford, J.A. Ogren, S. Sharma, N. Spichtinger, K. Stebel, R.S. Stone, J. Storm, K. Torseth, C. Wehrli and K.E. Yttri, 2006. Pan-Arctic enhancements of light absorbing aerosol concentrations due to North American boreal forest fires during summer 2004. Journal of Geophysical Research: Atmospheres, 111:D22214, doi:10.1029/2006JD007216.

Stohl, A., T. Berg, J.F. Burkhart, A.M. Fjaeraa, C. Forster, A. Herber, O. Hov, C. Lunder, W.W. McMillan, S. Oltmans, M. Shiobara, D. Simpson, S. Solberg, K. Stebel, J. Strom, K. Torseth, R. Treffeisen, K. Virkkunen and K.E. Yttri, 2007. Arctic smoke – record high air pollution levels in the European Arctic due to agricultural fires in Eastern Europe. Atmospheric Chemistry and Physics, 7:511-534.

Stohl, A., Z. Klimont, S. Eckhardt, K. Kupiainen, V.P. Shevchenko, V.M. Kopeikin and A.N. Novigatsky, 2013. Black carbon in the Arctic: the underestimated role of gas flaring and residential combustion emissions. Atmospheric Chemistry and Physics, 13:8833-8855.

Stone, R.S., A. Herber, V. Vitale, M. Mazzola, A. Lupi, R.C. Schnell, E.G. Dutton, P.S.K. Liu, S.M. Li, K. Dethloff, A. Lampert, C. Ritter, M. Stock, R. Neuber and M. Maturilli, 2010. A three-dimensional characterization of Arctic aerosols from airborne Sun photometer observations: PAM-ARCMIP, April 2009. Journal of Geophysical Research: Atmospheres, 115:doi 10.1029/2009jd013605.

Stone, R.S., S. Sharma, A. Herber, K.S. Eleftheriadis and D.W. Nelson, 2014. A characterization of Arctic aerosols on the basis of aerosol optical depth and black carbon measurements. Elementa, 2:000027, doi:10.12952/journal.elementa.000027.

Strunin, M.A., A.A. Postnov and M.Y. Mezrin, 1997. Meteorological potential for contamination of arctic troposphere: Boundary layer structure and turbulent diffusion characteristics. Atmospheric Research, 44:37-51.

Sweitlicki, E., H.C. Hansson, K. Hameri, B. Svenningsson, A. Massling, G. McFiggans, P.H. McMurry, T. Petaja, P. Tunved, M. Gysel, D. Topping, E. Weingartner, U. Baltensperger, J. Rissler, A. Wiedensohler and M. Kulmala, 2008. Hygroscopic properties of submicrometer atmospheric aerosol particles measured with H-TDMA instruments in various environments - a review. Tellus, 60:432-469.

Thomas, J.L., J. Dibb, L.G. Huey, J. Liao, D. Tanner, B. Lefer, R. von Glasow and J. Stutz, 2012. Modeling chemistry in and above snow at Summit, Greenland – Part 2: Impact of snowpack chemistry on the oxidation capacity of the boundary layer. Atmospheric Chemistry and Physics, 12:6537-6554.

Thomas, J.L., J.C Raut, K.S Law, L. Marelle, G. Ancellet, F. Ravetta, J.D Fast, G. Pfister, L.K Emmons, G.S Diskin, A. Weinheimer, A. Roiger and H. Schlager, 2013. Pollution transport towards Greenland during summer 2008. Atmospheric Chemistry and Physics, 13:3825-3848.

Tjernström, M., C. Leck, C.E. Birch, J.W. Bottenheim, B.J. Brooks, I.M. Brooks, L. Bäcklin, R.Y.-W. Chang, G. de Leeuw, L. Di Liberto, S. de la Rosa, E. Granath, M. Graus, A. Hansel, J. Heintzenberg, A. Held, A. Hind, P. Johnston, J. Knulst, M. Martin, P.A. Matrai, T. Mauritsen, M. Müller, S.J. Norris, M.V. Orellana, D.A. Orsini, J. Paatero, P.O.G. Persson, Q. Gao, C. Rauschenberg, Z. Ristovski, J. Sedlar, M.D. Shupe, B. Sierau, A. Sirevaag, S. Sjogren, O. Stetzer, E. Swietlicki, M. Szczodrak, P. Vaattovaara, N. Wahlberg, M. Westberg and C.R. Wheeler, 2014. The Arctic Summer Cloud Ocean Study (ASCOS): overview and experimental design. Atmospheric Chemistry and Physics, 14:2823-2869.

Tol, R.S.J., T. Berntsen, B.C. O'Neill, J.S. Fuglestvedt and K.P. Shine, 2012. A unifying framework for metrics for aggregating the climate effect of different emissions. Environmental Research Letters, 7: 044006, doi: 10.1088/1748-9326/7/4/044006.

Tomasi, C., V. Vitale, A. Lupi, C. Di Carmine, M. Campanelli, A. Herber, R. Treffeisen, R.S. Stone, E. Andrews, S. Sharma, V. Radionov, W. von Hoyningen-Huene, K. Stebel, G.H. Hansen, C.L. Myhre, C. Wehrli, V. Aaltonen, H. Lihavainen, A. Virkkula, R. Hillamo, J. Strom, C. Toledano, V.E. Cachorro, P. Ortiz, A.M. de Frutos, S. Blindheim, M. Frioud, M. Gausa, T. Zielinski, T. Petelski and T. Yamanouchi, 2007. Aerosols in polar regions: A historical overview based on optical depth and in situ observations. Journal of Geophysical Research: Atmospheres, 112:D16205, doi:10.1029/2007JD008432.

Tomasi, C., A. Lupi, M. Mazzola, R.S. Stone, E.G. Dutton, A. Herber, V. Radionov, B. Holben, M. Sorokin and S. Sakerin, 2012. An update on polar aerosol optical properties using POLAR-AOD and other measurements performed during the International Polar Year. Atmospheric Environment, 52:29-47.

Tomasi, C., A.A. Kokhanovsky, A. Lupi, C. Ritter, A. Smirnov, N.T. O'Neill, R.S. Stone, B.N. Holben, S. Nyeki, C. Wehrli, A. Stohl, M. Mazzola, C. Lanconelli, V. Vitale, K. Stebel, V. Aaltonen, G. de Leeuw, E. Rodriguez, A.B. Herber, V.F. Radionov, T. Zielinski, T. Petelski, S.M. Sakerin, D.M. Kabanov, Y. Xue, L. Mei, L. Istomina, R. Wagener, B. McArthur, P.S. Sobolewski, R. Kivi, Y. Courcoux, P. Larouche, S. Broccardo and S.J. Piketh, 2015. Aerosol remote sensing in polar regions. Earth-Science Reviews, 140:108-157.

Tritscher, T., Z. Jurányi, M. Martin, R. Chirico, M. Gysel, M.F. Heringa, P.F. DeCarlo, B. Sierau, A.S.H. Prévôt, E. Weingartner and U. Baltensperger, 2011. Changes of hygroscopicity and morphology during ageing of diesel soot. Environmental Research Letters, 6:034026, doi:10.1088/1748-9326/6/3/034026.

Tunved, P., J. Ström and R. Krejci, 2013. Arctic aerosol life cycle: linking aerosol size distributions observed between 2000 and 2010 with air mass transport and precipitation at Zeppelin station, Ny-Ålesund, Svalbard. Atmospheric Chemistry and Physics, 13:3643-3660.

Turpin, B.J., R.A. Cary and J.J. Huntzicker, 1990. An in-situ time resolved analyzer for aerosol organic and elemental carbon. Aerosol Science and Technology, 12:161-171.

Twomey, S., 1977. The influence of pollution on the shortwave albedo of clouds. Journal of Atmospheric Sciences, 34:1149-1152.

UNEP/WMO, 2011. Integrated Assessment of Black Carbon and Tropospheric Ozone. United Nations Environment Programme / World Meteorological Organization, Nairobi, Kenya.

US EPA, 2012. Report to Congress on Black Carbon. United States Environmental Protection Agency, EPA-450/R-12-001.

van der Werf, G.R., J.T. Randerson, L. Giglio, G.J. Collatz, P.S. Kasibhatla and J. Arellano, 2006. Interannual variability in global biomass burning emissions from 1997 to 2004. Atmospheric Chemistry and Physics, 6:3423-3441.

van der Werf, G.R., J.T. Randerson, L. Giglio, G.J. Collatz, M. Mu, P.S. Kasibhatla, D.C. Morton, R.S. DeFries, Y. Jin and T.T. Leeuwen, 2010. Global fire emissions and the contribution of deforestation, savanna, forest, agricultural, and peat fires. Atmospheric Chemistry and Physics, 11:11707-11735.

van Vuuren, D.P., M.G.J. Den Elzen, P. Lucas, B.E. Eickhout, B.J. Strengers, B. Van Ruijven, S. Wonink and R. Van Houdt, 2007. Stabilizing greenhouse gas concentrations at low levels: an assessment of reduction strategies and costs. Climatic Change, 81:119-159.

Vignati, E., M. Karl, M. Krol, J.C. Wilson, P. Stier and F. Cavalli, 2010. Sources of uncertainties in modelling black carbon at the global scale. Atmospheric Chemistry and Physics, 10:2595-2611.

Virkkula, A., N.C. Ahlquist, D.S. Covert, W.P. Arnott, P.J. Sheridan, P.K. Quinn and D.J. Coffman, 2005. Modification, calibration, and a field test of an instrument for measuring light absorption by particles. Aerosol Science and Technology, 39:68-73.

von Hardenberg, J., L. Vozella, C. Tomasi, V. Vitale, A. Lupi, M. Mazzola, T.P.C. van Noije, A. Strunk and A. Provenzale, 2012. Aerosol optical depth over the Arctic: a comparison of ECHAM-HAM and TM5 with ground-based, satellite and reanalysis data. Atmospheric Chemistry and Physics, 12:6953-6967.

von Salzen, K., 2006. Piecewise log-normal approximation of size distributions for aerosol modelling. Atmospheric Chemistry and Physics, 6:1351-1372.

von Salzen, K., J.F. Scinocca, N.A. McFarlane, J. Li, J.N.S. Cole, D. Plummer, D. Verseghy, M.C. Reader, X. Ma, M. Lazare and L. Solheim, 2013. The Canadian Fourth Generation Atmospheric Global Climate Model (CanAM4). Part I: Representation of Physical Processes. Atmosphere-Ocean, 51:104-125.

von Schneidemesser, R., J.J. Schauer, G.S.W. Hagler and M.H. Bergin, 2009. Concentrations and sources of carbonaceous aerosol in the atmosphere of Summit, Greenland. Atmospheric Environment, 43:4155-4162.

Walker, T.W., D.B.A. Jones, M. Parrington, D.K. Henze, L.T. Murray, J.W. Bottenheim, K. Anlauf, J.R. Worden, K.W. Bowman, C. Shim, K. Singh, M. Kopacz, D.W. Tarasick, J. Davies, P. von der Gathen, A.M. Thompson and C.C. Carouge, 2012. Impacts of midlatitude precursor emissions and local photochemistry on ozone abundances in the Arctic. Journal of Geophysical Research: Atmospheres, 117:D01305, doi:10.1029/2011JD016370.

Wang, Q., D.J. Jacob, J.A. Fisher, J. Mao, E.M. Leibensperger, C.C. Carouge, P. Le Sager, Y. Kondo, J.L. Jimenez, M.J. Cubison and S.J. Doherty, 2011. Sources of carbonaceous aerosols and deposited black carbon in the Arctic in winter-spring: Implications for radiative forcing. Atmospheric Chemistry and Physics, 11:12453-12473.

Wang, H., R. Easter, P.J. Rasch, M. Wang, X. Liu, S. Ghan, Y. Qian, J.H. Yoon, P.L. Ma and V. Velu, 2013. Sensitivity of remote aerosol distributions to representation of cloud–aerosol interactions in a global climate model. Geoscientific Model Development, 6:765-782.

Wang, Q., D.J. Jacob, J.R. Spackman, A.E. Perring, J.P. Schwarz, N. Moteki, E.A. Marais, C. Ge, J. Wang, and S.R.H. Barrett, 2014a. Global budget and radiative forcing of black carbon aerosol: Constraints from pole-to-pole (HIPPO) observations across the Pacific. Journal of Geophysical Research: Atmospheres, 119:195-206.

Wang, H., P.J. Rasch, R.C. Easter, B. Singh, R. Zhang, P.-L. Ma, Y. Qian, S.J. Ghan and N. Beagley, 2014b. Using an explicit emission tagging method in global modeling of source-receptor relationships for black carbon in the Arctic: Variations, sources, and transport pathways. Journal of Geophysical Research: Atmospheres, 119:12,888-12,909.

Warneke, C., R. Bahreini, J. Brioude, C.A. Brock, J.A. de Gouw, D.W. Fahey, K.D. Froyd, J.S. Holloway, A. Middlebrook, L. Miller, S. Montzka, D.M. Murphy, J. Peischl, T.B. Ryerson, J.P. Schwarz, J.R. Spackman and P. Veres, 2009. Biomass burning in Siberia and Kazakhstan as an important source for haze over the Alaskan Arctic in April 2008. Geophysical Research Letters, 36:L02813, doi:10.1029/2008GL036194.

Warneke, C., K.D. Froyd, J. Brioude, R. Bahreini, C.A. Brock, J. Cozic, J.A. de Gouw, D.W. Fahey, R. Ferrare, J.S. Holloway, A.M. Middlebrook, L. Miller, S. Montzka, J.P. Schwarz, H. Sodemann, J.R. Spackman and A. Stohl, 2010. An important contribution to springtime Arctic aerosol from biomass burning in Russia. Geophysical Research Letters, 37:L01801, doi:10.1029/2009GL041816.

Wendl, I.A., J.A. Menking, R. Färber, M. Gysel, S.D. Kaspari, M.J.G. Laborde and M. Schwikowski, 2014. Optimized method for black carbon analysis in ice and snow using the Single Particle Soot Photometer. Atmospheric Measurement Techniques, 7:2667-2681.

Wespes, C., L.K. Emmons, D.P. Edwards, J. Hannigan, D. Hurtmans, M. Saunois, P.F. Coheur, C. Clerbaux, M.T. Coffey, R.L. Batchelor, R. Lindenmaier, K. Strong, A. Weinheimer, J.B. Nowak, T.B. Ryerson, J.D. Crounse and P.O. Wennberg, 2012. Analysis of ozone and nitric acid in spring and summer Arctic pollution using aircraft, ground-based, satellite observations and MOZART-4 model: source attribution and partitioning. Atmospheric Chemistry and Physics, 12:237-259.

West, J.J., A.M. Fiore, V. Naik, L. Horowitz, M.D. Schwarzkopf and D.L. Mauzerall, 2007. Ozone air quality and radiative forcing consequences of changes in ozone precursor emissions. Geophysical Research Letters, 34:L06806, doi:10.1029/2006GL029173.

Wiedinmyer, C., S.K. Akagi, R.J. Yokelson, L.K. Emmons, J.A. Al-Saadi, J.J. Orlando and A.J. Soja, 2011. The Fire Inventory from NCAR (FINN): A high resolution global model to estimate the emissions from open burning. Geoscientific Model Development, 4:625-641.

Williams, E.J., F.C. Fehsenfeld, B.T. Jobson, W.C. Kuster, P.D. Goldan, J. Stutz and W.A. McClenny, 2006. Comparison of ultraviolet absorbance, chemiluminescence, and DOAS instruments for ambient ozone monitoring. Environmental Science and Technology, 40:5755-5762.

Winther, M. and O.-K. Nielsen, 2011. Technology dependent BC and OC emissions for Danmark, Greenland and the Faroe Islands calculated for the time period 1990–2030. Atmospheric Environment, 45:5880-5895.

Winther, M., J.H. Christensen, M.S. Plejdrup, E.S. Ravn, O.F. Eriksson and H.O. Kristensen, 2014. Emission inventories for ships in the Arctic based on satellite sampled AIS data. Atmospheric Environment, 91:1-14.

Wise, M.A., K.V. Calvin, A.M. Thomson, L.E. Clarke, B. Bond-Lamberty, R.D. Sands, S.J. Smith, A.C. Janetos and J.A. Edmonds, 2009. Implications of limiting CO_2 concentrations for land use and energy. Science, 324:1183-1186.

Wofsy, S.C., 2011. HIAPER Pole-to-Pole Observations (HIPPO): fine-grained, global-scale measurements of climatically important atmospheric gases and aerosols. Philosophical Transactions of the Royal Society, 369:2073-2086.

Wuebbles, D.J. and K. Hayhoe, 2002. Atmospheric methane and global change. Earth-Science Reviews, 57:177-210.

Yang, Q., C.M. Bitz and S.J. Doherty, 2014. Offsetting effects of aerosols on Arctic and global climate in the late 20th century. Atmospheric Chemistry and Physics, 14:3969-3975.

Yttri, K.E., C. Lund Myhre, S. Eckhardt, M. Fiebig, C. Dye, D. Hirdman, J. Ström, Z. Klimont and A. Stohl, 2014. Quantifying black carbon from biomass burning by means of levoglucosan – a one-year time series at the Arctic observatory Zeppelin. Atmospheric Chemistry and Physics, 14:6427-6442.

Zaveri, R.A., and L.K. Peters, 1999. A new lumped structure photochemical mechanism for large-scale applications. Journal of Geophysical Research: Atmospheres, 104:30387-30415.

Zaveri, R.A., R. Easter, J.D. Fast and L.K. Peters, 2008. Model for Simulating Aerosol Interactions and Chemistry (MOSAIC). Journal of Geophysical Research: Atmospheres, 113:D13204, doi: 10.1029/2007JD008782.

Zhang, Y., C. Seigneur, M. Bocquet, V. Mallet and A. Baklanov, 2012a. Real-time air quality forecasting, Part I: History, techniques, and current status. Atmospheric Environment, 60:632-655.

Zhang, Y., C. Seigneur, M. Bocquet, V. Mallet and A. Baklanov, 2012b. Real-time air quality forecasting, Part II: State of the science, current research needs, and future prospects. Atmospheric Environment, 60:656-676.

Zhang, K., D. O'Donnell, J. Kazil, P. Stier, S. Kinne, U. Lohmann, S. Ferrachat, B. Croft, J. Quaas, H. Wan, S. Rast and J. Feichter, 2012c. The global aerosol-climate model ECHAM-15 HAM, version 2: sensitivity to improvements in process representations. Atmospheric Chemistry and Physics, 12:8911-8949.

Zhang, J.L., R. Lindsay, A. Schweiger and M. Steele, 2013. The impact of an intense summer cyclone on 2012 Arctic sea ice retreat. Geophysical Research Letters, 40:720-726.

Zhou, C., J.E. Penner, M.G. Flanner, M.M. Bisiaux, R. Edwards and J.R. McConnell, 2012. Transport of black carbon to polar regions: Sensitivity and forcing by black carbon. Geophysical Research Letters, 39:L22804, doi: 10.1029/2012GL053388.

Zilitinkevich, S. and A. Baklanov, 2002. Calculation of the height of stable boundary layers in practical applications. Boundary Layer Meteorology, 105:389-409.

Zilitinkevich, S., A. Baklanov, J. Rost, A.S. Smedman, V. Lykosov and P. Calanca, 2002. Diagnostic and prognostic equations for the depth of the stably stratified Ekman boundary layer. Quarterly Journal of the Royal Meteorological Society, 128:25-46.

Acronyms and abbreviations

σ_{ap}	Particle light absorption coefficient
ACCMIP	Atmospheric Chemistry and Climate Model Intercomparison Project
AeroCom	Aerosol Comparisons between Observations and Models (project)
AMAP	Arctic Monitoring and Assessment Programme
AOD	Aerosol optical depth
asl	Above sea level
BC	Black carbon
C2010	Arctic shipping emission inventory by Corbett et al. (2010)
CCM	Chemistry Climate Model
CESM	Community Earth System Model
CH_4	Methane
CLM	Land component of CESM
CLRTAP	Convention on Long-range Transboundary Air Pollution
CMIP5	Coupled Model Intercomparison Project Phase 5
CTM	Chemistry Transport Model
CO	Carbon monoxide
CO_2	Carbon dioxide
DNV	Det Norske Veritas
eBC	Equivalent black carbon
EC	Elemental carbon
ESM	Earth System Model
GAINS	Greenhouse gas and Air pollutant Interactions and Synergies model
GTP	Global Temperature change Potential
GWP	Global Warming Potential
HNO_3	Nitric acid
IIASA	International Institute for Applied Systems Analysis, Austria
IPCC AR5	Intergovernmental Panel on Climate Change, Fifth Assessment Report
LAC	Light-absorbing carbon
MAC	Mass-specific Absorption Cross section
nmOP	Non-methane ozone precursor
nmVOC	Non-methane volatile organic compound
NO_X	Nitrogen oxides
nss SO_4^{2-}	Non-sea salt sulfate
O_3	Ozone
OC	Organic carbon
OEUR	Other (i.e. non-Arctic) Europe
OH	Hydroxyl radical
OM	Organic matter
P2011	Arctic shipping emission inventory by Peters et al. (2011)
PAMARCMiP	Polar Airborne Measurements and Arctic Regional Climate Model Simulation Project
PAN	Peroxyacetyl nitrate
PAS	Photoacoustic spectrometer
PM	Particulate matter
ppb	Parts per billion
ppbv	Parts per billion by volume
POLARCAT	Polar Study using Aircraft, Remote Sensing, Surface Measurements and Models of Climate, Chemistry, Aerosols, and Transport
PSAP	Particle Soot Absorption Photometer
rBC	Refractory black carbon
RF	Radiative forcing
ROW	Rest-of-World
RTP	Regional temperature potential
SLCFs	Short-lived climate forcers
SO_2	Sulfur dioxide
SO_4	Sulfate
SP2	Single Particle Soot Photometer
SST	Sea-surface temperature
TOA	Top-of-Atmosphere
UNFCCC	United Nations Framework Convention on Climate Change
VOC	Volatile organic compound
W2014	Arctic shipping emission inventory by Winther et al. (2014)

Arctic Monitoring and Assessment Programme

The Arctic Monitoring and Assessment Programme (AMAP) was established in June 1991 by the eight Arctic countries (Canada, Denmark, Finland, Iceland, Norway, Russia, Sweden and the United States) to implement parts of the Arctic Environmental Protection Strategy (AEPS). AMAP is now one of six working groups of the Arctic Council, members of which include the eight Arctic countries, the six Arctic Council Permanent Participants (indigenous peoples' organizations), together with observing countries and organizations.

AMAP's objective is to provide 'reliable and sufficient information on the status of, and threats to, the Arctic environment, and to provide scientific advice on actions to be taken in order to support Arctic governments in their efforts to take remedial and preventive actions to reduce adverse effects of contaminants and climate change'.

AMAP produces, at regular intervals, assessment reports that address a range of Arctic pollution and climate change issues, including effects on health of Arctic human populations. These are presented to Arctic Council Ministers in 'State of the Arctic Environment' reports that form a basis for necessary steps to be taken to protect the Arctic and its inhabitants.

This report has been subject to a formal and comprehensive peer review process. The results and any views expressed in this series are the responsibility of those scientists and experts engaged in the preparation of the reports.

The AMAP Secretariat is located in Oslo, Norway. For further information regarding AMAP or ordering of reports, please contact the AMAP Secretariat (Gaustadalléen 21, N-0349 Oslo, Norway) or visit the AMAP website at www.amap.no.

AMAP Secretariat

Gaustadalléen 21
N-0349 Oslo, Norway

T +47 21 08 04 80
F +47 21 08 04 85

www.amap.no

ISBN – 978-82-7971-092-9

ARCTIC COUNCIL

AMAP
Arctic Monitoring and Assessment Programme